

# **Modular Ligation Chemistry as an Avenue to Novel Acrylonitrile- Butadiene Copolymer Architectures**

Zur Erlangung des akademischen Grades eines

DOKTORS DER NATURWISSENSCHAFTEN

(Dr. rer. nat.)

Fakultät für Chemie und Biowissenschaften

Karlsruher Institut für Technologie (KIT) – Universitätsbereich

genehmigte

DISSERTATION

von

Dipl.-Chem. Christoph Jürgen Dürr

aus

Lüneburg, Deutschland

Dekan: Prof. Dr. Martin Bastmeyer

Referent: Prof. Dr. Christopher Barner-Kowollik

Korreferent: Prof. Dr. Michael Meier

Tag der mündlichen Prüfung: 19.07.2013



Die vorliegende Arbeit wurde von Mai 2010 bis Juni 2013 unter Anleitung von Prof. Dr. Christopher Barner-Kowollik am Karlsruher Institut für Technologie (KIT) – Universitätsbereich angefertigt.



Ich erkläre hiermit, dass ich die vorliegende Arbeit im Rahmen der Betreuung durch Prof. Dr. Christopher Barner-Kowollik selbstständig verfasst und keine anderen als die angegebenen Quellen und Hilfsmittel verwendet habe. Des Weiteren erkläre ich, dass ich mich derzeit in keinem laufenden Promotionsverfahren befinde und auch keine vorausgegangenen Promotionsversuche unternommen habe.

Karlsruhe, den 19.07.2013



*Für meine Familie*

*Claudi und Isabella*



## Zusammenfassung

Trotz der hohen industriellen Relevanz von Nitril-Butadien-Kautschuken (Nitrile-Butadiene-Rubber, NBR) und der großen Bedeutung orthogonaler Konjugationsmethoden zur Synthese anspruchsvoller makromolekularer Architekturen haben modulare Konjugationsmethoden bis heute keine Anwendung in der Darstellung komplexer NBR Architekturen gefunden.

Um diese Lücke zu schließen beschreibt die vorliegende Arbeit Strategien zur Synthese neuartiger Acrylnitril-Butadien Copolymerstrukturen mittels modularer Konjugationsmethoden. Die verwendeten NBR Blöcke wurden dazu in einem Lösungs-basierten Verfahren unter Verwendung mehrerer neuartiger Trithiocarbonat-Kettentransferagenzien über die reversible Additions-Fragmentierungs-Kettenübertragungspolymerisation erhalten. Es wurde gezeigt, dass die Kupfer-vermittelte Azid-Alkin-Cycloaddition eine effektive Methode zur Synthese linearer und verzweigter hochmolekularer NBR Architekturen darstellt. Die hetero-Diels-Alder Cyclisierungsreaktion von Cyclopentadienen mit den elektronenarmen Thiocarbonyl-Gruppen von Pyridinyldithioestern wurde zur Synthese von NBR-*b*-poly(Styrol-*co*-Acrylnitril) Blockcopolymer- und 4-Miktoarm-sternpolymerarchitekturen ausgenutzt. Durch den Vergleich von experimentellen Daten und simulierten Werten konnten für den Fall der Blockcopolymerbildung die mit der reversiblen Deaktivierungs-Polymerisationstechnik verbundenen Vorteile sowie Einschränkungen der modularen Synthese makromolekularer Architekturen aufgezeigt werden. Außerdem wurde gezeigt, dass die Nitrilimin-vermittelte Tetrazol-En-Kopplung eine außerordentlich reine und effektive modulare Methode zur Synthese hochmolekularer NBRs darstellt. Die Arbeit umfasst außerdem die detaillierte chromatographische Untersuchung der NBR Mikrostrukturen sowie die Bestimmung der Mark-Houwink-Kuhn-Sakurada-Parameter von Nitrilkautschuken azeotroper Zusammensetzung.



## Abstract

Despite the industrial importance of nitrile-butadiene rubber (NBR) and the high attention orthogonal ligation techniques have received for the construction of complex macromolecular architectures, the application of modular ligation strategies for the design of complex NBRs has not been addressed in polymer science. Herein, the synthesis of novel acrylonitrile-butadiene copolymer architectures via modular ligation techniques is reported. NBR building blocks were obtained via the reversible addition-fragmentation chain transfer polymerization in solution employing several novel trithiocarbonate chain transfer agents. The copper mediated azide-alkyne cycloaddition proved to be an efficient method for the synthesis of linear and crosslinked high molecular weight NBR architectures. The hetero-Diels-Alder cyclization of cyclopentadienes with the electron-deficient thiocarbonyl moieties of pyridinyl dithioesters was exploited for the synthesis of NBR-*b*-poly(styrene-*co*-acrylonitrile) block and 4-miktoarm star copolymer architectures. In the context of the block copolymer formation, comparison of simulation and experimental data uncovered the limitations and advantages of reversible-deactivation polymerization techniques for the construction of macromolecular architectures. In addition, the nitrile imine mediated tetrazole-ene coupling was shown to be an extraordinarily pure and efficient example of a modular ligation technique for the synthesis of high molecular weight NBR. The thesis is completed by a detailed investigation of the polymer microstructure and the determination of the Mark-Houwink-Kuhn-Sakurada parameters of NBR by chromatographic means.



## Publications Arising from the Thesis

- (5) *Photo-Induced Ligation of Acrylonitrile-Butadiene Rubber: Selective Tetrazole-Ene Coupling of Chain-End Functionalized Copolymers of 1,3-Butadiene*  
Dürr, C. J.; Lederhose, P.; Hlalele, L.; Abt, D.; Kaiser, A.; Brandau, S.; Barner-Kowollik, C. *Macromolecules* **2013**, *46*, 5915-5923.
- (4) *Determining the Mark-Houwink Parameters of Nitrile Rubber: A Chromatographic Investigation of the NBR Microstructure*  
Dürr, C. J.; Hlalele, L.; Schneider-Baumann, M.; Kaiser, A.; Brandau, S.; Barner-Kowollik, C. *Polym. Chem.* **2013**, *4*, 4755-4767.
- (3) *Mild and Efficient Modular Synthesis of Poly(acrylonitrile-co-butadiene) Block and Miktoarm Star Copolymer Architectures*  
Dürr, C. J.; Hlalele, L.; Kaiser, A.; Brandau, S.; Barner-Kowollik, C. *Macromolecules* **2013**, *46*, 49-62.
- (2) *High Molecular Weight Acrylonitrile-Butadiene Architectures via a Combination of RAFT Polymerization and Orthogonal Copper Mediated Azide-Alkyne Cycloaddition*  
Dürr, C. J.; Emmerling, S. G. J.; Lederhose, P.; Kaiser, A.; Brandau, S.; Klimpel, M.; Barner-Kowollik, C. *Polym. Chem.* **2012**, *3*, 1048-1060.
- (1) *A Detailed Investigation of the Experimental Conditions for the Reversible Addition Fragmentation Chain Transfer-Mediated Copolymerization of Acrylonitrile and Butadiene*  
Dürr, C. J.; Emmerling, S. G. J.; Kaiser, A.; Brandau, S.; Habicht, A. K. T.; Klimpel, M.; Barner-Kowollik, C. *J. Polym. Sci. – Polym. Chem.* **2012**, *50*, 174-180.



# Contents

<b>1. Introduction</b> .....	<b>1</b>
1.1 Motivation .....	1
1.2 Thesis Overview.....	3
1.3 References.....	6
<b>2. Theory and Background</b> .....	<b>7</b>
2.1 Conventional Free Radical Polymerization .....	7
2.2 Reversible-Deactivation Radical Polymerization .....	8
2.2.1 Reversible Addition–Fragmentation Chain Transfer Polymerization	10
2.2.2 Nitroxide Mediated Polymerization .....	14
2.2.3 Atom Transfer Radical Polymerization .....	15
2.3 Modular Ligation Strategies .....	16
2.3.1 Macromolecular Architectures .....	16
2.3.2 The Concept of “Click” Chemistry .....	19
2.3.3 Azide-Alkyne Cycloaddition.....	21
2.3.4 Diels–Alder Cyclization.....	25
2.3.5 Hetero-Diels–Alder Cyclization .....	26
2.3.6 Nitrile Imine Mediated Tetrazole-Ene Coupling.....	28
2.3.7 Other Modular Ligation Techniques.....	30
2.4 Nitrile-Butadiene Rubber.....	31
2.4.1 Synthesis and Applications .....	31
2.4.2 Recent Advances in the Controlled Synthesis of NBR.....	33

---

2.5	References.....	37
<b>3.</b>	<b>High Molecular Weight Acrylonitrile-Butadiene Architectures via a Combination of RAFT Polymerization and Orthogonal Copper Mediated Azide-Alkyne Cycloaddition .....</b>	<b>49</b>
3.1	Introduction.....	49
3.2	Experimental Section.....	51
3.2.1	Materials.....	51
3.2.2	Synthesis of the Alkyne-Functional RAFT Agent Prop-2-yn-1-yl 2-(((dodecylsulfanyl)carbonothioyl)-sulfanyl)propanoate ( <b>2</b> ) .....	52
3.2.3	Synthesis of TMS Protected Alkyne-Functional RAFT Agent ( <b>2-TMS</b> ).....	52
3.2.4	Synthesis of Bis-Triazole Model Compound <b>6</b> .....	53
3.2.5	Synthesis of Acrylonitrile-Butadiene Copolymers with Terminal Alkyne Functionality ( <b>3</b> ).....	53
3.2.6	Synthesis of Acrylonitrile-Butadiene-Prop-2-ynyl Methacrylate Terpolymer <b>7</b> .....	54
3.2.7	Typical Procedure for the Coupling of NBR Building Blocks.....	55
3.2.8	Modification of Acrylonitrile-Butadiene-Prop-2-ynyl Methacrylate Terpolymers with 1-Undecane azide.....	55
3.2.9	General Procedure for the Copper Mediated Crosslinking of Terpolymer <b>7</b> .....	55
3.2.10	Instrumentation.....	55
3.3	Results and Discussion.....	56
3.3.1	RAFT Agent Synthesis .....	56
3.3.2	RAFT Polymerizations.....	58
3.3.3	Conjugation of NBR Building Blocks.....	64
3.3.4	Detection of the Triazole Moiety.....	69

---

3.3.5	Side-Chain Modification of NBR via CuAAC .....	71
3.3.6	Crosslinking.....	75
3.4	Conclusions.....	77
3.5	Appendix.....	78
3.6	References.....	85
<b>4.</b>	<b>Mild and Efficient Modular Synthesis of Poly(acrylonitrile-<i>co</i>-butadiene) Block and Miktoarm Star Copolymer Architectures.....</b>	<b>89</b>
4.1	Introduction .....	89
4.2	Experimental Section.....	90
4.2.1	Materials.....	90
4.2.2	Synthesis of <sup>t</sup> Br RAFT Agent ( <b>1</b> ).....	91
4.2.3	Synthesis of Midfunctionalized <sup>t</sup> Br RAFT Agent ( <b>11</b> ).....	92
4.2.4	Synthesis of Diene-Functional Chain Transfer Agent Hexa-2,4-dien-1-yl 2-((dodecylthio)carbonothioylthio)propanoate ( <b>2</b> ). .....	93
4.2.5	Synthesis of Cp-Functional RAFT Agent.....	94
4.2.6	Experimental Determination of the Benzylthiodihydrothiopyranylpyridine Structure <b>3+BD</b> Responsible for the Loss of Control in AN/BD Copolymerizations Utilizing Controlling Agent <b>3</b> .....	94
4.2.7	Polymerizations.....	95
4.2.8	Cp-Functionalization of NBRs .....	96
4.2.9	Hetero-Diels–Alder Reactions.....	96
4.2.10	PREDICI Simulations.....	96
4.2.11	SEC Deconvolution .....	99
4.2.12	Instrumentation .....	99
4.3	Results and Discussion.....	100
4.3.1	RAFT Polymerizations .....	100

---

4.3.2	Synthesis of Cp-Functional NBRs .....	109
4.3.3	Block Copolymer Formation .....	112
4.3.4	Miktoarm Star Copolymers .....	117
4.3.5	Theoretical Aspects and Simulations .....	127
4.4	Conclusions .....	136
4.5	Appendix .....	137
4.6	References .....	142
<b>5.</b>	<b>Photo-Induced Ligation of Acrylonitrile-Butadiene Rubber: Selective Tetrazole-Ene Coupling of Chain-End Functionalized Copolymers of 1,3-Butadiene .....</b>	<b>147</b>
5.1	Introduction .....	147
5.2	Experimental Section .....	149
5.2.1	Materials .....	149
5.2.2	Synthesis of Tetrazole-Functional RAFT Agent <b>3</b> .....	150
5.2.3	Synthesis of Ethyl-Functionalized RAFT Agent <b>8</b> .....	151
5.2.4	Coupling of Tetrazole-Functionalized NBR via NITEC .....	152
5.2.5	Polymerizations .....	152
5.2.6	DFT Calculations .....	152
5.2.7	Instrumentation .....	152
5.3	Results and Discussion .....	153
5.4	Conclusion .....	170
5.5	Appendix .....	171
5.6	References .....	174
<b>6.</b>	<b>Determining the Mark-Houwink Parameters of Nitrile Rubber: A Chromatographic Investigation of the NBR Microstructure .....</b>	<b>179</b>
6.1	Introduction .....	179

---

6.2	Experimental Section.....	181
6.2.1	Materials.....	181
6.2.2	Polymerizations.....	182
6.2.3	NMR Measurements.....	182
6.2.4	Size Exclusion Chromatography and Data Evaluation.....	182
6.3	Results and Discussion.....	184
6.3.1	Experimental Determination of the NBR Microstructure .....	188
6.3.2	Can a Unique Set of MHKS Parameters be Obtained for NBR? .....	201
6.4	Conclusions.....	209
6.5	Appendix.....	211
6.6	References.....	222
<b>7.</b>	<b>Concluding Remarks and Outlook .....</b>	<b>227</b>
	<b>List of Abbreviations .....</b>	<b>231</b>
	<b>Curriculum Vitae .....</b>	<b>235</b>
	Education.....	235
	Employment History.....	235
	<b>List of Publications and Conference Contributions.....</b>	<b>237</b>
	Refereed Journal Publications.....	237
	Patents.....	239
	Conference Contributions.....	239
	<b>Acknowledgement – Danksagung.....</b>	<b>241</b>

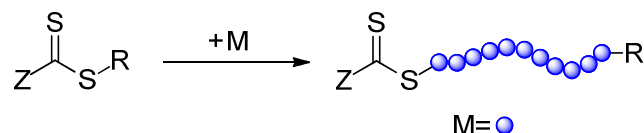


# 1 ■ Introduction

## 1.1 Motivation

Nitrile-butadiene rubbers (NBRs) are technically important synthetic elastomers. Due to their high resistance to aggressive environmental surroundings and their temperature stability in a wide range between  $-40$  and  $+125$  °C,<sup>1</sup> NBRs find applications in the automotive and aeronautical industries. On an industrial scale, to date NBR is solely produced in an emulsion polymerization process in a capacity of several hundreds of thousand tons per year. Two major drawbacks are associated with the emulsion process: Firstly, control over the degree of polymerization can be achieved over a limited range of molar mass only. Secondly, polymers obtained in an emulsion process mainly exhibit branched or crosslinked structures, typically displaying a broad molecular weight distribution with dispersities above 2. However, for specialty applications, fine control over molar mass and molecular architecture is highly desirable to allow for the access of sophisticated polymeric materials.

Recently, Barner-Kowollik and coworkers in collaboration with Lanxess Deutschland GmbH have introduced a reversible-deactivation polymerization technique for the synthesis of NBR.<sup>2</sup> In contrast to the large-scale aqueous emulsion polymerization system, the novel method allows for the copolymerization of acrylonitrile (AN) and 1,3-butadiene (BD) in organic solution and provides nitrile rubber with narrow molecular weight distributions and molar mass control. Control over molar mass was achieved via the reversible addition-fragmentation chain transfer (RAFT) mediated polymerization process<sup>3</sup> by employing trithiocarbonate or dithioester chain transfer agents.



**Scheme 1.1.** Synthesis of chain-end functionalized polymers via the RAFT technique. When monomer (M) incorporation occurs, the R- and the Z-group of the RAFT agent are relocated at the  $\alpha$ - and  $\omega$ -chain-end of the RAFT polymer, respectively.

In addition to the control over molar mass and molecular weight distribution, the RAFT technique offers a further powerful tool for the synthesis of sophisticated polymeric materials. As a result of the mechanism controlling the radical polymerization, chain-end functionalized polymers are obtained. As schematically depicted in Scheme 1.1, monomers are incorporated into the controlling agent leading to the formation of  $\alpha,\omega$ -functionalized polymers. When orthogonal to the polymerization, the RAFT R- and Z-group moieties are located at the polymer chain-end and remain unaffected in their chemical structures.

Alternative reversible-deactivation polymerization techniques, such as nitroxide mediated polymerization (NMP) or atom transfer radical copolymerization (ATRP) allow for the synthesis of chain-end functionalized polymers, too, however, the control over polymerizations is achieved via a fundamentally different conceptual approach.<sup>4</sup> One of the main advantages of the RAFT process over other reversible-deactivation polymerization techniques is the constant and high radical concentration, allowing the polymerization to proceed at polymerization rates similar to those observed in conventional free radical copolymerization. The high radical concentration is an outstanding superiority of the RAFT process when targeting industrial applications, since it provides high conversion-over-time ratios, important for the economical large-scale synthesis.

The scope of the current work is to harness the accessibility of chain-end functionalized NBRs for the modular construction of advanced polymer architectures. These architectures include block and miktoarm star copolymers and the synthesis of linear high molecular weight NBR by coupling linear NBR precursor blocks upon addition of small organic linker molecules. Block and star copolymers often provide material properties superior to those of polymer blends of the respective polymer building blocks. In the last decade, significant efforts

have been devoted to the development of efficient modular ligation strategies in polymer science. These strategies mainly comprise cycloaddition reactions such as the (hetero-)Diels–Alder coupling or 1,3-dipolar addition. However, the transfer of the established techniques to the orthogonal conjugation of nitrile-rubber entities is challenging. One of the main obstacles is the high density of functional moieties among the NBR backbone potentially interfering with the coupling techniques.

## 1.2 Thesis Overview

A focus of the work presented in the current thesis is directed toward the application of orthogonal ligation protocols on the construction of complex macromolecular architectures of nitrile rubber. The content of the thesis is graphically illustrated in Figure 1.1. The investigated modular construction routes for the synthesis of complex macromolecular architectures of NBR are summarized in the following:

- The synthesis of linear high molecular weight acrylonitrile-butadiene architectures via the copper mediated azide-alkyne cycloaddition of alkyne-functionalized NBR building blocks is presented (chapter 3). The study is extended to the construction of covalently crosslinked networks, allowing for the control of the extent of crosslinking.
- The synthesis of (acrylonitrile-*co*-butadiene)-*b*-(styrene-*co*-acrylonitrile) block copolymer and miktoarm star copolymer architectures via the hetero-Diels–Alder reaction of cyclopentadiene-functionalized NBR building blocks is described (chapter 4). The study is underpinned by simulations of the polymerizations for assessing the density of chain-end functionality, quantifying the limitations of reversible-deactivation protocols for the modular construction of macromolecular architectures of NBR.
- The photo-induced ligation of chain-end functionalized NBR to obtain polymers of high molecular weight via the nitrile imine mediated tetrazole-ene coupling reaction is described (chapter 5). An appropriate choice of the linking agent and the aryl substituents of the tetrazole-functionalized chain

transfer agent allowed for a selective conjugation orthogonal to reactive moieties of the NBR backbone.

The application of modular ligation strategies, either for polymer-polymer coupling reactions or the coupling of small organic molecules to polymeric substrates requires the knowledge of the actual molar masses of polymer precursors.<sup>5</sup> Molecular weight determination of polymers is commonly performed on size exclusion chromatography (SEC) instruments with concentration sensitive on-line detectors. SEC with concentration sensitive detectors is a relative method;

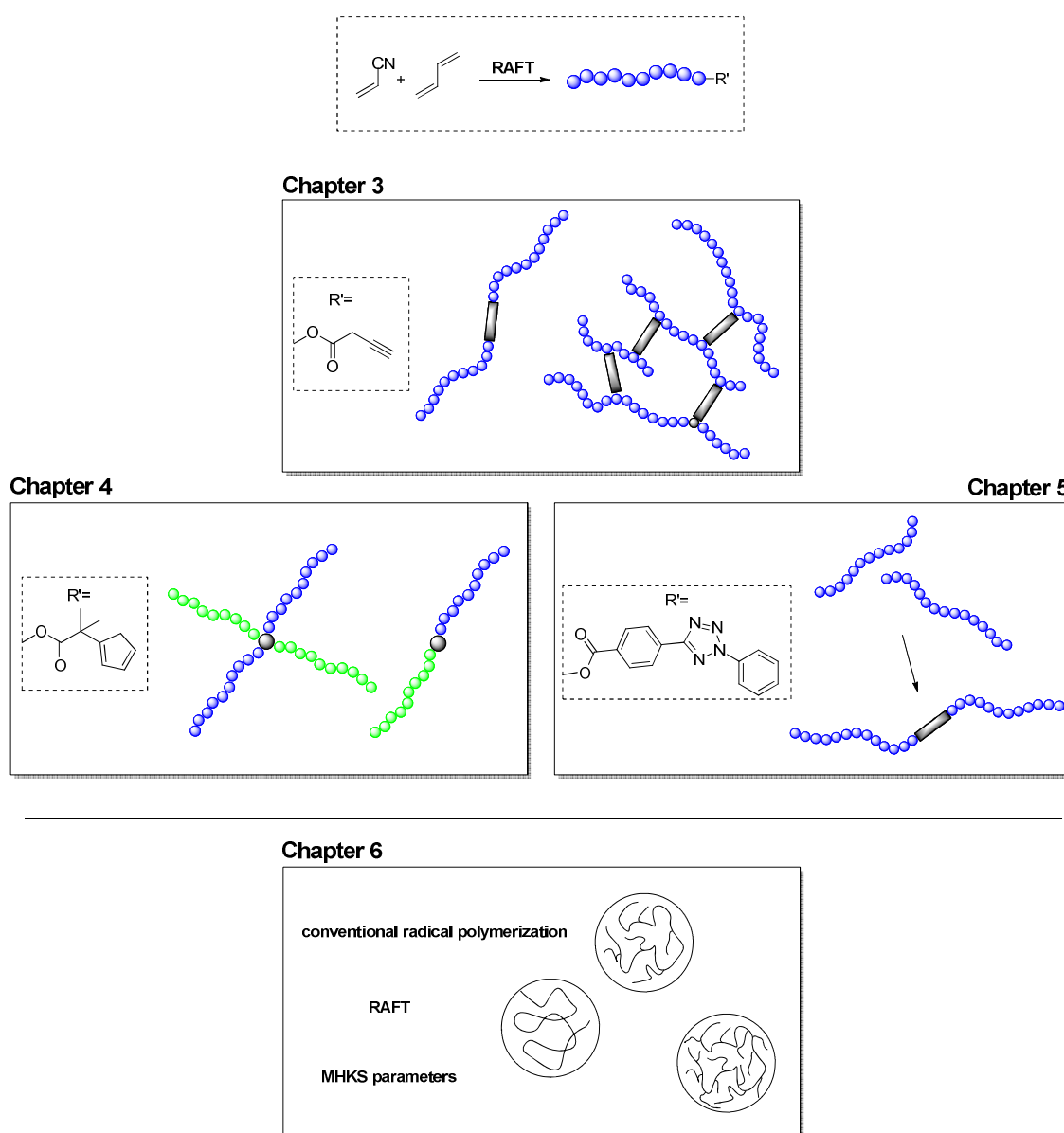


**Figure 1.1.** Overview of the projects presented in the current thesis.

the instruments are calibrated with narrowly dispersed standards. Therein, the molar masses of polymers are obtained either as values relative to the polymer type employed in the SEC calibration, or – when Mark–Houwink–Kuhn–Sakurada (MHKS) parameters are accessible – more accurate via the universal calibration principle.<sup>6</sup> In academia and industry to date molar masses of NBR are obtained as polystyrene relative values only. In contrast to most other technically important polymers, the MHKS parameters necessary for the evaluation of SEC data via universal calibration have not been determined. In chapter 6, the lack of the MHKS parameters of NBR is addressed in a detailed investigation of nitrile rubber samples via SEC with on-line mass sensitive detection (triple SEC). The investigations include:

- The detailed description of the NBR microstructure by chromatographic means. Insights are obtained by comparing data of on-line viscometry and on-line multi-angle laser light scattering as a function of retention time.
- The determination of the MHKS parameters of NBR by establishing the Mark–Houwink relation for a collection of NBR samples ranging over a broad region of molar mass.
- A plausibility check of molar mass data obtained by re-evaluating polystyrene relative SEC data (taken from chapter 3) via universal calibration employing the MHKS parameters determined herein.

Since MHKS parameters of NBR were not accessible at the time the experiments and sample evaluation of the investigations presented in chapter 3 and 4 were performed, molar masses are given as values relative to polystyrene standards. In contrast, molar masses provided in chapter 5 are accurate molar masses obtained via universal calibration with the MHKS parameters of NBR.

Given the high importance of nitrile rubber in industrial applications and the vast scale of production thereof, it is surprising that – to the best of our knowledge – to date no academic interest has been devoted to the synthesis of advanced macromolecular architectures of NBR. The lack of established procedures is addressed in the current thesis opening up a wide field for future applications of sophisticated NBR materials.

### 1.3 References

1. International Institute of Synthetic Rubber Producers. <http://iisrp.com/synthetic-rubber.html>.
2. Kaiser, A.; Brandau, S.; Klimpel, M.; Barner-Kowollik, C. *Macromol. Rapid Commun.* **2010**, *31*, 1616-1621.
3. Moad, G.; Rizzardo, E.; Thang, S. H. *Aust. J. Chem.* **2005**, *58*, 379-410.
4. *Handbook of RAFT Polymerization*. Barner-Kowollik, C., Ed.; Wiley-VCH: Weinheim, 2009.
5. Guillaneuf, Y.; Castignolles, P. *J. Polym. Sci. Part A: Polym. Chem.* **2008**, *46*, 897-911.
6. Grubisic, Z.; Rempp, P.; Benoit, H. *J. Polym. Sci. Part B: Polym. Lett.* **1967**, *5*, 753-759.

# 2 ■ Theory and Background

## 2.1 Conventional Free Radical Polymerization

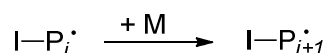
Polymers play a fundamental role in modern society and a life without the countless polymer-based articles of daily use is almost impossible to imagine. A high share of the commodity polymers such as polystyrene or low-density polyethylene is commercially synthesized in free radical polymerization processes. Per year, around 100 million tons of polymer are produced by free radical polymerization processes worldwide.<sup>1</sup>

Since the last century, free radical polymerization has attracted a substantial amount of interest and various methods were invented to perform polymerizations in homogeneous systems such as bulk and solution or in heterogeneous media, *i.e.* suspension, emulsion<sup>2</sup> and the associated processes such as mini- and microemulsion polymerization.<sup>3-4</sup> Free radical polymerization reactions proceed via four individual reaction steps, illustrated in Scheme 2.1. During initiation a nonradical initiator generates radical species, triggered by physical or chemical stimuli. The radicals react with the unsaturated monomers forming the propagating radical species. Over the lifetime of the radical ( $\sim 1$  s), these species add monomer units and a polymer chain is obtained.<sup>5</sup> As a result of the high propensity of radicals to undergo stabilization, radical termination reactions are observed. Termination either occurs via the recombination of two propagating polymer chains or via radical transfer reactions such as the transfer to monomer or disproportionation. In the latter, a saturated ( $I-P_m^{\text{sat}}$ ) and an unsaturated polymer chain ( $I-P_n^{\cdot}$ ) are formed simultaneously. To obtain polymers

*Initiation*

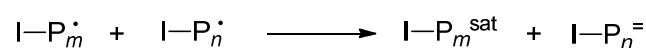


*Propagation*

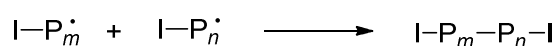


*Termination*

*Disproportionation*



*Recombination*



**Scheme 2.1.** Mechanism of free radical polymerization.

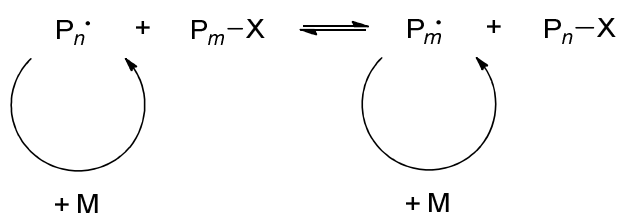
of adequate chain-length, radical concentrations need to be kept low and are typically in the range of ppm.<sup>6</sup> One of the main advantages of free radical polymerization over other polymerization techniques is the high tolerance toward functional moieties and the low susceptibility to impurities, allowing for the polymerization of a broad variety of monomers. Nevertheless, control over the polymerization to obtain narrow dispersed and/or chain-end functionalized polymers as accessible in anionic polymerization<sup>7</sup> cannot be achieved. To combine the outstanding versatility of conventional free radical polymerization with the advantages of molecular weight control and chain-end manipulation, several sophisticated methods of radical polymerization have been introduced. The following paragraphs are devoted to the description of the fundamental aspects of these advanced radical polymerization techniques.

## 2.2 Reversible-Deactivation Radical Polymerization

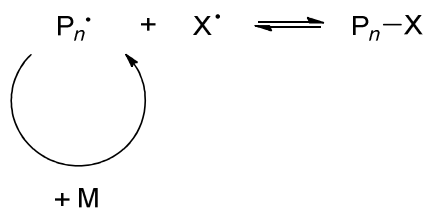
In the recent decades, radical polymerization processes have been developed that allow control over molecular weight and molecular weight distributions, imparting many of the characteristics observed in living anionic polymerization protocols.<sup>7</sup> A central feature of all these reversible-deactivation radical polymerization techniques is a dynamic equilibrium between growing radical chains and dormant

species.<sup>8</sup> The growing radical chains either undergo degenerative chain transfer, depicted in Scheme 2.2, or are reversibly terminated as illustrated in Scheme 2.3, while control over the polymerization is achieved by the persistent radical effect.<sup>9</sup> In contrast to conventional free radical polymerization, where essentially all polymer chains except the ppm amounts of propagating radicals are “dead” polymer chains, in reversible-deactivation radical polymerization the fractions of the dead polymer chains are typically in the range of 1-10 mol%.<sup>1,8</sup>

The reversible addition–fragmentation chain transfer (RAFT) polymerization has been studied in detail within the work presented in the thesis at hand and background information on RAFT thus will be given in the current chapter. Moreover, nitroxide mediated radical polymerization (NMP)<sup>10-11</sup> and atom transfer radical polymerization (ATRP)<sup>1,12</sup> are two other prominent examples of reversible-deactivation strategies that will be described. Other reversible-deactivation radical polymerization methods exist, *e.g.* iodine mediated polymerization<sup>13</sup> – a method based on degenerative chain transfer – or cobalt mediated radical polymerization<sup>14</sup> – in part relying on the persistent radical effect – yet are beyond the scope of the thesis and will not be described in detail. Note that the utilization of the commonly used term “controlled/living” radical polymerization is discouraged by the Subcommittee on Polymer Terminology of the International



**Scheme 2.2.** General mechanism of degenerative chain transfer.

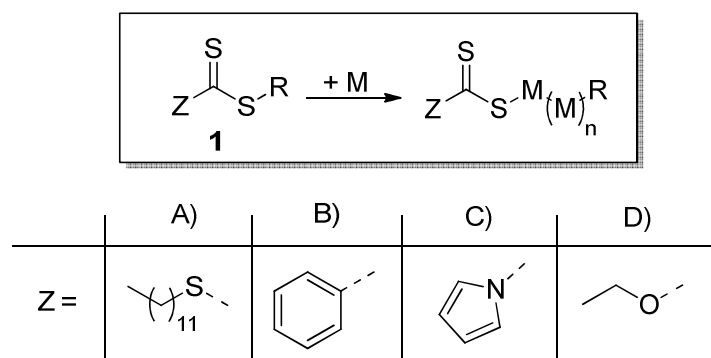


**Scheme 2.3.** General mechanism of reversible chain deactivation.

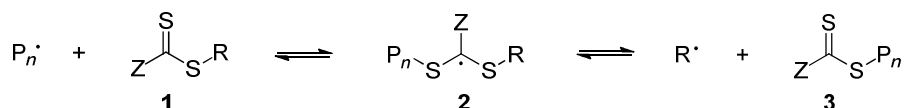
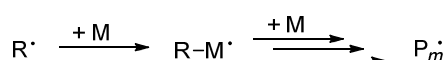
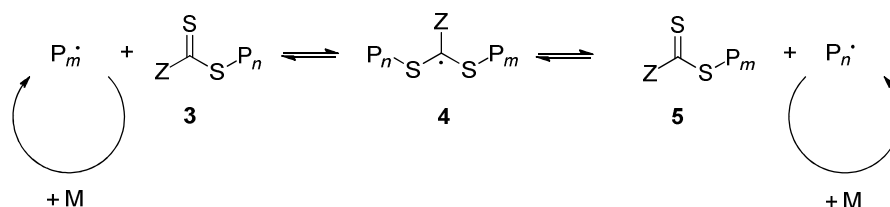
Union of Pure and Applied Chemistry's Polymer Division and should be substituted by the term "reversible-deactivation radical polymerization".<sup>15</sup>

### 2.2.1 Reversible Addition–Fragmentation Chain Transfer Polymerization

Since its invention in 1998 in the laboratories of the Australian Commonwealth Scientific and Industrial Research Organization (CSIRO),<sup>16</sup> the RAFT process has attracted high interest in polymer science. The versatility of the RAFT process is documented by a total of more than 4000 articles published between 1998 and 2012,<sup>17</sup> and a continuous interest can be expected.<sup>18</sup> The crucial characteristic of the RAFT process is the presence of a transfer agent **1**, able to capture growing radical chains and to transfer the radical to a second polymer chain. During RAFT polymerization, the R- and Z-group moieties of the transfer agent **1** are sustained to give functionalized polymers with the R- and Z-group moieties at the  $\alpha$ - and  $\omega$ -chain-end, respectively (Figure 2.1). RAFT polymerizations have been shown to proceed in bulk, homogenous solution and heterogeneous media.<sup>19-21</sup> The underlying chemical structure of all RAFT agents is the thiocarbonylthio moiety, allowing the release of a carbon centered radical species after a radical addition. The three typical classes of controlling agents are trithiocarbonates, dithioesters and dithiocarbamates, depicted in Figure 2.1A-C. Reversible-deactivation radical polymerization with xanthates is widely termed "macromolecular design by interchange of xanthates" (MADIX), albeit identical to the RAFT process with the



**Figure 2.1.** Examples of typical Z-group moieties of the different types of thiocarbonylthio compounds employed as controlling agents in RAFT mediated polymerizations and the MADIX technique. A) Trithiocarbonates, B) dithioesters, C) dithiocarbamates and D) xanthates. During polymerization, monomers M (formally) incorporate in between the R-group and the thiocarbonylthio moiety.

*Initiation**Reversible Chain Transfer**Reinitiation**Chain Equilibration**Termination***Scheme 2.4.** Mechanism of the RAFT process.<sup>22</sup>

only difference being the chemical nature of the employed controlling agent (Figure 2.1D).<sup>23</sup> Almost simultaneously with the RAFT mechanism the MADIX technique was invented by a group of researchers in France independent from the findings of CSIRO.<sup>24</sup>

The RAFT polymerization process relies on a degenerative chain transfer mechanism and can be divided into five individual reaction steps as illustrated in Scheme 2.4. The initiation is equivalent to the initiation in conventional free radical polymerization. The initiator radicals are formed by the fragmentation of a nonradical initiator that can be chosen from initiators commonly employed in conventional radical polymerizations. Caution is required when the initiation strategies might interfere with the RAFT agent, *e.g.* for oxidizing agents such as peroxides,<sup>25</sup> yet examples of peroxide initiated RAFT polymerizations exist.<sup>26</sup> The initiator fragments react with the monomers forming a macroradical,  $\text{P}_n^\cdot$ . At the

early stages of the polymerization the macroradical adds to the controlling agent **1**, forming the intermediate radical **2**. Radical **2** now either undergoes back reaction to the starting materials  $P_n^\bullet$  and **1**, or  $\beta$ -scission releasing the R-group radical  $R^\bullet$ . After release, the latter can add monomers in a radical addition reaction, the so-called reinitiation step, forming a macroradical  $P_m^\bullet$ . The step essential for molecular weight control in RAFT polymerization is the chain equilibration. The growing radical chains  $P_m^\bullet$  and  $P_n^\bullet$  are in equilibrium with dormant macroRAFT species **5** and **3**, respectively. While  $P_m^\bullet$  is in its propagating state,  $P_n^\bullet$  is in its dormant form **3**. Chain transfer of  $P_m^\bullet$  with the latter converts  $P_m^\bullet$  into its dormant form **5** via the intermediate radical **4**.  $P_n^\bullet$  is released and propagates by the radical addition of monomers. The rapid addition of the macroradicals to the dormant species and the fast successive fragmentation of the intermediate radicals provide all chains with an equal probability to grow and thus lead to an equilibration of the degree of polymerization giving narrow molecular weight distributions. In comparison to conventional radical polymerization the overall radical concentration is not significantly reduced by the presence of the RAFT agent. Since the intermediate radical **4** exhibits a fast fragmentation, each silencing of a propagating macroradical via the addition to a dormant species evokes the formation of another radical species able to further propagate with the monomers. As a result of the high radical concentration, the termination occurs in analogy to conventional free radical polymerization by termination events such as recombination or disproportionation. In return, the loss of radical species by termination events requires the steady formation of radical species from a radical source throughout the entire polymerization.

The constant and high radical concentration is an important advantage of the RAFT process over radical polymerization techniques where the control over molecular weights is achieved via the reversible chain termination (*vide infra*). The high radical concentration allows a high conversion-to-time ratio crucial for industrial applications. As noted above, in RAFT polymerization the polymerization rates are theoretically expected to be unaffected by the presence of the transfer agent. Nevertheless, rate retardation is observed especially when dithiobenzoates are employed as chain transfer agents.<sup>27</sup> However, the underlying

mechanisms for rate retardation are still under debate,<sup>28</sup> and might be related to the irreversible reaction of intermediate radicals **4** with propagating radical species,<sup>29-30</sup> or a high stability of the intermediate radical itself.<sup>31-32</sup>

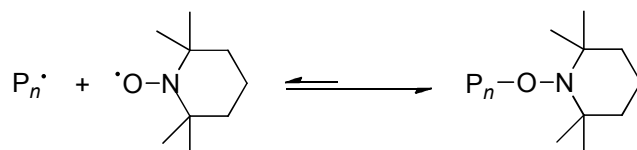
An appropriate choice of the transfer agent in RAFT mediated polymerization is crucial for an effective polymerization control. The RAFT R- and Z-group moieties have to be chosen in a way that the stability of the intermediate radicals **2** and **4** allow for a rapid fragmentation without the occurrence of side reactions. To obtain RAFT polymers with a high density of  $\alpha,\omega$ -functionalization, the intermediate radical **2** needs to fragment in favor of the R-group radical R $\cdot$ , in turn required to be capable of reinitiating the polymerization.<sup>33</sup> The type of monomer employed in RAFT polymerization is an important factor for the design of the RAFT agent. The R-group radical R $\cdot$  has to be a good leaving group for the homolytic S-C bond dissociation relative to the dissociation ability of the propagating macroradical. However, if stability of R $\cdot$  is too high, reinitiation of the polymerization will be slow or – in cases of very high stability – not be observed. Especially in polymerizations of methyl methacrylate (MMA) where the propagating polymer chains are tertiary radical species, RAFT agents providing primary or secondary R-group radicals are widely inefficient in controlling the polymerizations.<sup>22</sup> A simple choice of the R-group moiety based on the structure of the growing radicals will, however, not be sufficient, since penultimate effects influence the behavior of the macroradicals.<sup>34</sup> The Z-group moiety strongly influences the radical addition behavior of the macroradicals to the RAFT and the macroRAFT agent and controls the ability of the intermediate radical to release the R-group radicals R $\cdot$  and the macroradicals by electronic and steric effects, respectively.<sup>35</sup> The behavior of the RAFT agents can be predicted by low-level molecular orbital calculations<sup>33,35-36</sup> or high-level *ab initio* calculations.<sup>32,37-38</sup> However, as suggested by Moad *et al.* in principle two RAFT agents – a tertiary cyanoalkyl trithiocarbonate and a cyanoalkane xanthate should allow to perform polymerizations with the majority of commodity and specialty monomers.<sup>22</sup> While radical polymerization in principle provides good stereoselectivity, regioselectivity is rather low. Nevertheless, approaches to control tacticity in RAFT polymerization have been presented.<sup>39</sup>

Exhaustive summaries of RAFT mediated polymerization systems investigated from the early beginnings in 1998 to 2012 can be found in the literature.<sup>17,22,40-41</sup>

### 2.2.2 Nitroxide Mediated Polymerization

Nitroxide mediated polymerization (NMP) is a further prominent method of reversible-deactivation radical polymerization. NMP was first reported in 1986 in a patent and invented in the laboratories of CSIRO before the emergence of RAFT polymerization.<sup>10</sup> In contrast to RAFT, control in NMP relies on a reversible chain termination mechanism,<sup>42</sup> illustrated in Scheme 2.5. The propagating radicals  $P_n^\bullet$  are reversibly deactivated in a dynamic equilibrium with dormant alkoxyamines. The reduction of the radical concentration via alkoxyamine formation decelerates bimolecular termination reactions. Under steady state conditions, *i.e.* a constant concentration of radical species, the rate of bimolecular termination is a second order reaction with respect to the radical concentration. In contrast, polymerization adheres to a first order law, thus the influence of the decrease in radical concentration on the polymerization rate is one order of magnitude lower. The deceleration of termination relative to propagation is the underlying principle inducing living characteristics in NMP.<sup>43</sup> Termination is observed for the propagating radical species only. The mediating nitroxides do not undergo termination and thus accumulate in the polymerization system. The phenomenon is known as the persistent radical effect and enhances the efficiency of the persistent radicals to reversibly trap the propagating species.<sup>9</sup>

First reports in the scientific literature employ 2,2,6,6-tetramethylpiperidine 1-oxyl (TEMPO) at elevated temperatures for trapping the propagating radicals.<sup>44</sup> In analogy to conventional free radical polymerization, propagation was initiated with thermal initiators such as benzoyl peroxide. Better control over the polymerization is achieved when unimolecular initiators are employed.<sup>45-46</sup> In such

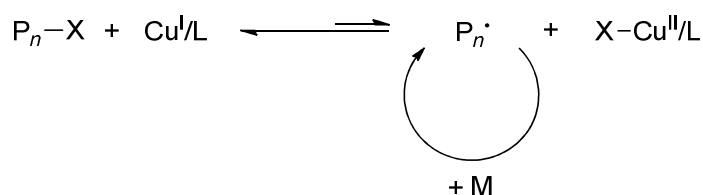


**Scheme 2.5.** Reversible chain deactivation in nitroxide mediated polymerization (NMP).

an approach, an external radical source is not required. The radical species form upon heating from the pre-formed alkoxyamines that initiate the chain growth. NMP was early exploited for the synthesis of homopolymers,<sup>47</sup> random copolymers,<sup>48</sup> block copolymers,<sup>48-49</sup> graft and star polymers.<sup>50</sup> Due to the strong covalent C-O bond of the alkoxyamines formed in the deactivation of the propagating radicals, the controlled polymerization of acrylates and several other monomers employing TEMPO proved to be unsuccessful.<sup>6</sup> For this reason, other nitroxides have been developed by the introduction of  $\alpha$ -substituents increasing the bulkiness of the piperidine 1-oxyl.<sup>51</sup> Nevertheless, it was pointed out that enhanced bulkiness can result in low control as the rate of reversible trapping is reduced.<sup>52</sup>

### 2.2.3 Atom Transfer Radical Polymerization

Redox equilibria of metal complexes provide another interesting basic principle for the reversible-deactivation radical polymerization. In atom transfer radical polymerization (ATRP), redox-active transition metal complexes are employed for the reversible silencing of propagating radical species. The mechanism and the kinetics of ATRP have been investigated intensively.<sup>53-54</sup> The overall concept is depicted in Scheme 2.6. The growing radical chains  $P_n^\bullet$  reversibly react with a (nonradical)  $Cu^{II}/\text{ligand (L)}$  complex transferring a halide ligand X. The dormant alkyl halide  $P_n-X$  is reactivated by reduction with the reducing  $Cu^I/L$  complex. Several other transition metal catalysts have been successfully employed in ATRP including Fe, Ru, Mo and Os.<sup>55</sup> Addition of a radical source as employed in NMP or RAFT polymerization is not required. Propagating radicals are formed *in situ* from small organic alkyl halides – the ATRP initiators – via the atom transfer reaction. Nevertheless, a “reverse” ATRP process has been described, where the mediating



**Scheme 2.6.** Atom transfer radical polymerization (ATRP).

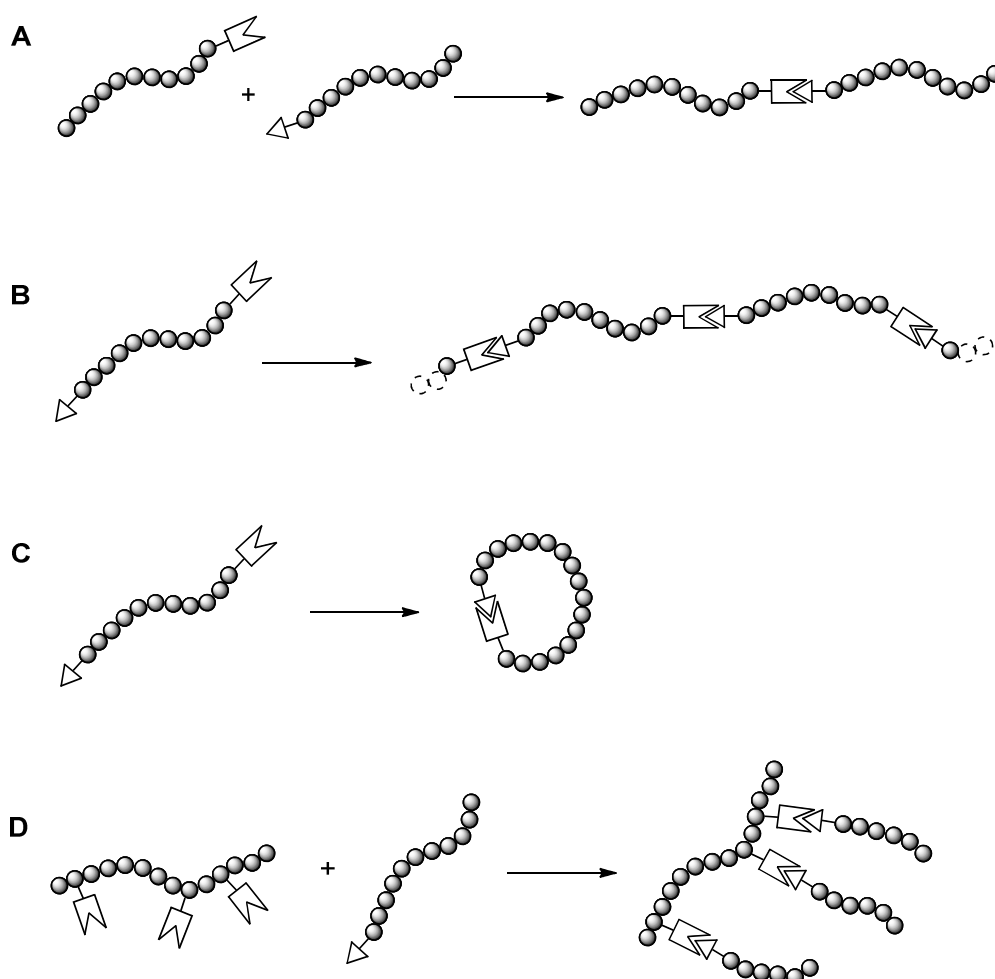
Cu<sup>I</sup> complex is obtained by reduction from its higher oxidation state with a conventional radical initiator, allowing for the utilization of more reactive metal complexes.<sup>56</sup> To overcome problems related to the formation of small amounts of polymer chains initiated with the conventional radical initiator, the latter was later replaced by reducing agents such as metal species in a process named activators generated by electron transfer (AGET) ATRP.<sup>57</sup> The AGET process served as a precursor for a further refined polymerization process termed activators regenerated by electron transfer (ARGET) ATRP. A continuous regeneration of Cu<sup>I</sup> species is ensured by the presence of reducing agents such as ascorbic acid,<sup>58</sup> glucose,<sup>59</sup> or zerovalent metals,<sup>60</sup> to antagonize the accumulation of Cu<sup>II</sup> species via the unavoidable termination of the propagating radical species. Further advances in ATRP include the employment of Cu catalyst concentrations in the region of ppm with a continuous activator regeneration by a source of free radicals of organic nature (initiators for continuous activator regeneration, ICAR ATRP),<sup>61</sup> or electrochemical ATRP.<sup>62</sup> The bromo-telechelic polymers obtained in ATRP have been proven to be versatile precursors for the postpolymerization modification and their application in modular ligation strategies.<sup>63-64</sup> The countless studies performed on ATRP have been summarized in several review articles.<sup>1,6,65</sup>

## 2.3 Modular Ligation Strategies

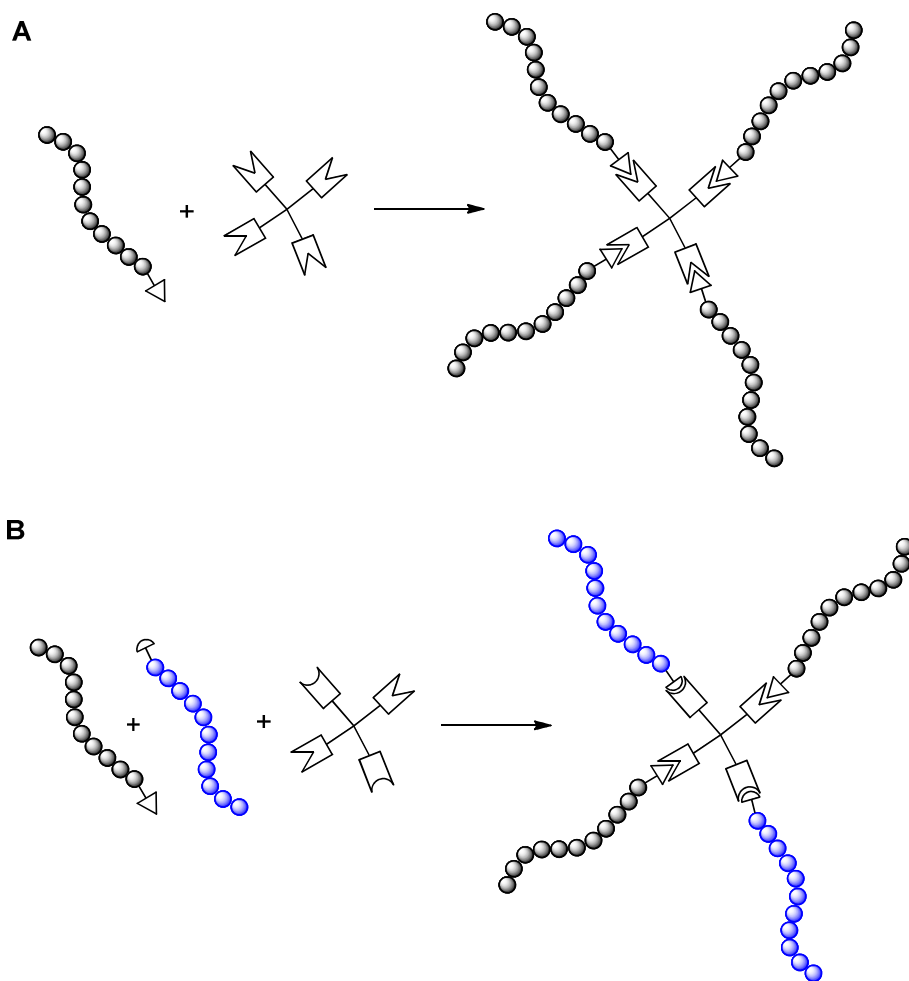
### 2.3.1 Macromolecular Architectures

With the advent of reversible-deactivation radical polymerization and the thereby arising possibilities to obtain polymers with defined chain-end functionality, various modular ligation strategies have been developed and employed in the synthesis of advanced macromolecular architectures.<sup>63,66-67</sup> With respect to modular ligation, chain-end functionalized polymers can be considered as polymeric building blocks allowing for the construction of sophisticated macromolecular structures. Some of these structures, however, could be achieved in sequential polymerization processes. Nevertheless, the essentially endless possibilities to construct polymeric architectures from a single polymer sample are an important advantage of the modular approach.

Several macromolecular architectures that can be obtained in modular ligation reactions are depicted in Scheme 2.7. If two polymer building blocks are functionalized with correlating chemical functionalities, orthogonal ligation allows for the conjugation of the polymers (Scheme 2.7A). The polymer building blocks can be either of similar type, thus providing polymers of high molecular weight, or in case two different polymer types are employed, providing a simple route to access block copolymers. The superiority of the modular construction over a sequential synthesis of block copolymers via chain extension arises from the incompatibility of several monomer types with one another due to kinetic or solubility issues. As described above, RAFT polymerization requires an individual adjustment of the reaction conditions including the structure of the controlling



**Scheme 2.7.** Selected advanced macromolecular architectures that can be obtained in modular ligation strategies.



**Scheme 2.8.** Modular ligation chemistry as an avenue to A) star polymers and B) miktoarm star polymers.

agent on the polymerization performed. Several combinations of monomers cannot be polymerized with a single RAFT agent structure. In contrast, the modular approach allows for the individual choice of the controlling agent and the reaction conditions for the different polymer types before combining the polymers in orthogonal conjugation reactions.

Two different types of polymer topology can be obtained when  $\alpha,\omega$ -functionalized polymer chains with correlating reactive moieties at the two opposite chain-ends are employed in orthogonal ligation reactions. When the conjugation is performed in high concentrations of the polymer building block, linear chains are obtained in a polyaddition type reaction (Scheme 2.7B). In contrast, when the conjugation reactions are performed in high dilution, cyclic polymer structures will be obtained (Scheme 2.7C). Cyclic polymers often exhibit

unique physical properties when compared to their linear analogues.<sup>68</sup> With an appropriate functionalization of polymers along the backbone – either achieved by employing functionalized monomer units or the postpolymerization modification of the polymers – orthogonal ligation allows for the access of comb polymers, depicted in Scheme 2.7D.

The topology strongly influences the physical properties of polymers. Branched architectures show increased densities at their branching points, arising from the compact structure induced by the steric constraints at those positions. A star polymer is a specific type of a branched polymer where linear chains – the individual arms of the star polymer – evolve from a single branching point – termed the core. As depicted in Scheme 2.8A, star polymers are accessible via the orthogonal ligation of chain-end functionalized polymer building blocks to a multifunctional (small molecular) core. The major advantage of the modular ligation route over other approaches as the core first approach where *e.g.* a multifunctional RAFT agent or ATRP initiator is employed, or the arm first approach, where a successive polymerization of a mono- and a bifunctional monomer provides a crosslinked star polymer core, is the high level of control over the length and the number of arms of the targeted star polymers without the occurrence of star-star coupling. If a core structure with more than one type of coupling functionality is employed, modular ligation allows for the facile construction of miktoarm star polymers, illustrated in Scheme 2.8B. In miktoarm star polymers, the different arms consist of two or more different polymer types. For an efficient synthesis of miktoarm star polymers, orthogonality of the two modular ligation techniques employed for the immobilization of the different types of arms is required.

### 2.3.2 The Concept of “Click” Chemistry

The term “modular ligation” describes a collection of reactions allowing for the efficient construction of larger structures from smaller building block units. Chemistry provides an infinitely large toolbox for the construction of such structures. However, only a few reactions fulfill certain requirements of effective linking, defined in the concept of “click” chemistry by Sharpless and coworkers.

There are several criteria a reaction must meet to be categorized as a “click” reaction:<sup>69</sup>

- The reaction must be modular. The reactions need to be orthogonal to other reaction steps involved.
- The reaction has to be wide in scope.
- The reaction needs to give quantitative or almost quantitative yields.
- The reaction should give inoffensive byproducts. To fulfill the criteria of an economic process these byproducts need to be easily separated by purification other than chromatography. Purification methods such as distillation or recrystallization are admissible.
- The reaction needs to be stereospecific. However, an enantioselective character of the reaction is not necessarily required.
- The process should proceed under simple reaction conditions. These conditions include ambient temperature and the insensitivity to oxygen and water.
- The starting materials and reagents need to be readily available.
- If a solvent is required, the solvent needs to be environmentally benign or easily removable.
- Moreover, the product needs to be simply isolated and to be stable under physiological conditions.

Sharpless and coworkers derived their concept from (bio-)chemical processes observed in nature such as the *in vivo* synthesis of proteins and polysaccharides and compared the “click” type reactions metaphorically with reactions being spring-loaded for a single reaction trajectory. From the above mentioned criteria, the authors derived several classes of chemical reactions that might adhere to the “click” criteria. Reactions that display a high thermodynamic driving force of  $20 \text{ kcal}\cdot\text{mol}^{-1}$  and more widely comply with the above mentioned criteria.<sup>70</sup> These reactions include:

- 1,3-dipolar cycloaddition reactions;
- Diels–Alder transformations;

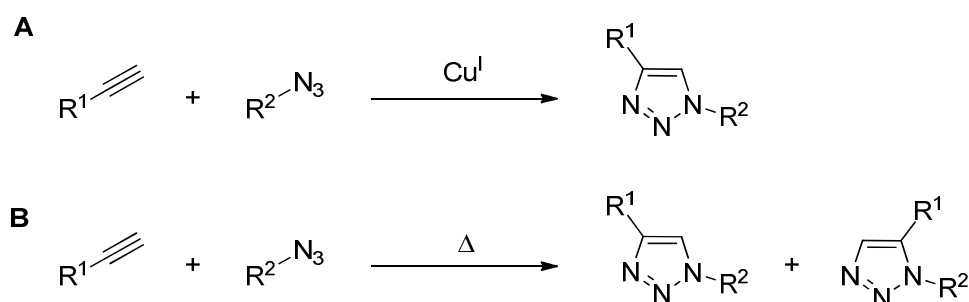
- nucleophilic substitution, especially ring-opening of strained heterocycles, *e.g.* epoxides or aziridines;
- carbonyl chemistry, *e.g.* formation of ureas, thioureas, oxime ethers or amides;
- the addition to multiple carbon-carbon bonds, *e.g.* epoxidation, aziridination or Michael type additions.

Originally intended for the synthesis of metabolites and pharmaceuticals, “click” chemistry has achieved much greater interest in the field of polymer science. Barner-Kowollik *et al.* extended the definition of the “click” concept on polymer coupling and suggested several further criteria that need to be met for efficient polymer-polymer conjugation reactions.<sup>71</sup> In light of Sharpless’ criterion of the simple isolation of the reaction product, polymer-polymer conjugation requires the utilization of equimolar amounts of the polymeric reactands. The criterion of equimolarity arises from the fact that the purification of polymers is difficult and in some cases impossible to achieve. Most importantly, technical approaches such as preparative liquid chromatography cannot be considered as a simple purification method.

Orthogonal ligation techniques have been intensively studied for the construction of advanced macromolecular architectures. In the following paragraphs, several orthogonal ligation reactions – while some of them adhere to “click” criteria – with relevance to the field of polymer science will be presented.

### 2.3.3 Azide-Alkyne Cycloaddition

Within the numerous modular ligation techniques, the Cu<sup>I</sup> mediated 1,3-dipolar cycloaddition of azides and terminal alkynes (CuAAC)<sup>72-73</sup> is among the most powerful methods and has obtained the highest interest in all fields of chemistry.<sup>74-77</sup> The CuAAC is virtually quantitative, robust and insensitive and was shown to adhere to the criteria of “click” reactions.<sup>78</sup> The wide applicability of the CuAAC reaction in biomedical applications derives from the bio-orthogonality of the azides and alkynes,<sup>79</sup> and their high stability under biological conditions.<sup>75</sup> The



**Scheme 2.9.** Regioisomers obtained in the A) copper(I) mediated and B) thermal 1,3-dipolar cycloaddition of azides and alkynes.

CuAAC is a regioselective variant of the 1,3-dipolar Huisgen cycloaddition and solely provides 1,4-substituted 1,2,3-triazoles (Scheme 2.9A). In contrast, the thermally induced 1,3-dipolar Huisgen reaction in the absence of  $\text{Cu}^{\text{I}}$  provides mixtures of 1,4- and 1,5-substituted 1,2,3-triazoles, depicted in Scheme 2.9B. Several catalyst systems have been introduced in recent years. The catalytically active species is a  $\text{Cu}^{\text{I}}$  complex. Generally, a  $\text{Cu}^{\text{I}}$  source and a ligand are employed. It was found that in step-growth click coupling reactions aliphatic ligands provided significant rate enhancements over pyridine based ligands, while tridentate ligands were superior to tetradentate ligands.<sup>80</sup> A typical catalyst system, consisting of  $\text{CuBr}$  and  $N,N,N',N'',N''$ -pentamethyldiethylenetriamine (PMDETA), is provided in Figure 2.2A. A drawback of such catalysts is the affinity of the  $\text{Cu}^{\text{I}}$  species toward oxidation and the therefore required exclusion of oxygen during the coupling process. Sodium ascorbate is known to reduce  $\text{Cu}^{\text{II}}$  species to  $\text{Cu}^{\text{I}}$ ,<sup>81</sup> and thus can be employed in combination with  $\text{CuSO}_4$  as a catalyst system insensitive to air, illustrated in Figure 2.2B. Herein, the  $\text{Cu}^{\text{I}}$  is obtained *in situ* via the reduction of the

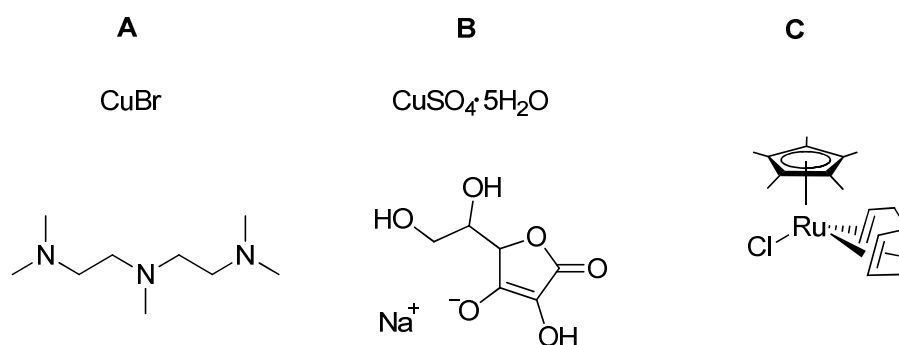
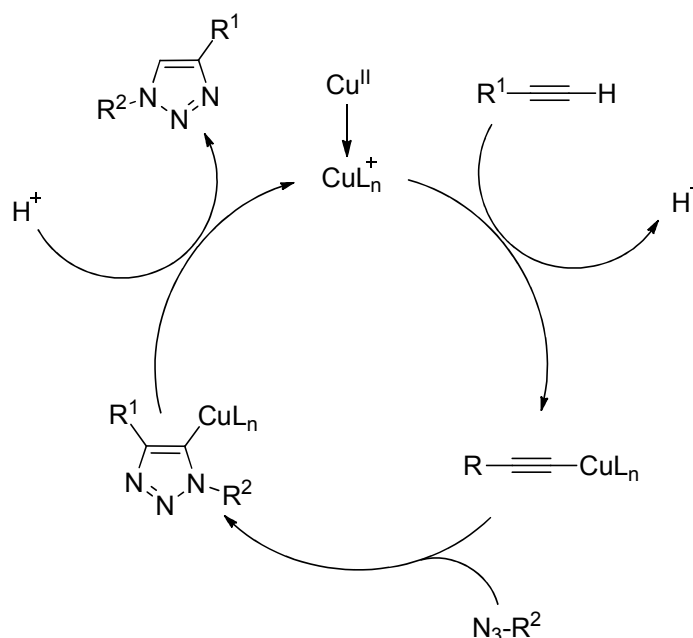


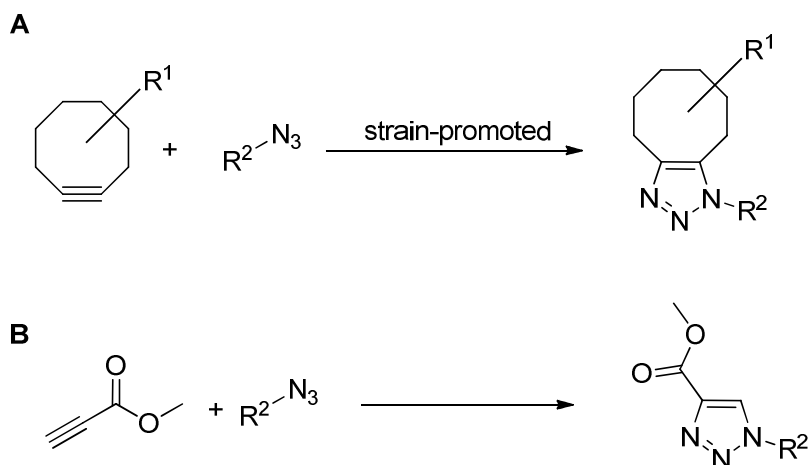
**Figure 2.2.** Catalyst systems typically employed in the metal mediated azide-alkyne cycloadditions.

copper(II) sulfate pentahydrate. Ligations can be performed in aqueous solution or organic solvents. A possible catalytic cycle for the CuAAC is provided in Scheme 2.10.<sup>82</sup> A  $\text{Cu}^{\text{I}}$  species reacts with the alkyne under abstraction of the alkyne proton and a copper acetylide complex is formed. After a cycloaddition with the azide, a neutral 1,2,3-triazole is released and the  $\text{Cu}^{\text{I}}$  active species is regenerated. 1,2,3-Triazoles were reported to enhance reaction rates during the CuAAC as auto-acceleration was observed in the synthesis of tris(triazolyl)amine via CuAAC.<sup>83</sup> While the CuAAC selectively yields 1,4-substituted 1,2,3-triazoles, azide-alkyne cycloadditions catalyzed with ruthenium complexes (RuAAC) provide 1,5-substituted 1,2,3-triazoles.  $\text{Cp}^*\text{RuCl}(\text{COD})$ , depicted in Figure 2.2C, for example, provides quantitative conversion of benzyl azide with phenyl acetylene.<sup>84</sup> However, RuAAC has to date only found minor interest in the field of polymer science.<sup>85-86</sup>

The CuAAC was introduced to the field of polymer science by Hawker, Fokin and Sharpless.<sup>87</sup> In their early studies, a convergent synthesis of triazole based dendrimers was reported and was later complemented with a divergent approach.<sup>88</sup> Inspired by their work, CuAAC was employed for the synthesis of block



**Scheme 2.10.** Possible catalytic cycle for the copper catalyzed azide-alkyne cycloaddition.<sup>82</sup>



**Scheme 2.11.** Catalyst-free 1,3-dipolar cycloaddition reactions of alkynes and azides. A) Strain-promoted cycloaddition of azides and cyclooctynes.<sup>89</sup> B) The utilization of electron-deficient alkynes for accelerating the rate of cycloaddition.<sup>90</sup>

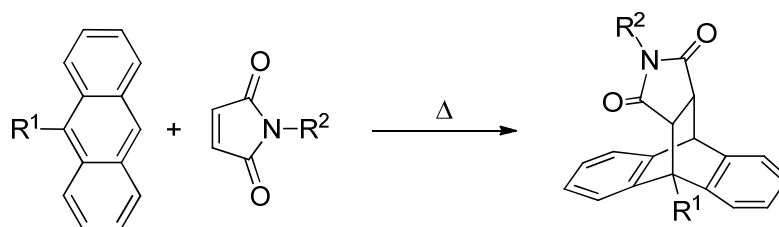
copolymers. Opsteen *et al.* reported the synthesis of amphiphilic poly(methyl methacrylate)-*b*-poly(ethylene glycol) and polystyrene-*b*-poly(ethylene glycol) block copolymers by coupling azide-telechelic poly(ethylene glycol) with the alkyne-functionalized hydrophobic polymers.<sup>91</sup> Shortly after, the bromide termini of polystyrenes obtained in ATRP were shown to be efficient handles that can be transformed into azide moieties and employed in a subsequent chain-end functionalization with small molecule alkynes.<sup>92-93</sup> Moreover, the synthesis of hyperbranched polymers,<sup>94</sup> shell crosslinked nanoparticles,<sup>95</sup> hydrogels,<sup>96</sup> cyclic polymers,<sup>97</sup> dendronized polymers,<sup>98</sup> and dendrimers,<sup>87-88</sup> the stepgrowth reaction of  $\alpha,\omega$ -functionalized polymers,<sup>99</sup> and the synthesis of combs,<sup>100</sup> star,<sup>101</sup> and miktoarm star polymers<sup>102-103</sup> via the CuAAC was investigated. Several review articles summarize the major achievements of the application of CuAAC in the field of polymer science.<sup>63,66,74,104-107</sup>

Catalyst-free strategies to allow for a fast azide-alkyne ligation at ambient conditions were developed. Rate enhancement of the cycloaddition was achieved either by inducing ring strain to the alkyne (Scheme 2.11A),<sup>89</sup> by introducing electron-withdrawing substituents on the alkyne (Scheme 2.11B),<sup>90</sup> or a combination of both approaches. While neat cyclooctynes gave the cycloadduct at rather low reaction rates,<sup>108</sup> the cycloaddition was accelerated by the introduction of electron-withdrawing fluorine moieties in  $\alpha$ -position to the carbon-carbon triple

bond,<sup>109-111</sup> or the employment of merged cyclooctyne-aryl structures, further enhancing the ring strain.<sup>112</sup>

### 2.3.4 Diels–Alder Cyclization

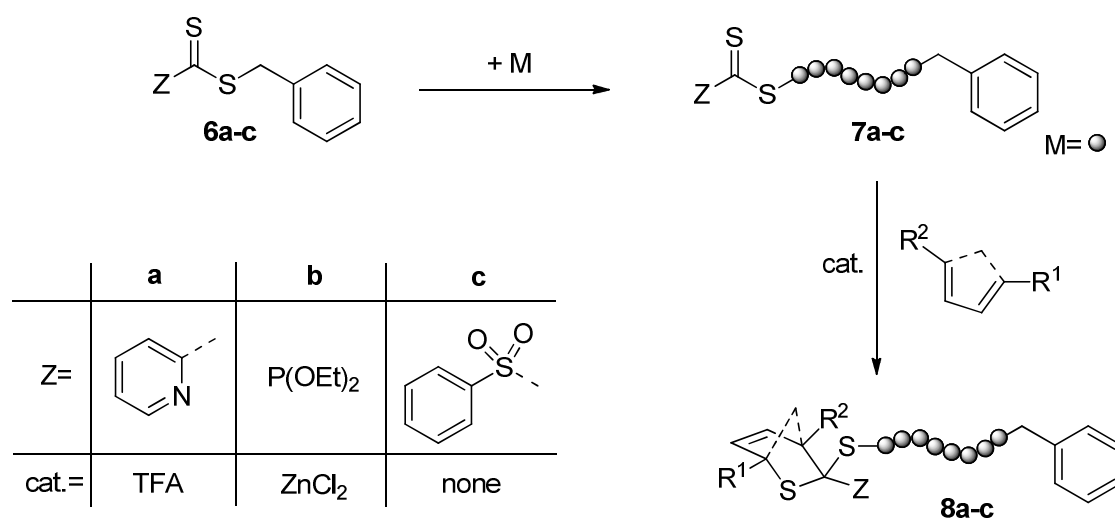
The invention of the Diels–Alder (DA) cyclization reaction by Otto Diels and Kurt Alder has been a milestone in organic chemistry.<sup>113</sup> DA reactions are thermally induced [4 + 2] cycloaddition reactions of electron-rich conjugated dienes and electron-poor dienophiles.<sup>114</sup> An example of a DA cyclization commonly employed in the field of polymer science is depicted in Scheme 2.12. The reaction of anthracene and maleimide was reported to proceed at elevated temperatures within several hours to days and was described to adhere to the “click” concept.<sup>115</sup> DA cyclization of anthracene and maleimide has been used for the construction of (stereo-)block copolymers,<sup>116-117</sup> graft,<sup>118</sup> and star polymers.<sup>115</sup> Moreover, the orthogonality of the reaction to the CuAAC has been demonstrated and exploited for the construction of advanced macromolecular architectures, either in sequential reactions or in simultaneous one-pot protocols.<sup>119-120</sup> The reversibility of the DA cyclization has been harnessed for the synthesis of thermoreversible materials.<sup>121-122</sup> DA systems that were employed as a reversible handle for the preparation of self-healing materials include the reactions of furan and maleimide,<sup>123</sup> and the dimerization of cyclopentadiene (Cp) moieties.<sup>124</sup> An exhaustive description of work performed on the modular construction of macromolecular architectures is beyond the scope of the present thesis. The interested reader is referred to a recent review article by Tasdelen.<sup>125</sup>



**Scheme 2.12.** [4 + 2] cycloaddition of anthracene and maleimide as an example of Diels–Alder cycloaddition, commonly employed in polymer science (R<sup>1</sup>, R<sup>2</sup> = polymer chains).

### 2.3.5 Hetero-Diels–Alder Cyclization

Hetero-Diels–Alder (HDA) reactions play a key role in the preparation of polymer architectures and were proven to often adhere to the “click” criteria.<sup>126</sup> The combination of RAFT polymerization using specific electron-deficient dithioester controlling agents and a successive utilization of these RAFT polymers in HDA ligation reactions in the so-called RAFT-HDA approach provides a versatile and atom-efficient method for modular ligation chemistries on polymeric substrates.<sup>127</sup> The key component in both, the reversible-deactivation polymerization and the orthogonal ligation reaction, is the electron-deficient thiocarbonyl moiety of the dithioester RAFT agents. In Scheme 2.13, three different Z-group moieties of dithioester controlling agents **6a-c** commonly employed in RAFT-HDA reactions are depicted exemplarily. The overall reaction strategy of the RAFT-HDA approach is depicted in Scheme 2.13. Electron-deficient dithioesters **6a-c** are employed as controlling agents in the RAFT mediated polymerization. Monomer is incorporated in the reversible-deactivation polymerization process and hetero-dienophile telechelic polymers **7a-c** are obtained. Under specific reaction conditions, the hetero-dienophiles undergo a reaction with conjugated open-chain dienes and form dihydrothiopyran linkage structures **8a-c**. The DA cyclization of the pyridinyl dithioester derived polymers **7a** is triggered by the addition of trifluoroacetic acid (TFA). Phosphoryl dithioester derived polymers **7b** widely require the presence of



**Scheme 2.13.** Overall reaction strategy of the RAFT-HDA approach.

ZnCl<sub>2</sub> as an activating species. Both catalytic species, TFA, a Brønsted acid, and ZnCl<sub>2</sub>, a Lewis acid, enhance the electron-deficient character of the thiocarbonyl dienophile either by protonation or coordination.<sup>127</sup> In contrast, the HDA cyclization of sulfonyl dithioester derived polymers **7c** proceeds within hours in absence of activating species.<sup>128</sup> It is noted that due to the structural similarity of the dithioesters **6a-c** and the macroRAFT species **7a-c** the reactivities of the thiocarbonyl moieties of the polymers **7a-c** are widely equivalent to those of the small molecular analogues **6a-c**.

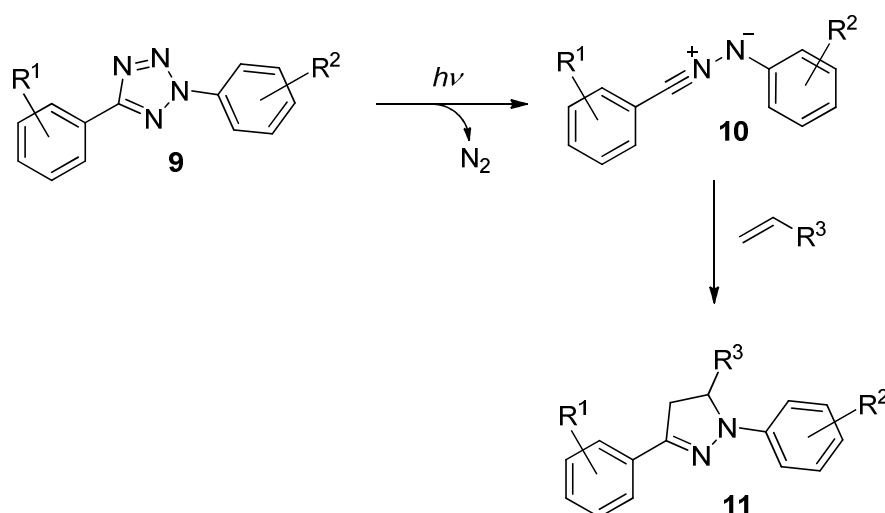
The rates of HDA cyclization in organic solution strongly depend on the type of the employed diene structure. While HDA cyclizations of dienophiles **7a-b** with open-chain dienes, *e.g.* derived from sorbic alcohols (R<sup>1</sup> = CH<sub>2</sub>OH, R<sup>2</sup> = Me), generally require elevated temperatures (~50 °C) and the presence of activating species to allow for a quantitative conjugation within hours,<sup>127</sup> the utilization of Cp derived structures drastically reduces the reaction rates (a technique termed ultrafast RAFT-HDA). HDA reactions of **7a-b** with Cp derived enophiles proceed at ambient conditions within minutes.<sup>129-130</sup> While pyridinyl dithioesters **7a** still require the addition of TFA, the HDA cyclization of **7b** with Cp derived structures proceeds under ambient conditions in the absence of a ZnCl<sub>2</sub> catalyst.<sup>129</sup> With the more reactive sulfonyl dithioesters **6c**, reaction times are severely reduced when Cp derived enophiles are employed instead of open-chain dienes. While cyclizations with both, Cp derived and open-chain diene derived reactands readily proceed at ambient conditions, the coupling products of **7c** with cyclic dienes in part undergo degradation.<sup>128</sup> Most interestingly, the reactivity of the thiocarbonyl moiety of the sulfonyl controlling agents **6c** is sufficiently high to allow for a HDA reaction with the residual pendant styrenes of poly(divinylbenzene) microspheres, breaking up delocalized electronic systems.<sup>131</sup> In aqueous media, open-chain diene reactands were shown to undergo conjugation with polymers of type **7a-b** within hours or minutes under ambient conditions while no catalyst was required.<sup>132</sup>

The utilization of diene-capped polymers (Scheme 2.13, R<sup>1</sup> = polymer) allows the access of various complex macromolecular architectures. A major achievement for the applicability of the ultrafast RAFT-HDA technique was the preparation of Cp-telechelic polymers from bromide-capped polymers employing nickelocene

(NiCp<sub>2</sub>) as the source of the diene.<sup>133</sup> The numerous side reactions that were observed when NaCp was employed as a source of nucleophiles were suppressed and pure Cp-functionalized poly(acrylates) and poly(methacrylates) were obtained. The HDA technique was employed for the synthesis of block copolymers,<sup>134-135</sup> graft,<sup>136</sup> and star polymers,<sup>137</sup> and the immobilization of (bio-)polymers on solid substrates.<sup>138-140</sup> Moreover, HDA cyclization was exploited in step-growth polymerizations.<sup>141-142</sup> The dihydrothiopyran coupling moieties were shown to be stable up to temperatures of 100 °C in case the open-chain dienes were employed.<sup>143</sup> Nevertheless, the potential of the retro-DA reaction was exploited in thermally reversible polymerizations,<sup>141-142,144</sup> and in the synthesis of reversibly colour-switchable polymeric materials.<sup>145</sup>

### 2.3.6 Nitrile Imine Mediated Tetrazole-Ene Coupling

In the field of biochemistry, the introduction of highly selective, unique chemical motifs and their utilization in bioorthogonal conjugation techniques has been proven to be an efficient tool for the tracking of cellular processes in living systems.<sup>146</sup> The photo-induced nitrile imine mediated tetrazole-ene coupling (NITEC) is such an example of bioorthogonal conjugation.<sup>147</sup> The technique was employed for the rapid labeling of encoded proteins *in vivo*<sup>148-149</sup> and *in vitro*,<sup>150</sup>



**Scheme 2.14.** Mechanism of the nitrile imine mediated tetrazole-ene coupling (NITEC) approach.

and the structural reinforcement of peptide helices.<sup>151</sup> The NITEC technique is a photo-induced cycloaddition reaction of a 1,3-dipole provided *in situ* from a light-sensitive diaryl tetrazole precursor. The mechanism of the NITEC approach is depicted in Scheme 2.14. Under irradiation with UV light, the diaryl tetrazoles **9** undergo cycloreversion and release molecular nitrogen. In the presence of olefins, the therein formed nitrile imine intermediates **10** readily undergo a cyclization reaction giving the pyrazolines **11**.<sup>152</sup> The modification of the substituents R<sup>1</sup> and R<sup>2</sup> of the aryl moieties provides an efficient handle for connecting the tetrazoles with various substrates.

The NITEC was shown to proceed with unsaturated compounds ranging from acrylic, methacrylic and vinylic olefins over maleimides to unactivated olefins such as 1-decene.<sup>153</sup> The light absorption properties strongly depend on the substituents R<sup>1</sup> and R<sup>2</sup> of the tetrazole precursors. Lin and coworkers investigated a series of substituted diaryl tetrazoles to identify reagents that can be photoactivated at longer wavelengths and thus employed for an improved ligation strategy in living systems.<sup>154-155</sup> The reactivity of the nitrile imine intermediates toward pyrazoline formation was demonstrated to strongly depend on the energy level of the highest occupied molecular orbital (HOMO) of the nitrile imine. The effective labeling of an alkene-encoded protein inside *E. coli* cells was observed within less than 60 s when a diaryl tetrazole **9** (R<sup>1</sup> = H, R<sup>2</sup> = *para*-OMe) with a low HOMO energy level was employed.<sup>148</sup>

Recently, the NITEC reaction has found interest among polymer scientists. The principal ability of the NITEC approach to allow for the joining of polymer building blocks was demonstrated by Dietrich *et al.*<sup>156</sup> Under irradiation with UV light of 254 nm, a tetrazole-telechelic poly(ethylene glycol) was coupled to a maleimide-functionalized poly(ethylene glycol) polymer building block within 20 min under ambient conditions. The concept was further exploited for the immobilization of various poly(methacrylates) on tetrazole-functionalized cellulose or silicon wafers and was proven to allow for a spatially resolved surface patterning.<sup>156-157</sup> De Hoog *et al.* utilized the NITEC technique for the functionalization of polymersomes, *i.e.* self-assembled diblock copolymer vesicles, and highlighted the benefits of the protocol facility, the ease of preparation and the pro-fluorescent character for the

*in situ* tracking of the functionalization progress.<sup>158</sup> In their study, tetrazole-functionalized horseradish peroxidase was coupled to the methacrylate chain-ends of a commercially available triblock copolymer employed for the formation of the polymersomes. The fast reaction rates in the absence of catalysts or additives at nondemanding reaction conditions make the NITEC approach a promising alternative to the strain-promoted catalyst-free cycloaddition of azides and activated alkynes.<sup>89</sup>

### 2.3.7 Other Modular Ligation Techniques

In addition to the modular ligation techniques with particular interest for the thesis at hand, *i.e.* the CuAAC, the RAFT-HDA approach and the NITEC route, several other modular ligation techniques have been developed and applied for the construction of complex macromolecular architectures. In recent years, the thiol-ene reaction – the addition of a thiol to an olefin – has attracted a particular interest.<sup>159</sup> The thiol-ene reaction can be performed via two different reaction pathways. A radical reaction pathway gives the anti-Markownikov thioethers<sup>160</sup> and proceeds either via the thermal initiation with a radical initiator,<sup>161</sup> or under photoinitiation with UV light<sup>162</sup> or sunlight.<sup>163</sup> In the second approach, a reaction of the thiols with the double bonds of  $\alpha,\beta$ -unsaturated carbonyls occurs via a *Michael*-type reaction pathway in the presence of amines.<sup>164</sup> Thiol-yne chemistry, *i.e.* the addition of two thiols to an alkyne via a radical mechanism,<sup>165</sup> the thio-bromo coupling, *i.e.* the formation of thioethers via nucleophilic substitution,<sup>166-167</sup> and the thiol-isocyanate chemistry<sup>168</sup> are three further powerful methods that make use of the relatively high stability of the thio-carbon single bond.<sup>159</sup> Since RAFT polymerization involves trithiocarbonate or dithioester chain transfer agents, a simple aminolysis of the RAFT polymers allows for a facile access of the thiol-telechelic polymer building blocks that can be subsequently employed in the construction of macromolecular architectures.<sup>169-170</sup> Other modular ligation strategies involve the (light-triggered) formation of oximes,<sup>171-172</sup> or the *in situ* formation of isocyanates via the Curtius rearrangement that readily undergo reaction with alcohols.<sup>173</sup> Moreover, metal-free 1,3-dipolar addition of nitrile oxides and alkynes has been reported.<sup>174</sup> Due to the high interest of polymer

scientists in orthogonal ligation techniques and the high number of publications, the herein presented list is incomplete. Moreover, the continuing search for innovative ligation strategies will certainly lead to further rapid, selective and efficient approaches.

## 2.4 Nitrile-Butadiene Rubber

### 2.4.1 Synthesis and Applications

Nitrile-butadiene rubber (NBR) is a synthetic rubber and is obtained as a statistic copolymer of acrylonitrile (AN) and 1,3-butadiene (BD). Several other synthetic rubbers exist, commonly known as chloroprene rubber (CR), butadiene rubber (BR), styrene-butadiene rubber (SBR) and butyl rubber (IIR), to name a few. In contrast to polymers classified in category M (*e.g.* ethylene propylene diene monomer (EPDM) rubber) these types of synthetic rubbers display unsaturated carbon-carbon bonds within the polymer backbone, thus classified into category R. NBR has a history of almost one century and was invented in the 1930 by the Bayer company as the first-ever oil resistant rubber. On an industrial scale, NBR is manufactured in an emulsion polymerization process. Today, NBR is commercially available as products named Nipol® (Zeon),<sup>175</sup> Europrene® (Eni),<sup>176</sup> Perbunan®, Krynac® or in a pulverized version as Baymod® N (all Lanxess).<sup>177</sup> NBR is merchandised in different grades of AN contents between 18 and 50%, depending on the targeted application. The AN content influences important properties such as the swelling behavior or oil resistance.<sup>178</sup> NBR displays a heat resistance of temperatures of up to 120 °C. Substantially improved temperature stability is obtained when NBR is hydrogenated (HNBR). HNBR of different grades regarding the AN content and the content of residual double bonds is commercially available as Therban® (Lanxess) and exhibits a temperature stability of up to 165 °C, or for short-term heating of up to 190 °C.<sup>179</sup>

Due to its pronounced oil resistance, NBR finds applications in the automotive and aeronautical industry as seals, fuel supply hoses, hydraulic hoses, fabric linings, gaskets and drive belts, yet can be found in shoe soles and flooring

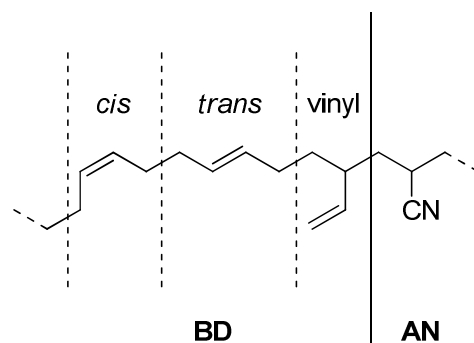


**Figure 2.3.** Different channels of monomer incorporation in the radical copolymerization of AN and BD.

materials.<sup>180</sup> The excellent temperature stability at high levels of oil resistance observed for HNBR makes it an outstanding candidate for the production of items employed in the oil exploration industries, such as blow-out preventers or stators. Elastomeric items therein are subjected to severe conditions while exposed to hostile media such as oil, methane, carbon dioxide and hydrogen sulfide.<sup>181</sup> Several applications require a transition of the visco-plastic properties of pristine NBR into a visco-elastic material generally achieved via vulcanization with sulfur or other crosslinking agents.<sup>182</sup> However, vulcanization of the synthesized rubber materials is not targeted within the work performed in the current thesis.

The typical structure of the NBR chain is depicted in Figure 2.3. While AN allows a single channel of incorporation only, BD incorporates in three distinct structures.<sup>183</sup> NBR obtained in free radical polymerization typically comprises 78% of the double bonds formed upon 1,4-incorporation of BD in a *trans* configuration. Around 12% exist in *cis* configuration while 10% of BD is incorporated in a 1,2-fashion giving vinyl groups. The nitrile monomers and the BD monomers providing a vinyl structure may be incorporated in a 1,2- or a 2,1-fashion, giving several possible combinations of patterns of monomer incorporation. Due to the relatively low stability of the primary radicals in comparison to the secondary radicals, 1,2-incorporation will be preferred. However, head-head or tail-tail pattern of two consecutively incorporated monomer units might be observed.<sup>183</sup>

### 2.4.2 Recent Advances in the Controlled Synthesis of NBR

On an industrial scale, to date NBR is synthesized in an emulsion polymerization process. In the emulsion polymerization, a hydrophobic monomer is dispersed in water by an oil-in-water emulsifier employed in concentrations above the critical micelle concentration. Radical species are released from a water soluble radical source and react with the small amounts of the hydrophobic monomer dissolved in the aqueous phase forming a short propagating polymer chain. After a certain number of monomer addition steps, a critical chain-length is reached, the polymer chain collapses and forms a primary particle. After the primary particle has entered a monomer-swollen micelle, propagation proceeds while monomer is continuously delivered from the monomer droplet reservoirs. Due to the spatial constraints within the particles, a single radical can exist per particle only. If a second radical enters a micelle, immediate termination occurs. The number of free radicals per polymer particle equals approximately 0.5 (zero-one kinetics).<sup>184</sup> The spatial segregation of the propagating radicals inside the monomer swollen “micro-reactor” compartments allows for a high polymerization rate while radical termination reactions are heavily reduced. Nevertheless, the two major drawbacks associated with the emulsion process are the low degree of control over molecular weights and the broad molecular weight distributions obtained. Due to the exothermic nature of radical polymerization and the low heat transfer capacity of large-scale reactors, industrial emulsion polymerization processes are mainly conducted in continuous reaction systems. When reactor cascades are employed, the residence time distribution of the growing particles is broad and results in broad particle size distributions.<sup>2</sup>

For an efficient polymerization process and the effective stabilization of the large oil-water interfacial area of the polymer latex a high amount of salts and additives is required. In contrast, solution-based polymerization can be considered to be a “pure” system, consisting of the monomer, the initiator and the solvent, only. A major advantage of a solution-based polymerization system of NBR becomes obvious when the synthesis of HNBR as a secondary product is considered.

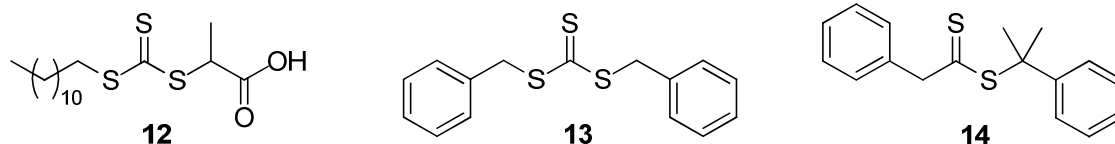


**Figure 2.4.** Trithiocarbonate **12** and **13** and dithioester controlling agent **14** employed in RAFT mediated copolymerizations of AN and BD.<sup>185</sup>

Hydrogenation of unsaturated polymers is commonly performed in solution.<sup>186</sup> A solvent allowing for both, the polymerization and hydrogenation, thus allows for a subsequent polymerization and hydrogenation of NBR without a workup procedure except monomer stripping.<sup>187</sup> There have been a few reports of solution-based copolymerization attempts of AN and BD.<sup>187-189</sup> However, poor control over molecular weights and a low monomer-to-polymer conversion were observed.

Recently, polymer scientists from the Karlsruhe Institute of Technology in collaboration with Lanxess Deutschland GmbH reported a solution-based process

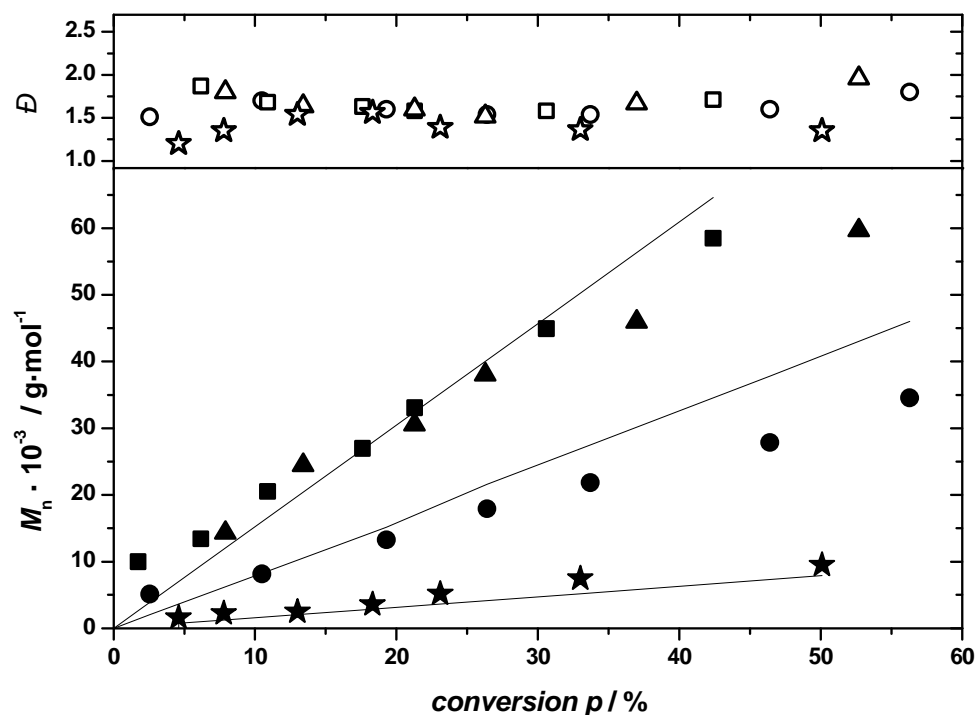


**Figure 2.5.** Evolution of molar mass with conversion of RAFT mediated copolymerizations of AN and BD employing trithiocarbonate **12** in concentrations of 3.2 mM (triangles), 3.3 mM (squares), 6.4 mM (circles) and 32.0 mM (stars) and an overall monomer concentration of 9.4 M. For further experimental details see reference 185. Adapted from reference 185. Copyright © 2010 WILEY-VCH Verlag GmbH & Co. KGaA, Weinheim.

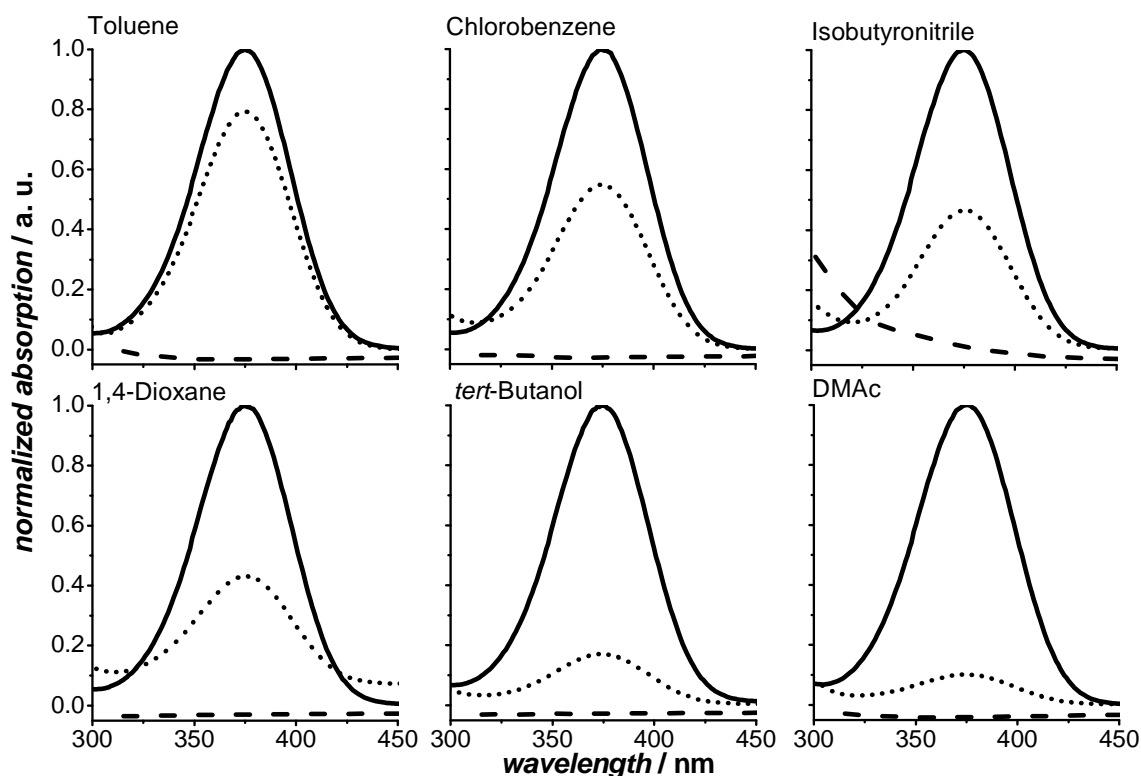


**Figure 2.6.** Tracking of the decomposition of a 0.1 mol·L<sup>-1</sup> solution of 2,2'-azobis(*N*-butyl-2-methylpropionamide) at 100 °C in various solvents as illustrated by the UV-vis spectroscopic data of the azo absorption band around 375 nm before (solid line) and after (dotted line) a heating period of 22 h. Adapted from reference 190. Copyright © 2011 Wiley Periodicals, Inc.

for the synthesis of NBR under controlled conditions.<sup>185</sup> In the presence of a chain transfer agent and at elevated temperatures, AN and BD were copolymerized to high conversions of approximately 60%. Molar masses of up to 60 000 g·mol<sup>-1</sup> were obtained while dispersities were kept below 2. The controlling agents employed in the study are depicted in Figure 2.4. Either trithiocarbonates **12** or **13**, or dithioester **14** allowed for the control over molar mass. As depicted in Figure 2.5, a linear evolution of molar mass with conversion was obtained for polymerizations performed at various concentrations of trithiocarbonate **12**. In light of the outline of the current thesis targeting novel NBR architectures, the potential ability to modify trithiocarbonate **12** via manipulation of the carboxy moiety is highlighted. As discussed above, the utilization of functionalized chain transfer agents in RAFT polymerization allows for the direct synthesis of chain-end functionalized NBR without successive postpolymerization modifications.

The RAFT mediated copolymerization of AN and BD was further optimized in its experimental conditions by variation of the solvent and the type of azo initiator employed. To facilitate a constant radical flux at elevated temperatures, azo initiators with ten hour half-life decomposition temperatures of 88-110 °C were employed.<sup>190</sup> The solvent proved to have a major impact on the interrelation of the achievable conversion within a pre-assigned reaction time. UV-vis spectra of the azo absorption band of 0.1 M solutions of high temperature initiator 2,2'-azobis(*N*-butyl-2-methylpropionamide) in *N,N*-dimethylacetamide, *tert*-butanol, 1,4-dioxane, isobutyronitrile, chlorobenzene or toluene before (solid line) and after (dotted line) tempering the solution to 100 °C for a period of 22 h are depicted in Figure 2.6. In analogy to a high conversion observed in polymerizations performed in *N,N*-dimethylacetamide, almost complete decomposition of the azo initiator was observed within 22 h. In contrast, decomposition in toluene proceeded to an extent of only 20%, in line with the low conversion/time ratios observed in a respective polymerization experiment. The differences were shown to derive from solvent-solute interactions and to solely influence the initiation step of the polymerizations. With respect to the ecology of RAFT mediated copolymerizations of AN and BD on an industrial scale, the advantages of the high conversion/time ratio observed for polymerizations in *N,N*-dimethylacetamide are exceeded by the potential of chlorobenzene to be employed in both, polymerization and a successive hydrogenation to obtain the specialty polymer HNBR.<sup>186</sup>

## 2.5 References

1. Matyjaszewski, K. *Macromolecules* **2012**, *45*, 4015-4039.
2. Chern, C. S. *Prog. Polym. Sci.* **2006**, *31*, 443-486.
3. Yuan, H. G.; Kalfas, G.; Ray, W. H. *J. Macromol. Sci. Polym. Rev.* **1991**, *31*, 215-299.
4. *Emulsion polymerization and emulsion polymers*. Lovell, P. A.; El-Aasser, M. S., Eds.; John Wiley & Sons: New York, 1997.
5. *Handbook of Radical Polymerization*. Matyjaszewski, K.; Davis, T. P., Eds.; Wiley-Interscience: Hoboken, 2002.
6. Braunecker, W. A.; Matyjaszewski, K. *Prog. Polym. Sci.* **2007**, *32*, 93-146.
7. Szwarc, M. *Nature* **1956**, *178*, 1168-1169.
8. Goto, A.; Fukuda, T. *Prog. Polym. Sci.* **2004**, *29*, 329-385.
9. Fischer, H. *Macromolecules* **1997**, *30*, 5666-5672.
10. Solomon, D. H.; Rizzardo, E.; Cacioli, P. *Polymerization Process and Polymers Produced Thereby*. US. Pat., 4 581 429, 1986.
11. Grubbs, R. B. *Polym. Rev.* **2011**, *51*, 104-137.
12. Wang, J.-S.; Matyjaszewski, K. *J. Am. Chem. Soc.* **1995**, *117*, 5614-5615.
13. Matyjaszewski, K.; Gaynor, S.; Wang, J.-S. *Macromolecules* **1995**, *28*, 2093-2095.
14. Kumar, K. S. S.; Gnanou, Y.; Champouret, Y.; Daran, J.-C.; Poli, R. *Chem. Eur. J.* **2009**, *15*, 4874-4885.
15. Jenkins, A. D.; Jones, R. G.; Moad, G. *Pure Appl. Chem.* **2010**, *82*, 483-491.
16. Chiefari, J.; Chong, Y. K.; Ercole, F.; Krstina, J.; Jeffery, J.; Le, T. P. T.; Mayadunne, R. T. A.; Meijs, G. F.; Moad, C. L.; Moad, G.; Rizzardo, E.; Thang, S. H. *Macromolecules* **1998**, *31*, 5559-5562.
17. Moad, G.; Rizzardo, E.; Thang, S. H. *Aust. J. Chem.* **2012**, *65*, 985-1076.
18. *Handbook of RAFT Polymerization*. Barner-Kowollik, C., Ed.; Wiley-VCH: Weinheim, 2009.
19. O'Donnell, J. M. *Chem. Soc. Rev.* **2012**, *41*, 3061-3076.
20. Monteiro, M. J. *Macromolecules* **2010**, *43*, 1159-1168.
21. McLeary, J. B.; Klumperman, B. *Soft Matter* **2006**, *2*, 45-53.

22. Moad, G.; Rizzardo, E.; Thang, S. H. *Aust. J. Chem.* **2005**, *58*, 379-410.
23. Taton, D.; Destarac, M.; Zard, S. Z., The RAFT Process as a Kinetic Tool: Accessing Fundamental Parameters of Free Radical Polymerization. In *Handbook of RAFT Polymerization*. 1<sup>st</sup> ed.; Barner-Kowollik, C., Ed.; Wiley-VCH: Weinheim, 2008; p 373 ff.
24. Biadatti, T.; Charmot, D.; Corpart, P.; Michelet, D.; Zard, S. Z. *Method for Block Polymer Synthesis by Controlled Radical Polymerisation*. WO Pat., 9858974 A1, 1998.
25. Moad, G.; Rizzardo, E.; Thang, S. H. *Polym. Int.* **2011**, *60*, 9-25.
26. Xu, J.; He, J.; Fan, D.; Tang, W.; Yang, Y. *Macromolecules* **2006**, *39*, 3753-3759.
27. Moad, G.; Chiefari, J.; Chong, Y. K.; Krstina, J.; Mayadunne, R. T. A.; Postma, A.; Rizzardo, E.; Thang, S. H. *Polym. Int.* **2000**, *49*, 993-1001.
28. Barner-Kowollik, C.; Buback, M.; Charleux, B.; Coote, M. L.; Drache, M.; Fukuda, T.; Goto, A.; Klumperman, B.; Lowe, A. B.; McLeary, J. B.; Moad, G.; Monteiro, M. J.; Sanderson, R. D.; Tonge, M. P.; Vana, P. *J. Polym. Sci. Part A: Polym. Chem.* **2006**, *44*, 5809-5831.
29. Monteiro, M. J.; de Brouwer, H. *Macromolecules* **2001**, *34*, 349-352.
30. Kwak, Y.; Goto, A.; Fukuda, T. *Macromolecules* **2004**, *37*, 1219-1225.
31. Vana, P.; Davis, T. P.; Barner-Kowollik, C. *Macromol. Theory Simul.* **2002**, *11*, 823-835.
32. Coote, M. L. *Macromolecules* **2004**, *37*, 5023-5031.
33. Chong, Y. K.; Krstina, J.; Le, T. P. T.; Moad, G.; Postma, A.; Rizzardo, E.; Thang, S. H. *Macromolecules* **2003**, *36*, 2256-2272.
34. Fukuda, T.; Goto, A.; Kwak, Y.; Yoshikawa, C.; Ma, Y.-D. *Macromol. Symp.* **2002**, *182*, 53-64.
35. Chiefari, J.; Mayadunne, R. T. A.; Moad, C. L.; Moad, G.; Rizzardo, E.; Postma, A.; Thang, S. H. *Macromolecules* **2003**, *36*, 2273-2283.
36. Farmer, S. C.; Patten, T. E. *J. Polym. Sci. Part A: Polym. Chem.* **2002**, *40*, 555-563.
37. Benaglia, M.; Rizzardo, E.; Alberti, A.; Guerra, M. *Macromolecules* **2005**, *38*, 3129-3140.

38. Coote, M. L.; Radom, L. *J. Am. Chem. Soc.* **2003**, *125*, 1490-1491.
39. Ishitake, K.; Satoh, K.; Kamigaito, M.; Okamoto, Y. *Polym. Chem.* **2012**, *3*, 1750-1757.
40. Moad, G.; Rizzardo, E.; Thang, S. H. *Aust. J. Chem.* **2006**, *59*, 669-692.
41. Moad, G.; Rizzardo, E.; Thang, S. H. *Aust. J. Chem.* **2009**, *62*, 1402-1472.
42. Nicolas, J.; Guillaneuf, Y.; Lefay, C.; Bertin, D.; Gigmes, D.; Charleux, B. *Prog. Polym. Sci.* **2013**, *38*, 63-235.
43. Fukuda, T.; Terauchi, T.; Goto, A.; Ohno, K.; Tsujii, Y.; Miyamoto, T.; Kobatake, S.; Yamada, B. *Macromolecules* **1996**, *29*, 6393-6398.
44. Georges, M. K.; Veregin, R. P. N.; Kazmaier, P. M.; Hamer, G. K. *Macromolecules* **1993**, *26*, 2987-2988.
45. Hawker, C. J. *J. Am. Chem. Soc.* **1994**, *116*, 11185-11186.
46. Hawker, C. J.; Barclay, G. G.; Orellana, A.; Dao, J.; Devonport, W. *Macromolecules* **1996**, *29*, 5245-5254.
47. Greszta, D.; Mardare, D.; Matyjaszewski, K. *Macromolecules* **1994**, *27*, 638-644.
48. Fukuda, T.; Terauchi, T.; Goto, A.; Tsujii, Y.; Miyamoto, T.; Shimizu, Y. *Macromolecules* **1996**, *29*, 3050-3052.
49. Yoshida, E.; Ishizone, T.; Hirao, A.; Nakahama, S.; Takata, T.; Endo, T. *Macromolecules* **1994**, *27*, 3119-3124.
50. Hawker, C. J. *Angew. Chem. Int. Ed.* **1995**, *34*, 1456-1459.
51. Studer, A.; Schulte, T. *Chem. Rec.* **2005**, *5*, 27-35.
52. Studer, A.; Harms, K.; Knoop, C.; Müller, C.; Schulte, T. *Macromolecules* **2003**, *37*, 27-34.
53. Matyjaszewski, K.; Patten, T. E.; Xia, J. *J. Am. Chem. Soc.* **1997**, *119*, 674-680.
54. Kajiwara, A.; Matyjaszewski, K.; Kamachi, M. *Macromolecules* **1998**, *31*, 5695-5701.
55. di Lena, F.; Matyjaszewski, K. *Prog. Polym. Sci.* **2010**, *35*, 959-1021.
56. Wang, J.-S.; Matyjaszewski, K. *Macromolecules* **1995**, *28*, 7572-7573.
57. Matyjaszewski, K.; Coca, S.; Gaynor, S. G.; Wei, M.; Woodworth, B. E. *Macromolecules* **1997**, *30*, 7348-7350.
58. Min, K.; Gao, H.; Matyjaszewski, K. *Macromolecules* **2007**, *40*, 1789-1791.

59. Jakubowski, W.; Matyjaszewski, K. *Angew. Chem. Int. Ed.* **2006**, *45*, 4482-4486.
60. Matyjaszewski, K.; Tsarevsky, N. V.; Braunecker, W. A.; Dong, H.; Huang, J.; Jakubowski, W.; Kwak, Y.; Nicolay, R.; Tang, W.; Yoon, J. A. *Macromolecules* **2007**, *40*, 7795-7806.
61. Matyjaszewski, K.; Jakubowski, W.; Min, K.; Tang, W.; Huang, J.; Braunecker, W. A.; Tsarevsky, N. V. *Proc. Natl. Acad. Sci. USA* **2006**, *103*, 15309-15314.
62. Magenau, A. J. D.; Strandwitz, N. C.; Gennaro, A.; Matyjaszewski, K. *Science* **2011**, *332*, 81-84.
63. Lutz, J.-F.; Schlaad, H. *Polymer* **2008**, *49*, 817-824.
64. Altintas, O.; Vogt, A. P.; Barner-Kowollik, C.; Tunca, U. *Polym. Chem.* **2012**, *3*, 34-45.
65. Siegwart, D. J.; Oh, J. K.; Matyjaszewski, K. *Prog. Polym. Sci.* **2012**, *37*, 18-37.
66. Iha, R. K.; Wooley, K. L.; Nyström, A. M.; Burke, D. J.; Kade, M. J.; Hawker, C. J. *Chem. Rev.* **2009**, *109*, 5620-5686.
67. Nandivada, H.; Jiang, X.; Lahann, J. *Adv. Mater.* **2007**, *19*, 2197-2208.
68. Kricheldorf, H. R. *J. Polym. Sci. Part A: Polym. Chem.* **2010**, *48*, 251-284.
69. Kolb, H. C.; Finn, M. G.; Sharpless, K. B. *Angew. Chem. Int. Ed.* **2001**, *40*, 2004-2021.
70. Guthrie, J. P. *Can. J. Chem.* **1978**, *56*, 962-973.
71. Barner-Kowollik, C.; Du Prez, F. E.; Espeel, P.; Hawker, C. J.; Junkers, T.; Schlaad, H.; Van Camp, W. *Angew. Chem. Int. Ed.* **2011**, *50*, 60-62.
72. Rostovtsev, V. V.; Green, L. G.; Fokin, V. V.; Sharpless, K. B. *Angew. Chem. Int. Ed.* **2002**, *41*, 2596-2599.
73. Tornøe, C. W.; Christensen, C.; Meldal, M. *J. Org. Chem.* **2002**, *67*, 3057-3064.
74. Lutz, J.-F. *Angew. Chem. Int. Ed.* **2007**, *46*, 1018-1025.
75. Bock, V. D.; Hiemstra, H.; van Maarseveen, J. H. *Eur. J. Org. Chem.* **2006**, *2006*, 51-68.
76. Moses, J. E.; Moorhouse, A. D. *Chem. Soc. Rev.* **2007**, *36*, 1249-1262.
77. Kolb, H. C.; Sharpless, K. B. *Drug Discov. Today* **2003**, *8*, 1128-1137.

78. Meldal, M.; Tornøe, C. W. *Chem. Rev.* **2008**, *108*, 2952-3015.
79. Speers, A. E.; Adam, G. C.; Cravatt, B. F. *J. Am. Chem. Soc.* **2003**, *125*, 4686-4687.
80. Golas, P. L.; Tsarevsky, N. V.; Sumerlin, B. S.; Matyjaszewski, K. *Macromolecules* **2006**, *39*, 6451-6457.
81. Kuijpers, B. H. M.; Groothuys, S.; Keereweer, A. R.; Quaedflieg, P. J. L. M.; Blaauw, R. H.; van Delft, F. L.; Rutjes, F. P. J. T. *Org. Lett.* **2004**, *6*, 3123-3126.
82. Bräse, S.; Gil, C.; Knepper, K.; Zimmermann, V. *Angew. Chem. Int. Ed.* **2005**, *44*, 5188-5240.
83. Wang, Q.; Chan, T. R.; Hilgraf, R.; Fokin, V. V.; Sharpless, K. B.; Finn, M. G. *J. Am. Chem. Soc.* **2003**, *125*, 3192-3193.
84. Boren, B. C.; Narayan, S.; Rasmussen, L. K.; Zhang, L.; Zhao, H.; Lin, Z.; Jia, G.; Fokin, V. V. *J. Am. Chem. Soc.* **2008**, *130*, 8923-8930.
85. Pola, R.; Laga, R.; Ulbrich, K.; Siegllová, I.; Král, V.; Fábry, M.; Kabešová, M.; Kovář, M.; Pechar, M. *Biomacromolecules* **2013**, *14*, 881-889.
86. Brantley, J. N.; Konda, S. S. M.; Makarov, D. E.; Bielawski, C. W. *J. Am. Chem. Soc.* **2012**, *134*, 9882-9885.
87. Wu, P.; Feldman, A. K.; Nugent, A. K.; Hawker, C. J.; Scheel, A.; Voit, B.; Pyun, J.; Fréchet, J. M. J.; Sharpless, K. B.; Fokin, V. V. *Angew. Chem. Int. Ed.* **2004**, *43*, 3928-3932.
88. Joralemon, M. J.; O'Reilly, R. K.; Matson, J. B.; Nugent, A. K.; Hawker, C. J.; Wooley, K. L. *Macromolecules* **2005**, *38*, 5436-5443.
89. Agard, N. J.; Prescher, J. A.; Bertozzi, C. R. *J. Am. Chem. Soc.* **2004**, *126*, 15046-15047.
90. Li, Z.; Seo, T. S.; Ju, J. *Tetrahedron Lett.* **2004**, *45*, 3143-3146.
91. Opsteen, J. A.; van Hest, J. C. M. *Chem. Commun.* **2005**, 57-59.
92. Lutz, J.-F.; Börner, H. G.; Weichenhan, K. *Macromol. Rapid Commun.* **2005**, *26*, 514-518.
93. Gao, H.; Louche, G.; Sumerlin, B. S.; Jahed, N.; Golas, P.; Matyjaszewski, K. *Macromolecules* **2005**, *38*, 8979-8982.

94. Scheel, A. J.; Komber, H.; Voit, B. I. *Macromol. Rapid Commun.* **2004**, *25*, 1175-1180.
95. Joralemon, M. J.; O'Reilly, R. K.; Hawker, C. J.; Wooley, K. L. *J. Am. Chem. Soc.* **2005**, *127*, 16892-16899.
96. Malkoch, M.; Vestberg, R.; Gupta, N.; Mespouille, L.; Dubois, P.; Mason, A. F.; Hedrick, J. L.; Liao, Q.; Frank, C. W.; Kingsbury, K.; Hawker, C. J. *Chem. Commun.* **2006**, *0*, 2774-2776.
97. Laurent, B. A.; Grayson, S. M. *J. Am. Chem. Soc.* **2006**, *128*, 4238-4239.
98. Helms, B.; Mynar, J. L.; Hawker, C. J.; Fréchet, J. M. J. *J. Am. Chem. Soc.* **2004**, *126*, 15020-15021.
99. Tsarevsky, N. V.; Sumerlin, B. S.; Matyjaszewski, K. *Macromolecules* **2005**, *38*, 3558-3561.
100. Vogt, A. P.; Sumerlin, B. S. *Macromolecules* **2006**, *39*, 5286-5292.
101. Hoogenboom, R.; Moore, B. C.; Schubert, U. S. *Chem. Commun.* **2006**, 4010-4012.
102. Whittaker, M. R.; Urbani, C. N.; Monteiro, M. J. *J. Am. Chem. Soc.* **2006**, *128*, 11360-11361.
103. Altintas, O.; Hizal, G.; Tunca, U. *J. Polym. Sci. Part A: Polym. Chem.* **2006**, *44*, 5699-5707.
104. Sumerlin, B. S.; Vogt, A. P. *Macromolecules* **2010**, *43*, 1-13.
105. Binder, W. H.; Sachsenhofer, R. *Macromol. Rapid Commun.* **2007**, *28*, 15-54.
106. Binder, W. H.; Sachsenhofer, R. *Macromol. Rapid Commun.* **2008**, *29*, 952-981.
107. Hawker, C. J.; Wooley, K. L. *Science* **2005**, *309*, 1200-1205.
108. Wittig, G.; Krebs, A. *Chem. Ber.* **1961**, *94*, 3260-3275.
109. Agard, N. J.; Baskin, J. M.; Prescher, J. A.; Lo, A.; Bertozzi, C. R. *ACS Chem. Biol.* **2006**, *1*, 644-648.
110. Codelli, J. A.; Baskin, J. M.; Agard, N. J.; Bertozzi, C. R. *J. Am. Chem. Soc.* **2008**, *130*, 11486-11493.
111. Baskin, J. M.; Prescher, J. A.; Laughlin, S. T.; Agard, N. J.; Chang, P. V.; Miller, I. A.; Lo, A.; Codelli, J. A.; Bertozzi, C. R. *Proc. Natl. Acad. Sci. USA* **2007**, *104*, 16793-16797.

112. Ning, X.; Guo, J.; Wolfert, M. A.; Boons, G.-J. *Angew. Chem. Int. Ed.* **2008**, *47*, 2253-2255.
113. Diels, O.; Alder, K. *Liebigs Ann. Chem.* **1928**, *460*, 98-122.
114. Sauer, J.; Sustmann, R. *Angew. Chem. Int. Ed.* **1980**, *19*, 779-807.
115. Dag, A.; Durmaz, H.; Hizal, G.; Tunca, U. *J. Polym. Sci. Part A: Polym. Chem.* **2008**, *46*, 302-313.
116. Durmaz, H.; Colakoglu, B.; Tunca, U.; Hizal, G. *J. Polym. Sci. Part A: Polym. Chem.* **2006**, *44*, 1667-1675.
117. Masutani, K.; Kawabata, S.; Aoki, T.; Kimura, Y. *Polym. Int.* **2010**, *59*, 1526-1530.
118. Gacal, B.; Durmaz, H.; Tasdelen, M. A.; Hizal, G.; Tunca, U.; Yagci, Y.; Demirel, A. L. *Macromolecules* **2006**, *39*, 5330-5336.
119. Dag, A.; Durmaz, H.; Demir, E.; Hizal, G.; Tunca, U. *J. Polym. Sci. Part A: Polym. Chem.* **2008**, *46*, 6969-6977.
120. Durmaz, H.; Sanyal, A.; Hizal, G.; Tunca, U. *Polym. Chem.* **2012**, *3*, 825-835.
121. Bergman, S. D.; Wudl, F. *J. Mater. Chem.* **2008**, *18*, 41-62.
122. Sanyal, A. *Macromol. Chem. Phys.* **2010**, *211*, 1417-1425.
123. Chen, X.; Dam, M. A.; Ono, K.; Mal, A.; Shen, H.; Nutt, S. R.; Sheran, K.; Wudl, F. *Science* **2002**, *295*, 1698-1702.
124. Murphy, E. B.; Bolanos, E.; Schaffner-Hamann, C.; Wudl, F.; Nutt, S. R.; Auad, M. L. *Macromolecules* **2008**, *41*, 5203-5209.
125. Tasdelen, M. A. *Polym. Chem.* **2011**, *2*, 2133-2145.
126. Inglis, A. J.; Barner-Kowollik, C. *Macromol. Rapid Commun.* **2010**, *31*, 1247-1266.
127. Sinnwell, S.; Inglis, A. J.; Davis, T. P.; Stenzel, M. H.; Barner-Kowollik, C. *Chem. Commun.* **2008**, 2052-2054.
128. Nebhani, L.; Sinnwell, S.; Lin, C. Y.; Coote, M. L.; Stenzel, M. H.; Barner-Kowollik, C. *J. Polym. Sci. Part A: Polym. Chem.* **2009**, *47*, 6053-6071.
129. Inglis, A. J.; Sinnwell, S.; Stenzel, M. H.; Barner-Kowollik, C. *Angew. Chem. Int. Ed.* **2009**, *48*, 2411-2414.
130. Inglis, A. J.; Stenzel, M. H.; Barner-Kowollik, C. *Macromol. Rapid Commun.* **2009**, *30*, 1792-1798.

131. Nebhani, L.; Schmiedl, D.; Barner, L.; Barner-Kowollik, C. *Adv. Funct. Mater.* **2010**, *20*, 2010-2020.
132. Glassner, M.; Delaittre, G.; Kaupp, M.; Blinco, J. P.; Barner-Kowollik, C. *J. Am. Chem. Soc.* **2012**, *134*, 7274-7277.
133. Inglis, A. J.; Paulöhrl, T.; Barner-Kowollik, C. *Macromolecules* **2010**, *43*, 33-36.
134. Espinosa, E.; Glassner, M.; Boisson, C.; Barner-Kowollik, C.; D'Agosto, F. *Macromol. Rapid Commun.* **2011**, *32*, 1447-1453.
135. Inglis, A. J.; Barner-Kowollik, C. *Polym. Chem.* **2011**, *2*, 126-136.
136. Bousquet, A.; Barner-Kowollik, C.; Stenzel, M. H. *J. Polym. Sci. Part A: Polym. Chem.* **2010**, *48*, 1773-1781.
137. Inglis, A. J.; Sinnwell, S.; Davis, T. P.; Barner-Kowollik, C.; Stenzel, M. H. *Macromolecules* **2008**, *41*, 4120-4126.
138. Goldmann, A. S.; Tischer, T.; Barner, L.; Bruns, M.; Barner-Kowollik, C. *Biomacromolecules* **2011**, *12*, 1137-1145.
139. Tischer, T.; Goldmann, A. S.; Linkert, K.; Trouillet, V.; Börner, H. G.; Barner-Kowollik, C. *Adv. Funct. Mater.* **2012**, *22*, 3853-3864.
140. Blinco, J. P.; Trouillet, V.; Bruns, M.; Gerstel, P.; Gliemann, H.; Barner-Kowollik, C. *Adv. Mater.* **2011**, *23*, 4435-4439.
141. Zhou, J.; Guimard, N. K.; Inglis, A. J.; Namazian, M.; Lin, C. Y.; Coote, M. L.; Spyrou, E.; Hilf, S.; Schmidt, F. G.; Barner-Kowollik, C. *Polym. Chem.* **2012**, *3*, 628-639.
142. Guimard, N. K.; Ho, J.; Brandt, J.; Lin, C. Y.; Namazian, M.; Mueller, J. O.; Oehlenschlaeger, K. K.; Hilf, S.; Lederer, A.; Schmidt, F. G.; Coote, M. L.; Barner-Kowollik, C. *Chem. Sci.* **2013**, DOI: 10.1039/C3SC50642H.
143. Sinnwell, S.; Synatschke, C. V.; Junkers, T.; Stenzel, M. H.; Barner-Kowollik, C. *Macromolecules* **2008**, *41*, 7904-7912.
144. Inglis, A. J.; Nebhani, L.; Altintas, O.; Schmidt, F. G.; Barner-Kowollik, C. *Macromolecules* **2010**, *43*, 5515-5520.
145. Paulöhrl, T.; Inglis, A. J.; Barner-Kowollik, C. *Adv. Mater.* **2010**, *22*, 2788-2791.
146. Prescher, J. A.; Bertozzi, C. R. *Nat. Chem. Biol.* **2005**, *1*, 13-21.

147. Song, W.; Wang, Y.; Yu, Z.; Rivera Vera, C. I.; Qu, J.; Lin, Q. *ACS Chem. Biol.* **2010**, *5*, 875-885.
148. Wang, Y.; Song, W.; Hu, W. J.; Lin, Q. *Angew. Chem. Int. Ed.* **2009**, *48*, 5330-5333.
149. Song, W.; Wang, Y.; Qu, J.; Lin, Q. *J. Am. Chem. Soc.* **2008**, *130*, 9654-9655.
150. Wang, J.; Zhang, W.; Song, W.; Wang, Y.; Yu, Z.; Li, J.; Wu, M.; Wang, L.; Zang, J.; Lin, Q. *J. Am. Chem. Soc.* **2010**, *132*, 14812-14818.
151. Madden, M. M.; Rivera Vera, C. I.; Song, W.; Lin, Q. *Chem. Commun.* **2009**, 5588-5590.
152. Clovis, J. S.; Eckell, A.; Huisgen, R.; Sustmann, R. *Chem. Ber.* **1967**, *100*, 60-70.
153. Wang, Y.; Rivera Vera, C. I.; Lin, Q. *Org. Lett.* **2007**, *9*, 4155-4158.
154. Wang, Y.; Hu, W. J.; Song, W.; Lim, R. K. V.; Lin, Q. *Org. Lett.* **2008**, *10*, 3725-3728.
155. Yu, Z.; Ho, L. Y.; Wang, Z.; Lin, Q. *Bioorg. Med. Chem. Lett.* **2011**, *21*, 5033-5036.
156. Dietrich, M.; Delaittre, G.; Blinco, J. P.; Inglis, A. J.; Bruns, M.; Barner-Kowollik, C. *Adv. Funct. Mater.* **2012**, *22*, 304-312.
157. Rodriguez-Emmenegger, C.; Preuss, C.; Yameen, B.; Pop-Georgievski, O.; Bachmann, M.; Mueller, J. O.; Bruns, M.; Goldmann, A. S.; Bastmeyer, M.; Barner-Kowollik, C. **2013**, unpublished data.
158. de Hoog, H.-P. M.; Nallani, M.; Liedberg, B. *Polym. Chem.* **2012**, *3*, 302-306.
159. Dondoni, A. *Angew. Chem. Int. Ed.* **2008**, *47*, 8995-8997.
160. Griesbaum, K. *Angew. Chem. Int. Ed.* **1970**, *9*, 273-287.
161. Campos, L. M.; Killops, K. L.; Sakai, R.; Paulusse, J. M. J.; Damiron, D.; Drockenmuller, E.; Messmore, B. W.; Hawker, C. J. *Macromolecules* **2008**, *41*, 7063-7070.
162. Gress, A.; Völkel, A.; Schlaad, H. *Macromolecules* **2007**, *40*, 7928-7933.
163. ten Brummelhuis, N.; Diehl, C.; Schlaad, H. *Macromolecules* **2008**, *41*, 9946-9947.
164. Pounder, R. J.; Stanford, M. J.; Brooks, P.; Richards, S. P.; Dove, A. P. *Chem. Commun.* **2008**, 5158-5160.

165. Hoogenboom, R. *Angew. Chem. Int. Ed.* **2010**, *49*, 3415-3417.
166. Rosen, B. M.; Lligadas, G.; Hahn, C.; Percec, V. *J. Polym. Sci. Part A: Polym. Chem.* **2009**, *47*, 3940-3948.
167. Rosen, B. M.; Lligadas, G.; Hahn, C.; Percec, V. *J. Polym. Sci. Part A: Polym. Chem.* **2009**, *47*, 3931-3939.
168. Shin, J.; Matsushima, H.; Chan, J. W.; Hoyle, C. E. *Macromolecules* **2009**, *42*, 3294-3301.
169. Xu, J.; Tao, L.; Boyer, C.; Lowe, A. B.; Davis, T. P. *Macromolecules* **2010**, *43*, 20-24.
170. Li, H.; Yu, B.; Matsushima, H.; Hoyle, C. E.; Lowe, A. B. *Macromolecules* **2009**, *42*, 6537-6542.
171. Heredia, K. L.; Tolstyka, Z. P.; Maynard, H. D. *Macromolecules* **2007**, *40*, 4772-4779.
172. Pauloehrl, T.; Delaittre, G.; Bruns, M.; Meißler, M.; Börner, H. G.; Bastmeyer, M.; Barner-Kowollik, C. *Angew. Chem. Int. Ed.* **2012**, *51*, 9181-9184.
173. Gody, G.; Rossner, C.; Moraes, J.; Vana, P.; Maschmeyer, T.; Perrier, S. *J. Am. Chem. Soc.* **2012**, *134*, 12596-12603.
174. Singh, I.; Zarafshani, Z.; Lutz, J.-F. o.; Heaney, F. *Macromolecules* **2009**, *42*, 5411-5413.
175. Zeon Web Page. <http://www.zeonchemicals.com/nipol/>.
176. Eni Web Page. [http://www.eni.com/en\\_IT/products-services/elastomers/elastomers.shtml](http://www.eni.com/en_IT/products-services/elastomers/elastomers.shtml).
177. Lanxess Web Page. <http://lanxess.de/de/corporate/produkte-loesungen/business-units/high-performance-elastomers/>.
178. Mori, T.; Kondo, T.; Ohtake, Y. *Nippon Gomu Kyokaishi* **2011**, *84*, 182-188.
179. Therban Web Page. [http://therban.com/therban/en/about/why\\_use\\_therban/](http://therban.com/therban/en/about/why_use_therban/).
180. Lanxess Web Page. <http://techcenter.lanxess.com/hpe/emea/en/products/description/article.jsp?docId=4048>.
181. Therban Web Page. [http://therban.com/therban/en/about/success\\_stories/oil\\_well\\_specialities/](http://therban.com/therban/en/about/success_stories/oil_well_specialities/).
182. Coran, A. Y. *J. Appl. Polym. Sci.* **2003**, *87*, 24-30.

183. Hertz, D. L.; Bussem, H.; Ray, T. W. *Rubber Chem. Technol.* **1995**, *68*, 540-546.
184. Smith, W. V.; Ewart, R. H. *J. Chem. Phys.* **1948**, *16*, 592-599.
185. Kaiser, A.; Brandau, S.; Klimpel, M.; Barner-Kowollik, C. *Macromol. Rapid Commun.* **2010**, *31*, 1616-1621.
186. Buding, H.; Fiedler, P.; Königshofen, H.; Thörmer, J. *Hydrierung nitrilgruppenhaltiger ungesättigter Polymerer*. DE Pat., 3433392 A1, 1986.
187. Cherubin, T. *Über die Bestimmung von Copolymerisationsparametern in der radikalischen Copolymerisation von Acrylnitril mit Butadien*. Ph.D. Thesis, University of Essen, 1999.
188. Hollbeck, C.; Bandermann, F.; Gunther, C. *Angew. Makromol. Chem.* **1996**, *242*, 47-64.
189. Bardeck, S. *Kinetik der Nitril-Butadien-Kautschuk-Synthese in Lösung*. Ph.D. Thesis, University of Essen, 1996.
190. Dürr, C. J.; Emmerling, S. G. J.; Kaiser, A.; Brandau, S.; Habicht, A. K. T.; Klimpel, M.; Barner-Kowollik, C. *J. Polym. Sci. Part A: Polym. Chem.* **2012**, *50*, 174-180.



# 3 ■ High Molecular Weight Acrylonitrile-Butadiene Architectures via a Combination of RAFT Polymerization and Orthogonal Copper Mediated Azide-Alkyne Cycloaddition\*

## 3.1 Introduction

In the solution-based RAFT mediated copolymerization of acrylonitrile (AN) and 1,3-butadiene (BD), recently reported by Kaiser *et al.*,<sup>1</sup> molecular weights up to 60 000 g·mol<sup>-1</sup> with  $\bar{D} < 2.0$  and conversions above 50% within 9 h reaction time were obtained. The living character of the process was evidenced by a linear relation between molecular weight and conversion, as well as the possibility to perform chain extension after isolation of the polymer. The process was further optimized with regard to its experimental conditions<sup>2</sup> and is most probably one of the reversible-deactivation radical polymerization processes closest to a large-scale industrial application.<sup>3-4</sup> The present chapter extends the scope of the recently developed RAFT mediated copolymerization of AN and BD toward the synthesis of chain-end functionalized nitrile-butadiene rubbers (NBRs) as well as the incorporation of functional moieties and their utilization in modular ligation chemistry protocols.

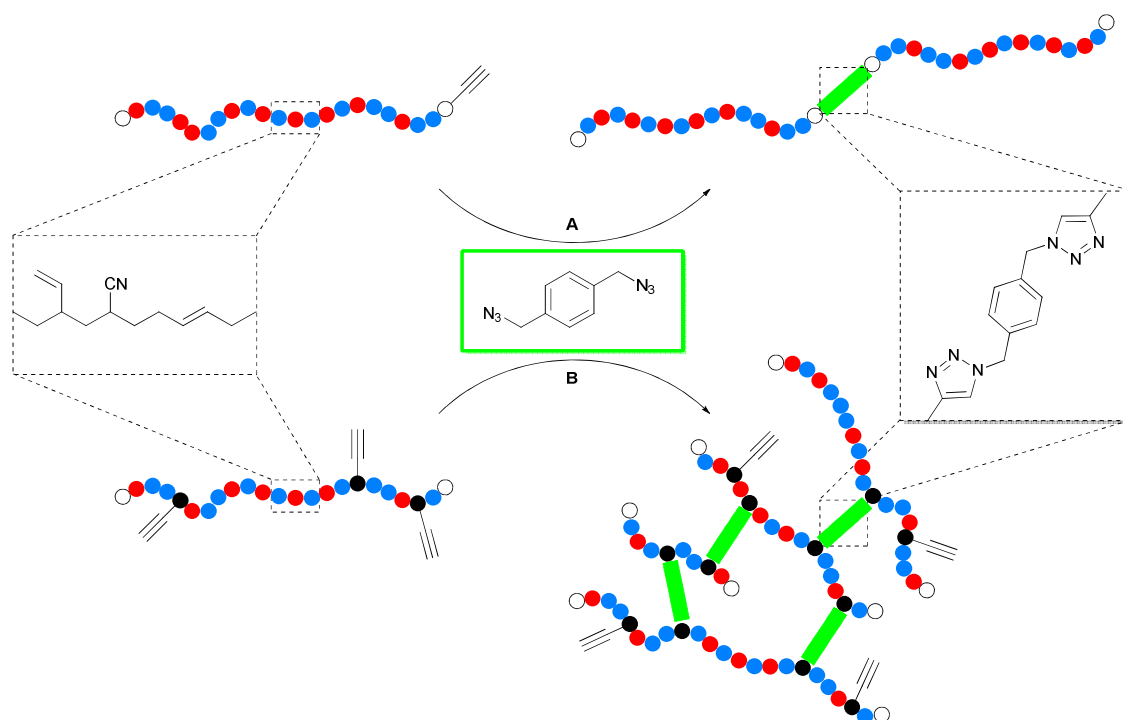
The application of modular ligation chemistry techniques for the synthesis of complex macromolecular architectures has been investigated intensively in recent years.<sup>5-11</sup> Modular ligation chemistry has been applied to polymers of all kind of origin, composition and functionality. Examples, however, mainly focus on

---

\* Dürr, C. J.; Emmerling, S. G. J.; Lederhose, P.; Kaiser, A.; Brandau, S.; Klimpel, M.; Barner-Kowollik, C. *Polym. Chem.* **2012**, *3*, 1048-1060. DOI: 10.1039/C2PY00547F – Reproduced and adapted by permission of the Royal Society of Chemistry.

polymers with molecular weights of less than  $40\,000\text{ g}\cdot\text{mol}^{-1}$ .<sup>12-13</sup> In contrast, examples of macromolecular conjugation of two polymer strands yielding polymers with molecular weights higher  $40\,000\text{ g}\cdot\text{mol}^{-1}$  are rare.<sup>14</sup> Inglis *et al.* reported the synthesis of block copolymers of polystyrene and poly(isobornyl acrylate) of up to  $100\,000\text{ g}\cdot\text{mol}^{-1}$  via a combination of RAFT polymerization and ultrafast hetero-Diels–Alder chemistry.<sup>15</sup> Their block copolymers exhibit the highest reported molecular weight obtained by modular conjugation of polymer building blocks to date. The method suffers, however, from the necessity to perform two post-polymerization modification steps.

In the present chapter an approach toward the synthesis of NBR of high molecular weight under preservation of a linear microstructure is presented. For this purpose a novel alkyne-functional trithiocarbonate **2** was synthesized and employed in RAFT polymerization. A copper mediated Huisgen cycloaddition upon addition of an aromatic diazido compound was subsequently performed (see Scheme 3.1A). Earlier studies showed that NBR with molecular weights higher



**Scheme 3.1.** Utilization of 1,4-bis(azidomethyl)benzene for the formation of high molecular weight AN-BD architectures. A)  $\alpha$ -Functional NBRs are employed for the formation of linear polymers. B) The utilization of NBR with alkyne moieties distributed among the polymer backbone affords crosslinked polymeric structures.

60 000 g·mol<sup>-1</sup> and low dispersity cannot be obtained via a classical sequential RAFT process.<sup>1</sup> The modular ligation technique is a powerful route to allow the synthesis of narrowly distributed AN-BD copolymers within a commercially interesting molecular weight range above 60 000 g·mol<sup>-1</sup>. Moreover, the incorporation of alkyne functions into the polymer was proven to be an efficient tool for the controlled crosslinking of linear AN-BD copolymer strands (see Scheme 3.1B) as well as the introduction of short chain branches, as for example alkyl moieties. The herein reported results provide the first successful approach to apply modular conjugation techniques for the generation of the industrially highly important polymer class.

## 3.2 Experimental Section

### 3.2.1 Materials

Acrylonitrile (AN, > 99%, Acros), 1,3-butadiene (BD, > 99.5%, Air Liquide), *N,N'*-dicyclohexylcarbodiimide (DCC, 99%, Acros), 4-(dimethylamino)pyridine (DMAP, 99%, Aldrich), methacryloyl chloride (purum, Fluka), propargyl alcohol (99%, Acros), triethyl amine (99%, ABCR), 1,4-bis(bromomethyl)benzene (98%, Acros), 1-bromoundecane (> 97%, Fluka), sodium azide (99%, Acros), copper sulfate pentahydrate (98+%, Aldrich), sodium (L)-ascorbate (> 98%, Aldrich), 1,1'-azobis(cyclohexane-1-carbonitrile) (98%, Aldrich), chlorobenzene (Acros, 99+%), *N,N*-dimethylacetamide (Acros, 99.5%) and *N,N*-dimethylformamide (DMF, Alfa Aesar, 99%) were used without further purification. Other solvents (p. a.) were obtained from VWR and used as received. 2-((dodecylsulfanyl)-carbonothioyl)sulfanyl propanoic acid (DoPAT, **1**) was obtained from Orica Pty Ltd., Melbourne, Australia. 1,4-bis(azidomethyl)benzene,<sup>16</sup> 1-azidoundecane,<sup>17</sup> 3-(trimethylsilyl)propargyl alcohol<sup>18</sup> and prop-2-yn-1-yl methacrylate<sup>19</sup> were synthesized according to the literature.

### 3.2.2 Synthesis of the Alkyne-Functional RAFT Agent Prop-2-yn-1-yl 2-(((dodecylsulfanyl)carbonothioyl)-sulfanyl)propanoate (**2**)

DoPAT (**1**, 12.000 g, 34.2 mmol), propargyl alcohol (6.276 g, 112.0 mmol) and DMAP (0.834 g, 6.8 mmol) were dissolved in dry methylene chloride (50 mL) and cooled to 0 °C. A solution of DCC (7.056 g, 34.2 mmol) in dry methylene chloride (10 mL) was added, the cooling bath was removed and the mixture was stirred overnight at ambient temperature. The white precipitate was filtered off, methylene chloride (100 mL) was added, the solution was extracted with 0.5 N hydrochloric acid (2 × 100 mL) and washed with saturated NaHCO<sub>3</sub> solution (100 mL). The organic layer was dried over MgSO<sub>4</sub> and concentrated under reduced pressure. The crude product was purified via column chromatography on silica gel with hexane/ethyl acetate (10:1, v/v, R<sub>f</sub> 0.73) as the eluent and dried under high vacuum to yield the RAFT agent **2** (8.409 g, 64%) as a yellow oil.

<sup>1</sup>H NMR (400 MHz, CDCl<sub>3</sub>) δ 4.84 (q, *J* = 7.4 Hz, 1H, CH(CH<sub>3</sub>)), 4.72 (d, *J* = 2.4 Hz, 2H, C(O)-O-CH<sub>2</sub>), 3.34 (t, *J* = 7.4 Hz, 2H, S-CH<sub>2</sub>), 2.49 (t, *J* = 2.5 Hz, 1H, C≡CH), 1.74 – 1.63 (m, 2H, S-CH<sub>2</sub>-CH<sub>2</sub>), 1.61 (d, *J* = 7.4 Hz, 3H, CH(CH<sub>3</sub>)), 1.46 – 1.34 (m, 2H, S-CH<sub>2</sub>-CH<sub>2</sub>-CH<sub>2</sub>), 1.34 – 1.16 (m, 16H, aliphatic Hs), 0.87 (t, *J* = 6.9 Hz, 3H, CH<sub>2</sub>-CH<sub>3</sub>).

<sup>13</sup>C NMR (101 MHz, CDCl<sub>3</sub>) δ 221.77 (S-C(S)), 170.55 (O-C(O)), 77.13, 75.52, 53.24, 47.69, 37.42, 32.01, 29.72, 29.65, 29.53, 29.44, 29.19, 29.00, 27.96, 22.79, 16.80, 14.22.

Elemental analysis calculated (%) for C<sub>19</sub>H<sub>32</sub>O<sub>2</sub>S<sub>3</sub>: C, 58.72; H, 8.30; O, 8.23; S, 24.75, found: C, 58.13; H, 8.07; O, 8.23; S, 24.75.

### 3.2.3 Synthesis of TMS Protected Alkyne-Functional RAFT Agent (**2-TMS**)

The trimethylsilyl (TMS) protected alkyne-functional trithiocarbonate **2-TMS** was synthesized similar to controlling agent **2** from DoPAT (**1**) and 3-(trimethylsilyl)propargyl alcohol. The crude product was purified via column chromatography on silica gel with hexane/ethyl acetate (20:1, v/v, R<sub>f</sub> 0.53) and yielded as a yellow oil (74%).

<sup>1</sup>H NMR (400 MHz, CDCl<sub>3</sub>) δ 4.82 (q, *J* = 7.4 Hz, 1H, CH(CH<sub>3</sub>)), 4.72 (s, 2H, C(O)-O-CH<sub>2</sub>), 3.34 (t, *J* = 7.4 Hz, 2H, S-CH<sub>2</sub>), 1.75 – 1.63 (m, 2H, S-CH<sub>2</sub>-CH<sub>2</sub>), 1.60 (d, *J* =

7.4 Hz, 3H, CH(CH<sub>3</sub>)), 1.44 – 1.33 (m, 2H, S-CH<sub>2</sub>-CH<sub>2</sub>-CH<sub>2</sub>), 1.33 – 1.15 (m, 16H, aliphatic Hs), 0.87 (t, *J* = 6.9 Hz, 3H, CH<sub>2</sub>-CH<sub>3</sub>), 0.18 (s, 9H, Si(CH<sub>3</sub>)<sub>3</sub>).

<sup>13</sup>C NMR (101 MHz, CDCl<sub>3</sub>) δ 221.77 (S-C(S)), 170.53 (O-C(O)), 98.45, 92.82, 54.04, 47.86, 37.39, 32.02, 29.73, 29.65, 29.54, 29.45, 29.19, 29.02, 28.00, 22.80, 16.83, 14.23, -0.23 (Si(CH<sub>3</sub>)<sub>3</sub>).

### 3.2.4 Synthesis of Bis-Triazole Model Compound 6

A solution of RAFT agent **2** (151.4 mg, 0.390 mmol), 1,4-bis(azidomethyl)benzene (36.7 mg, 0.195 mmol), CuSO<sub>4</sub>·5H<sub>2</sub>O (9.7 mg, 0.039 mmol) and sodium ascorbate (7.7 mg, 0.039 mmol) in DMF (2 mL) was stirred for 16 h at ambient temperature. The mixture was filtered over a short column of neutral aluminum oxide and concentrated under reduced pressure to quantitatively give **6** as determined via NMR. However, an additional faint spot was observed in TLC and the product was further purified by column chromatography on silica gel using hexane/ethyl acetate (1:1, v/v, *R*<sub>f</sub> 0.68) as the eluent for analysis.

<sup>1</sup>H NMR (400 MHz, CDCl<sub>3</sub>) δ 7.53 (s, 2H, triazole-H), 7.27 (s, 4H, C<sub>6</sub>H<sub>4</sub>), 5.51 (s, 4H, N-CH<sub>2</sub>), 5.25 (s, 4H, CH<sub>2</sub>-O), 4.77 (q, *J* = 7.4 Hz, 2H, CH(CH<sub>3</sub>)), 3.35 – 3.27 (m, 4H, S-CH<sub>2</sub>), 1.72 – 1.61 (m, 4H, S-CH<sub>2</sub>-CH<sub>2</sub>), 1.55 (d, *J* = 7.4 Hz, 6H, CH(CH<sub>3</sub>)), 1.42 – 1.32 (m, 4H, S-CH<sub>2</sub>-CH<sub>2</sub>-CH<sub>2</sub>), 1.33 – 1.18 (m, 32H, aliphatic Hs), 0.87 (t, *J* = 6.9 Hz, 6H, CH<sub>2</sub>-CH<sub>3</sub>).

<sup>13</sup>C NMR (101 MHz, CDCl<sub>3</sub>) δ 221.88 (S-C(S)), 171.09 (O-C(O)), 142.90, 135.19, 128.79, 123.91, 58.88, 53.66, 47.80, 37.32, 31.91, 29.62, 29.55, 29.44, 29.33, 29.10, 28.92, 27.86, 22.68, 16.69, 14.12.

Elemental analysis (%) calculated for C<sub>103</sub>H<sub>168</sub>N<sub>6</sub>O<sub>10</sub>S<sub>15</sub>: C, 57.22; H, 7.52; N, 8.70; O, 6.63; S, 19.93, found: C, 57.63; H, 7.48; N, 8.79; O, 6.23; S, 20.37.

### 3.2.5 Synthesis of Acrylonitrile-Butadiene Copolymers with Terminal Alkyne Functionality (3)

Copolymers of AN and BD were synthesized in a pressurized glass reactor utilizing a setup described earlier.<sup>1</sup> A general procedure is provided for experiment II, all other polymerizations were performed in a similar manner. The respective concentrations of initiator, RAFT agent and monomers are given in Table 3.1 (see

page 59). Alkyne-functional RAFT agent **2** (996.1 mg, 2.56 mmol), AN (21.7 mL, 330 mmol) and 1,1'-azobis(cyclohexane-1-carbonitrile) (78.2 mg, 0.32 mmol) were dissolved in chlorobenzene (25 mL). The solution was purged with nitrogen for 10 min and transferred into a pressure stable glass reactor. Oxygen was removed from the reactor by three vacuum/nitrogen cycles and BD (45 mL, 541 mmol) was added via a metal burette. The reactor was sealed and heated with an oil bath. By the time the bath temperature reached 100 °C, the starting time was set. Samples were taken at pre-set time intervals and monomer conversion was determined gravimetrically. Thus the weight of the samples was determined before and after removing all volatile components at 110 °C in a vacuum oven. Additionally, at each time interval samples were taken for the determination of molecular weights by precipitating the hot polymer solution in cold ethanol. The supernatant was discarded and polymers were dried in high vacuum. The reaction was stopped by removing the heating bath, the reactor was depressurized and the polymer was isolated by precipitating the polymer solution in cold ethanol. The supernatant was discarded; the polymer was dried in vacuum and analyzed by size exclusion chromatography (SEC) and NMR spectroscopy.

### 3.2.6 Synthesis of Acrylonitrile-Butadiene-Prop-2-ynyl Methacrylate

#### Terpolymer 7

A terpolymer of AN, BD and prop-2-ynyl methacrylate (PMA) was synthesized in analogy to AN-BD copolymers. AN (4.7 mL, 71.4 mmol), PMA (2.350 g, 18.9 mmol), 1,1'-azobis(cyclohexane-1-carbonitrile) (0.030 g, 0.125 mmol) and DoPAT (**1**, 0.439 g, 1.250 mmol) were dissolved in *N,N*-dimethylacetamide (5 mL) and degassed with nitrogen for 10 minutes. The solution was transferred into the glass reactor and oxygen was removed with three vacuum/nitrogen cycles. BD (9.6 mL, 115.4 mmol) was added, the vessel was sealed and heated for 5 h to 100 °C. The heating source was removed, the reactor was depressurized and the solution was poured into a cold mixture of hexane/diethyl ether (2:1, v/v) before drying in high vacuum, yielding terpolymer **7** ( $M_n$  3900 g·mol<sup>-1</sup>,  $D = 1.3$ ).

### 3.2.7 Typical Procedure for the Coupling of NBR Building Blocks

Alkyne-functional NBR **3**, CuSO<sub>4</sub>·5H<sub>2</sub>O and sodium ascorbate were weighed into a glass vial and the appropriate volume of a stock solution of 1,4-bis(azidomethyl)benzene in DMF was added. The reaction was stirred for 16 h at ambient temperature, filtered over a short column of neutral aluminum oxide and concentrated in vacuum to afford NBR **5**. Conjugated polymers with molecular weights > 15 000 g·mol<sup>-1</sup> were diluted with 2 mL of DMF prior to filtration to facilitate a fast elution of the polymer from the aluminum oxide column. Detailed information for each experiment is provided in Table 3.3 in the *Appendix* at the end of the current chapter.

### 3.2.8 Modification of Acrylonitrile-Butadiene-Prop-2-ynyl Methacrylate Terpolymers with 1-Undecane azide

1-undecane azide (44 mg, 0.22 mmol), terpolymer **7** (50 mg, 0.013 mmol), CuSO<sub>4</sub> pentahydrate (2.8 mg, 0.11 mmol) and sodium ascorbate (2.5 mg, 0.013 mmol) were stirred for 16 h in DMF (0.5 mL) at ambient temperature. The mixture was filtered over a short column of neutral aluminum oxide and concentrated in vacuum to give polymer **8** ( $M_n$  5900 g·mol<sup>-1</sup>,  $D = 1.2$ ).

### 3.2.9 General Procedure for the Copper Mediated Crosslinking of Terpolymer 7

In a typical procedure, terpolymer **7** (60 mg), CuSO<sub>4</sub>·5H<sub>2</sub>O (1.9 mg, 0.008 mmol) and sodium ascorbate (1.5 mg, 0.008 mmol) were weighted into a glass vial. The appropriate amount of a 1,4-bis(azidomethyl)benzene (**4**) stock solution was added and the mixture was stirred in DMF for 16 h. After filtration over neutral aluminum oxide the solvent was removed under reduced pressure. More detailed information for each experiment is provided in Table 3.4 in the *Appendix* at the end of the current chapter.

### 3.2.10 Instrumentation

<sup>1</sup>H NMR and <sup>13</sup>C NMR spectra were recorded at room temperature on a Bruker Advance 400 NMR and referenced to the remaining solvent signal.

Molecular weight determination was performed on a SEC system (PL-GPC 50 Plus, Polymer Laboratories) consisting of an auto injector, a guard column (PLgel Mixed C, 50 × 7.5 mm), three linear columns (PLgel Mixed C, 300 × 7.5 mm, 5 μm bead-size) and a differential refractive index detector using tetrahydrofuran (THF) as the eluent at 35 °C and a flow rate of 1 mL·min<sup>-1</sup>. The system was calibrated using narrow polystyrene (PS) standards (obtained from PSS) ranging from 160 to 6 × 10<sup>6</sup> g·mol<sup>-1</sup>. Samples were injected from solutions in THF (2 mg·mL<sup>-1</sup>) and molecular weight distributions were referenced versus PS standards (Mark-Houwink-Kuhn-Sakurada parameters for PS:  $\alpha = 0.70$ ,  $K = 14.1 \times 10^{-5}$  dL·g<sup>-1</sup>).

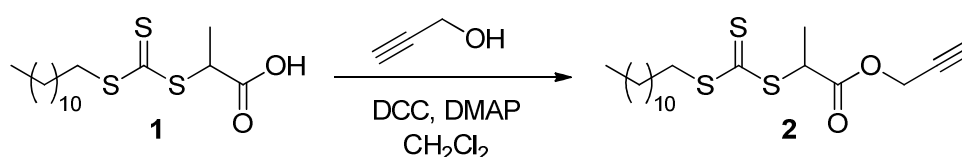
SEC-electrospray ionization mass spectrometry (ESI-MS) spectra were recorded on a LXQ mass spectrometer (ThermoFisher Scientific, San Jose, CA, USA) equipped with an atmospheric pressure ionization source operating in the nebulizer assisted electrospray mode. The system was calibrated with a standard containing caffeine, Met-Arg-Phe-Ala acetate and a mixture of fluorinated phosphazenes (Ultramark 1621), purchased from Aldrich. A spray voltage of 4.5 kV, a dimensionless sweep gas flow rate of 2 and a dimensionless sheath gas flow-rate of 12 were applied. The capillary voltage, the tube lens offset voltage and the capillary temperature were set to 60 V, 110 V and 275 °C. The mass spectrometer was coupled to a Series 1200 HPLC-system (Agilent, Santa Clara, CA, USA) with THF as the eluent in accordance to a setup described earlier.<sup>20</sup> Polymer samples were dissolved in THF in concentrations of 2 mg·mL<sup>-1</sup> and injected onto the HPLC-system.

### 3.3 Results and Discussion

#### 3.3.1 RAFT Agent Synthesis

The RAFT polymerization is widely used for the synthesis of end-functionalized polymers.<sup>21-23</sup> The RAFT polymerization technique produces polymers incorporating the R- and Z-group of the RAFT agent, *e.g.* dithioesters or trithiocarbonates. The R- and Z-groups are relocated at the  $\alpha$ - and  $\omega$ -chain-ends of the macromolecule, respectively.<sup>24</sup> The first aim was the synthesis of end-functionalized AN-BD copolymers and their application in the conjugation with a second NBR polymer chain. As noted above, the key point of the current chapter

aims at generating high molecular weight NBRs with low dispersities, which are not obtainable via a classical sequential RAFT process. Copper mediated azide-alkyne cycloaddition was chosen as the conjugation technique due to its selectivity and orthogonality to a wide variety of functional groups. A novel alkyne-functional RAFT agent **2** was synthesized with good yields in this context. A Steglich esterification of DoPAT (**1**) with propargyl alcohol using *N,N'*-dicyclohexylcarbodiimide (DCC) as the coupling reagent and catalytic amounts of 4-(dimethylamino)pyridine (DMAP) as shown in Scheme 3.2 was carried out. The R-group approach was chosen as herein all polymer chains formed within the RAFT process – the RAFT polymer as well as growing chains terminated via disproportionation or recombination – possess the alkyne functionality. The trithiocarbonate **2** was



**Scheme 3.2.** Synthesis of alkyne-functional RAFT agent **2** via Steglich esterification.

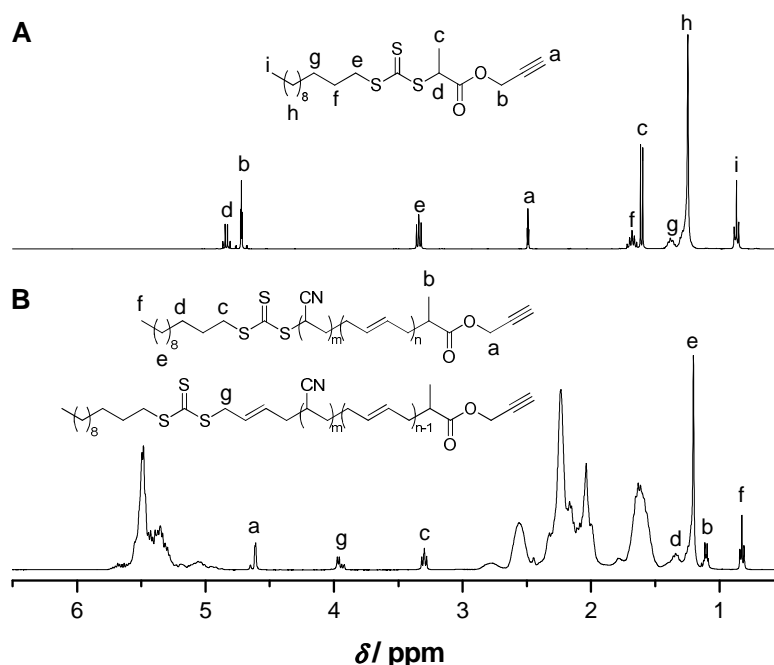
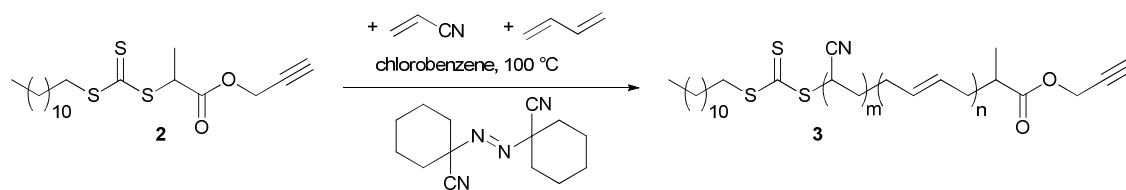


**Figure 3.1.** <sup>1</sup>H NMR characterization of A) alkyne-functional trithiocarbonate **2** and B) 6300 g·mol<sup>-1</sup> (PS reference) alkyne terminal AN-BD copolymer obtained via RAFT mediated copolymerization using RAFT agent **2**. A complete assignment of the NBR backbone proton signals was published elsewhere.<sup>25</sup>



**Scheme 3.3.** Reversible-deactivation radical polymerization using trithiocarbonate **2** and 1,1'-azobis(cyclohexane-1-carbonitrile) at 100 °C in chlorobenzene for the synthesis of statistical copolymers of AN and BD. 1,2-Linked incorporation of BD is observed but omitted for clarity.

characterized by elemental analysis and NMR spectroscopy. Elemental analysis was in agreement with the calculated results. Peak assignments of the proton signals are provided in Figure 3.1A, demonstrating the presence of the alkyne resonances around 2.5 ppm (a) and 4.7 ppm (b), respectively. A Fourier transform IR spectrum is depicted in Figure 3.11A in the *Appendix* at the end of the present chapter. A strong  $C\equiv C-H$  stretching vibration absorption band at  $3300\text{ cm}^{-1}$  provides further evidence for the presence of the terminal alkyne moiety. In previous studies on the reversible-deactivation radical copolymerization of AN and BD, DoPAT was proven to be a suitable controlling agent.<sup>1</sup> DoPAT was thus chosen as the underlying basic RAFT agent structure for the herein presented investigations. Ranjan and Brittain have previously synthesized a similar alkyne-functional RAFT agent based on a slightly different trithiocarbonate.<sup>26-27</sup>

### 3.3.2 RAFT Polymerizations

The novel alkyne-functional RAFT agent **2** was tested toward its ability to control the free radical copolymerization of AN and BD (see Scheme 3.3), *i.e.* to obtain linear polymers with an  $\alpha$ -functional alkyne moiety. Polymerizations were performed in a pressure stable glass reactor at 100 °C, using the high temperature azo initiator 1,1'-azobis(cyclohexane-1-carbonitrile) with a ten hour half-life decomposition temperature of 88 °C.<sup>28</sup> Chlorobenzene or *N,N*-dimethylacetamide was chosen as the solvent, since these were shown to be excellent media for RAFT mediated AN/BD copolymerization.<sup>2</sup> In the case of low molecular weight polymer unable to precipitate in common organic solvents (targeted  $M_n < 2000\text{ g}\cdot\text{mol}^{-1}$ ) acetone was employed to afford a simple isolation of the polymer via solvent evaporation. To reduce the number of dead polymer chains – and thus the number

of macromolecules unable to undergo a successive conjugation reaction – a RAFT agent to initiator ratio of 5:1 to 15:1, depending on the desired chain length, conversion and reaction time was chosen (for polymerization details see Table 3.1).

In a typical polymerization AN and BD were employed in the azeotropic ratio of 38 (AN) to 62 (BD) to enable a constant statistic incorporation of the monomers at each time during the polymerization. Samples were taken at pre-set time intervals and the conversion was determined gravimetrically by weight analysis before and after removing all volatile components in a vacuum oven. Subsequently, a sample was taken from the reaction mixture, precipitated in ethanol and analyzed by SEC. As at the time experiments and sample evaluation was performed, Mark–Houwink–Kuhn–Sakurada (MHKS) parameters were not available for NBR, molecular weights were thus calculated via conventional calibration and

**Table 3.1.** Experimental details of RAFT mediated polymerizations at 100 °C.<sup>a</sup>

exp.-No.	RAFT agent	[RAFT] <sub>0</sub> (mmol·L <sup>-1</sup> )	[Ini] <sub>0</sub> (mmol·L <sup>-1</sup> )	<i>t</i> <sup>b</sup> (h)	<i>p</i> <sup>c</sup> (%)		<i>M</i> <sub>n</sub> <sup>d</sup> (g·mol <sup>-1</sup> )	<i>D</i> <sup>d</sup>
I <sup>e,f</sup>	<b>2</b>	83.5	5.6	3	-	<b>3a</b>	1000	1.3
II <sup>g</sup>	<b>2</b>	27.9	3.5	5	19.1	<b>3b</b>	6300	1.2
III <sup>g</sup>	<b>2</b>	14.0	1.4	8	19.5	<b>3c</b>	10 300	1.3
IV <sup>g</sup>	<b>2</b>	1.7	0.2	22	10.9	<b>3d</b>	42 000	1.5
V <sup>g</sup>	<b>2</b>	0.9	0.2	22	10.0	<b>3e</b>	69 000	1.5
VI <sup>g</sup>	<b>2</b>	3.5	0.3	16	15.1	-	25 000	1.4
VII <sup>g</sup>	<b>2-TMS</b>	3.5	0.3	16	14.3	-	25 000	1.4
VIII <sup>f,h,i</sup>	<b>1</b>	57.8	5.8	5	-	<b>7</b>	3900	1.3
IX <sup>h</sup>	<b>1</b>	47.9	4.8	5	18.8	-	4000	1.2

<sup>a</sup> [RAFT]<sub>0</sub> is the initial concentration of RAFT agent. [Ini]<sub>0</sub> is the initial concentration of initiator 1,1'-azobis(cyclohexane-1-carbonitrile). Polymerizations were performed with an initial overall monomer concentration [M]<sub>0</sub> of 9.5 mol·L<sup>-1</sup>. Monomers are used in the azeotropic ratio of 62/38 (BD/AN). <sup>b</sup> The starting point of the reaction was set as the time the temperature of the heating bath reached 100 °C. <sup>c</sup> Gravimetrically determined conversion. <sup>d</sup> Obtained from SEC versus PS standards. <sup>e</sup> Solution in acetone, the polymer was recovered by solvent/monomer evaporation. <sup>f</sup> The total volume was too small for the determination of conversion. <sup>g</sup> Solution in chlorobenzene. <sup>h</sup> Solution in *N,N*-dimethylacetamide. <sup>i</sup> BD, AN and PMA were used in the ratio of 56:35:9 (*n/n/n*).

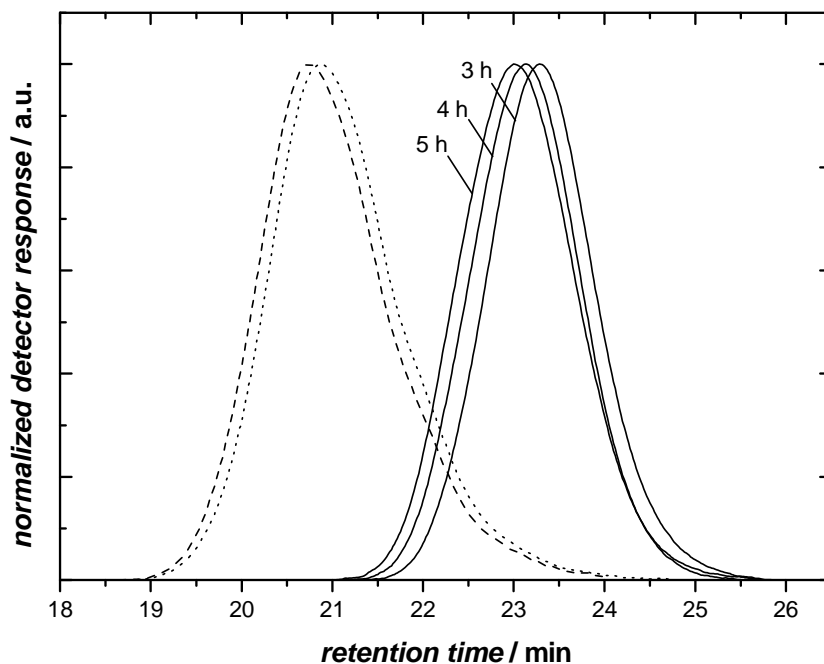


**Figure 3.2.** SEC traces for a selection of AN-BD copolymerization experiments at the azeotropic ratio of 62 (BD) to 38 (AN). The evolution of molecular weight with increasing reaction time is depicted for a RAFT mediated copolymerization in chlorobenzene at 100 °C using trithiocarbonate **2** (27.9 mmol·L<sup>-1</sup>, experiment II) after 3, 4 and 5 h (solid lines). The SEC traces clearly demonstrate the shift toward lower retention times with reaction time. SEC traces of comparative studies using unprotected RAFT agent **2** (dotted lines, experiment VI) and TMS protected RAFT agent **2-TMS** (dashed lines, experiment VII) under identical conditions are provided and do not exhibit pronounced differences in shape and position.

referenced to PS standards. Several polymerizations within a wide range of molecular weights were performed as summarized in Table 3.1. Trithiocarbonate **2** was employed in concentrations ranging from 83.5 mmol·L<sup>-1</sup> to 0.9 mmol·L<sup>-1</sup> to obtain alkyne-functional polymers with molecular weights from 1000 to 69 000 g·mol<sup>-1</sup>. RAFT agent **2** enabled good control over molecular weights with dispersities of up to 1.4 in each case. Polymers with  $M_n$  higher than 25 000 g·mol<sup>-1</sup> exhibit dispersities above this value. These data are in good agreement with previous results, providing RAFT mediated AN-BD copolymers with molecular weights up to 60 000 g·mol<sup>-1</sup> and dispersities ranging from 1.2 to 2.0, depending on the monomer to polymer conversion.<sup>1</sup> SEC traces shown in Figure 3.2 depict the time dependent evolution of molecular weights for a polymerization with a RAFT agent concentration of 27.9 mmol·L<sup>-1</sup> (experiment II) at 3, 4 and 5 h, respectively. Retention time decreased with increasing reaction time under preservation of the

distribution. However, all investigated polymers exhibit a slight tailing toward low molecular weights, most probably caused by the formation of dead polymeric chains.

The evolution of molar mass with conversion is depicted in Figure 3.3 and exhibits a linear dependency as expected for a reversible-deactivation radical polymerization. The discrepancy between experimental values represented by symbols and theoretical values represented by the solid lines may be explained with the inaccuracy of the molecular weights obtained from SEC via conventional calibration versus PS standards. In addition, a distinct hybrid behavior was observed, as molecular weights higher than  $DP_n = 1$  are obtained for the limit of zero conversion.<sup>29</sup> The hybrid behavior is more pronounced for polymerizations aimed at higher molecular weights (Figure 3.3B) than in the synthesis of polymers lower than  $10\,000\text{ g}\cdot\text{mol}^{-1}$  (Figure 3.3A).

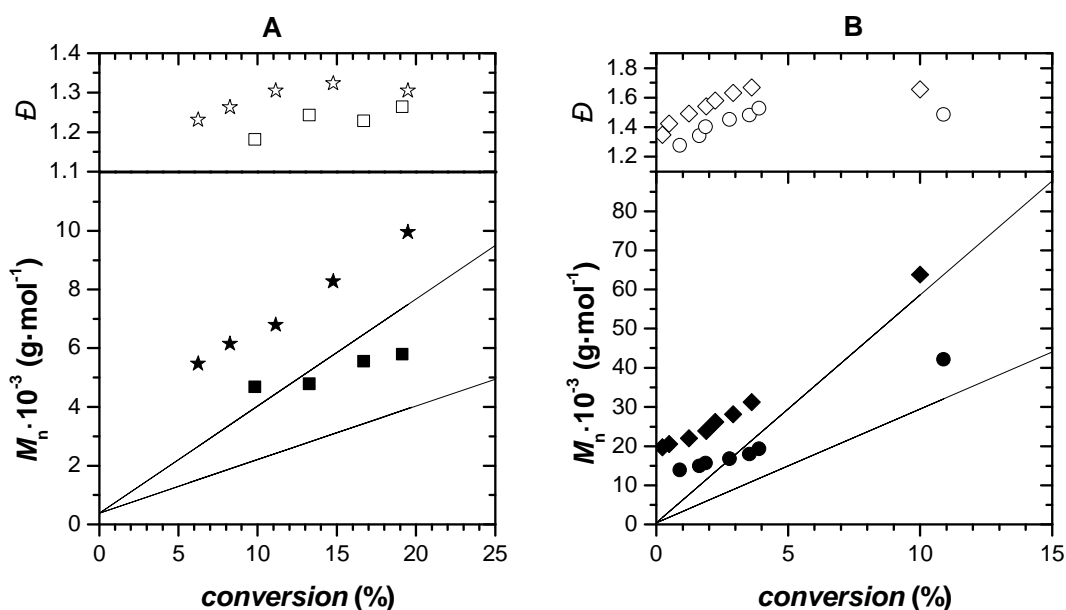


**Figure 3.3.** Evolution of molar mass (filled symbols) and  $\bar{D}$  (empty symbols) with conversion for several RAFT polymerizations using alkyne-functional RAFT agent **2**. Theoretically calculated molecular weights are indicated by solid lines. Conditions:  $100\text{ }^\circ\text{C}$ , initiator 1,1'-azobis(cyclohexane-1-carbonitrile), monochlorobenzene,  $[\text{M}]_0\text{ }9.5\text{ mol}\cdot\text{l}^{-1}$ . A) Experiment II:  $[\text{Ini}]_0\text{ }3.5\text{ mmol}\cdot\text{L}^{-1}$ ,  $[\mathbf{2}]_0\text{ }27.9\text{ mmol}\cdot\text{L}^{-1}$ , 5 h (boxes). Experiment III:  $[\text{Ini}]_0\text{ }1.4\text{ mmol}\cdot\text{L}^{-1}$ ,  $[\mathbf{2}]_0\text{ }14.0\text{ mmol}\cdot\text{L}^{-1}$ , 8 h (stars). B) Experiment IV:  $[\text{Ini}]_0\text{ }0.2\text{ mmol}\cdot\text{L}^{-1}$ ,  $[\mathbf{2}]_0\text{ }1.7\text{ mmol}\cdot\text{L}^{-1}$ , 22 h (circles). Experiment V:  $[\text{Ini}]_0\text{ }0.2\text{ mmol}\cdot\text{L}^{-1}$ ,  $[\mathbf{2}]_0\text{ }0.9\text{ mmol}\cdot\text{L}^{-1}$ , 22 h (rhombs).

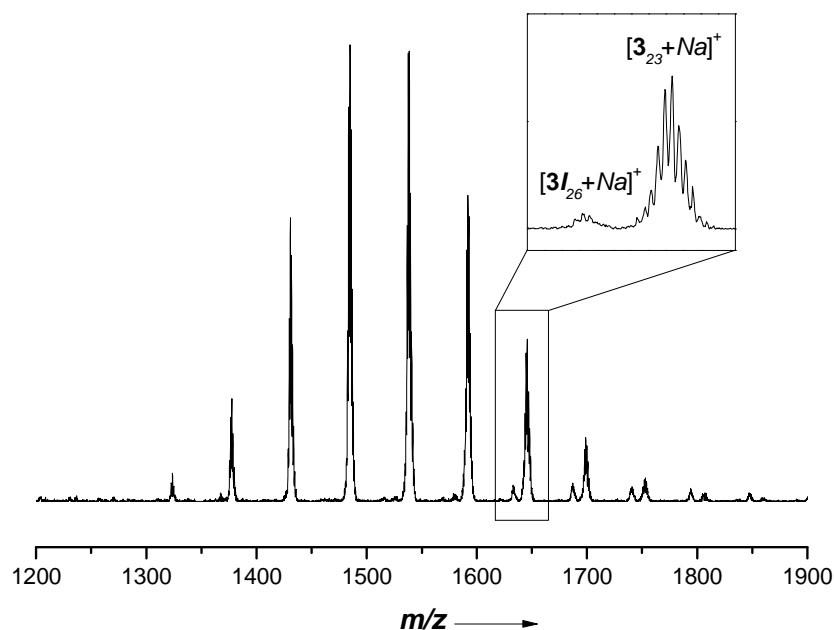


**Figure 3.4.** Section of the SEC-ESI mass spectra of alkyne-capped polymer **3** of  $6300 \text{ g}\cdot\text{mol}^{-1}$ . Signals repeat in intervals of 53 to 54 Da and are assigned to the sodium adducts of the alkyne-capped polymer  $[\mathbf{3}_{(m+n)}+\text{Na}]^+$  of various chain length,  $m+n$ . The small but yet resolved signals  $[\mathbf{3I}_{(m+n)}+\text{Na}]^+$  (see inset) are assigned to a polymer formed by the recombination of two growing polymer chains initiated by the azo initiator instead of the alkyne-functionalized R-group radical.

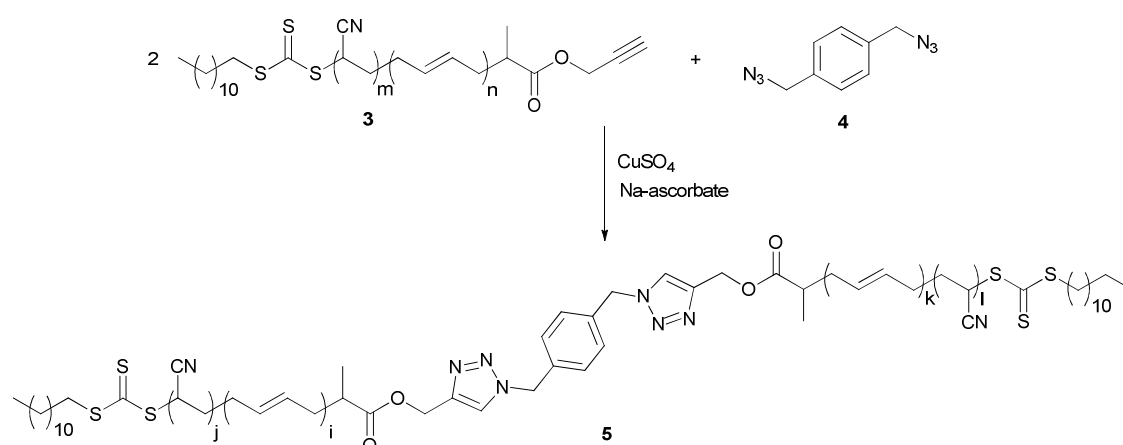
Low molecular weight AN-BD copolymers were investigated with SEC-ESI mass spectrometry to prove the formation of RAFT polymers with the respective R- and Z-groups. Figure 3.4 provides a section of the SEC-ESI mass spectrum of an alkyne-capped NBR of  $6300 \text{ g}\cdot\text{mol}^{-1}$ , obtained at the end of experiment II by precipitation of the polymer. Despite its potential ability to undergo radical reactions and to be incorporated into the polymer, no such interaction of the terminal alkyne moiety of RAFT agent **2** with the growing radical chain is observed under the experimental conditions. Main signals repeat in an interval of 53 to 54 Da and are assigned to the alkyne-capped polymers  $[\mathbf{3}_{(m+n)}+\text{Na}]^+$ . The rather unusual isotopic pattern (see inset) can be traced back to the superposition of the isotope pattern of copolymers with similar chain length  $m+n$  but different ratios of incorporated AN and BD  $m/n$  and is a direct result of the fact that molecular weights of AN and BD building blocks differ by only one atomic unit. Signals of very low yet resolved intensity are located in between the repeating signals of  $[\mathbf{3}_{(m+n)}+\text{Na}]^+$  and are assigned to NBRs  $[\mathbf{3I}_{(m+n)}+\text{Na}]^+$ . These NBRs **3I** are polymer strands that were initiated by the

fragment 1-cyanide-cyclohexyl of the azo initiator and terminated with a second 1-cyanide-cyclohexyl-initiated strand by recombination. These species – inaccessible for a successive utilization in modular conjugation – are an inevitable side product of the RAFT process, but are minimized in quantity by an appropriate choice of RAFT agent and initiator concentrations providing a high degree of alkyne-functional polymer.<sup>30</sup>

<sup>1</sup>H NMR spectroscopy was employed to further prove the formation of terminal alkyne moieties within the polymerization. A spectrum of a 6300 g·mol<sup>-1</sup> polymer **3b** is provided in Figure 3.1B (see page 57). Methylene protons of the propargyl alcohol resonate as doublet signals (a) around 4.6 ppm. Signals of the methyl protons (b) of the propanoate moiety are located at 1.2 ppm and thus shifted toward higher fields when compared to its signals in the RAFT agent structure (Figure 3.1A). Alkyl protons of the dodecyl tail (c, d, e, and f) exhibit only minor variation in its chemical shifts compared to trithiocarbonate **2**. The intensive doublet signals at 3.9 ppm (g) are assigned to the methylene protons in  $\alpha$ -position to the trithiocarbonate moiety of the final 1,4-incorporated BD. A 1,4-incorporated BD unit in  $\alpha$ -position to the trithiocarbonate is present in approximately 85-90% of all polymer chains, as determined by integration of signals c, f and g. Olefinic signals of the incorporated BD concentrate around 5.5 ppm. Aliphatic protons of the polymer backbone resonate between 1.5 ppm and 3.0 ppm and were previously assigned in more detail.<sup>25</sup> Fourier transform IR spectroscopy provides evidence for the incorporation of the terminal alkyne moiety, resonating at 3280 cm<sup>-1</sup> and further proving the incorporation of AN by the  $C\equiv N$  stretching vibration at 2240 cm<sup>-1</sup> (see Figure 3.11B in the *Appendix*). Moreover, SEC analysis of polymerizations utilizing TMS-protected RAFT agent **2-TMS** and unprotected compound **2** provides similar results, which serves as proof for the orthogonality of the alkyne moiety toward the incorporation into the polymer backbone. SEC traces provided in Figure 3.2 exhibit no substantial difference in shape and position of the curves using unprotected RAFT agent **2** (dotted lines, experiment VI) and protected alkyne-functional RAFT agent **2-TMS** (dashed lines, experiment VII).

### 3.3.3 Conjugation of NBR Building Blocks

The obtained alkyne-functional AN-BD building blocks were coupled in a copper mediated 1,3-dipolar Huisgen cycloaddition reaction. The application of azide-alkyne "click" reactions on polymer conjugation has been studied intensively for the formation of AB block copolymers.<sup>31-34</sup> However, no conjugation of AN-BD copolymers has been reported to date. A potential difficulty for the application of the copper mediated azide-alkyne cycloaddition on alkyne-capped NBR is the high density of functional groups present in the polymer backbone. Incorporated BD units retain an olefinic moiety, either internal when incorporated in a 1,4-fashion or terminal when incorporated in a 1,2-mode and might compete for the 1,3-dipolar cycloaddition with the  $\alpha$ -alkyne moiety present in much lower quantities. AN units are distributed along the polymer backbone and are known to interfere with transition metals such as copper. Coordination between the strongly polar nitrile moieties and transition metals can occur.<sup>35</sup> It was shown that nitrile-copper coordination within NBR/poly(vinyl chloride)/CuSO<sub>4</sub> blends is resulting in altered glass transition temperatures and swelling properties. In the study, physical crosslinks were established between chains by copper sulfate particles.<sup>36</sup> Golas *et al.* showed that the ligand free copper catalyzed cycloaddition of methyl 2-azidopropionate and propargyl alcohol decreases by a factor of 30 when replacing *N,N*-dimethylformamide with acetonitrile as the solvent. They explained



**Scheme 3.4.** Coupling of NBR building blocks via the copper mediated azide-alkyne cycloaddition of alkyne-functional NBR with a difunctional aromatic azide, 1,4-bis(azidomethyl)benzene (**4**).

their observation with a coordination of copper to the nitrile reducing the formation of the copper-acetylide complex. Moreover, a negative effect of the nitrile moieties in substrates such as poly(styrene-*co*-acrylonitrile) on copper catalyzed cycloaddition reactions was suggested.<sup>37</sup>

The coupling of two alkyne-functional NBR building blocks was the first aim of the study presented in the current chapter. Coupling occurred upon addition of a difunctional aromatic azide, 1,4-bis(azidomethyl)benzene (**4**, see Scheme 3.4) in

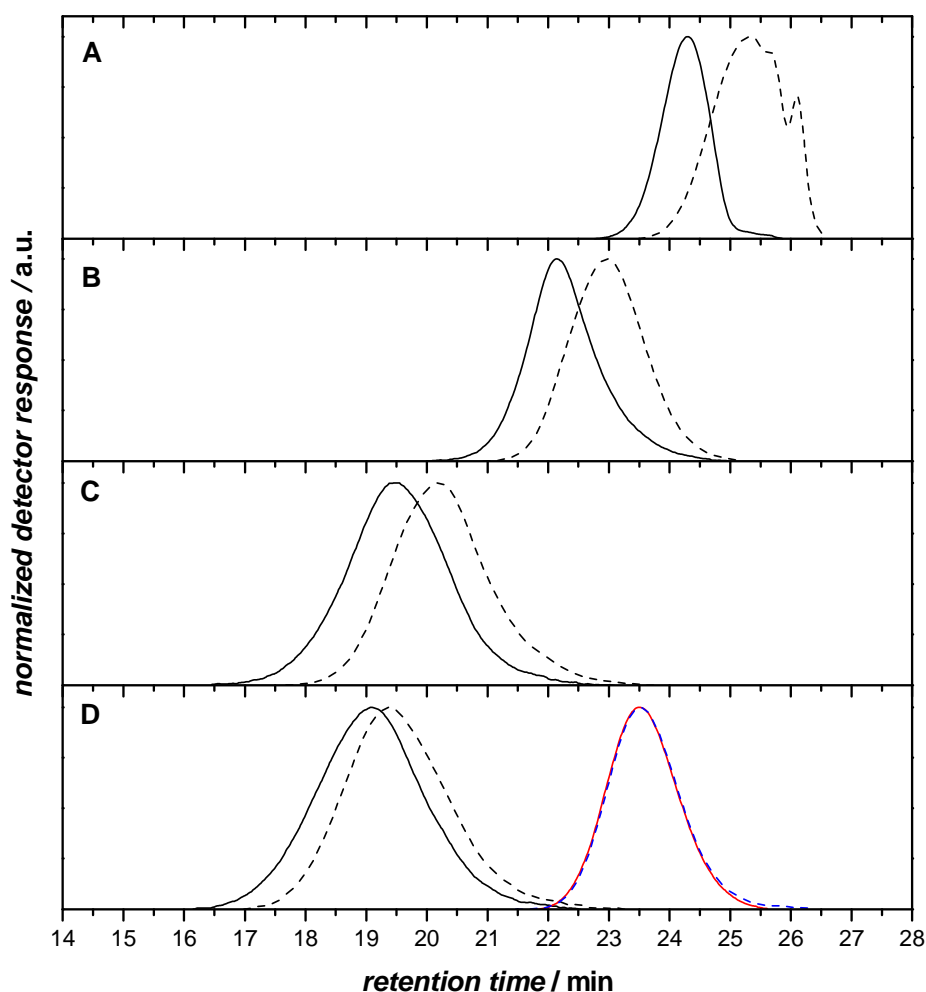


**Figure 3.5.** SEC traces of alkyne-functional NBR **3** (dashed lines) and the respective (long-chain) polymers **5** obtained via azide-alkyne cycloaddition (solid lines). A) Conjugation experiment 1 yielding 2500 g·mol<sup>-1</sup> polymer **5a**. B) Conjugation experiment 2 yielding 10 600 g·mol<sup>-1</sup> polymer **5b**. C) Conjugation experiment 4 yielding 72 000 g·mol<sup>-1</sup> polymer **5d**. D) Conjugation experiment 5 yielding 97 000 g·mol<sup>-1</sup> polymer **5e**. As depicted in layer D), comparative exposure of an 4200 g·mol<sup>-1</sup> alkyne-free carboxylic acid terminal NBR (blue dashed line) to 1,4-bis(azidomethyl)benzene under similar conditions does not lead to a significantly altered molecular weight distribution (red line).

the presence of  $\text{CuSO}_4$  pentahydrate and sodium ascorbate under air. A central challenge for the exhaustive conjugation of polymer strands was proven to meet the exact stoichiometric conditions of NBR to aromatic diazide (0.5 equivalents). Both an over- and underestimation of the required amount of diazide might lead to an incomplete ligation reaction. The required ratio of alkyne and azido compound can merely be approximately estimated since molecular weights of the investigated copolymers were obtained from conventional calibration SEC analysis without knowledge of the actual MHKS parameters of NBR. Stoichiometric variations were thus necessary. Figure 3.5 provides SEC results for several conjugation experiments with alkyne-functional polymers of various chain lengths. SEC traces of the coupled polymer blocks **5** are represented by solid lines and the respective alkyne-functional polymer **3** by dashed lines. All coupling products **5** depict a distinct shift toward lower retention time and thus toward higher molecular weight in comparison to the starting material **3**, while the unimodal shape of all curves is conserved. Molar mass and dispersity data of alkyne-functional polymers and the respective conjugation products are summarized in Table 3.2, experimental details of each conjugation experiment can be found in Table 3.3 in the *Appendix*.

Figure 3.5A provides SEC traces of a  $1000 \text{ g}\cdot\text{mol}^{-1}$  alkyne-functional polymer (**3a**, dashed line) and the respective conjugation product (**5a**, solid line) obtained via cycloaddition in a  $111 \text{ mmol}\cdot\text{L}^{-1}$  solution of **4** with a 13 mol% (in respect to the azide moieties) of copper catalyst (conjugation experiment 1). The resulting molar mass of  $2500 \text{ g}\cdot\text{mol}^{-1}$  of the conjugation product **5a** is slightly higher with respect to the molar masses of the two building blocks and linker molecule ( $2190 \text{ g}\cdot\text{mol}^{-1}$ ). However, these values are in agreement with theoretical ones considering that the molar masses were determined via conventional SEC versus PS standards and were rather rough approximations. The dispersity of the polymer is decreasing from 1.3 to 1.1 within the conjugation process. Such a decrease meets the theoretical expectations as conjugation is not a co-addition but a convolution procedure.<sup>38-39</sup> The rather unusual structure of the SEC trace of the alkyne-functional polymer **3a** exhibiting distinct features toward low molecular weight is

**Table 3.2.** Molar masses of alkyne-functional NBR building blocks **3a-e** and their respective coupling products **5a-e** obtained in the 1,3-dipolar cycloaddition with 1,4-bis(azidomethyl)benzene (**4**).<sup>a</sup>

conj. exp.	alkyne-functional NBR <b>3</b>			conjugation product <b>5</b>		
		$M_n$ (g·mol <sup>-1</sup> )	$\bar{D}$		$M_n$ (g·mol <sup>-1</sup> )	$\bar{D}$
1 <sup>b</sup>	<b>3a</b>	1000	1.3	<b>5a</b>	2500	1.1
2 <sup>c</sup>	<b>3b</b>	6300	1.2	<b>5b</b>	10 600	1.3
3 <sup>d</sup>	<b>3c</b>	10 300	1.3	<b>5c</b>	17 400	1.3
4 <sup>e</sup>	<b>3d</b>	42 000	1.5	<b>5d</b>	72 000	1.6
5 <sup>f</sup>	<b>3e</b>	69 000	1.5	<b>5e</b>	97 000	1.6

<sup>a</sup> Conditions: Reactions were stirred for 16 h in DMF at room temperature. Equimolar amounts of CuSO<sub>4</sub>·5H<sub>2</sub>O and sodium ascorbate were employed. <sup>b</sup> 13 mol% CuSO<sub>4</sub>. <sup>c</sup> 119 mol% CuSO<sub>4</sub>. <sup>d</sup> 198 mol% CuSO<sub>4</sub>. <sup>e</sup> 1951 mol% CuSO<sub>4</sub>. <sup>f</sup> 3324 mol% CuSO<sub>4</sub> (percentages calculated vs. azide moieties).

attributed to the almost complete separation of low molecular weight polymer of different chain length on the high resolution SEC column. For the identification of the narrow signal of close to 26.1 min a chromatographic separation of polymer **3a** on silica was performed as demonstrated in Figure 3.12 in the *Appendix*. <sup>1</sup>H NMR spectroscopy allows assignment to the molecular species where a single BD was incorporated into the alkyne-functional RAFT agent **2**.

Similarly, an increase in molar mass was obtained from reacting 6300 g·mol<sup>-1</sup> alkyne-functional NBR **3b**, depicted in Figure 3.5B. The coupled polymer building blocks **5b** exhibit a molar mass of 10 600 g·mol<sup>-1</sup> and a slight tailing toward low molecular weight is observed. Here, an approximately equimolar concentration of azide moieties and copper was applied (conjugation experiment 2) in order to successfully couple the polymer blocks. A coupling of two 10 300 g·mol<sup>-1</sup> building blocks **3c** gave coupled polymer **5c** with a molar mass of 17 400 g·mol<sup>-1</sup> (conjugation experiment 3). However, dispersities of the coupling product in **5b** and **5c** did not decrease within the conjugation process, indicating a small fraction of dead polymer chains obtained from chain termination unable to undergo a 1,3-dipolar cycloaddition.

The current work focuses on an application of the conjugation process on AN-BD copolymers within an industrially interesting range of molecular weights. Therefore, a 42 000 g·mol<sup>-1</sup> alkyne-functional NBR **3d** was subjected to conjugation via addition of the aromatic diazido compound **4** to obtain coupling product **5d** of 72 000 g·mol<sup>-1</sup> (see Figure 3.5C). However, a twentyfold excess of copper in relation to the amount of azide moieties is necessary to successfully perform a polymer conjugation. Equimolar amounts of copper salt did not evoke any shift in molecular weight, although equimolar amounts of copper had been high enough for the conjugation of lower molecular weight materials. The necessity of such high amounts of copper is attributed to a catalyst deactivation by coordination of the copper to the nitrile moieties of the polymer backbone as predicted earlier by Golas *et al.* (*vide supra*).<sup>37</sup> High amounts of copper likely enable an adequate formation of the acetylide-copper complex, which is crucial for a successful conjugation. Equimolar amounts, in turn, allowing nitrile-copper coordination, prevent the metal from catalyzing the cycloaddition. The addition of a “catalyst” in the ligand free copper mediated 1,3-dipolar cycloaddition of nitrile containing polymer substrates needs to be adjusted on a per gram rather than on a molar basis therefore. A conjugation experiment with a 69 000 g·mol<sup>-1</sup> alkyne-functional NBR **3e** afforded a polymer-polymer coupling product **5e** of 97 000 g·mol<sup>-1</sup> and a dispersity of 1.6 (conjugation experiment 5, Figure 3.5D). The herein reported results are among the highest reported molar masses obtained via modular ligation of two polymer strands.

Several possibilities for a coupling reaction are conceivable for the alkyne-functional AN-BD copolymer with its high density of nitrile and olefinic moieties. Tsarevsky *et al.*, for example, exploited the presence of nitrile moieties in homo- and copolymers of AN for the post-polymerization formation of vinyltetrazole units using a cycloaddition reaction with sodium azide.<sup>40</sup> This modification, however, requires a Zn(II) catalyst and harsh conditions such as elevated temperatures and prolonged reaction times. A blind experiment was therefore performed to preclude a coupling mechanism other than the copper mediated Huisgen type conjugation of the alkyne-functional chain-end and the aromatic diazido compound. Herein, no reaction between 1,4-bis(azidomethyl)benzene (**4**)

and an alkyne-free, carboxylic acid terminal NBR – synthesized from DoPAT (see Table 3.1, experiment IX) – was observed under experimental conditions identical to conjugation experiment 2. SEC traces of the polymer before (blue dashed line) and after exposure (red line) to the aromatic diazide, as provided in Figure 3.5D, do not significantly differ. This result serves as further proof for the orthogonality of the investigated system toward nitrile or olefinic moieties present in the polymer backbone. Conjugation pathways other than the formation of the triazole moiety can be ruled out with this experiment, providing evidence for the alkyne moiety to be the key component in the presented conjugation system.

### 3.3.4 Detection of the Triazole Moiety

SEC results indicate that the 1,3-dipolar Huisgen conjugation occurs between the alkyne-functional chain-ends of the two polymer strands and the bisfunctional aromatic azido component. A molecular verification of the triazole moiety via NMR spectroscopy and ESI mass spectrometry for the exclusion of other conjugation mechanisms was nevertheless substantial. Thus compound **2** was linked directly. RAFT agent **2** has proven to quantitatively react with 0.5 equivalents of diazide **4**

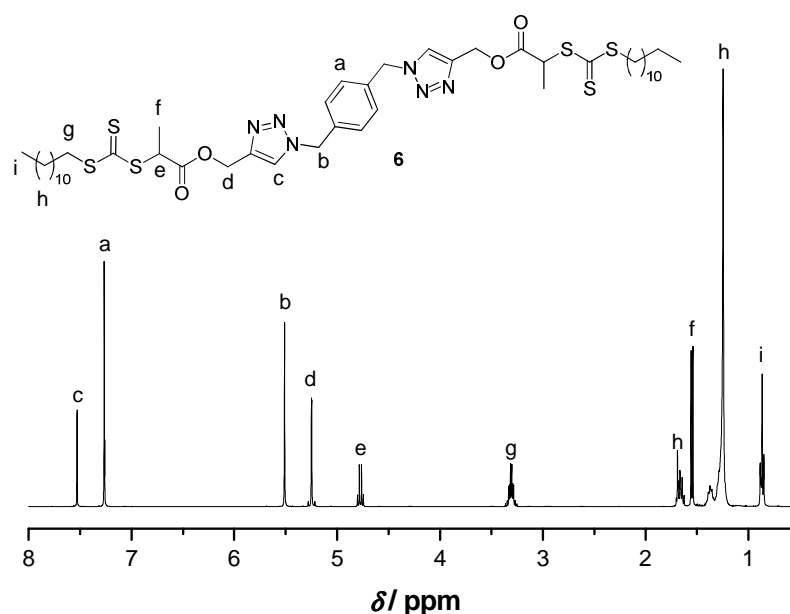


**Figure 3.6.**  $^1\text{H}$  NMR characterization of the 1,4-bis(triazolylmethyl)benzene linked model compound **6** demonstrating the ability of RAFT agent **2** to undergo a quantitative 1,3-dipolar Huisgen cycloaddition reaction with 1,4-bis(azidomethyl)benzene **4** (0.5 equivalents). Conditions: DMF, 25 °C, 16 h, 10 mol%  $\text{CuSO}_4 \cdot 5\text{H}_2\text{O}$ .

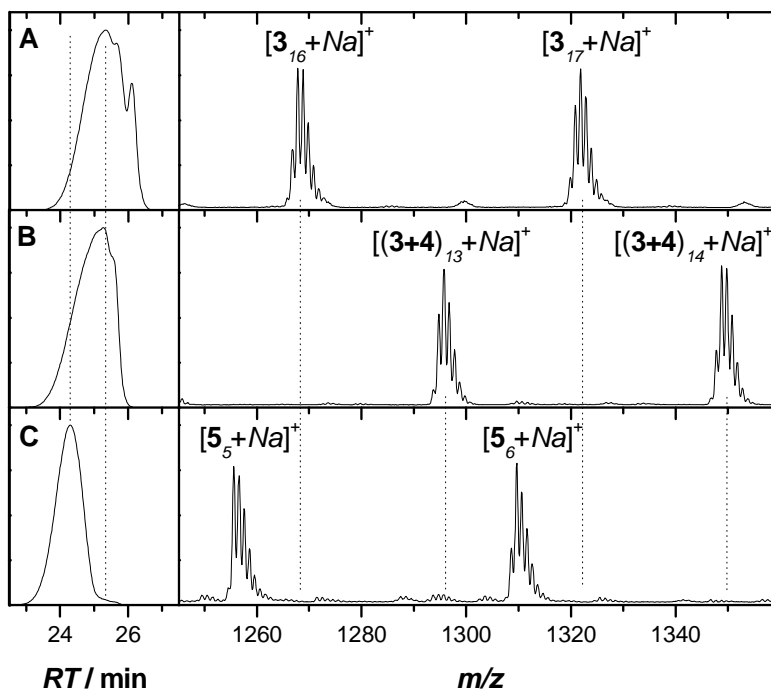


**Figure 3.7.** SEC-ESI mass spectrometric analysis of the copper mediated cycloaddition of alkyne-functional NBR **3a** with 1,4-bis(azidomethyl)benzene (**4**) yielding coupled NBR **5a** (right), and the respective SEC traces (left). The mass spectra exhibit signals of the sodium adducts of A) alkyne-functional NBR  $[3_{(m+n)}+Na]^+$  repeating with monomer mass, B) alkyne-functional NBR after reacting with an excess of **4**, resulting in the one-sided cycloaddition product  $[(3+4)_{(m+n)}+Na]^+$  and C) coupling product  $[5_{(i+j+k+l)}+Na]^+$ . Full mass spectra are provided in Figure 3.15, Figure 3.16 and Figure 3.17 in the *Appendix*.

forming the 1,4-bis(triazolylmethyl)benzene linked compound **6**. A  $^1H$  NMR spectrum is provided in Figure 3.6. For copper mediated 1,3-dipolar cycloadditions one expects a regioselective formation of the 1,2,3-triazole with the RAFT agent in the 4-position and the aryl linker in the 1-position. The single unsplit signal of the triazole proton around 7.5 ppm and the presence of only one signal for each methylene moiety (b, d) adjacent to the newly formed five-membered heteroaromatic cycle serves as a proof.  $^1H$  NMR spectroscopy on coupled polymer **5a** reveals analogous signals and is provided in Figure 3.13 in the *Appendix*. Herein, resonances of the methylene protons of the propargyl moiety at 4.6 ppm decrease in intensity during conjugation, along with the appearance of signals between 5.1 and 5.4 ppm. These signals can be assigned to the respective methylene protons of the coupling product. Conjugation was proven to proceed in a quantitative manner, as no signals of unreacted linker **4** can be observed and no purification steps other than filtration over aluminum oxide were performed.

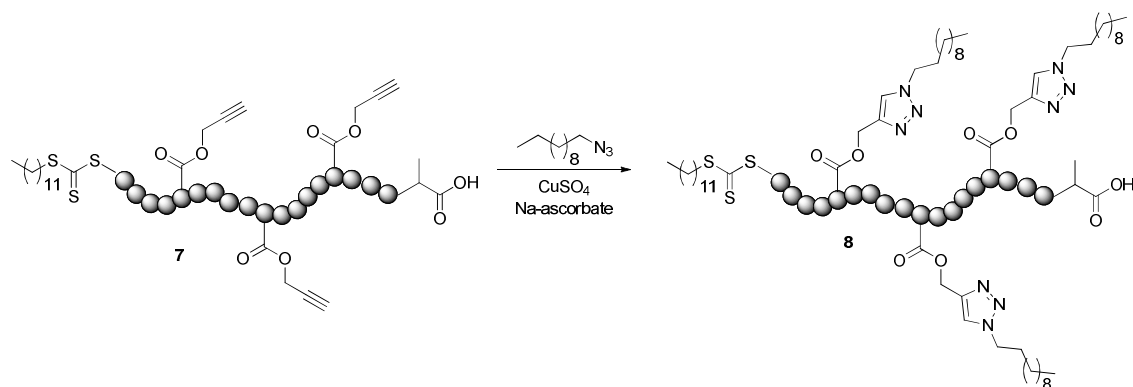
Minor resonances (< 5%) of the alkyne-functional NBR after conjugation are attributed to an insufficient adjustment of stoichiometry. Signals of the newly formed triazole protons resonate at 7.6 ppm but are significantly broadened, however.

A further proof for the formation of the coupling product is the investigation of the cycloaddition product **5a** via SEC-ESI mass spectrometry. Figure 3.7 provides a magnified view of the region of 1245-1360 Da for the alkyne-functional NBR **3a** (layer A) in comparison with the coupling product **5a** (layer C). For completeness, the respective SEC traces are provided on the left side of Figure 3.7. Layer B provides the ESI mass spectrum of the one-sided cycloaddition product (**3a+4**), obtained by reacting the alkyne-functional NBR **3a** with an excess of 1,4-bis(azidomethyl)benzene (**4**), indicated by a shift in mass-to-charge ratio and retention time. Signals of the sodium adducts of the alkyne-functional starting material  $[3_{(m+n)}+Na]^+$  disappear in favor of the signals of the sodium adducts of the coupling product  $[5_{(i+j+k+l)}+Na]^+$  within the conjugation process. However, the full mass spectrum of coupled polymer **5a**, provided in Figure 3.17 in the *Appendix*, exhibits a very small amount of unreacted alkyne-functional NBR, with a value estimated to less than 5%. No signals of the sodium adducts of the respective one-sided coupling product  $[(3+4)_{(m+n)}+Na]^+$  can be found in the mass spectrum of the coupled polymer blocks, nevertheless. Thus, the presence of unreacted alkyne-functional NBR can be related to an inaccurate stoichiometry rather than to an incomplete 1,3-dipolar cycloaddition process.

### 3.3.5 Side-Chain Modification of NBR via CuAAC

The application of the 1,3-dipolar Huisgen cycloaddition to NBR is not only limited to the chain-end modification and its deployment in the orthogonal conjugation of two polymer building blocks. A functional moiety within the polymer backbone accessible to modular modification would be highly desirable for several other applications such as the synthesis of polymer brushes. As the terminal alkyne moiety was proven to be highly orthogonal to the AN/BD polymerization process without any traceable incorporation of the triple bond into the polymer chain during chain growth, NBRs with several alkyne moieties along the polymer

backbone were targeted. In a RAFT mediated polymerization employing DoPAT (**1**), a terpolymer (**7**) of AN, BD and prop-2-ynyl methacrylate (PMA) was synthesized (Table 3.1, experiment VIII, see Scheme 3.5). The monomers were used in a molar ratio of 56:35:9 (BD:AN:PMA) and an overall monomer



**Scheme 3.5.** Copper mediated modification of AN-BD-PMA terpolymer **7** with 1-azidoundecane yielding brush-like structures.

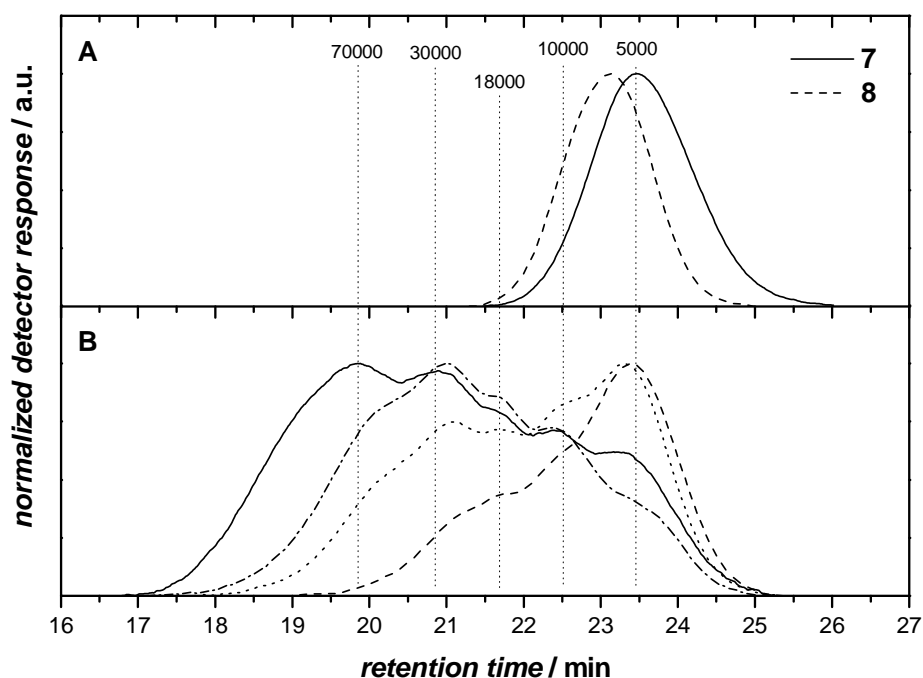


**Figure 3.8.** A) SEC traces of AN-BD-PMA terpolymer (**7**, solid line) and terpolymer after copper mediated side chain modification using undecane azide (**8**, dashed line). B) SEC analysis of the soluble parts of the crosslinking experiments for several ratios  $r = n(\mathbf{4})/n(\mathbf{7})$  of the molar amount of crosslinking reagent 1,4-bis(azidomethyl)benzene  $n(\mathbf{4})$  to the molar amount of alkyne-functional terpolymer  $n(\mathbf{7})$ : Dashed line:  $r = 0.5$ , dotted line:  $r = 1.0$ , solid line:  $r = 2.0$ , dash-dotted line:  $r = 5.0$ . Vertical dotted lines indicate molecular weights of narrow PS standards eluting at the respective retention time.

concentration of  $9.5 \text{ mol}\cdot\text{L}^{-1}$ . With an initiator concentration of  $5.8 \text{ mmol}\cdot\text{L}^{-1}$  and ten equivalents of RAFT agent, a terpolymer **7** of  $3900 \text{ g}\cdot\text{mol}^{-1}$  with a dispersity of 1.3 was obtained within 5 h. The obtained narrow SEC trace is provided in Figure 3.8A (solid line) and displays a slight tailing toward low molecular weight, due to the formation of a small amount of dead polymer chains. The incorporation of each of the three monomers was confirmed by IR spectroscopy (provided Figure 3.14 in the *Appendix*), SEC-ESI mass spectrometry (Figure 3.9) and  $^1\text{H}$  NMR spectroscopy

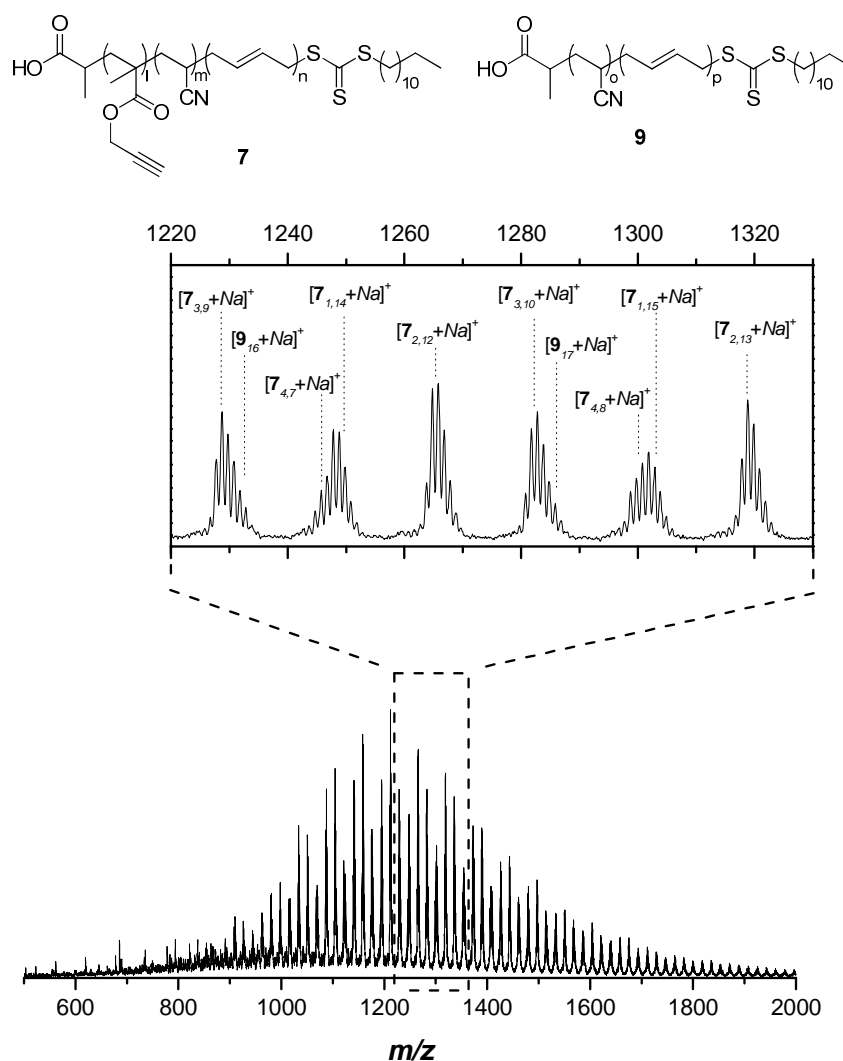


**Figure 3.9.** SEC-ESI-MS characterization of terpolymer **7**. An integral over a section of single charged species is provided, showing the typical NBR signal structure resulting from the superposition of the isotope pattern of macromolecules with a similar overall amount of AN and BD repeating units yet different AN/BD ratios. The main signals are assigned to the sodium adducts of the terpolymer  $[7_{(l,m+n)}+Na]^+$ . For statistical reason, a distinct amount of sodium adducts of polymer strands without propargyl methacrylate incorporation  $[9_{(o+p)}+Na]^+$  is observed.

(Figure 3.10). Remarkably, signals in the SEC-ESI-MS appear as distinct peaks, allowing the assignment to the respective polymer species. A small amount of AN-BD copolymer **9** is present besides the signals of terpolymer with one or more propargyl methacrylate units due to statistic effects.  $^1\text{H}$  NMR resonances of the aliphatic polymer backbone and the olefinic signals of the incorporated BD are located as described above, methylene protons of the propargyl moiety (d) resonate around 4.6 ppm (Figure 3.10). Correlation of the latter signal with the methylene protons (c) of the dodecyl tail in  $\alpha$ -position to the trithiocarbonate at

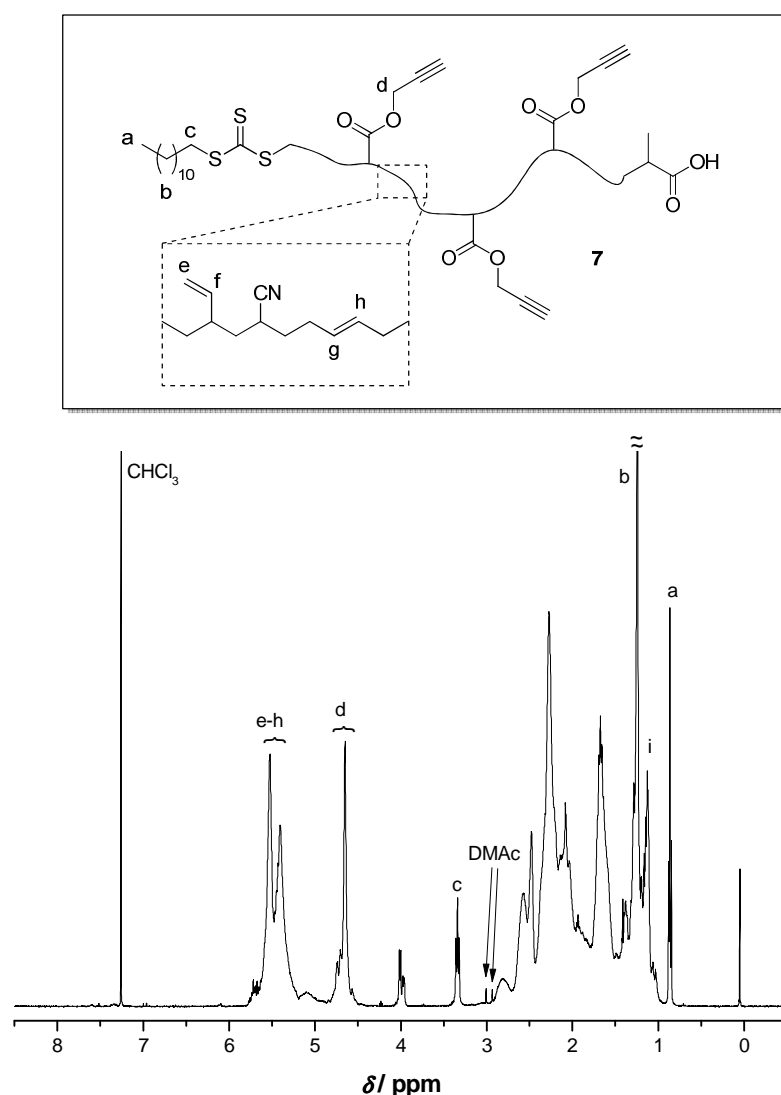


**Figure 3.10.**  $^1\text{H}$  NMR characterization ( $\text{CDCl}_3$ ) of a  $3900 \text{ g}\cdot\text{mol}^{-1}$  terpolymer **7** synthesized in a DoPAT (**1**) mediated polymerization of AN, BD and PMA within 5 h at  $100^\circ\text{C}$ , using 1,1'-azobis(cyclohexane-1-carbonitrile) as the initiator and *N,N*-dimethylacetamide (DMAc) as the solvent.

3.3 ppm accounts for an average incorporation of 5 alkyne moieties per polymer chain, in equivalence with the provided proportions. IR spectra evidence the presence of the alkyne moieties due to the presence of a strong  $C\equiv C-H$  stretching vibration absorption band around  $3285\text{ cm}^{-1}$  and display a  $C\equiv N$  vibration at  $2240\text{ cm}^{-1}$  (Figure 3.14 in the *Appendix*).

The alkyne moieties of terpolymer **7** were subjected to a 1,3-dipolar cycloaddition, as depicted in Scheme 3.5. An excess of 1-azidoundecane using  $\text{CuSO}_4$ /sodium ascorbate in DMF at room temperature was employed. SEC analysis of the resulting alkane branched terpolymer **8** is provided in Figure 3.8A (dashed line). A distinct shift toward lower retention times and thus higher molecular weight compared to the alkyne-functional terpolymer **7** (solid line) was found. A molecular weight of  $5900\text{ g}\cdot\text{mol}^{-1}$  corresponds to a percentage increase of 50%. This is in agreement with the calculated average incorporation of 5 alkyne monomers per polymer chain, considering the altered relation of hydrodynamic volume and molecular weight due to the influence of the established branched structure<sup>41</sup> as well as the lack of proper MHKS parameters, further documented by the slight decrease of the dispersity from 1.3 to 1.2.

### 3.3.6 Crosslinking

NBRs are among the most important technical rubber products worldwide. Many of its applications require crosslinked structures for the enhancement of viscoelasticity and swelling properties.<sup>42-43</sup> Several alternative crosslinking protocols have been developed,<sup>44-46</sup> since the invention of the vulcanization process by Charles Goodyear more than 150 years ago.<sup>47</sup> With the advent of orthogonal conjugation in polymer chemistry various methods have been exploited for the controlled generation of defined crosslinked polymer structures, recently reviewed by Wooley and Hawker *et al.*<sup>5</sup> Thiol-ene coupling has been studied extensively and was applied to the formation of hydrogels,<sup>48</sup> thin films<sup>49</sup> and lithographic applications.<sup>50</sup> Similar efforts were devoted to the generation of polymer networks using the copper catalyzed 1,3-dipolar Huisgen cycloaddition. Ossipov and Hilborn, for example, prepared novel acetylene and azide-functional poly(vinyl alcohols) and obtained polymer networks by crosslinking these under

mild conditions in presence of a Cu(I) catalyst system.<sup>51</sup> A PMA-methyl methacrylate-butyl acrylate terpolymer has been subjected to crosslinking under air using copper and tetramethylethylenediamine by a Hay-type coupling reaction, yielding bisacetylene linkage structures.<sup>52</sup> To the best of our knowledge, no successful attempts toward a controlled crosslinking of NBR by means of the copper mediated azide-alkyne cycloaddition have been reported to date. In the present chapter, 1,4-bis(azidomethyl)benzene (**4**) was shown to be an efficient agent in the conjugation of  $\alpha$ -functional NBR building blocks. Thus diazide **4** was investigated for its ability to support the formation of higher aggregates via coupling of the pendant alkyne moieties of terpolymer **7**. In the presence of the Cu(I) system (CuSO<sub>4</sub>/Na-ascorbate), solutions of terpolymer **7** were reacted with diazide **4** in various concentrations for 16 h in DMF at ambient temperature. Reactions were performed in high concentrations to minimize the amount of intramolecular cycloadditions of the pendant alkyne moieties. Metal salts were removed by filtration over a short column of neutral aluminum oxide and soluble fractions of the recovered polymer (in THF) were analyzed by size exclusion chromatography. Figure 3.8B provides SEC traces of a selection of crosslinking experiments for several ratios  $r = n(\mathbf{4})/n(\mathbf{7})$  of the molar amount of crosslinking reagent 1,4-bis(azidomethyl)benzene  $n(\mathbf{4})$  to the molar amount of alkyne-functional terpolymer  $n(\mathbf{7})$ . The dashed line represents the SEC results for  $r = 0.5$ , the dotted line for  $r = 1$ , the solid line for  $r = 2$  and the dash-dotted line for  $r = 5$ .  $r$ -Values are calculated under the assumption of a molar mass of 3900 g·mol<sup>-1</sup> for terpolymer **7**, as obtained from SEC via conventional calibration versus PS standards. Peak molecular weights at several positions of the elugram are illustrated by vertical dotted lines. All polymers obtained from the crosslinking experiments exhibit highly structured SEC traces with local maximum values at similar retention times. Retention times at these maxima refer to molecular weights that are approximately a multiple of the peak molecular weight of the unreacted terpolymer **7**. We therefore assume that polymeric species linked via 1,4-bis(triazolylmethyl)benzene moieties were formed in analogy to the coupling of  $\alpha$ -functionalized NBR building blocks. As expected, an addition of an amount of linker molecule **4** equimolar to the alkyne moieties present (*i.e.*  $r = 5$ , since

approximately five PMA units are incorporated per chain) yields a lower molecular weight polymer, compared to the addition of roughly 1 mol diazido linker molecule per 2 mol alkyne functionality (*i.e.*  $r = 2$ ).

### 3.4 Conclusions

$\alpha$ -Functional NBR building blocks were employed in the copper mediated 1,3-dipolar Huisgen coupling upon addition of 1,4-bis(azidomethyl)benzene (**4**), providing the first successful approach to employ the orthogonal conjugation technique on this technically important class of synthetic rubbers. Linear polymers with molar masses of up to 97 000 g·mol<sup>-1</sup> were obtained, clearly exceeding the ability of reversible-deactivation polymerization techniques (*i.e.* RAFT) in providing high molecular weight NBRs. Other examples of polymer-polymer conjugation in high molecular weight regions (> 40 000 g·mol<sup>-1</sup>) are rare, further highlighting the outstanding properties of the presented system. For this purpose, a novel alkyne-functional RAFT agent **2** was synthesized in good yields via the DCC mediated coupling of DoPAT (**1**) and propargyl alcohol and was shown to be an efficient controlling agent for the reversible-deactivation radical copolymerization of AN and BD. Moreover, the use of CuAAC was extended toward the side-chain modification of NBR as well as applied in the synthesis of branched and crosslinked NBR structures. With this toolbox in hand, a wide variety of future applications is accessible, as for example the synthesis of block-copolymers or the use of NBR in covalent surface immobilization.

### 3.5 Appendix

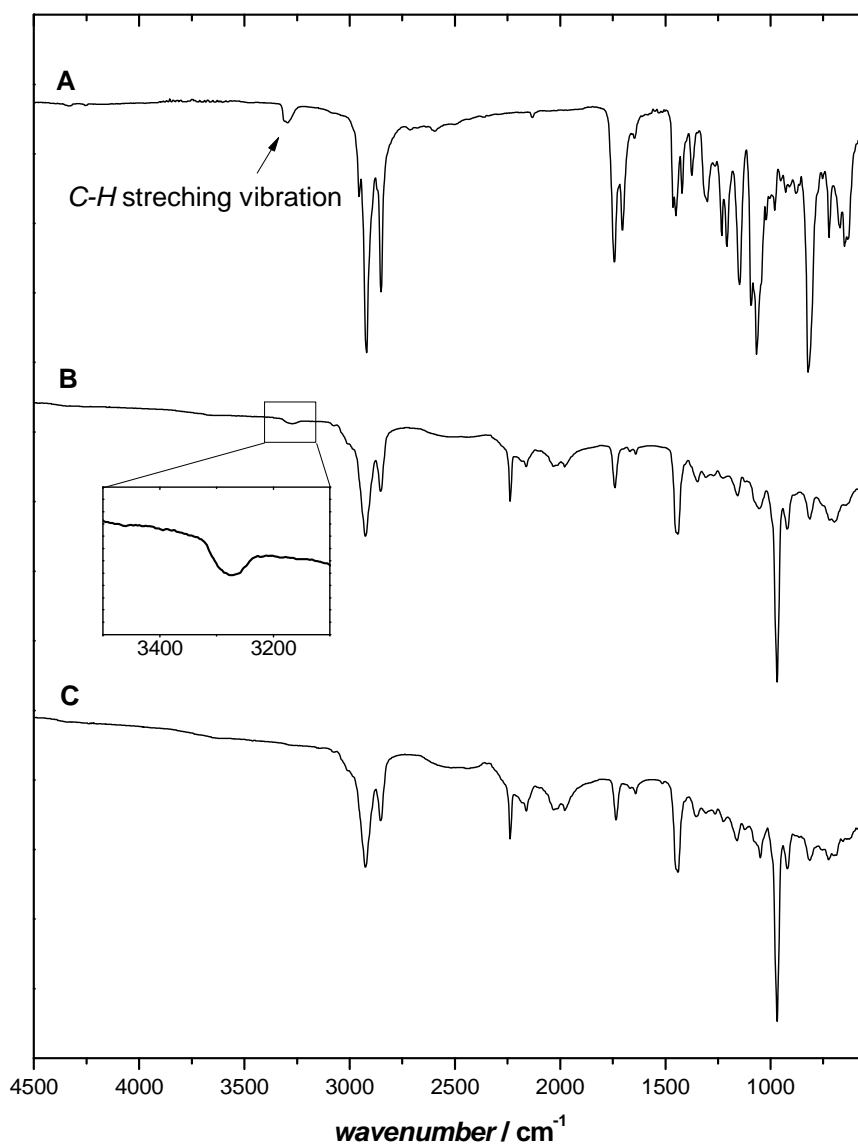


**Figure 3.11.** Fourier transform (FT)-IR spectra of A) alkyne-functional RAFT agent **2**, B) alkyne-capped AN-BD copolymer **3** and C) a comparative sample of a NBR synthesized from DoPAT.

**Table 3.3.** Experimental details of the 1,3-dipolar cycloaddition reactions of alkyne-functional NBR building blocks **3** with 1,4-bis(azidomethyl)benzene (**4**).<sup>a</sup>

conj. exp.	[ <b>3</b> ] <sub>0</sub> (mg·mL <sup>-1</sup> )	[ <b>4</b> ] <sub>0</sub> (mmol·L <sup>-1</sup> )	[CuSO <sub>4</sub> ·5H <sub>2</sub> O] (mmol·L <sup>-1</sup> )	coupling product	<i>M</i> <sub>n</sub> (g·mol <sup>-1</sup> )	<i>D</i>
1 <sup>b</sup>	167	111	29.4	<b>5a</b>	2500	1.1
2 <sup>c</sup>	98.0	13.2	31.4	<b>5b</b>	10 600	1.3
3 <sup>d</sup>	106	8.80	34.7	<b>5c</b>	17 400	1.3
4 <sup>e</sup>	214	4.05	158	<b>5d</b>	72 000	1.6
5 <sup>e</sup>	150	1.5	99.7	<b>5e</b>	97 000	1.6

<sup>a</sup> Conditions: Reactions were stirred for 16 h in DMF at room temperature. Equimolar amounts of CuSO<sub>4</sub>·5H<sub>2</sub>O and sodium ascorbate were employed. <sup>b</sup> Total volume of 300 μL.

<sup>c</sup> Total volume of 510 μL. <sup>d</sup> Total volume of 700 μL. <sup>e</sup> Total volume of 1000 μL.

**Table 3.4.** Experimental details for the crosslinking experiments of terpolymer **7**.<sup>a</sup>

crosslinking exp.	<i>n</i> ( <b>4</b> ) (μmol)	<i>r</i> = <i>n</i> ( <b>4</b> )/ <i>n</i> ( <b>7</b> )	<i>V</i> <sub>total</sub> (mL)	<i>M</i> <sub>n</sub> (g·mol <sup>-1</sup> )	<i>D</i>
1	7.69	0.5	0.3	6300	1.9
2	15.4	1	0.3	9200	2.7
3	30.8	2	0.5	14 900	4.0
4	76.9	5	1.1	14 200	2.7

<sup>a</sup> Conditions: 60 mg of terpolymer **7**. 3.2 mass% of CuSO<sub>4</sub>·5H<sub>2</sub>O. Addition of **4** from a 77 mM stock solution.

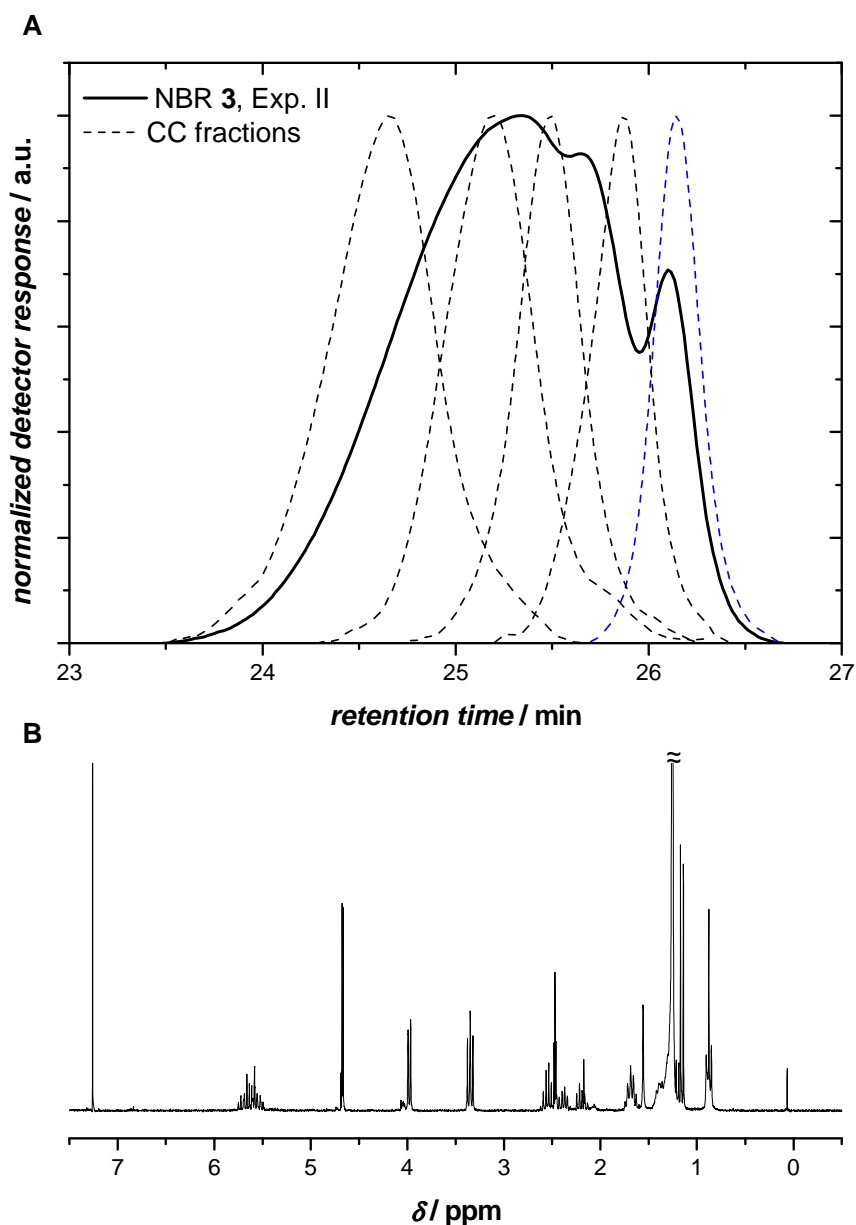
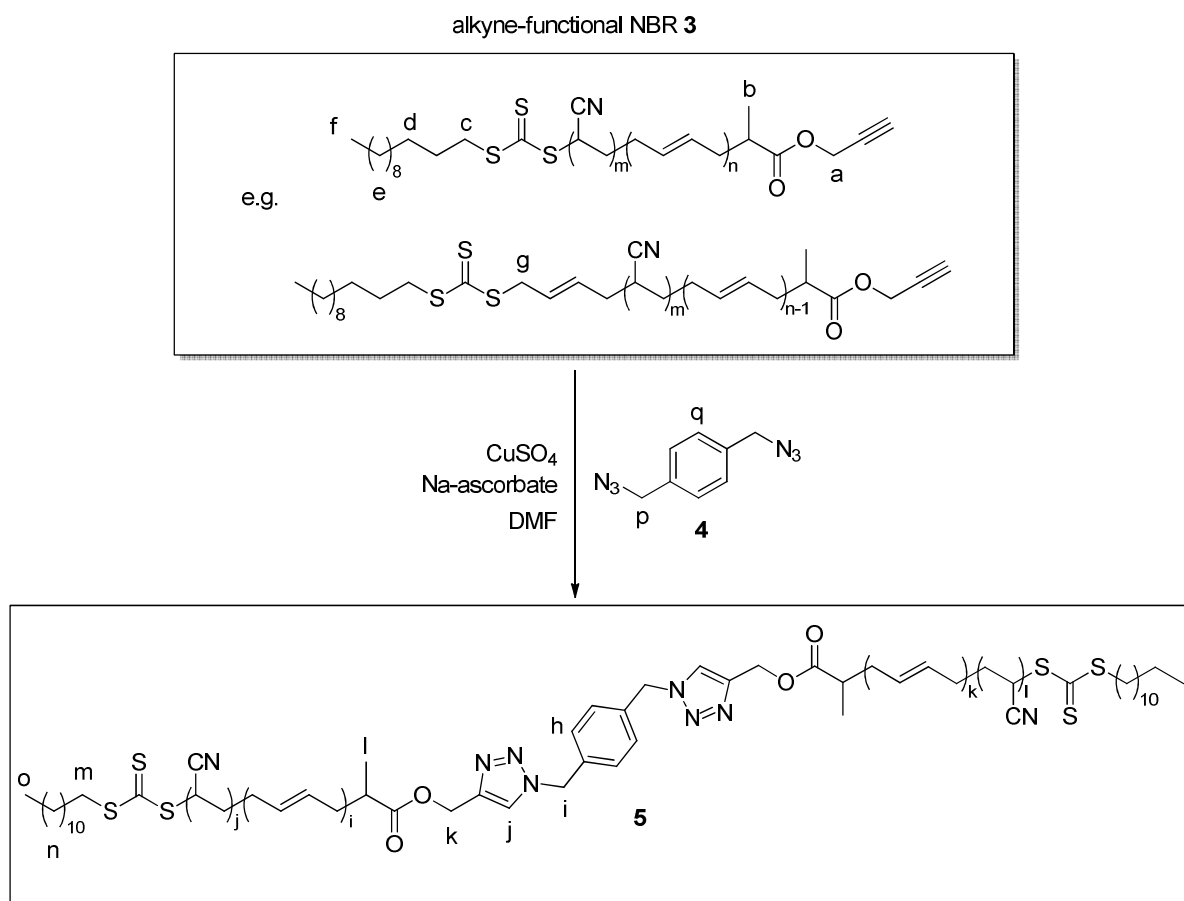


**Figure 3.12.** Separation of the components of alkyne-functional NBR **3a** of  $1000 \text{ g}\cdot\text{mol}^{-1}$  (exp. I) by column chromatography (CC) on silica gel in hexane/methylene chloride (1:1, v/v). A) SEC traces of the polymer as obtained from polymerization (solid line) and several fractions (dashed lines) after separation. B)  $^1\text{H}$  NMR spectrum of the first fraction eluting from the column (blue curve). For the latter, a  $M_n$   $500 \text{ g}\cdot\text{mol}^{-1}$  and a  $\mathcal{D} = 1.02$  was obtained in SEC versus PS standards.



**Scheme 3.6.** Coupling of two alkyne-functional NBR building blocks via CuAAC upon addition of 1,4-bis(azidomethyl)benzene (**4**). Lower case letters are provided for the facile assignment of <sup>1</sup>H NMR resonances (see Figure 3.13) to the respective protons.

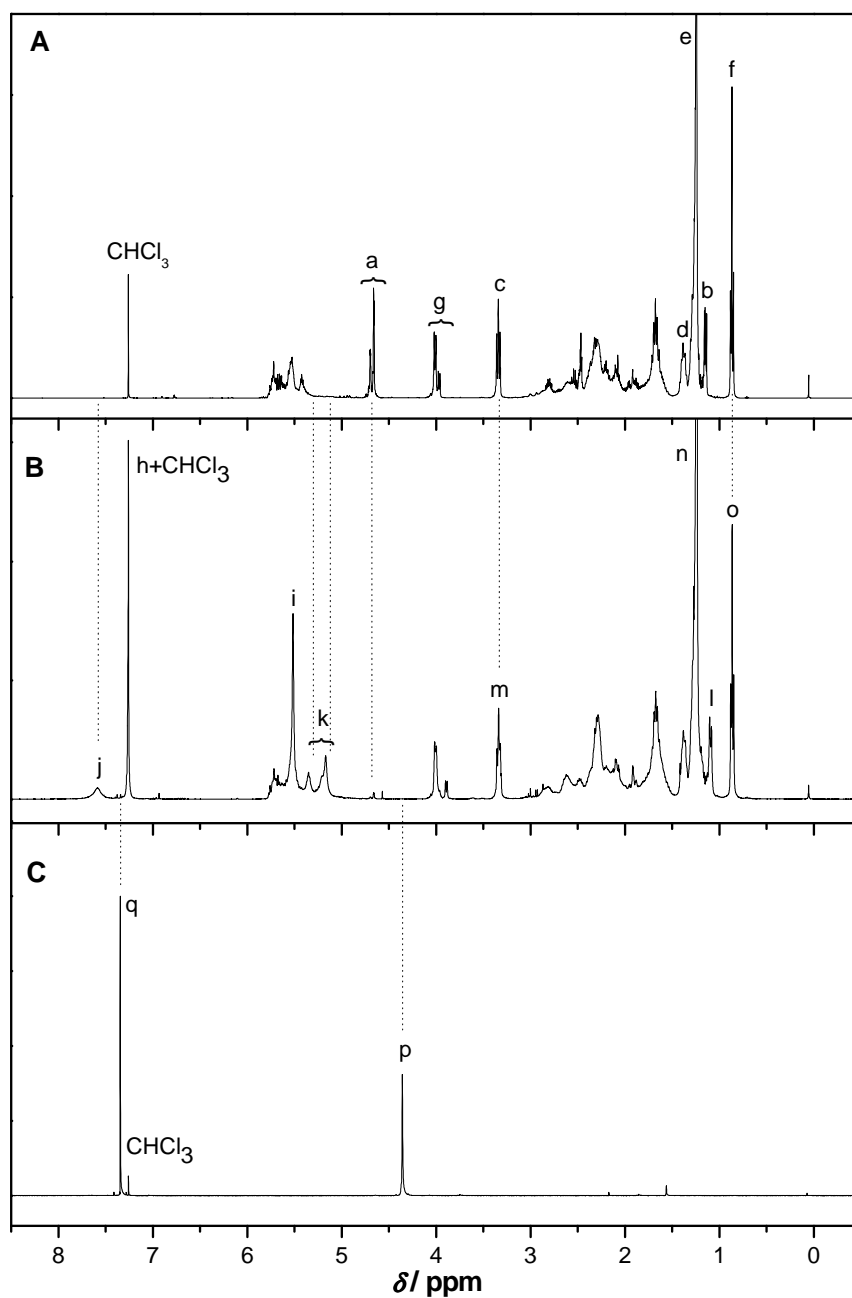


**Figure 3.13.** Molecular verification of the triazole moiety as the linking structure within the coupled polymer building blocks via ambient temperature  $^1\text{H}$  NMR spectroscopic analysis in  $\text{CDCl}_3$ . For comparison,  $^1\text{H}$  NMR spectra of A) the linear alkyne-functional NBR **3a** of  $1000\text{ g}\cdot\text{mol}^{-1}$ , B) polymer **5a** ( $M_n$   $2500\text{ g}\cdot\text{mol}^{-1}$ ) obtained from coupling of **3a** via addition of 1,4-bis(azidomethyl)benzene (**4**) in the presence of copper sulfate and sodium ascorbate and C) the linking agent 1,4-bis(azidomethyl)benzene (**4**) are depicted. Lower-case letters are provided for peak assignments and can also be found in Scheme 3.6.

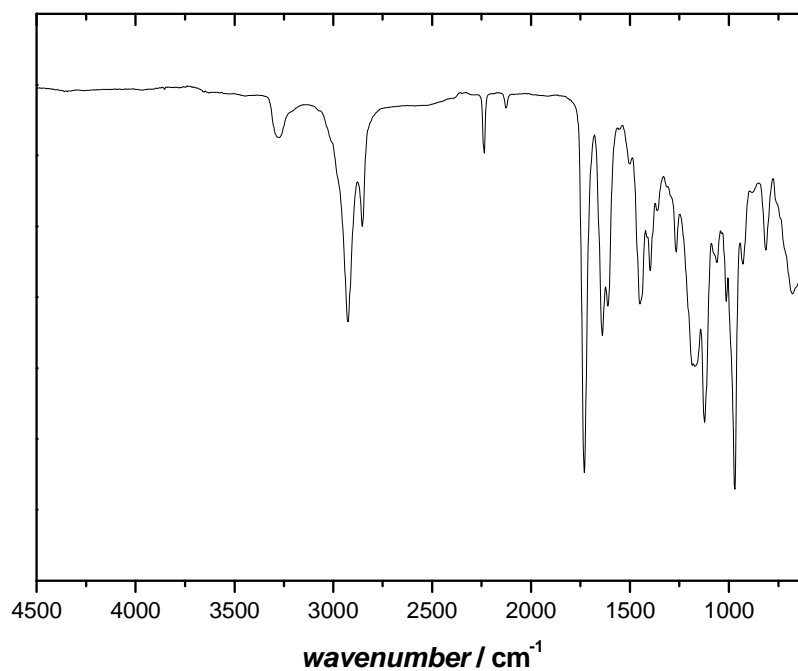


**Figure 3.14.** FT-IR spectrum of a 3900 g·mol<sup>-1</sup> terpolymer **7** synthesized in a DoPAT (**1**) mediated polymerization of AN, BD and PMA within 5 h at 100 °C, using 1,1'-azobis(cyclohexane-1-carbonitrile) as the initiator and *N,N*-dimethylacetamide as the solvent.

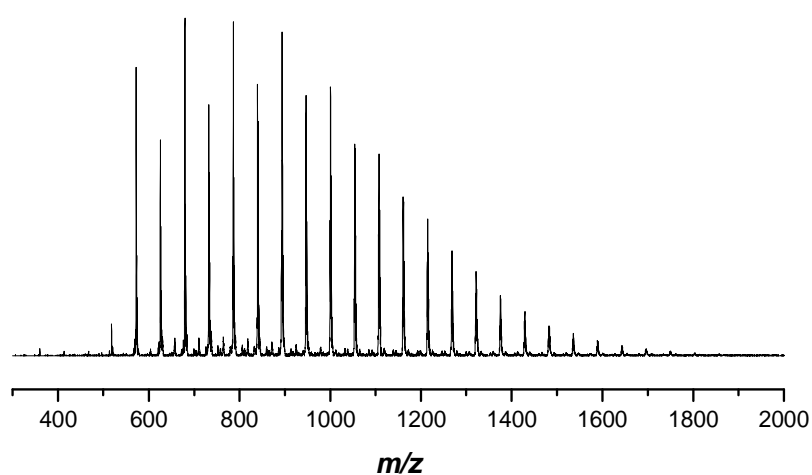


**Figure 3.15.** Full ESI mass spectrum of the 1000 g·mol<sup>-1</sup> alkyne-functional NBR **3a**.

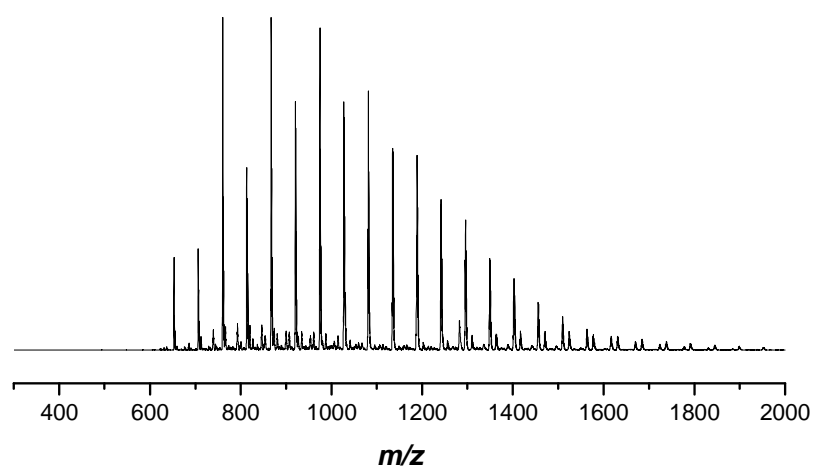


**Figure 3.16.** Full ESI mass spectrum of alkyne-functional NBR **3a** after reacting with an excess of **4**, resulting in the one-sided cycloaddition product (**3a+4**).  $M_n$  1400 g·mol<sup>-1</sup>,  $D = 1.2$ .

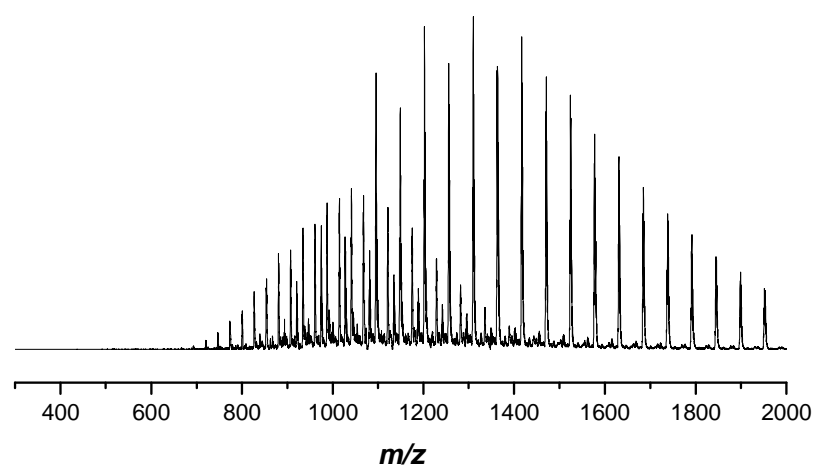


**Figure 3.17.** Full ESI mass spectrum of 2500 g·mol<sup>-1</sup> coupled NBR **5a**.

### 3.6 References

1. Kaiser, A.; Brandau, S.; Klimpel, M.; Barner-Kowollik, C. *Macromol. Rapid Commun.* **2010**, *31*, 1616-1621.
2. Dürr, C. J.; Emmerling, S. G. J.; Kaiser, A.; Brandau, S.; Habicht, A. K. T.; Klimpel, M.; Barner-Kowollik, C. *J. Polym. Sci. Part A: Polym. Chem.* **2012**, *50*, 174-180.
3. Klimpel, M.; Brandau, S.; Barner-Kowollik, C.; Kaiser, A. *Nitrilkautschuke und deren Herstellung in organischen Lösungsmitteln*. EU Pat., 2 298 824 A1, 2011.
4. Klimpel, M.; Brandau, S.; Westeppe, U.; Barner-Kowollik, C.; Kaiser, A. *Nitrilkautschuke und deren Herstellung in organischen Lösungsmitteln*. WO Pat., 2011/032832 A1, 2011.
5. Iha, R. K.; Wooley, K. L.; Nyström, A. M.; Burke, D. J.; Kade, M. J.; Hawker, C. *J. Chem. Rev.* **2009**, *109*, 5620-5686.
6. Sumerlin, B. S.; Vogt, A. P. *Macromolecules* **2010**, *43*, 1-13.
7. Inglis, A. J.; Barner-Kowollik, C. *Macromol. Rapid Commun.* **2010**, *31*, 1247-1266.
8. Barner-Kowollik, C.; Du Prez, F. E.; Espeel, P.; Hawker, C. J.; Junkers, T.; Schlaad, H.; Van Camp, W. *Angew. Chem. Int. Ed.* **2011**, *50*, 60-62.
9. Mansfeld, U.; Pietsch, C.; Hoogenboom, R.; Becer, C. R.; Schubert, U. S. *Polym. Chem.* **2010**, *1*, 1560-1598.
10. Tasdelen, M. A. *Polym. Chem.* **2011**, *2*, 2133-2145.
11. Vinson, N.; Gou, Y.; Becer, C. R.; Haddleton, D. M.; Gibson, M. I. *Polym. Chem.* **2011**, *2*, 107-113.
12. Binder, W. H.; Sachsenhofer, R. *Macromol. Rapid Commun.* **2007**, *28*, 15-54.
13. Binder, W. H.; Sachsenhofer, R. *Macromol. Rapid Commun.* **2008**, *29*, 952-981.
14. Quémener, D.; Davis, T. P.; Barner-Kowollik, C.; Stenzel, M. H. *Chem. Commun.* **2006**, 5051-5053.
15. Inglis, A. J.; Stenzel, M. H.; Barner-Kowollik, C. *Macromol. Rapid Commun.* **2009**, *30*, 1792-1798.

16. Thomas, J. R.; Liu, X.; Hergenrother, P. J. *J. Am. Chem. Soc.* **2005**, *127*, 12434-12435.
17. Díaz, L.; Bujons, J.; Casas, J.; Llebaria, A.; Delgado, A. *J. Med. Chem.* **2010**, *53*, 5248-5255.
18. Hensarling, R. M.; Doughty, V. A.; Chan, J. W.; Patton, D. L. *J. Am. Chem. Soc.* **2009**, *131*, 14673-14675.
19. Geng, J.; Mantovani, G.; Tao, L.; Nicolas, J.; Chen, G.; Wallis, R.; Mitchell, D. A.; Johnson, B. R. G.; Evans, S. D.; Haddleton, D. M. *J. Am. Chem. Soc.* **2007**, *129*, 15156-15163.
20. Dietrich, M.; Glassner, M.; Gruending, T.; Schmid, C.; Falkenhagen, J.; Barner-Kowollik, C. *Polym. Chem.* **2010**, *1*, 634-644.
21. Moad, G.; Rizzardo, E.; Thang, S. H. *Aust. J. Chem.* **2005**, *58*, 379-410.
22. Moad, G.; Rizzardo, E.; Thang, S. H. *Aust. J. Chem.* **2006**, *59*, 669-692.
23. Moad, G.; Rizzardo, E.; Thang, S. H. *Aust. J. Chem.* **2009**, *62*, 1402-1472.
24. Moad, G.; Chong, Y. K.; Postma, A.; Rizzardo, E.; Thang, S. H. *Polymer* **2005**, *46*, 8458-8468.
25. Cherubin, T. *Über die Bestimmung von Copolymerisationsparametern in der radikalischen Copolymerisation von Acrylnitril mit Butadien*. Ph.D. Thesis, University of Essen, 1999.
26. Ranjan, R.; Brittain, W. J. *Macromol. Rapid Commun.* **2007**, *28*, 2084-2089.
27. Ranjan, R.; Brittain, W. J. *Macromolecules* **2007**, *40*, 6217-6223.
28. Wako Pure Chemical Industries Ltd. Web Page. <http://www.wako-chem.co.jp/specialty/oilazo/V-40.htm>.
29. Barner-Kowollik, C.; Quinn, J. F.; Nguyen, T. L. U.; Heuts, J. P. A.; Davis, T. P. *Macromolecules* **2001**, *34*, 7849-7857.
30. Lowe, A. B.; McCormick, C. L., RAFT Polymerization in Homogeneous Aqueous Media: Initiation Systems, RAFT Agent Stability, Monomers and Polymer Structures. In *Handbook of RAFT Polymerization*. 1<sup>st</sup> ed.; Barner-Kowollik, C., Ed.; Wiley-VCH: Weinheim, 2008; p 235 ff.
31. Opsteen, J. A.; van Hest, J. C. M. *Chem. Commun.* **2005**, 57-59.
32. Fournier, D.; Hoogenboom, R.; Schubert, U. S. *Chem. Soc. Rev.* **2007**, *36*, 1369-1380.

33. Lutz, J.-F. *Angew. Chem. Int. Ed.* **2007**, *46*, 1018-1025.
34. Meldal, M. *Macromol. Rapid Commun.* **2008**, *29*, 1016-1051.
35. Loo, B. H.; Kato, T. *Surf. Sci.* **1993**, *284*, 167-174.
36. Shen, F.; Li, H.; Wu, C. *J. Polym. Sci. Part B: Polym. Phys.* **2006**, *44*, 378-386.
37. Golas, P. L.; Tsarevsky, N. V.; Matyjaszewski, K. *Macromol. Rapid Commun.* **2008**, *29*, 1167-1171.
38. Barner-Kowollik, C. *Macromol. Rapid Commun.* **2009**, *30*, 1625-1631.
39. Preuss, C. M.; Barner-Kowollik, C. *Macromol. Theory Simul.* **2011**, *20*, 700-708.
40. Tsarevsky, N. V.; Bernaerts, K. V.; Dufour, B.; Du Prez, F. E.; Matyjaszewski, K. *Macromolecules* **2004**, *37*, 9308-9313.
41. Douglas, J. F.; Roovers, J.; Freed, K. F. *Macromolecules* **1990**, *23*, 4168-4180.
42. Flory, P. J. *Chem. Rev.* **1944**, *35*, 51-75.
43. Flory, P. J.; Rabjohn, N.; Shaffer, M. C. *J. Polym. Sci.* **1949**, *4*, 225-245.
44. Tillet, G.; Boutevin, B.; Ameduri, B. *Prog. Polym. Sci.* **2011**, *36*, 191-217.
45. Coran, A. Y. *J. Appl. Polym. Sci.* **2003**, *87*, 24-30.
46. Coran, A. Y. *Rubber Chem. Technol.* **1995**, *68*, 351-375.
47. Calzonetti, J. A.; Laursen, C. J. *Rubber Chem. Technol.* **2010**, *83*, 303-321.
48. Simpson, N.; Takwa, M.; Hult, K.; Johansson, M.; Martinelle, M.; Malmstrom, E. *Macromolecules* **2008**, *41*, 3613-3619.
49. Wei, H. Y.; Senyurt, A. F.; Jonsson, S.; Hoyle, C. E. *J. Polym. Sci. Part A: Polym. Chem.* **2007**, *45*, 822-829.
50. Khire, V. S.; Yi, Y.; Clark, N. A.; Bowman, C. N. *Adv. Mater.* **2008**, *20*, 3308-3313.
51. Ossipov, D. A.; Hilborn, J. *Macromolecules* **2006**, *39*, 1709-1718.
52. Dirlikov, S.; Chen, Z. *Air Dried Cross-linkable Polymeric Vehicles Which Include Acetylenic Groups*. US Pat., 5 556 921, 1996.



# 4 ■ Mild and Efficient Modular Synthesis of Poly(acrylonitrile-*co*-butadiene) Block and Miktoarm Star Copolymer Architectures<sup>†</sup>

## 4.1 Introduction

Elastomers play an outstanding role in our everyday life and find applications in products ranging from general to speciality applications. Nitrile-butadiene rubbers (NBRs) are among the most important elastomers for the automotive and oil exploitation industries and can be found in tubings, sealing gaskets, dampers or stators due to their high resistance to aggressive surroundings in a wide temperature range.

In chapter 3, the synthesis of high molecular weight NBR by combining reversible addition–fragmentation chain transfer (RAFT) mediated polymerization and orthogonal copper mediated azide-alkyne cycloaddition (CuAAC) was reported. NBRs with molar masses up to 97 000 g·mol<sup>-1</sup> and dispersities between 1.1 and 1.6 were obtained. As it was shown earlier, linear copolymers of acrylonitrile (AN) and 1,3-butadiene (BD) with molar masses above 60 000 g·mol<sup>-1</sup> and low dispersities cannot be easily synthesized by a sequential RAFT process.<sup>1</sup> The CuAAC method, however, suffers from the need for high concentrations of copper catalyst to facilitate quantitative conjugation. The need for a high catalyst concentration was attributed to nitrile-copper coordination of the AN backbone competing with the formation of the copper-acetylide complex essential for azide-alkyne cycloaddition.<sup>2</sup> Copper-free azide-alkyne cycloaddition protocols exist,

---

<sup>†</sup> Adapted with permission from Dürr, C. J.; Hlalele, L.; Kaiser, A.; Brandau, S.; Barner-Kowollik, C. *Macromolecules* **2013**, *46*, 49-62. DOI: 10.1021/ma302017c. Copyright 2013 American Chemical Society.

namely strain promoted azide-alkyne click reactions,<sup>3-4</sup> and have been applied to the synthesis of complex macromolecular architectures. Nevertheless, strained alkynes are not readily available and require a complex multistep synthesis.

Diels–Alder (DA) cyclization is an alternative copper-free ligation technique that has been investigated extensively in polymer science.<sup>5</sup> An elegant and efficient method for the construction of complex macromolecular architectures is the RAFT-hetero-Diels–Alder (HDA) approach. Herein, a diene reacts with the electron-deficient C=S double bond of a dithioester RAFT agent after polymerization resulting in the formation of a dihydrothiopyran ring. Depending on the employed diene and the dienophile RAFT agent, coupling products provide temperature stability up to 120 °C that can be further enhanced by hydrogenation of the linkage structure.<sup>6</sup> RAFT-HDA reactions have been investigated for a broad range of common monomers and have been used for the synthesis of block copolymers,<sup>7</sup> star shaped<sup>8</sup> and comb polymers<sup>9</sup> as well as for the surface immobilization of polymer on microspheres<sup>10</sup> or solid (bio)substrates.<sup>11-12</sup>

In the present chapter, the first successful approach applying RAFT-HDA chemistry for the synthesis of complex NBR (star) block copolymers is presented. The application of orthogonal conjugation on NBR is challenging, considering the high density of functional moieties and the difficulties associated with preparing these polymers in a controlled fashion.

## 4.2 Experimental Section

### 4.2.1 Materials

Acrylonitrile (AN, > 99%, Acros), 1,3-butadiene (BD, > 99.5%, Air Liquide), styrene (S, Acros, 99%), *N,N'*-dicyclohexylcarbodiimide (DCC, 99%, Acros), 4-(dimethylamino)pyridine (DMAP, 99%, Aldrich), *trans,trans*-2,4-hexadien-1-ol (> 97%, SAFC), propane-1,3-diol (98%, Aldrich), 2-bromo-2-methylpropionyl bromide (98%, Acros), sodium azide (99%, Acros), copper sulfate pentahydrate (98+%, Aldrich), sodium (L)-ascorbate (> 98%, Aldrich), 1,1'-azobis(cyclohexane-1-carbonitrile) (98%, Aldrich), 2,2'-azobis(*N*-butyl-2-methylpropionamide) (Wako Ltd.), ethylenediaminetetraacetic acid disodium salt (Na<sub>2</sub>EDTA, Roth, 85%),

nickelocene (NiCp<sub>2</sub>, 99%, strem chemicals), triphenyl phosphine (VWR), NaI (> 99%, Fluka), butadiene diepoxide (97%, Aldrich), trifluoroacetic acid (TFA, Sigma, 99%), chlorobenzene (Acros, 99+%), *N,N*-dimethylacetamide (99.5%, Acros) and *N,N*-dimethylformamide (DMF, Alfa Aesar, 99%), methylene chloride (99.8%, extra dry, Acros), tetrahydrofuran (THF, 99.5%, extra dry, Acros) were used without further purification. Triethylamine (99%, ABCR) was dried over CaH<sub>2</sub> and distilled prior to use. Other solvents (synthesis grade) were obtained from VWR and used as received. 2-((dodecylsulfanyl)carbonothioyl)sulfanyl propanoic acid (DoPAT) was obtained from Orica Pty Ltd., Melbourne, Australia. Prop-2-yn-1-yl 2-(((dodecylsulfanyl)carbonothioyl)-sulfanyl)propanoate (see 3.2.2), 3-hydroxypropyl 2-bromo-2-methylpropanoate,<sup>13</sup> 1,4-diazidobutane-2,3-diol,<sup>14</sup> 1-benzyl pyridin-2-ylidithioformate,<sup>15</sup> 1-phenylethyl pyridin-2-ylidithioformate and 1-phenylethyl (diethoxyphosphoryl)dithioformate<sup>6</sup> were synthesized according to the literature.

#### 4.2.2 Synthesis of <sup>t</sup>Br RAFT Agent (1)

DoPAT (3.000 g, 8.56 mmol), DMAP (0.105 g, 0.86 mmol) and 3-hydroxypropyl 2-bromo-2-methylpropanoate (3.852 g, 17.1 mmol) were dissolved in methylene chloride (20 mL) and cooled to 0 °C with a water/ice bath. After addition of a solution of DCC (1.765 g, 8.58 mmol) in methylene chloride (10 mL) the cooling bath was removed and the mixture was stirred overnight at ambient temperature. The white precipitate was filtered off, the solution was diluted with methylene chloride (70 mL), extracted with 0.5 M aqueous HCl (2 × 100 mL) and washed with saturated NaHCO<sub>3</sub> solution (1 × 100 mL). The organic layer was dried over MgSO<sub>4</sub> and concentrated under vacuum. The crude product was purified by column chromatography on silica with hexane/ethyl acetate (5:1, v/v, *R<sub>f</sub>* 0.52) and dried under high vacuum to give RAFT agent **1** (3.882 g, 81%) as a yellow liquid.

<sup>1</sup>H NMR (400 MHz, CDCl<sub>3</sub>) δ 4.80 (q, *J* = 7.4 Hz, 1H, CH(CH<sub>3</sub>)), 4.31 – 4.18 (m, 4H, CH<sub>2</sub>-CH<sub>2</sub>-CH<sub>2</sub>), 3.34 (t, *J* = 7.4 Hz, 2H, S-CH<sub>2</sub>), 2.10 – 1.99 (m, 2H, CH<sub>2</sub>-CH<sub>2</sub>-CH<sub>2</sub>), 1.93 (s, 6H, Br-C(CH<sub>3</sub>)<sub>2</sub>), 1.73 – 1.64 (m, 2H, S-CH<sub>2</sub>-CH<sub>2</sub>), 1.59 (d, *J* = 7.4 Hz, 3H, CH(CH<sub>3</sub>)), 1.44 – 1.33 (m, 2H, S-CH<sub>2</sub>-CH<sub>2</sub>-CH<sub>2</sub>), 1.33 – 1.20 (m, 16H, CH<sub>3</sub>-(CH<sub>2</sub>)<sub>8</sub>), 0.87 (t, *J* = 6.9 Hz, 3H, CH<sub>3</sub>-CH<sub>2</sub>).

$^{13}\text{C}$  NMR (101 MHz,  $\text{CDCl}_3$ )  $\delta$  222.18 ( $\text{C}(\text{S})$ ), 171.62, 171.20, 62.33, 62.13, 55.75, 47.92, 37.42, 32.03, 30.82, 29.74, 29.66, 29.55, 29.45, 29.20, 29.03, 27.99, 27.75, 22.80, 16.85, 14.24.

Elemental analysis calculated (%) for  $\text{C}_{23}\text{H}_{41}\text{BrO}_4\text{S}_3$ : C, 49.54; H, 7.41; S, 17.25, found: C, 50.05; H, 7.45; S, 17.00.

#### 4.2.3 Synthesis of Midfunctionalized $^t\text{Br}$ RAFT Agent (**11**)

A solution of 1,4-diazidobutane-2,3-diol (0.751 g, 4.36 mmol) in DMF (5 mL) was added dropwise to a stirred solution of prop-2-yn-1-yl 2-(((dodecylsulfanyl)-carbonothioyl)-sulfanyl)propanoate (3.389 g, 8.72 mmol),  $\text{CuSO}_4 \cdot 5\text{H}_2\text{O}$  (0.217 g, 0.87 mmol) and sodium ascorbate (0.172 g, 0.87 mmol) in DMF (10 mL). The solution was stirred overnight at ambient temperature and diluted with diethyl ether (50 mL). A 2 M aqueous  $\text{Na}_2\text{EDTA}$  solution (50 mL) was added under slow stirring. The formed yellow precipitate was filtered off, washed with diethyl ether and dried in high vacuum to give compound **10** (2.995 g, 72%) as a yellow solid without further purification.

$^1\text{H}$  NMR (400 MHz,  $\text{CDCl}_3$ )  $\delta$  7.80 (s, 2H, triazole-*H*), 5.21 (s, 4H, O- $\text{CH}_2$ -triazole), 4.77 (q,  $J = 7.4$  Hz, 2H,  $\text{CH}(\text{CH}_3)$ ), 4.65 – 4.47 (m, 4H, triazole- $\text{CH}_2$ - $\text{CH}(\text{OH})$ ), 4.08 (br s, 2H, triazole- $\text{CH}_2$ - $\text{CH}(\text{OH})$ ), 3.96 (br s, 2H, OH), 3.39 – 3.23 (m, 4H, S- $\text{CH}_2$ ), 1.71 – 1.61 (m, 4H, S- $\text{CH}_2$ - $\text{CH}_2$ ), 1.55 (d,  $J = 7.4$  Hz, 6H,  $\text{CH}(\text{CH}_3)$ ), 1.41 – 1.32 (m, 4H, S- $\text{CH}_2$ - $\text{CH}_2$ - $\text{CH}_2$ ), 1.32 – 1.18 (m, 32H,  $\text{CH}_3$ - $(\text{CH}_2)_8$ ), 0.87 (t,  $J = 6.8$  Hz, 6H,  $\text{CH}_3$ - $\text{CH}_2$ ).

$^{13}\text{C}$  NMR (101 MHz,  $\text{CDCl}_3$ )  $\delta$  222.07 ( $\text{C}(\text{S})$ ), 222.03 ( $\text{C}'(\text{S})$ ), 171.18 ( $\text{C}(\text{O})-\text{O}$ ), 70.31, 58.76, 47.94, 37.51, 32.02, 29.75, 29.73, 29.68, 29.57, 29.45, 29.23, 29.06, 27.96, 22.80, 16.86, 14.23.

2-Bromo-2-methylpropionyl bromide (820  $\mu\text{L}$ , 6.62 mmol) was added dropwise to a stirred solution of **10** (1.572 g, 1.66 mmol) and triethylamine (930  $\mu\text{L}$ , 6.62 mmol) in dry methylene chloride (25 mL) under argon at 0 °C. The cooling bath was removed and the mixture was stirred for 7 h until thinlayer chromatography (TLC) control did not reveal any residual compound **10**. The white solid was filtered off and the solvent was removed under reduced pressure. The oily residue was dissolved in diethyl ether (100 mL), washed with 1 N aqueous HCl (2  $\times$  50 mL), brine (50 mL) and dried over  $\text{MgSO}_4$ . The solvent was removed

under reduced pressure and the crude product was purified by column chromatography on silica with hexane/ethyl acetate (2:1, v/v,  $R_f$  0.28) to give RAFT agent **11** as a yellow oil (1.951 g, 94%).

$^1\text{H}$  NMR (400 MHz,  $\text{CDCl}_3$ )  $\delta$  7.77 (s, 1H, triazole-*H*), 7.77 (s, 1H, triazole-*H'*), 5.53 – 5.45 (m, 2H, triazole- $\text{CH}_2\text{-CH(OR)}$ ), 5.27 (s, 4H, O- $\text{CH}_2\text{-triazole}$ ), 5.00 – 4.90 (m, 2H, triazole- $\text{C(H)(H')-CH(OR)}$ ), 4.81 (q,  $J = 7.4$  Hz, 1H,  $\text{CH(CH}_3\text{)}$ ), 4.79 (q,  $J = 7.3$  Hz, 1H,  $\text{CH'(CH}_3\text{)}$ ), 4.68 (m, 2H, triazole- $\text{C(H)(H')-CH(OR)}$ ), 3.39 – 3.24 (m, 4H, S- $\text{CH}_2$ ), 1.91 (s, 6H, Br- $\text{C(CH}_3\text{)}_2$ ), 1.85 (s, 6H, Br- $\text{C(CH}_3\text{)}_2$ ), 1.71 – 1.62 (m, 4H, S- $\text{CH}_2\text{-CH}_2$ ), 1.56 (d,  $J = 7.4$  Hz, 6H,  $\text{CH(CH}_3\text{)}$ ), 1.42 – 1.32 (m, 4H, S- $\text{CH}_2\text{-CH}_2\text{-CH}_2$ ), 1.32 – 1.18 (m, 32H,  $\text{CH-(CH}_2\text{)}_8$ ), 0.86 (t,  $J = 6.8$  Hz, 6H,  $\text{CH}_2\text{-CH}_3$ ).

$^{13}\text{C}$  NMR (101 MHz,  $\text{CDCl}_3$ )  $\delta$  221.94 ( $\text{C(S)}$ ), 171.12, 171.08, 170.22, 142.96 (triazole- $\text{C}$ ), 125.63 (triazole- $\text{CH}$ ), 125.53 (triazole- $\text{C'H}$ ), 71.37, 58.87, 58.83, 55.26, 49.64, 47.89, 47.85, 37.45, 32.01, 30.50, 30.41, 29.72, 29.71, 29.65, 29.54, 29.43, 29.20, 29.02, 27.96, 22.78, 16.90, 16.86, 14.22.

Elemental analysis calculated (%) for  $\text{C}_{50}\text{H}_{82}\text{Br}_2\text{N}_6\text{O}_8\text{S}_6$ : C, 48.14; H, 6.63; N, 6.74; S, 15.42, found: C, 48.15; H, 6.48; N, 6.51; S, 14.61.

#### 4.2.4 Synthesis of Diene-Functional Chain Transfer Agent Hexa-2,4-dien-1-yl 2-((dodecylthio)carbonothioylthio)propanoate (**2**).

DoPAT (6.000 g, 17.1 mmol), DMAP (0.417 g, 3.4 mmol) and *trans,trans*-2,4-hexadien-1-ol (5.496 g, 56.0 mmol) were dissolved in dry methylene chloride (25 mL) and cooled to 0 °C. A solution of DCC (3.528 g, 17.1 mmol) in dry methylene chloride (5 mL) was added. The cooling bath was removed and the mixture was stirred overnight at ambient temperature. The white precipitate was filtered off and methylene chloride (50 mL) was added. The solution was washed with 0.5 N aqueous HCl (2 × 50 mL) and saturated aqueous  $\text{NaHCO}_3$  solution (50 mL). The organic layer was dried over  $\text{MgSO}_4$  and concentrated in vacuum. The crude product was purified by column chromatography on silica gel with n-hexane/ethyl acetate (15:1, v/v,  $R_f$  0.59) to give **2** (5.024 g, 68%) as a yellow oil.

$^1\text{H}$  NMR (400 MHz,  $\text{CDCl}_3$ )  $\delta$  6.26 (dd,  $J = 15.2, 10.5$  Hz, 1H, O- $\text{CH}_2\text{-CH=CH}$ ), 6.05 (ddd,  $J = 14.8, 10.5, 1.4$  Hz, 1H,  $\text{CH}_3\text{-CH=CH}$ ), 5.76 (dq,  $J = 14.8, 6.7$  Hz, 1H,  $\text{CH}_3\text{-CH=CH}$ ), 5.60 (dt,  $J = 15.2, 6.6$  Hz, 1H, O- $\text{CH}_2\text{-CH=CH}$ ), 4.83 (q,  $J = 7.4$  Hz, 1H,

CH(CH<sub>3</sub>)), 4.63 (d,  $J = 6.6$  Hz, 2H, O-CH<sub>2</sub>), 3.34 (t,  $J = 7.5$  Hz, 2H, S-CH<sub>2</sub>), 1.76 (d,  $J = 6.7$  Hz, 3H, CH<sub>3</sub>-CH=CH), 1.74 – 1.64 (m, 2H, S-CH<sub>2</sub>-CH<sub>2</sub>), 1.59 (d,  $J = 7.4$  Hz, 3H, CH(CH<sub>3</sub>)), 1.44 – 1.34 (m, 2H, S-CH<sub>2</sub>-CH<sub>2</sub>-CH<sub>2</sub>), 1.33 – 1.20 (m, 16H, aliphatic Hs), 0.88 (t,  $J = 6.8$  Hz, 3H, CH<sub>3</sub>-CH<sub>2</sub>).

<sup>13</sup>C NMR (101 MHz, CDCl<sub>3</sub>)  $\delta$  222.11, 171.04, 135.46, 131.70, 130.50, 123.10, 66.37, 48.11, 37.37, 32.04, 29.75, 29.68, 29.56, 29.47, 29.22, 29.03, 28.02, 22.81, 18.26, 17.09, 14.25.

Elemental analysis calculated (%) for C<sub>22</sub>H<sub>38</sub>O<sub>2</sub>S<sub>3</sub>: C, 61.35; H, 8.89; O, 7.43; S, 22.33, found: C, 59.52; H, 8.77; O, 7.84; S, 23.36.

#### 4.2.5 Synthesis of Cp-Functional RAFT Agent

In a glove box, **1** (0.299 g, 0.54 mmol), PPh<sub>3</sub> (0.282 g, 1.07 mmol), NaI (0.483 g, 3.22 mmol) and nickelocene (0.203 g, 1.07 mmol) was dissolved in dry THF (4 mL) and stirred under argon for 6 h at room temperature. The solution was diluted with THF and filtered over basic aluminum oxide. All volatiles were removed in vacuum, the residue was dissolved in methylene chloride (10 mL) and washed with deionized water (2 × 10 mL). The organic phase was dried over MgSO<sub>4</sub>, concentrated in vacuum and purified by column chromatography on silica gel with n-hexane/ethyl acetate (10:1, v/v,  $R_f$  0.28) to give the modified trithiocarbonate (0.207 g, 71%) as a yellow liquid. NMR characterization is provided in Figure 4.8 (see page 114).

#### 4.2.6 Experimental Determination of the Benzylthiodihydrothiopyranil-pyridine Structure **3**+BD Responsible for the Loss of Control in AN/BD Copolymerizations Utilizing Controlling Agent **3**.

A high pressure glass reactor was charged with controlling agent **3** (100 mg, 0.41 mmol) and butylated hydroxytoluene (BHT, 450 mg, 2.04 mmol) as an inhibitor. Oxygen was removed by three consecutive vacuum/nitrogen cycles and BD (45 mL, 542 mmol) was added via a metal burette. The reactor was sealed and heated to 100 °C. After 54 h the reactor was vented. Residual BD was removed in high vacuum and a crude <sup>1</sup>H NMR was recorded. The crude product was purified by column chromatography on silica. After residual controlling agent **3** eluted from

the column with hexane/methylene chloride (1:1, v/v,  $R_f$  0.47), the methylene chloride content of the liquid phase was increased to 1:2 (v/v). The cyclization product **3+BD** ( $R_f$  0.2 in hexane/methylene chloride 1:1, v/v) was washed from the column and analyzed by NMR spectroscopy.

The  $^1\text{H}$  NMR spectrum of **3+BD** is provided in Figure 4.25B in the *Appendix* at the end of the current chapter and is compared to the spectrum of controlling agent **3** (Figure 4.25A). Olefinic proton resonances d and e and allyl resonances c and f of the formed heterocycle indicate the degradation of controlling agent **3** via HDA reaction with BD. The formation of **3+BD** is accompanied by a shift of the aromatic signals ( $\text{H}^{\text{Py}}$  and  $\text{H}^{\text{Bn}}$  to  $\text{H}'^{\text{Py}}$  and  $\text{H}'^{\text{Bn}}$ ) as well as the methylene protons of the benzyl moiety (a to b). Moreover,  $^{13}\text{C}$  NMR experiments (not shown) reveal the loss of the downfield resonance at 226 ppm assigned to the dithioester carbonyl of **3** when reacting with BD.

Integration of signals a and b of the crude  $^1\text{H}$  NMR taken after the reaction of **3** and BD allows evaluation of the conversion of **3+BD** formation to be > 95%. A steady removal of controlling agent **3** from AN/BD copolymerization system via HDA cyclization over the polymerization is therefore expected. The resonances of the protons  $\text{H}'^{\text{Py}}$ ,  $\text{H}'^{\text{Bn}}$ , b, c, d, e and f of the cyclic adduct are also observed when analyzing polymerization mixtures of AN/BD/**3** polymerization system via  $^1\text{H}$  NMR spectroscopy. These results indicate formation of **3+BD** and the respective macromolecular HDA cyclization adducts to cause the loss of control over RAFT copolymerization of AN/BD when using controlling agent **3**.

#### 4.2.7 Polymerizations

Solution polymerizations of AN and BD under azeotropic conditions (AN/BD = 38/62) were performed at 100 °C in a pressure stable glass reactor setup as reported earlier.<sup>1,16</sup> Polymerizations were performed in chlorobenzene, *N,N*-dimethylacetamide or acetone as solvents and either 1,1'-azobis(cyclohexane-1-carbonitrile) or 2,2'-azobis(*N*-butyl-2-methylpropionamide) were used as initiators. Polymers were recovered by precipitation in cold ethanol. Bulk copolymerizations of AN and S were performed in a round bottom flask under argon. 1,1'-Azobis(cyclohexane-1-carbonitrile) was utilized as a initiator. The

polymerization mixture was purged with argon for 30 min prior to polymerization. The flasks were sealed and immersed in a pre-heated oil bath at 90 °C to start the reaction. Polymerizations were stopped by cooling the reaction mixture to 0 °C and opening the flask to air. The polymer was recovered by repeated precipitation in cold methanol and dried under high vacuum. When employed in S/AN copolymerizations, AN was de-inhibited via filtration over basic aluminum oxide. Experimental details for each polymerization are given in Table 4.3 (see page 103).

#### 4.2.8 Cp-Functionalization of NBRs

Under inert conditions <sup>t</sup>Br-functional NBR, NiCp<sub>2</sub>, NaI and triphenyl phosphine were dissolved in dry THF and stirred overnight at ambient temperature. Solids were filtered off and the solution was percolated over a short column of basic aluminium oxide. The obtained brown solution was concentrated in vacuum and the polymer was recovered by precipitation in cold ethanol. The polymer was dissolved in methylene chloride and subjected to an aqueous washing procedure before being recovered by repeated precipitation and drying under vacuum. Further experimental details are provided in Table 4.7 in the *Appendix*.

#### 4.2.9 Hetero-Diels–Alder Reactions

Equimolar amounts of dienophile end-capped styrene-acrylonitrile copolymer (SAN) and Cp-capped NBR were dissolved in chloroform and TFA was added. Solutions were stirred at ambient temperature and polymers were dried under high vacuum. For further experimental details see Table 4.4 (see page 113).

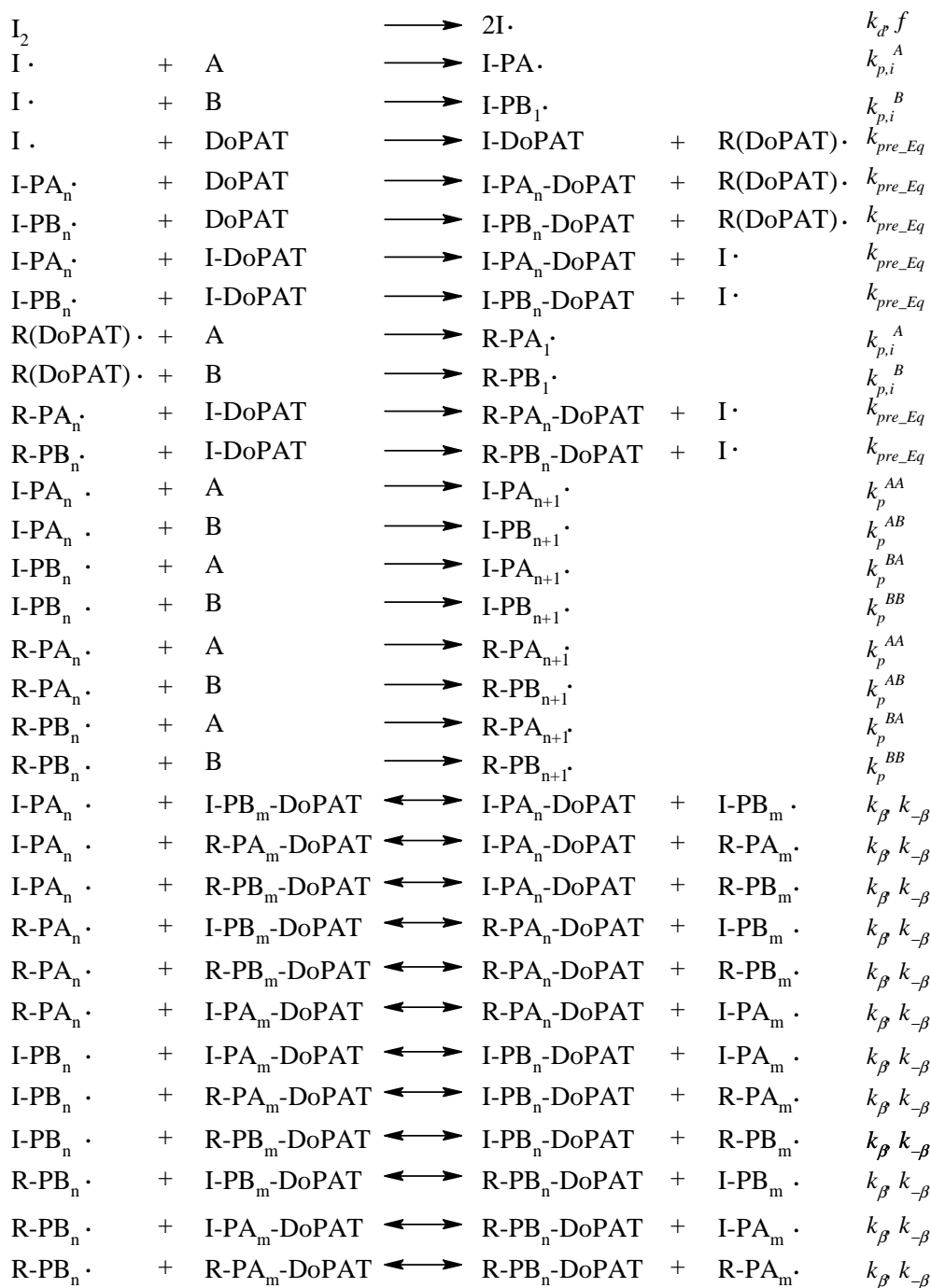
#### 4.2.10 PREDICI Simulations<sup>‡</sup>

The simulations were performed with the PREDICI<sup>®</sup> software package version 6.81.1 on a standard computer (2.4 GHz i5 processor, 4.0 GB RAM). The simulations were carried out in distribution mode. The implemented model for AN/BD copolymerization is illustrated in Scheme 4.1 with the relevant rate coefficients in Table 4.1. Scheme 4.2 illustrates the model implemented for simulation of AN/S copolymerization, with the employed rate coefficients shown in

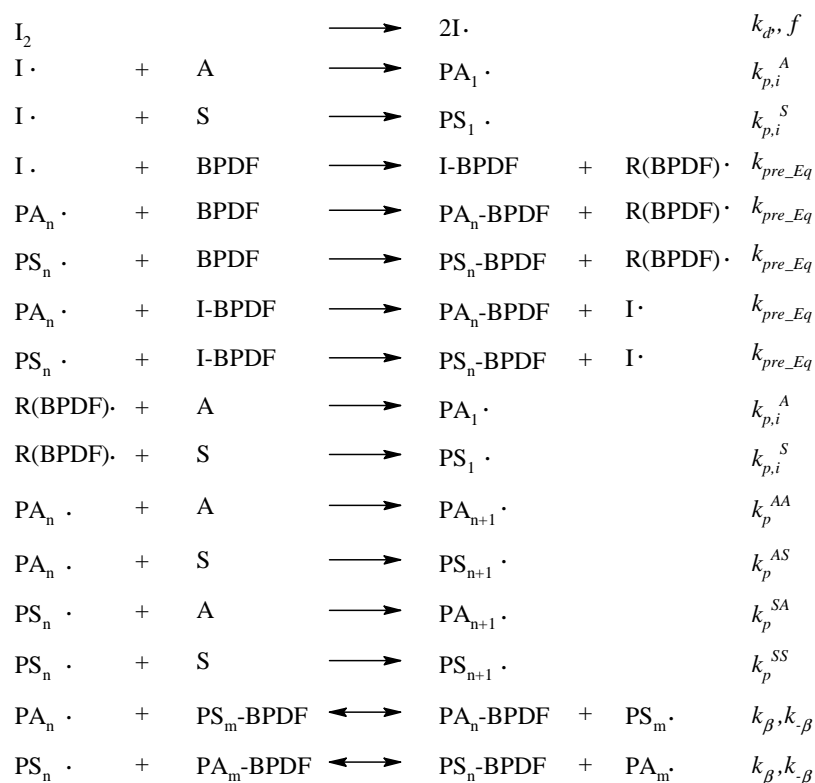
---

<sup>‡</sup> PREDICI simulations were performed by Dr. Lebohang Hlalele, Karlsruhe Institute of Technology, Institut für Technische Chemie und Polymerchemie.

Table 4.2. In both Schemes, termination reactions are not shown but were included in the implemented models at rates governed by the rate coefficients shown in Table 4.1 and Table 4.2, respectively. The “Q-type” system for the description of RAFT equilibrium reactions was adopted in both simulations.<sup>17-18</sup> A comparison of conversion and  $M_n$  data obtained experimentally, with that obtained from



**Scheme 4.1.** Implemented model for AN/BD copolymerization.



**Scheme 4.2.** Implemented model for AN/S copolymerization.

PREDICI<sup>®</sup> simulation is shown in Table 4.8 and Table 4.9 (both provided in the *Appendix*). Good correlation between experimental and simulated data is observed in both copolymerization processes. From simulation results in both cases of SAN and NBR preparations, the weight fractions of chains bearing the desired end group functionality required for subsequent conjugation reaction were computed.

In both copolymerization processes, the rate coefficient of addition of primary radical to monomer was assumed to be an order of magnitude larger than the corresponding rate coefficient of propagation for the respective monomer. The

**Table 4.1.** Relevant rate coefficients for AN/BD copolymerizations.

coefficient	A	$E_a$ (KJ·mol <sup>-1</sup> )	coefficient	ref.
$k_p^A$	$1.79 \times 10^6$	15.4		19
$k_p^B$	$1.20 \times 10^8$	38.91		20
$r_A$			0.016	20
$r_B$			0.408	20

**Table 4.2.** Relevant rate coefficients for AN/S copolymerizations.

coefficient	$A$	$E_a$ (KJ·mol <sup>-1</sup> )	coefficient	ref.
$k_p^A$	$1.79 \times 10^6$	15.4		19
$k_p^S$	$4.27 \times 10^7$	32.5		21
$r_A$			0.078	22
$r_S$			0.36	22

rate coefficient of addition of radicals to the RAFT agent in the pre-equilibrium steps was set to  $1.0 \times 10^6$  L·mol<sup>-1</sup>·s<sup>-1</sup>. The rate coefficients of addition ( $k_\beta$ ) and fragmentation ( $k_{-\beta}$ ) to the macro-RAFT were both set to  $1.0 \times 10^6$  L·mol<sup>-1</sup>·s<sup>-1</sup> and  $1.0 \times 10^6$  s<sup>-1</sup>. For termination processes, the rate coefficient of termination for processes involving primary radicals was set to  $1.0 \times 10^9$  L·mol<sup>-1</sup>·s<sup>-1</sup>, while it was set to  $1.0 \times 10^8$  L·mol<sup>-1</sup>·s<sup>-1</sup> for termination process involving two macro-radicals.

#### 4.2.11 SEC Deconvolution<sup>§</sup>

The SEC traces were deconvoluted using PeakFit version 4.12 (SeaSolve software). The method applied for the deconvolution process is described elsewhere.<sup>23</sup> Determination of the weight fractions of residual SAN or NBR was performed under the assumption of similar refractive index increments  $dn/dc$  of both polymer precursors. This simplification is necessary since  $dn/dc$  values of the NBR-*b*-SAN block copolymers (**8-b-7**) are not easily accessible. Determination of reliable refractive index increments in principle requires pure samples that do not contain impurities. However, the main message of the manuscript is that conjugation does not proceed to quantitative conversion for reasons explained in the following, thus not allowing determination of the respective  $dn/dc$ .

#### 4.2.12 Instrumentation

<sup>1</sup>H NMR and <sup>13</sup>C NMR spectra were recorded at room temperature on a Bruker Advance 400 NMR spectrometer and referenced to the remaining solvent signal.

<sup>§</sup> SEC deconvolution was performed by Dr. Lebohang Hlalele, Karlsruhe Institute of Technology, Institut für Technische Chemie und Polymerchemie.

Molecular weight determination was performed on a size exclusion chromatography (SEC) system (PL-GPC 50 Plus, Polymer Laboratories) consisting of an auto injector, a guard column (PLgel Mixed C, 50 × 7.5 mm), three linear columns (PLgel Mixed C, 300 × 7.5 mm, 5 μm bead-size) and a differential refractive index detector using THF as the eluent at 35 °C and a flow rate of 1 mL·min<sup>-1</sup>. The system was calibrated using narrow polystyrene (PS) standards (obtained from PSS) ranging from 160 to 6 × 10<sup>6</sup> g·mol<sup>-1</sup>. Samples were injected from solutions in THF (2 mg·mL<sup>-1</sup>) and molecular weight distributions were referenced versus PS standards. Molecular weight evaluations for NBR were performed employing the Mark–Houwink–Kuhn–Sakurada (MHKS) parameters of PS ( $\alpha = 0.70$ ,  $K = 14.1 \times 10^{-5} \text{ dL}\cdot\text{g}^{-1}$ ), SAN samples were evaluated using the appropriate MHKS parameters ( $\alpha = 0.68$ ,  $K = 21.5 \times 10^{-5} \text{ dL}\cdot\text{g}^{-1}$ ).<sup>24</sup>

Electrospray ionization (ESI) mass spectra were recorded on a LXQ mass spectrometer (ThermoFisher Scientific, San Jose, CA, USA) equipped with an atmospheric pressure ionization source operating in the nebulizer assisted electrospray mode. The system was calibrated with a standard containing caffeine, Met-Arg-Phe-Ala acetate and a mixture of fluorinated phosphazenes (Ultramark 1621), purchased from Aldrich. A spray voltage of 4.5 kV, a dimensionless sweep gas flow rate of 2 and a dimensionless sheath gas flow-rate of 12 were applied. The capillary voltage, the tube lens offset voltage and the capillary temperature were set to 60 V, 110 V and 275 °C, respectively. For SEC-ESI-MS measurements the mass spectrometer was coupled to a Series 1200 high performance liquid chromatography (HPLC) system (Agilent, Santa Clara, CA, USA) with THF as the eluent in accordance to a setup described earlier.<sup>25</sup> Polymer samples were dissolved in THF (2 mg·mL<sup>-1</sup>) and injected onto the HPLC system.

## 4.3 Results and Discussion

### 4.3.1 RAFT Polymerizations

The work presented in the current chapter aims at the development of a simple and rapid approach for the synthesis of block copolymers and miktoarm star copolymers of NBR with nonelastomeric polymer building blocks. Since NBRs are

an important commercial product with widespread applications, a facile route to conjugate NBR with diverse other building blocks is highly desirable. Such an approach allows for the synthesis of novel polymers combining the outstanding elastomeric properties of NBRs with those of other polymers such as thermoplastic materials, to just name one example. Elastomer blends often show incompatibility resulting in a coarse morphology and a poor interaction across the phase boundaries thus requiring compatibilization.<sup>26</sup> For this very reason the RAFT-HDA approach was chosen, as it allows conjugation of polymer building blocks at nondemanding reaction conditions without need for metallic catalysts, often influencing NBR ageing rates. The application of RAFT-HDA requires the synthesis of a diene- and a dienophile-functionalized polymer. The dienophile-functional polymer building block can be directly obtained by RAFT polymerization when employing distinct controlling agents containing an electron withdrawing Z-group.<sup>15,27</sup> Enophile chain-ends of the second polymer building block can be chosen from either open-chain dienes<sup>7</sup> or a cyclic diene structure.<sup>28</sup> Major advantages of the utilization of cyclic diene structures, *i.e.* cyclopentadienes (Cps), are the mild reaction conditions and short reaction times necessary to obtain full conversion of the HDA cyclization.<sup>29</sup>

The diene-functional NBR building blocks were obtained via RAFT polymerization. One of the main advantage of RAFT over other reversible-deactivation radical polymerization techniques – *i.e.* atom transfer radical polymerization (ATRP)<sup>30</sup> and nitroxide mediated polymerization (NMP)<sup>31</sup> – is a high and steady radical concentration resulting in nonreduced polymerization rates.<sup>32</sup> The RAFT process provides access to functional polymers by modification of the R- and Z-group of the controlling agent. In the herein presented study an R-group approach was chosen for the synthesis of diene-capped polymers. Nevertheless, a Cp moiety is not orthogonal to the investigated AN/BD copolymerization setup. Li *et al.* showed that at elevated temperatures Cp reacts with AN in a Diels–Alder reaction forming the cycloadduct 5-cyanobicyclo[2.2.1]-hept-2-ene.<sup>33</sup> The experiments were performed under conditions similar to the AN/BD copolymerization system, *i.e.* at elevated temperatures and in solution, and the cycloadduct was obtained with high yields within 24 h. Richards and co-

workers found that a Diels–Alder reaction of AN and Cp proceeds even at temperatures as low as 4 °C, albeit half-lives of 193 h were obtained.<sup>34</sup> Moreover, Cp moieties of small organic compounds have a high affinity toward dimerization,<sup>35</sup> yet sufficient stability is obtained when attached to polymeric substrates.<sup>36</sup>

Based on these previous studies diene-functional NBR polymers were synthesized, yet the reactive cyclic diene chain-end was introduced into the polymer building blocks in a postpolymerization modification step. A tertiary bromoalkane (<sup>t</sup>Br) end-group was considered to be a suitable precursor for the synthesis of Cp-modified NBRs via polymer analogue reaction. Thus, a novel bromide-functional transfer agent **1** (see Figure 4.1) was synthesized with good yields from DoPAT and 3-hydroxypropyl 2-bromo-2-methylpropanoate in a Steglich esterification.

**1** was applied in RAFT polymerizations to synthesize <sup>t</sup>Br-functional polymers with molecular weights ranging from 1000 to 70 000 g·mol<sup>-1</sup> under azeotropic conditions (38/62, AN/BD). In agreement with previous results (see chapter 3), dispersities below 1.6 were obtained. An overview of polymerizations discussed in the present chapter is provided in Table 4.3. Transfer agent to initiator ratios [1]<sub>0</sub>/[Ini]<sub>0</sub> were adjusted from 15:1 to 5:1 with respect to the desired molecular

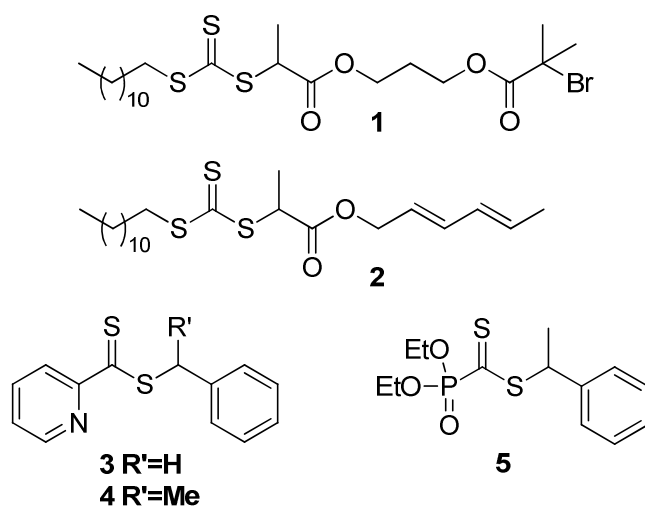


**Figure 4.1.** Trithiocarbonates and dithioesters employed during the RAFT mediated polymerization for the synthesis of block and miktoarm star copolymers of NBR and SAN via modular conjugation techniques.

**Table 4.3.** Experimental conditions of AN/BD and S/AN copolymerizations.<sup>a</sup>

entry	RAFT agent	type	[RAFT] <sub>0</sub> (mM)	[Ini] <sub>0</sub> (mM)	<i>t</i> (h)	<i>p</i> <sup>b</sup> (%)		<i>M</i> <sub>n</sub> (g·mol <sup>-1</sup> ) <sup>c</sup>	<i>D</i> <sup>c</sup>
1	<b>1</b>	NBR	27.9	3.5	5	29.1	<b>6a</b>	5900	1.3
2	<b>1</b>	NBR	2.0	0.3	22	12.3	<b>6b</b>	39 000	1.5
3	<b>1</b>	NBR <sup>d</sup>	96.2	6.4	3	27.0	<b>6c</b>	1300	1.3
4	<b>1</b>	NBR	14.0	1.7	7	21.8	<b>6d</b>	10 600	1.3
5	<b>1</b>	NBR	5.6	0.7	8	11.6	<b>6e</b>	15 600	1.4
6	<b>1</b>	NBR	0.9	0.2	22	10.6	<b>6f</b>	68 000	1.6
7	<b>2</b>	NBR	14.0	1.7	22	38.9		19 000	1.4
8	<b>3</b>	NBR <sup>e,f</sup>	12.7	2.5	22	14.5		23 000	1.8
9	<b>4</b>	NBR <sup>f</sup>	12.7	2.5	22	16.1		25 000	3.1
10	<b>5</b>	NBR <sup>f</sup>	12.7	2.5	6	7.8		180 000	2.1
11	<b>3</b>	SAN	13.9	1.4	4	9.8	<b>7a</b>	7900	1.2
12	<b>3</b>	SAN	7.0	0.7	7	22.9	<b>7b</b>	28 000	1.1
13	<b>3</b>	SAN	1.1	0.1	6	11.2	<b>7c</b>	76 000	1.2
14	<b>3</b>	SAN	20.9	2.1	5	17.8	<b>7d</b>	9200	1.2
15	<b>11</b>	NBR	31.5	4.2	5	37.2	<b>12a</b>	5100	1.1
16	<b>11</b>	NBR	2.2	0.3	22	16.4	<b>12b</b>	42 000	1.4

<sup>a</sup> Conditions: NBR was synthesized in chlorobenzene at 100 °C employing 1,1'-azobis(cyclohexane-1-carbonitrile) as initiator, except stated otherwise. AN and BD were employed at the azeotropic ratio of 38/62 at an overall monomer concentration of 9.5 mol·l<sup>-1</sup>. SAN polymerizations were performed in bulk at 90 °C. AN and S were employed at the azeotropic ratio of 38/62. <sup>b</sup> Conversion was determined gravimetrically. <sup>c</sup> Obtained from SEC versus PS standards. <sup>d</sup> Polymerization in acetone, polymer was recovered by solvent evaporation. <sup>e</sup> Polymerization in *N,N*-dimethylacetamide. <sup>f</sup> 2,2'-azobis(*N*-butyl-2-methylpropionamide) was used instead of 1,1'-azobis(cyclohexane-1-carbonitrile).

weight, conversion and polymerization time. SEC traces at various reaction times for two polymerizations employing **1** are provided in Figure 4.23 in the *Appendix* at the end of the current chapter. The elugrams exhibit monomodal molecular weight distributions, and peak retention time decreases with increasing conversion. While SEC traces of polymerizations aiming at low molecular weight do not provide any features (Figure 4.23A), high molecular weight samples exhibit a strong tailing toward longer retention time (Figure 4.23B). Formation of low

molecular weight material most probably proceeds by chain termination events and is an inevitable side reaction of the RAFT process.

Evolution of molar mass with conversion of several AN/BD copolymerizations employing transfer agent **1** is depicted in Figure 4.2. In all polymerizations a linear behavior is obtained, indicating the controlled character of the investigated system. Nevertheless, a slight hybrid behavior<sup>37</sup> is observed for polymerizations when low concentrations of controlling agent **1** are employed. Here, extrapolation of conversion toward the limit of zero conversion provides molecular weights corresponding to a  $DP_n > 1$ .

Polymers obtained in the RAFT mediated AN/BD copolymerization were analyzed by NMR spectroscopy. A  $^1\text{H}$  NMR spectrum of a  $10\,600\text{ g}\cdot\text{mol}^{-1}$   $^t\text{Br}$ -functional NBR **6d** (Table 4.3, entry 4) is provided in Figure 4.3A. A singlet resonance at 1.92 ppm is assigned to the methyl protons (a) of the isobutyryl bromide chain-end. Resonances of the methylene protons b and c of the propane

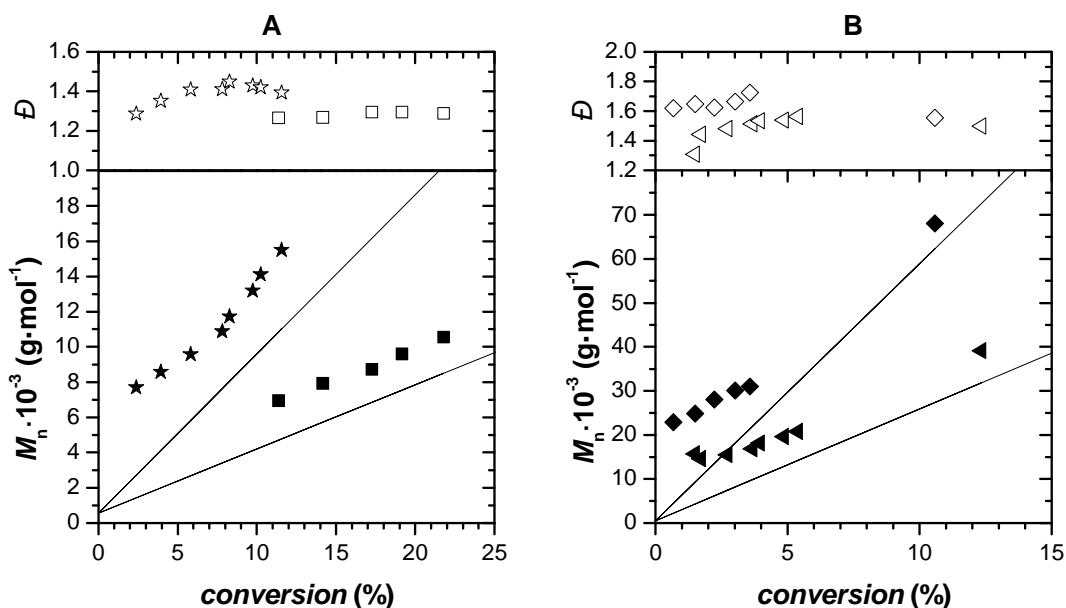


**Figure 4.2.** Evolution of molar mass (filled symbols) and dispersity (empty symbols) with conversion for RAFT mediated copolymerizations of AN and BD under azeotropic conditions (38/62) at 100 °C with an overall initial monomer concentration  $[\text{M}]_0$  of  $9.5\text{ mol}\cdot\text{L}^{-1}$ . Note the different scales of the axes. Conditions: A) Squares:  $[\text{RAFT}]_0$   $14.0\text{ mmol}\cdot\text{L}^{-1}$ ,  $[\text{Ini}]_0$   $1.7\text{ mmol}\cdot\text{L}^{-1}$ , samples taken after 3, 4, 5, 6 and 7 h, stars:  $[\text{RAFT}]_0$   $5.6\text{ mmol}\cdot\text{L}^{-1}$ ,  $[\text{Ini}]_0$   $0.7\text{ mmol}\cdot\text{L}^{-1}$ , samples taken after 1, 2, 3, 4, 5, 6, 7 and 8 h, B) triangles:  $[\text{RAFT}]_0$   $2.0\text{ mmol}\cdot\text{L}^{-1}$ ,  $[\text{Ini}]_0$   $0.3\text{ mmol}\cdot\text{L}^{-1}$ , samples taken after 1, 2, 3, 4, 5, 6, 7 and 22 h, rhombs:  $[\text{RAFT}]_0$   $0.9\text{ mmol}\cdot\text{L}^{-1}$ ,  $[\text{Ini}]_0$   $0.2\text{ mmol}\cdot\text{L}^{-1}$ , samples taken after 2, 3, 4, 5, 6 and 22 h.

linkage in  $\alpha$ -position to the ester moieties both appear around 4.2 ppm and 4.1 ppm, respectively. Methyl protons of the propanoate moiety (d) resonate around 1.1 ppm and are shifted toward higher field when compared to their resonances within the controlling agent **1** (for  $^1\text{H}$  NMR spectrum of **1** see Figure 4.22 in the *Appendix*). The high-field shift is proof for the successful incorporation of monomers into the controlling agent, as incorporation induces a separation of the propanoate moiety and the electron-withdrawing trithiocarbonate moiety during polymerization. The molar mass of sample **6d** was calculated to be  $6100\text{ g}\cdot\text{mol}^{-1}$  by comparison of the integrals of resonances b, c, f and h with those of the backbone signals. The elevated molar mass obtained from conventional SEC in comparison to NMR spectroscopy is a result of the determination of PS relative values in SEC due to the lack of Mark–Houwink–Kuhn–Sakurada (MHKS) parameters for NBR.

A high degree of functionality is a prerequisite for an efficient macromolecular conjugation. SEC-ESI mass spectrometry is a powerful tool for the determination of chain-end functionality of polymers and was applied to the analysis of a low molecular weight sample of  $^t\text{Br}$ -functional NBR **6c**. A magnified view into the

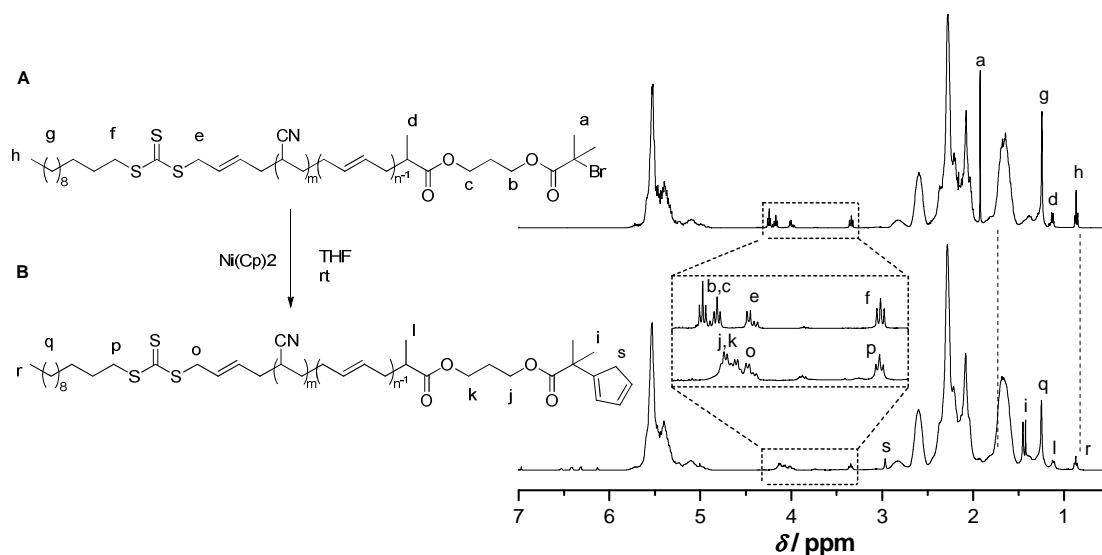


**Figure 4.3.** NMR spectra of A)  $^t\text{Br}$ -functional NBR **6d** of  $10\ 600\text{ g}\cdot\text{mol}^{-1}$  and B) the respective Cp-functional NBR **8d** obtained from substitution of the bromine. Lower case letters are provided for the assignment of the resonances of R- and Z-group protons. Signals of the polymer backbone have been assigned elsewhere in more detail.<sup>20</sup> 1,2-incorporation of BD into the polymer is observed yet omitted for clarity of the chemical structures.

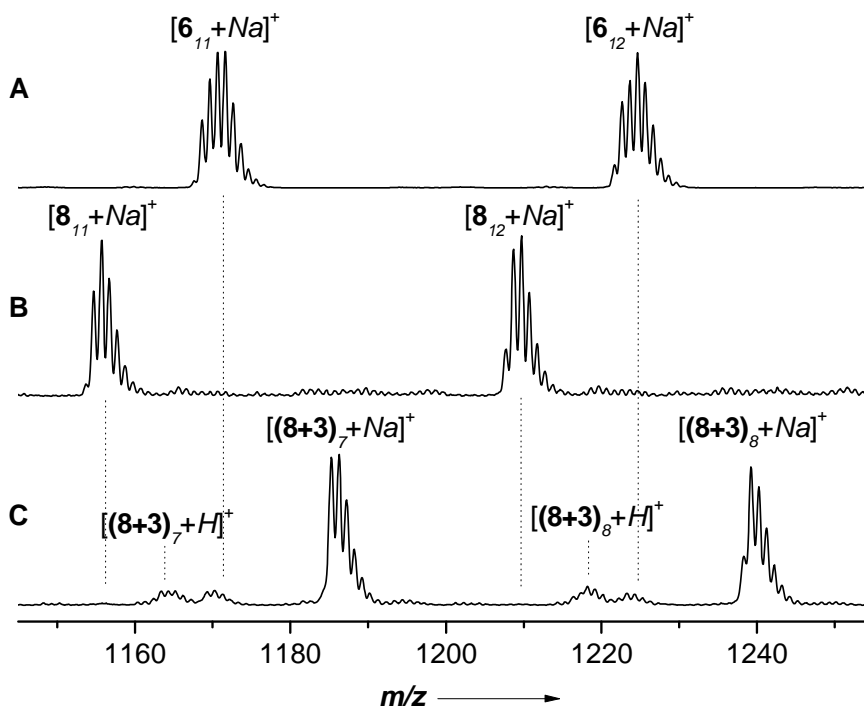


**Figure 4.4.** SEC-ESI mass spectrometric analysis of A)  $t$ Br-functional NBR **6c**, B) Cp-functional NBR **8c** and C) Cp-functional NBR **8c** after reaction with an excess of RAFT agent **3** in the presence of TFA.

region of 1145–1255 Da of a  $1300 \text{ g}\cdot\text{mol}^{-1}$   $t$ Br-functional NBR **6c** (Table 4.3, entry 3) is provided in Figure 4.4A. Signals repeat in intervals of 53–54 Da and are assigned to the sodium adducts  $[6_{m+n}+Na]^+$  of the RAFT polymers demonstrating a successful incorporation of the bromide end-group. Herein, almost exclusive formation of RAFT polymer is observed; small signals of initiator derived chains can barely be discerned from the noise. Nevertheless, formation of nonfunctional polymer chains is expected for higher molecular weight samples. The rather uncommon signal structure of the NBR ESI mass spectra has been observed earlier (see chapter 3.3.2) and is a result of the molecular weights of BD and AN differing in one atomic unit only. A comparative study of experimentally determined and theoretically calculated mass-to-charge ratios for a polymer **6** with  $m+n=11$  incorporated monomer units  $[6_{11}+Na]^+$  is provided in Figure 4.24 of the *Appendix*, demonstrating the presence of polymer chains with various  $m/n$  ratios. Nevertheless, signals derived from monomer compositions strongly deviating from the azeotrope of 38/62 (AN/BD) cannot be found or are observed in low quantities only.

Direct utilization of an open-chain diene-functional trithiocarbonate controlling agent (**2**, see Figure 4.1) initially studied as an alternative pathway to obtain diene-capped NBRs proved to be unsuitable. The unsuitability was due to side reactions of the conjugated olefin of the hexadienol chain-end with AN in a Diels–Alder reaction as shown in Figure 4.5 and Figure 4.6. Such a behavior is not expected since conjugated double bonds of diene-pendant acrylates were proven to be orthogonal to copolymerization with styrene.<sup>9</sup>

A chain transfer agent commonly used in the RAFT polymerization for a successive HDA reaction is benzyl pyridinyl dithioformate (**3**, see Figure 4.1). A characteristic feature of **3** is the C=S double bond with switchable electron-withdrawing properties. The C=S double bond readily reacts with conjugated olefins<sup>38</sup> in a HDA reaction when enhancing the electron-withdrawing properties of the heteroaromatic system by protonation of the pyridinyl nitrogen. The ability of **3** to undergo HDA reactions was exploited earlier for the synthesis of block copolymers<sup>7</sup> and the access of more complex macromolecular architectures.<sup>8</sup>

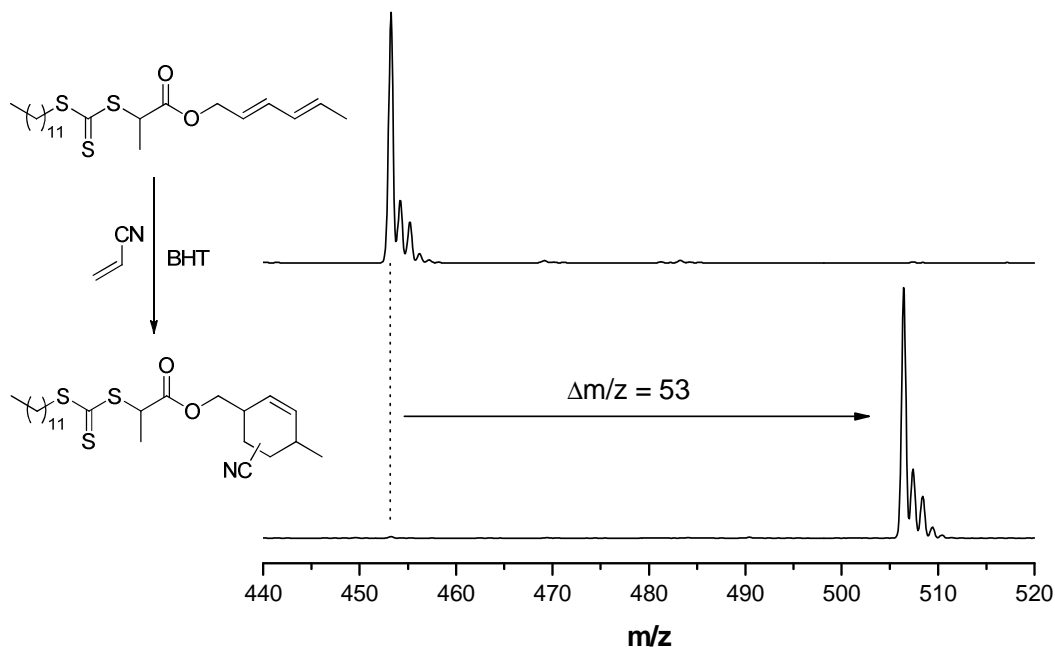


**Figure 4.5.** ESI mass spectra of the open-chain diene-functional trithiocarbonate **2** (upper panel) and the obtained Diels–Alder cyclization product (lower panel). Formation of the cyclohexene was observed after reaction of **2** with an excess of AN for 22 h at 100 °C in presence of butylated hydroxytoluene (BHT) as a radical inhibitor. Prior to analysis, the cycloadduct was separated from unreacted trithiocarbonate **2** by column chromatography.

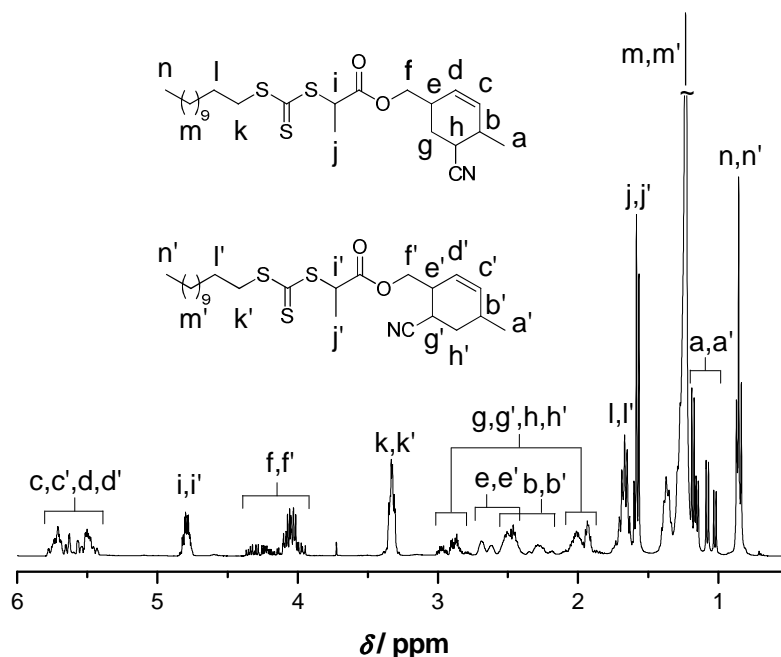


**Figure 4.6.**  $^1\text{H}$  NMR characterization of the Diels–Alder product of **2** and AN recorded in  $\text{CDCl}_3$  at ambient temperature. Prior to analysis, the cycloadduct was separated from unreacted trithiocarbonate **2** by column chromatography.

In the present study **3** was applied as a chain transfer agent in the RAFT mediated AN/S copolymerization in their azeotropic ratio<sup>39</sup> of 38 (AN) to 62 (S). Polymerizations were performed in bulk at 90 °C with initial concentrations of the controlling agent **3** ranging from 1.1 to 20.9  $\text{mmol}\cdot\text{L}^{-1}$  to obtain the random copolymers poly(S-*co*-AN) (**7**, SAN) with molecular weights of up to 80 000  $\text{g}\cdot\text{mol}^{-1}$ . SEC analysis provided narrow molecular weight distributions with dispersities < 1.2. Nevertheless, SEC traces of higher molecular weight SAN polymers obtained in RAFT polymerization exhibit a broadening of the elugrams, most probably due to the formation of dead polymer chains by chain termination events. NMR analysis of **7** (not shown) reveals the presence of proton resonances assigned to the pyridinyl protons of the RAFT Z-group from 8.7–7.6 ppm. Resonances of the benzyl protons of the RAFT R-group are superimposed by the aromatic resonances of styrene. Molar masses calculated from  $^1\text{H}$  NMR spectra are in agreement with the SEC results. The hereby obtained SAN copolymers are able to undergo HDA cyclization reactions with dienes when activated with TFA without any post-polymerization modification necessary. This is a unique feature of the RAFT-HDA approach making the method a powerful and atom-efficient

technique for orthogonal ligation. Experimental details of AN/S copolymerizations are provided in Table 4.3 (entry 11-14).

The inverse approach, *i.e.* the conjugation of enophile SAN with NBR copolymers synthesized from dithioester **3**, was also investigated. In contrast to the SAN system, RAFT polymerization of AN and BD employing **3** to synthesize dienophile NBR did not yield the targeted RAFT polymers. Under the applied polymerization conditions – *i.e.* elevated temperatures, a high excess of BD versus the RAFT agent and in absence of an acidic proton – **3** partly reacts with BD. The herein obtained structure was identified as a benzylthio dihydrothiopyranyl pyridine in an experiment described in detail in section 4.2.6. The heterocycle no longer behaves as a transfer agent, since the thiocarbonyl moiety is crucial for the degenerative chain transfer within the RAFT process. A similar reaction of the C=S double bond of RAFT polymers with BD proceeds during the polymerization. As a result of the steady degradation of the moiety controlling the polymerization process, molecular weight distributions broaden with increasing reaction time. Nevertheless, at the early polymerization stages narrow dispersities <1.1 are obtained. Similar problems arise when utilizing RAFT agent **4** and broad molecular weight distributions are obtained at later polymerization stages (Table 4.3, entry 9). AN/BD copolymerizations with controlling agent **5** yield high molecular weights and high dispersities after reaction times as short as 1 h (Table 4.3, entry 10). Such a behavior is not surprising, since the Z-group of **5** is a strongly electron withdrawing moiety and HDA reactions of **5** proceed without further activation of the C=S double bond.<sup>28</sup>

### 4.3.2 Synthesis of Cp-Functional NBRs

A common method for the introduction of Cp into organic compounds is via nucleophilic substitution with sodium cyclopentadiene. However, the highly reactive NaCp nucleophile is aggressive toward various functional groups such as ester moieties, and extensive purification is necessary to remove side products. In contrast, quantitative conversion is a prerequisite for macromolecular transformation, since preparative purification of macromolecules is challenging and – in most cases – impossible. A mild and efficient alternative route for the

synthesis of Cp-functional polymers utilizes nickelocene ( $\text{NiCp}_2$ ) as a source of Cp.<sup>36</sup> The method was recently introduced by Barner-Kowollik and coworkers and has allowed for synthesis of telechelic polymers of various kinds and origins.<sup>12,28</sup> In the herein presented work, a similar approach was applied to the synthesis of Cp-functional NBRs.  $^t\text{Br}$ -functional NBRs **6a-d** obtained from RAFT polymerization employing RAFT agent **1** were reacted with an excess of nickelocene in the presence of triphenylphosphine and sodium iodide. Cp-functional NBRs **8a-d** were obtained at ambient temperature with quantitative conversion within 16 h. Excess nickelocene was removed by filtration over basic aluminium oxide. Polymers were purified in an aqueous washing procedure and were recovered by repeated precipitation in cold ethanol. A comparison of  $^1\text{H}$  NMR spectra of  $^t\text{Br}$ -functional NBR **6d** and Cp-functional NBR **8d** after workup is provided in Figure 4.3 (see page 105). Substitution of the  $^t\text{Br}$  with cyclopentadienyl evokes an upfield shift of resonances b and c of the methyl protons of the propane diol linker of **6d** (see inset, upper panel) and the arising resonances j and k are relocated around 4.1 ppm (see inset, lower panel). No resonances b and c of residual  $^t\text{Br}$ -functional NBR **6d** are obtained, evidencing quantitative conversion. Formation of the Cp-functional NBR is further evidenced by an upfield shift of the methyl protons of the isobutyryl moiety dislocating from a singlet signal (a) at 1.9 ppm to a splitted signal (i) around 1.4 ppm. Methylene protons (s) of the Cp chain-end resonate at 2.97 ppm. Notably, a higher amount of nickelocene as reported for transformations on other bromide-telechelic polymers, *i.e.* polystyrene or polyacrylates, was necessary to obtain full conversion. Substitution employing 2 equivalents of nickelocene – a common protocol for Cp-substitutions of bromide-capped polyacrylates – resulted in the presence of approximately 10% of unreacted  $^t\text{Br}$ -functional NBR **6d**, as calculated from  $^1\text{H}$  NMR data. The elevated amount of nickelocene required for quantitative substitution is most probably due to the high concentration of nitrile moieties coordinating intermediate nickel complexes during substitution. A similar interference of the nitrile moieties of the NBR polymer backbone with transition metal complexes was observed in copper mediated azide-alkyne couplings of NBR building blocks (see chapter 3.3.3). These conjugations required increasing concentrations of copper sulfate with increasing

chain length of NBR copolymers. Experimental details of all Br-Cp substitution reactions are provided in Table 4.7 in the *Appendix*.

Cp-functional copolymer **8c** was further analyzed employing ESI mass spectrometry. Figure 4.4B shows a magnified view into the region of 1145-1255 Da of a 1000 g·mol<sup>-1</sup> polymer sample. Signals of the sodium adducts [**8**<sub>*m+n*</sub>+Na]<sup>+</sup> of the polymer with *m+n* incorporated monomer units repeat with 53-54 Da, equivalent to the mass of a BD or AN monomer unit. The signals are shifted toward a lower mass-to-charge ratio in comparison to the <sup>t</sup>Br-functional polymer precursor **6c** (Figure 4.4A), due to the lower weight of the Cp unit versus the bromine. Nevertheless, remaining signals of the polymer precursor **6c** are not obtained, documenting quantitative conversion of the bromide chain-end. Several signals of very low intensity are observed but were estimated to be less than 5%. These signals were not assigned in detail and are most probably a result of side reactions during the reaction with NiCp<sub>2</sub> as no side products were obtained in the synthesis of the <sup>t</sup>Br-functional precursor **6**. Similarly, ESI mass spectrometry of higher molecular weight Cp-functional NBRs **8** did not show any substantial side product formation. An ESI mass spectrum of the 10 000 g·mol<sup>-1</sup> Cp-telechelic polymer **8d** is provided in Figure 4.7.

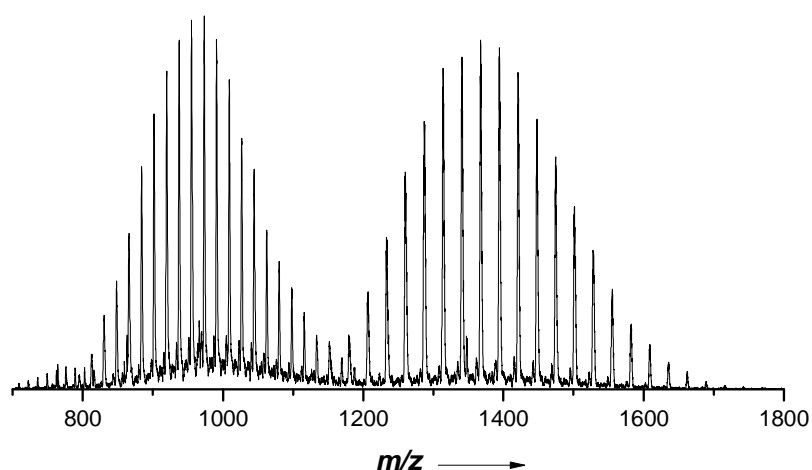
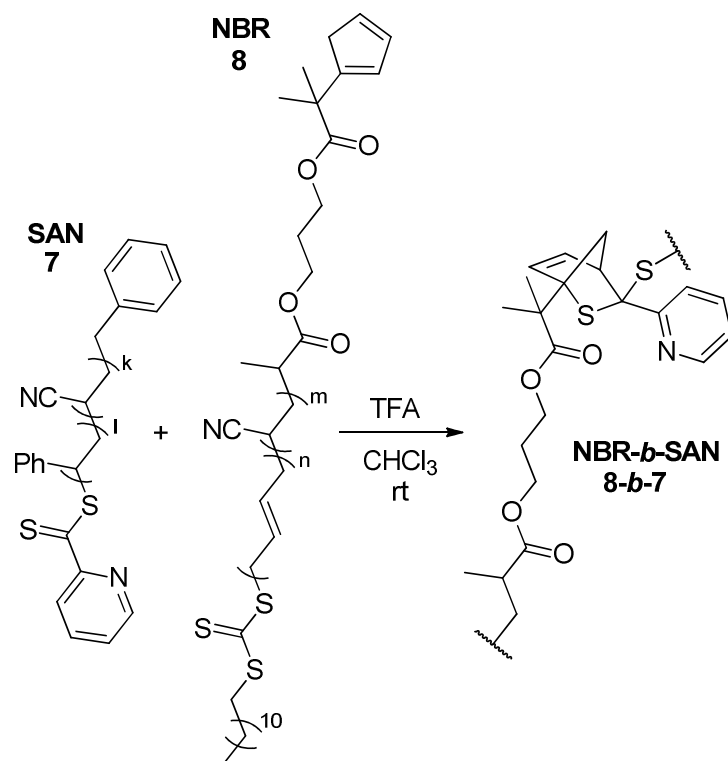


**Figure 4.7.** Integral over double and triple charges of the sodium adducts [**8**<sub>*m+n*</sub>+2Na]<sup>2+</sup> and [**8**<sub>*m+n*</sub>+3Na]<sup>3+</sup> of a SEC-ESI mass spectrum of Cp-capped NBR **8d** of 10 000 g·mol<sup>-1</sup>.

### 4.3.3 Block Copolymer Formation

The herein presented study was aiming at the synthesis of block copolymers of elastomeric and thermoplastic polymer building blocks via conjugation of Cp-functional NBR with dienophile-capped SAN polymers. As depicted in Scheme 4.3, the two polymer building blocks react under formation of a bicyclodihydrothiopyran coupling moiety and the block copolymer **8-b-7** is obtained. Conjugations proceeded in chloroform at ambient temperature. TFA is added to increase the reactivity of the C=S double bond by enhancing the electron-withdrawing properties of the heteroaromatic system. A major issue in obtaining block copolymers was the lack of reliable MHKS parameters for NBR. Efficient coupling requires equimolar amounts of diene and dienophile reactants. Molecular weights of NBR were obtained relative to PS, resulting in an overestimation of molar masses while SAN analysis was performed more accurately employing the Mark–Houwink relation. To compensate the errors in stoichiometry resulting thereof, several conjugation experiments for each pair of NBR/SAN were



**Scheme 4.3.** Formation of block copolymers of NBR and SAN. Both polymers are random copolymers; the structures are simplified for better legibility.

**Table 4.4.** SEC data of NBR and SAN precursor blocks and the resulting hetero-Diels-Alder conjugated linear block copolymers **8-b-7**.

entry	NBR			SAN			NBR- <i>b</i> -SAN		
		$M_n$ (g·mol <sup>-1</sup> ) <sup>a</sup>	$\mathcal{D}^a$		$M_n$ (g·mol <sup>-1</sup> ) <sup>b</sup>	$\mathcal{D}^b$		$M_n$ (g·mol <sup>-1</sup> ) <sup>a</sup>	$\mathcal{D}^a$
1 <sup>c</sup>	<b>8a</b>	6800	1.2	<b>7a</b>	7900	1.2	<b>8a-b-7a</b>	13 000	1.2
2 <sup>d</sup>	<b>8b</b>	43 000	1.4	<b>7b</b>	28 000	1.1	<b>8b-b-7b</b>	57 000	1.3
3 <sup>e</sup>	<b>8b</b>	43 000	1.4	<b>7c</b>	76 000	1.2	<b>8b-b-7c</b>	110 000	1.3

<sup>a</sup> Obtained from SEC employing the MHKS parameters of PS. <sup>b</sup> Obtained from SEC employing the MHKS parameters of SAN. <sup>c</sup> solid content 58 mg·mL<sup>-1</sup>, TFA 0.08 μL·mL<sup>-1</sup>, 2 h. <sup>d</sup> solid content 58 mg·mL<sup>-1</sup>, TFA 40 μL·mL<sup>-1</sup>, 20 min. <sup>e</sup> solid content 56 mg·mL<sup>-1</sup>, TFA 40 μL·mL<sup>-1</sup>, 20 min.

performed to cover a broad range of relative molar ratios of the two polymer building blocks. Polymers providing highest molecular weights in SEC analysis after conjugation were assumed to result from an optimum 1:1 stoichiometry of chain-end functionality and were thus used for all discussions. Molecular weight and dispersity data obtained from SEC for each conjugation experiment are provided in Table 4.4.

The ability of the Cp chain-end of the employed structures to undergo HDA cyclization was first investigated in a small molecule study. Such a study allows a comprehensive NMR characterization of the obtained structures in contrast to those of the polymeric species. Within the latter, resonances of the NBR-*b*-SAN polymer backbone cover a broad region of the <sup>1</sup>H NMR spectrum, thus superimposing signals of chain-end protons. <sup>t</sup>Br-functional trithiocarbonate **1** was therefore subjected to Cp-transformation. The bromine compound was allowed to react with nickelocene in the presence of triphenylphosphine and sodium iodide for 6 h. The short reaction time was chosen to compensate the high affinity of small organic Cps to undergo dimerization. The Cp-functional RAFT agent was purified by column chromatography and obtained with 71% yield. <sup>1</sup>H NMR analysis, shown in Figure 4.8 exhibits characteristic proton resonances at 6.6-6.1 ppm and at 2.9 ppm. These signals are assigned to the diene (b-d) and allyl protons (a) of the Cp, respectively, proving the substitution of the bromine with the diene. The

Cp-functional trithiocarbonate was then reacted with 1.05 equivalents of **3** in chloroform in the presence of 1.5 equivalents of TFA. Solvent removal after 20 min

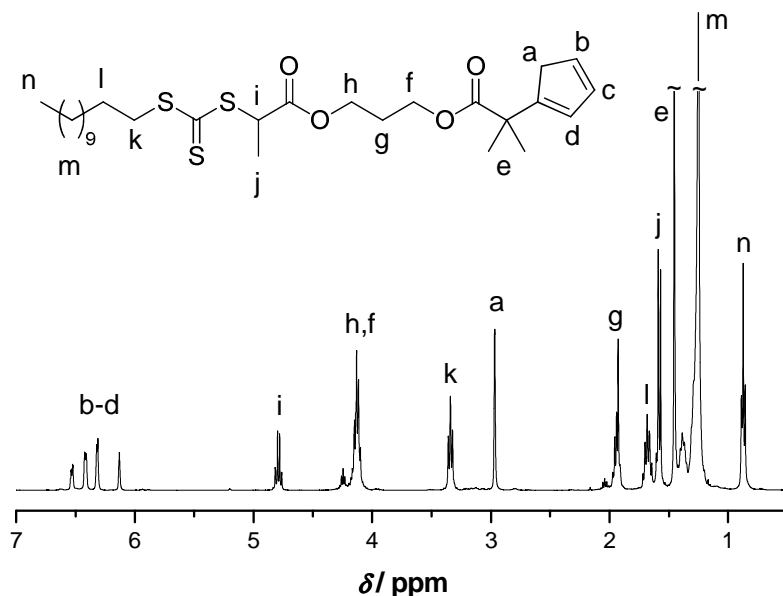


**Figure 4.8.**  $^1\text{H}$  NMR characterization ( $\text{CDCl}_3$ ) of Cp-functional RAFT agent obtained from Cp-transformation reaction of controlling agent **1**.

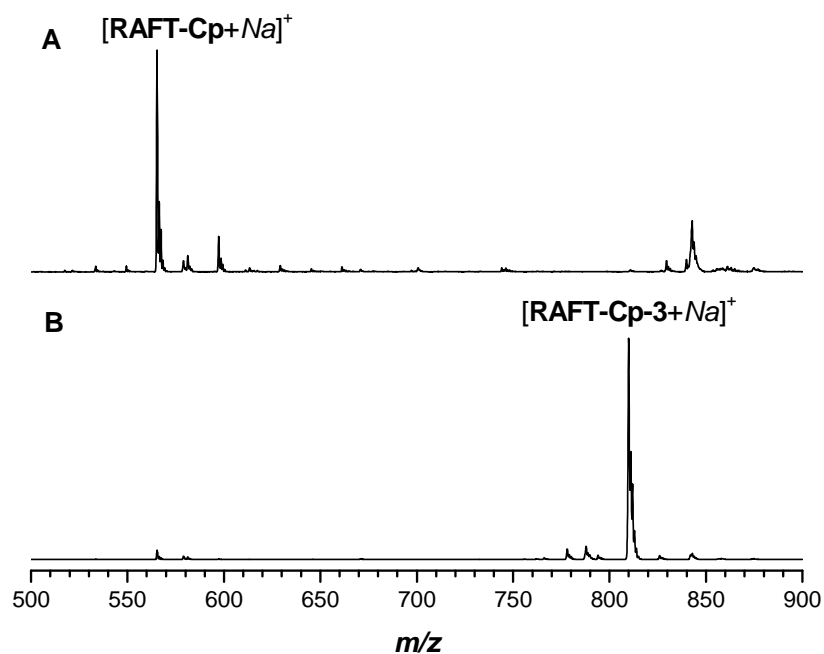


**Figure 4.9.** ESI-MS analysis of Cp-functional RAFT agent (**RAFT-Cp**) **A**) before and **B**) after HDA cyclization with controlling agent **3** in the presence of 1.5 equivalents of TFA. The HDA cycloadduct (**RAFT-Cp-3**) was neutralized by washing with saturated sodium bicarbonate solution prior to ESI-MS analysis.

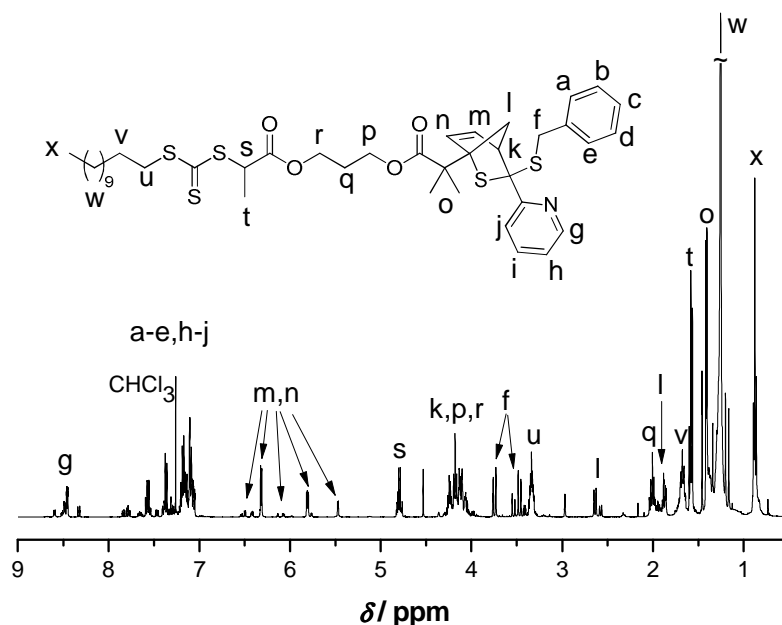


**Figure 4.10.**  $^1\text{H}$  NMR characterization of the Cp-functional RAFT agent after reaction with 1.05 eq. of **3** in the presence of TFA recorded in  $\text{CDCl}_3$ . Excess controlling agent **3** was removed via column chromatography prior to analysis.

and successive ESI mass spectrometry shows full conversion of the Cp-functional RAFT agent into the bicyclodihydrothiopyran-capped trithiocarbonate (Figure 4.9). The conjugation product was purified by column chromatography (to remove excess **3**) and subsequent NMR analysis, provided in Figure 4.10, allowed characterization of the dihydrothiopyran coupling structure but reveals the presence of several stereoisomers. In analogy, Cp-telechelic NBR **8c** undergoes HDA cyclization with the reactive thiocarbonyl moiety of neat controlling agent **3** without a preceding S/AN copolymerization. Here, **3** was used in excess to eliminate stoichiometric errors from the experimental setup (arising from molecular weight determination of **8c**). The obtained bicyclodihydrothiopyran end-capped NBR was identified via SEC-ESI mass spectrometry. A magnified view into the region of 1145 to 1255 Da of the obtained polymer is shown in Figure 4.4C (see page 106). Signals of residual Cp-telechelic NBR **8c** are not observed, evidencing the full conversion of the diene functionality. A minor polymeric species was observed but could not be identified. These preliminary experiments unambiguously confirm the dihydrothiopyran HDA cycle to be the coupling moiety in the investigated orthogonal ligation protocol.

Conjugation was subsequently applied for polymer-polymer coupling. Coupling of Cp-functional polymer **8a** ( $M_n$  6800 g·mol<sup>-1</sup>) and dienophile-capped SAN **7a** ( $M_n$  7900 g·mol<sup>-1</sup>) provided block copolymers **8a-b-7a** of 13 000 g·mol<sup>-1</sup>. The conjugation proceeded smoothly within 2 h, with ~20 mol% of TFA sufficient to obtain full conversion. Figure 4.11A shows SEC traces of **8a-b-7a** (solid line), together with the precursor blocks of Cp-functional NBR **8a** (dotted line) and dienophile-capped SAN **7a** (dashed line). Molecular weight distributions are monomodal, SEC traces of the conjugation product **8a-b-7a** appears at shorter retention time (21.80 minutes) relative to those of the precursor blocks. A slightly higher theoretical molar mass than obtained experimentally from SEC of 14 700 g·mol<sup>-1</sup> is calculated for **8a-b-7a** by summation of the molar masses of the individual building blocks. Given the lack of proper MHKS parameters of NBR at the time the experiments were performed and the investigation of conjugations of polymers of dissimilar chemical constitution, precise evaluation of coupling efficiency cannot be given simply based on molecular weight determined via SEC.

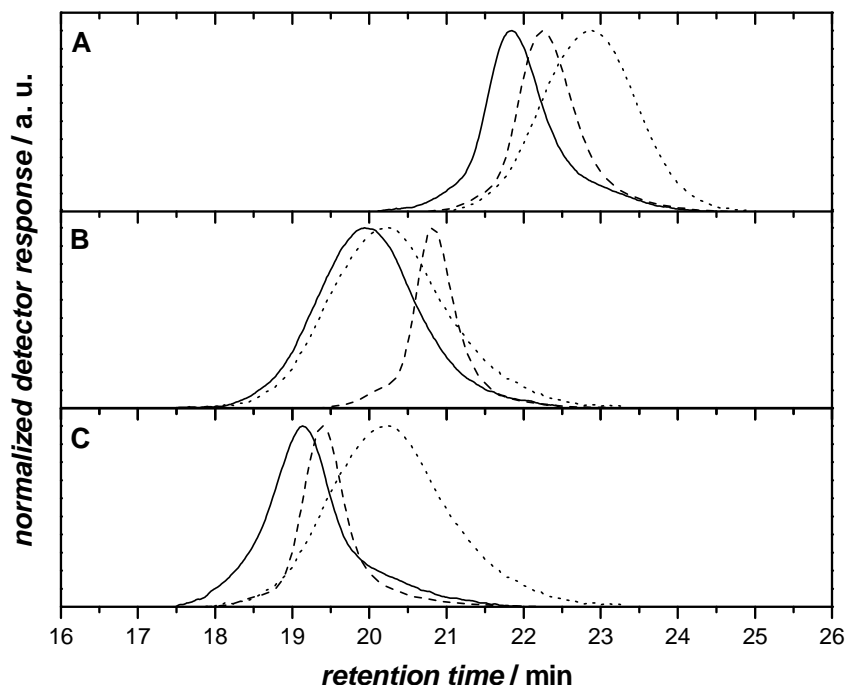


**Figure 4.11.** SEC traces of Cp-functional NBR **8** (dotted lines), dienophile SAN **7** (dashed lines) and the respective coupling product **8-b-7** (solid lines) of various conjugation experiments. A) Block copolymer **8a-b-7a** of 13 000 g·mol<sup>-1</sup> and a dispersity of 1.2 (Table 4.4, entry 1), B) **8b-b-7b** of 57 000 g·mol<sup>-1</sup> and a dispersity of 1.3 (Table 4.4, entry 2), and C) **8b-b-7c** of 110 000 g·mol<sup>-1</sup> and a dispersity of 1.3 (Table 4.4, entry 3) were obtained.

Nevertheless, a constant dispersity of 1.2 throughout the conjugation is an indication of the presence of a small fraction of polymer not undergoing ligation. As conjugation is a convolution process conjugations typically result in a narrowing of molecular weight distributions.<sup>40</sup> Conjugation of the higher molecular weight NBR **8b** ( $M_n$  43 000 g·mol<sup>-1</sup>) with SAN **7b** ( $M_n$  28 000 g·mol<sup>-1</sup>) gives **8b-b-7b** of 57 000 g·mol<sup>-1</sup> (Figure 4.11B). Conjugation of **8b** with a 76 000 g·mol<sup>-1</sup> SAN **7c** provides **8b-b-7c** of 110 000 g·mol<sup>-1</sup> (Figure 4.11C). Coupling of Cp-capped NBR **8b** with either **7b** or **7c** did not proceed upon activation with substoichiometric amounts of TFA. For reasons that could not be determined, conjugation efficiency strongly varied with the TFA concentration. Since complete conjugation was targeted, a high and constant concentration of TFA of 40  $\mu\text{L}\cdot\text{mL}^{-1}$  was applied, facilitating conversion within 20 min. A prolonged reaction time did not give any alteration to the SEC traces of **8-b-7**. In the present study, all provided block copolymers exhibit narrow molecular weight distributions with dispersities below 1.3. Molar masses of the herein presented block copolymers are among the highest molecular weights obtained in orthogonal conjugation and most studies focus on molecular weights below 20 000 g·mol<sup>-1</sup>.<sup>41-42</sup>

#### 4.3.4 Miktoarm Star Copolymers

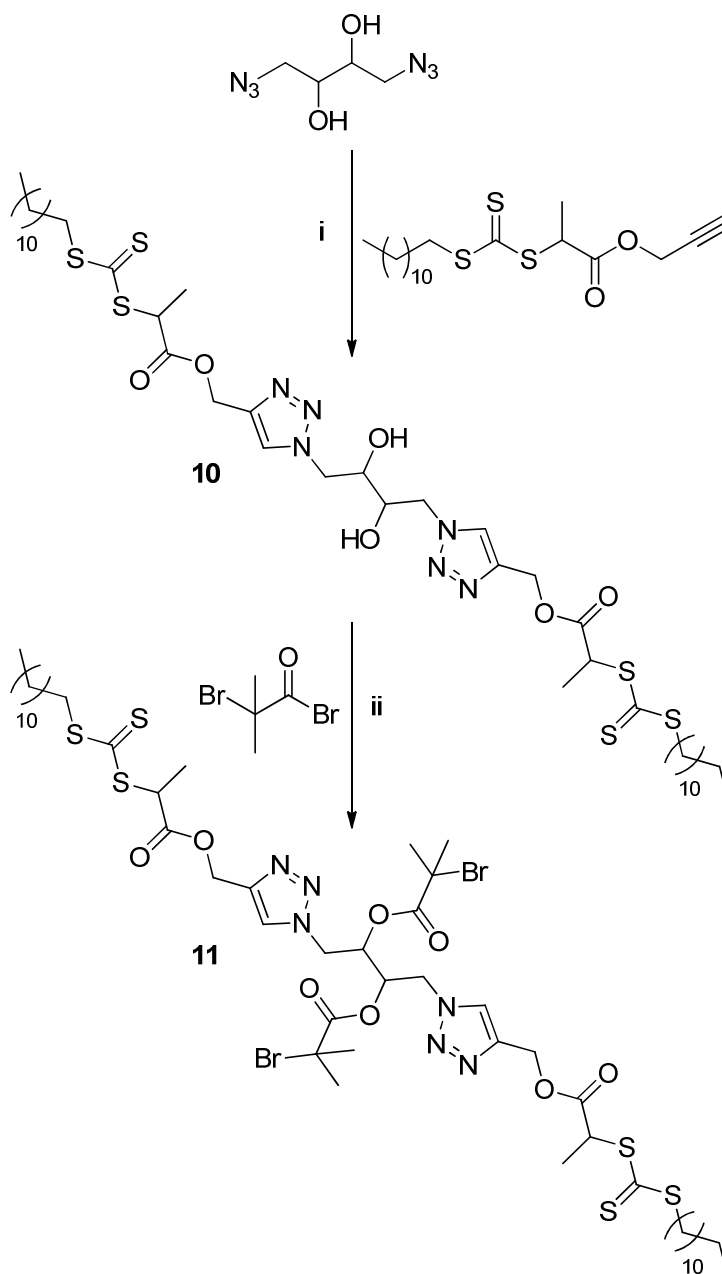
The material properties of block copolymers are determined by their structure and chemical constitution. A way to alter the physical properties of block copolymers is not only the variation of the chain lengths of the individual blocks, but also the variation of the topology. In the herein presented investigations, block copolymers of NBR and SAN were accessible over a broad range of molecular weight and it is mandatory to extend the current protocol toward the synthesis of various NBR block copolymers with other acrylate- or styrene-based polymer building blocks. A further variation of the properties of the block copolymers is achieved by modification of the architecture of the block copolymers targeting star-shaped geometries. With the advent of orthogonal ligation techniques, star shaped polymers have recently found renewed substantial interest and have been accessible for a broad range of commodity monomers via reversible-deactivation

radical polymerization protocols.<sup>43</sup> Moreover, other polymerization techniques such as living anionic polymerization and ring-opening polymerization have been thoroughly investigated in the synthesis of star shaped geometries.<sup>44-45</sup> Particular types of star configurations are miktoarm star polymers, comprising several arms of different chemical constitution.<sup>43,46</sup> Their outstanding self-assembly behavior in solution, as for example the formation of multicompartment micelles, makes these polymer types a promising candidate for drug delivery applications.<sup>47</sup>

Very recently, Frieberg *et al.* investigated time-dependent structural relaxations of thin films made from various linear and star-shaped polystyrenes.<sup>48</sup> They showed that physical ageing is decelerated in films prepared from star-shaped polystyrenes when compared to films prepared from linear ones. The slowdown was more pronounced when stars with a higher number of arms or shorter chain lengths of the polystyrene arms were employed. These results were explained in part with an increased rigidity of the star polymers close to the core, increasing entropic penalties for relaxations. Although these results indicate enhanced properties of star polymers over linear polymers, industrial applications of star polymers are still limited to a few examples.

To date, the synthesis of star polymers has not been applied to NBR, since reversible-deactivation polymerization protocols for the industrially important polymer have only been introduced very recently.<sup>1,16</sup> The work was therefore focused on the development of a facile and efficient protocol for the synthesis of 4-miktoarm star copolymers with two NBR and two “non-NBR” building blocks. To minimize the number of postpolymerization reaction steps, a combination of a “pre-“ and a “postclick” protocol was applied.<sup>49</sup> To implement the achievements of the <sup>t</sup>Br-precursor technique thoroughly investigated in the presented work, the synthesis of midchain functionalized <sup>t</sup>Br-functional NBR and thus a midfunctionalized symmetric RAFT agent was targeted. A 1,4-diazido butan-2,3-diol derived structure seemed to be a suitable core, since it is readily accessible from 1,3-butadiene diepoxide via ringopening nucleophilic attack with sodium azide.<sup>14</sup> As depicted in Scheme 4.4, the diazide was reacted in a copper-catalyzed 1,3-dipolar azide-alkyne cyclization with an alkyne-functional trithiocarbonate to obtain bifunctional controlling agent **10** with two midchain immobilized hydroxyl

moieties. The pure compound **10** was obtained in good yields by precipitation from DMF/diethyl ether upon addition of an aqueous Na<sub>2</sub>EDTA solution without any additional purification step such as column chromatography or extraction. Trithiocarbonate **10** was not tested as a controlling agent in the free radical polymerization of AN/BD, yet is expected to be a suitable transfer agent based on



**Scheme 4.4.** Synthesis of difunctional RAFT agent **11** bearing two <sup>t</sup>Br moieties in between the trithiocarbonate functionalities. Polymerization of AN and BD in the presence of RAFT agent **11** yields midchain functionalized polymers. Conditions: i) CuSO<sub>4</sub>·5H<sub>2</sub>O, Na-ascorbate, DMF, 25 °C, 16 h, ii) NEt<sub>3</sub>, CH<sub>2</sub>Cl<sub>2</sub>, 0-25 °C, 4 h.

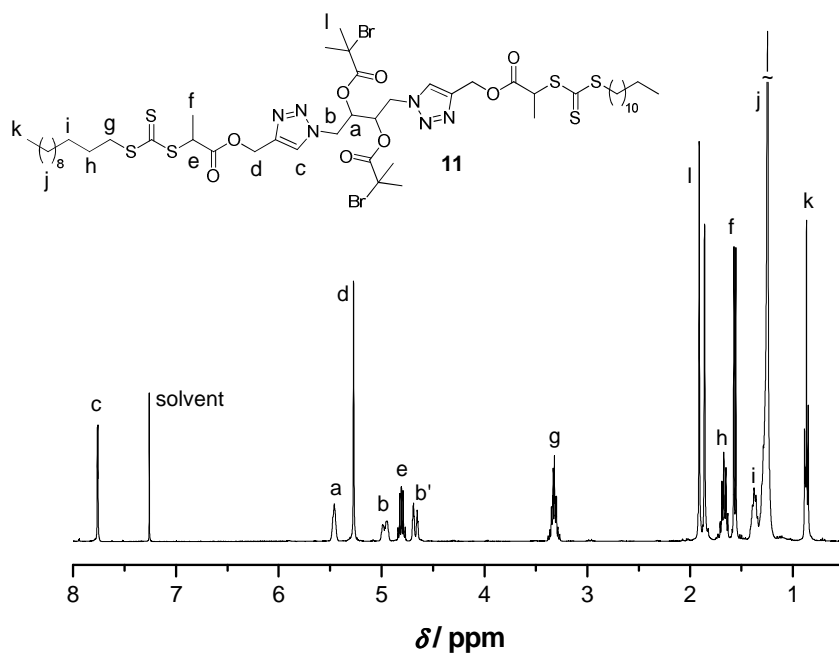


**Figure 4.12.**  $^1\text{H}$  NMR characterization of  $^t\text{Br}$ -functional symmetrical controlling agent **11** recorded in  $\text{CDCl}_3$ .

its structural similarity to controlling agent **1** and other trithiocarbonates recently investigated for the synthesis of AN-BD copolymers.<sup>1,16</sup> Utilization of **10** in RAFT polymerization would allow the synthesis of midchain hydroxyl-functionalized polymers.

The targeted  $^t\text{Br}$ -bifunctional controlling agent **11** was obtained with 94% isolated yield within 4 h via addition of bromoisobutyryl bromide to a solution of **10** in the presence of triethylamine, as visualized in Scheme 4.4. The herein obtained novel compound **11** contains two  $^t\text{Br}$  moieties and two trithiocarbonates centered around the 1,4-bis(triazolyl) butan-2,3-diol core.  $^1\text{H}$  NMR characterization of controlling agent **11** is provided in Figure 4.12. When employed in free radical polymerization, monomers incorporate on both sides of the core structure of **11**. Such incorporation allows the synthesis of a midchain functional NBR featuring two  $^t\text{Br}$  moieties located in the middle of the linear macromolecule.

RAFT agent **11** was assessed toward its ability of controlling the RAFT mediated copolymerization of AN and BD. Employment of **11** at  $31.5 \text{ mmol}\cdot\text{l}^{-1}$  in acetone at  $100^\circ\text{C}$  with an overall monomer concentration of  $9.5 \text{ mol}\cdot\text{l}^{-1}$  yielded a bromide-

functional NBR **12a** of  $5100 \text{ g}\cdot\text{mol}^{-1}$  and a dispersity of 1.1. The RAFT agent to initiator ratio  $[\mathbf{11}]_0/[\text{Ini}]_0$  was adjusted to 7.5:1 to allow for a high midchain functionality at a reasonable monomer-to-polymer conversion of 37% within 5 h. To prove that the incorporation of the RAFT agent proceeds without the loss of midchain functionality, the obtained polymer was investigated via SEC-ESI mass spectrometry. A magnified view into the region of 1850 to 1950 Da of a SEC-ESI-MS measurement is provided in Figure 4.13A. Signals exhibit a patterning similar to the one observed for the terminal  $^t\text{Br}$ -functional copolymers presented in the first part of the current chapter and repeat at intervals of 53 to 54 Da. The comparison with theoretical values allows assignment of these signals to the sodium adducts  $[\mathbf{12}_{m+n+o+p}+\text{Na}]^+$  of the targeted midchain functional NBR star precursors **12**. On closer inspection of the low molecular weight region of the SEC trace in SEC-ESI-MS, a small fraction of initiator derived chains<sup>50</sup> – having the initiator fragment on one chain-end and the trithiocarbonate RAFT Z-group on the other – can be identified. These species are an inevitable side product of the RAFT process and are formed before chain transfer with the RAFT agent occurs. Nevertheless, signals derived from these nonfunctional polymer chains are not observed in higher molecular weight regions, as clearly demonstrated by investigation of double and triple charged species  $[\mathbf{12}_{m+n+o+p}+2\text{Na}]^{2+}$  and  $[\mathbf{12}_{m+n+o+p}+3\text{Na}]^{3+}$  (see Figure 4.14). A further proof for the successful midchain

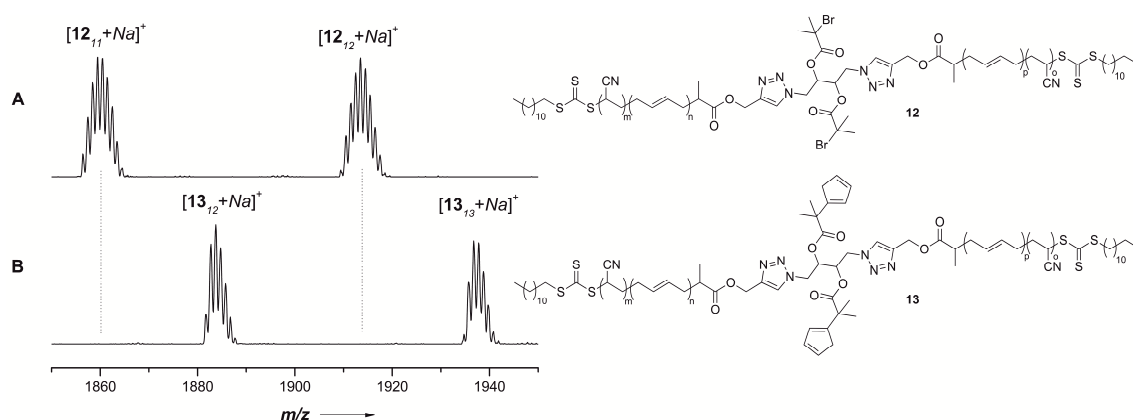


**Figure 4.13.** SEC-ESI-MS analysis of the NBR star precursor. A magnified view into the single charges of A) a  $5100 \text{ g}\cdot\text{mol}^{-1}$   $^t\text{Br}$ -functional NBR **12a** and B) the respective Cp-functional star precursor **13a** is provided, evidencing complete conversion of the midchain bromide functionalities into the highly reactive cyclic dienes.

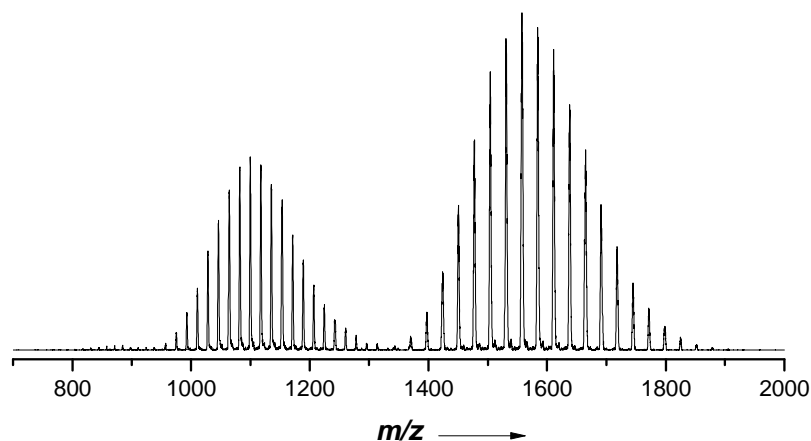


**Figure 4.14.** Integral over double and tripple charges of a SEC-ESI mass spectrum of midchain  $t$ Br-functional polymer **12a**.

functionalization of the polymer is obtained from  $^1\text{H}$  NMR analysis. The absence of a quadruplet resonance in the region of 4.8 ppm of a  $^1\text{H}$  NMR spectrum of polymer **12a** (see Figure 4.27 in the *Appendix*) is indicative that chain transfer occurred on both trithiocarbonates of the bifunctional RAFT agent. The quadruplet resonance is observed in the  $^1\text{H}$  NMR spectrum of controlling agent **11** and assigned to the methine proton in  $\alpha$ -position to the trithiocarbonate (see Figure 4.12, signal e). Incorporation of monomer occurs via homolytic cleavage of the methine-trithiocarbonate C-S-bond resulting in an upfield shift of the methine proton resonance.

Polymerization employing **11** depicts a linear behavior of the number average molecular weight with conversion, indicating living characteristics. Linearity was demonstrated over a period of 24 h; a plot of the evolution of  $M_n$  and dispersity with conversion for a polymerization in chlorobenzene is provided in Figure 4.15. A starting concentration of the controlling agent  $[\mathbf{11}]_0 = 2.2 \text{ mmol}\cdot\text{l}^{-1}$  was provided at a ratio of controlling agent to initiator of 7.5 to 1. Conversion was kept below 20% to prevent coupling of the growing NBR precursors via recombination of the macroradicals. SEC analysis of the  $t$ Br-functional (“two arm”) star precursor **12** reveals a monomodal molecular weight distribution with no evidence of “star-star” coupling. Occurrence of star-star coupling is expected to result in high molecular weight tailing of the SEC traces. After 24 h of polymerization, a molar mass of  $42\,000 \text{ g}\cdot\text{mol}^{-1}$  and a dispersity of 1.4 were obtained.

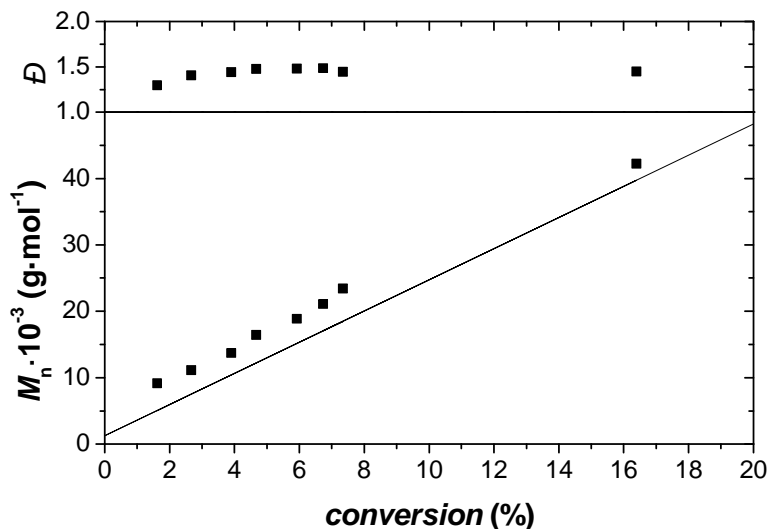


**Figure 4.15.** Evolution of molar mass and dispersity of an AN/BD copolymerization employing controlling agent **11**. Conditions:  $[\mathbf{11}]_0$  2.2 mmol·L<sup>-1</sup>,  $[\text{Ini}]_0$  0.3 mmol·L<sup>-1</sup>, 24 h, 100 °C, chlorobenzene, for further details see Table 4.3, entry 16.

Transformation of the midchain bromide-functionalized AN-BD copolymers **12** into their Cp analogues **13** was performed under similar conditions as applied for the synthesis of linear Cp-functionalized NBRs. The transformation proceeded quantitatively overnight at ambient temperature. As depicted in Figure 4.13B, SEC-ESI-MS analysis of the Cp-functional star precursor **13a** of 5600 g·mol<sup>-1</sup> did not provide any evidence of remaining bromo-functional polymer **12a**. Moreover, polymer species revealing one bromine and one Cp moiety are not obtained. A clear shift of the signals assigned to the sodium adducts of the Cp-functional polymer  $[\mathbf{13}_{m+n+o+p}+\text{Na}]^+$  is observed when compared to those of the bromo-functional polymer, provided in Figure 4.13A. The significant narrowing of the signals of **13a** when compared to the bromo-functional analogues **12a** can be ascribed to the loss of the bromine with its characteristic isotope pattern of 79 and 81 Da in an approximately one-to-one ratio. In the low molecular weight region of the SEC trace of the SEC-ESI mass spectrum, signals assigned to initiator derived chains are observed with no variation to those observed in the bromo-functional precursor polymer **12a**. NMR analysis of the Cp-functional NBR **13a** is provided in Figure 4.28 in the *Appendix* and exhibits the characteristic resonances of the olefin and allyl protons of the Cp moiety. No remaining proton signals of the 1,4-bis(triazolyl)butan-2,3-diol core of the bromide precursor are observed,

indicating the full conversion during the reaction with NiCp<sub>2</sub>. Conversion of the bromine in the higher molecular weight analogue **12b** provided the Cp-functional star precursor **13b** without a significant alteration of the molar masses obtained via SEC.

The coupling of Cp-functionalized NBR star precursors **13** with SAN **7** was performed in chloroform upon addition of TFA. Each of the two midchain-immobilized Cp rings reacts with the electron-deficient thiocarbonyl moiety of the dithioester chain-end of a SAN building block in a HDA cyclization establishing covalent linkages. Since conjugation occurs in the middle of the NBR macromolecule two NBR arms are “generated” directly from one linear polymer chain upon cycloaddition of the two SAN building blocks. The core structure of the herein obtained 4-miktoarm stars is depicted in Figure 4.16. In analogy to the

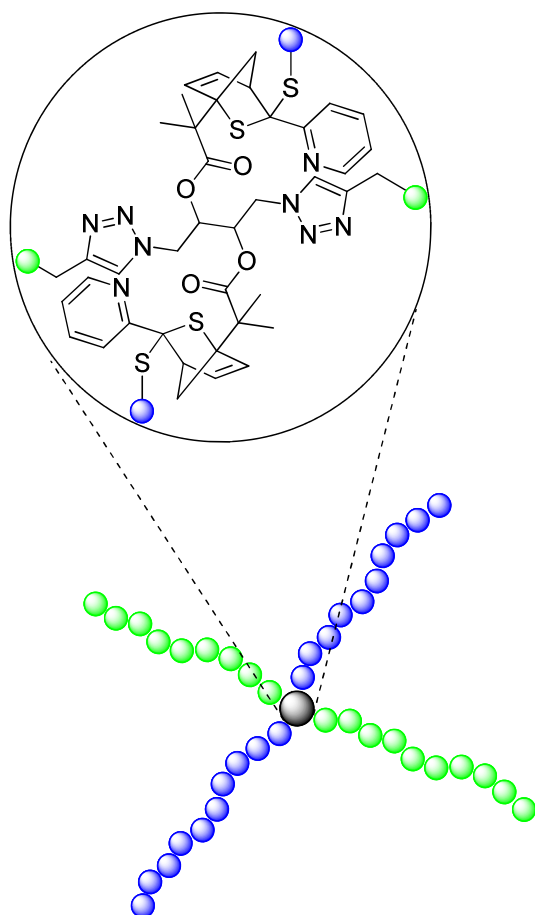


**Figure 4.16.** Core structure of the 4-miktoarm star copolymers (NBR)<sub>2</sub>(SAN)<sub>2</sub>. NBR blocks (green) are anchored to the core by 1,4-triazole moieties, SAN (blue) blocks are joined via bicyclodihydrothiopyran rings.

block copolymer formation with the linear end-capped NBRs, the 4-miktoarm stars are obtained via formation of two bicyclodihydrothiopyran moieties, immobilizing the SAN building blocks. As noted above, HDA cyclization gives several stereo- and regioisomers; for simplification one structure is provided exemplarily.

Polymers **7** and **13** were mixed in a molar ratio of roughly 2:1 and the obtained coupling products were analyzed by SEC. Since proper MHKS parameters of NBR have not been determined at the time the experiments were performed, molecular weight determination of NBRs **13** has been performed by SEC relative to narrow PS standards. These values provide a rather rough approximation of the actual molecular weight biased toward an overestivation of  $M_n$  and thus resulting in inaccurate calculations of initial sample weights. To account for errors resulting from an inaccurate stoichiometry, several conjugation experiments were performed (in analogy to the stoichiometry variations for the synthesis of linear block copolymers) to cover a broad range of relative molar ratios of the two polymer building blocks. The experiments exhibiting the highest molecular weights after block formation result from the optimum coupling conditions and are further discussed. SEC results of two miktoarm star formation experiments for two Cp-functional NBR star precursors of different molar mass are provided in Figure 4.17 (solid lines). The SEC traces of the midchain functional NBR star precursors **13a** and **13b** are depicted as dotted lines; dashed lines indicate the SAN building blocks **7d** and **7b** obtained from RAFT polymerization in the presence of controlling agent **3**. Conjugations proceeded rapidly at ambient temperature.

**Table 4.5.** SEC data of NBR and SAN precursor blocks and the resulting hetero-Diels-Alder conjugated miktoarm star copolymers.

entry	NBR			SAN			$(\text{NBR})_2(\text{SAN})_2$		
	$M_n$ ( $\text{g}\cdot\text{mol}^{-1}$ ) <sup>a</sup>	$\mathcal{D}^a$		$M_n$ ( $\text{g}\cdot\text{mol}^{-1}$ ) <sup>b</sup>	$\mathcal{D}^b$		$M_n$ ( $\text{g}\cdot\text{mol}^{-1}$ ) <sup>a</sup>	$\mathcal{D}^a$	
1 <sup>c</sup>	<b>13a</b>	5600	1.2	<b>7d</b>	9200	1.2	<b>(13a)(7d)<sub>2</sub></b>	20 000	1.2
2 <sup>d</sup>	<b>13b</b>	36 000	1.7	<b>7b</b>	28 000	1.2	<b>(13b)(7b)<sub>2</sub></b>	63 000	1.3

<sup>a</sup> Obtained from SEC employing MHKS parameters of PS. <sup>b</sup> Obtained from SEC employing MHKS parameters of SAN. <sup>c</sup> Solid content 66  $\text{mg}\cdot\text{mL}^{-1}$ , TFA 40  $\mu\text{L}\cdot\text{mL}^{-1}$ , 20 min. <sup>d</sup> Solid content 51  $\text{mg}\cdot\text{mL}^{-1}$ , TFA 40  $\mu\text{L}\cdot\text{mL}^{-1}$ , 20 min.

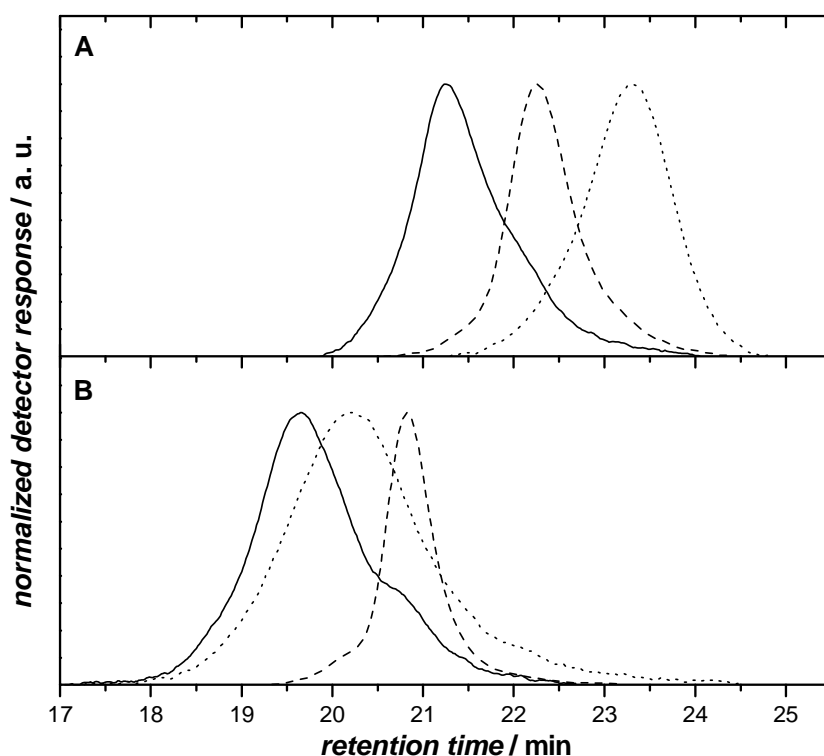


**Figure 4.17.** SEC traces documenting the formation of  $(\text{NBR})_2(\text{SAN})_2$  miktoarm star copolymers (solid lines) from midchain Cp-functional NBR **13** (dotted lines) and dienophile SAN **7** (dashed lines). A) NBR **13a** is reacted with SAN **7d** yielding a miktoarm star polymer with a molar mass of  $20\,000\text{ g}\cdot\text{mol}^{-1}$ , B) NBR **13b** and SAN **7b** convert into a miktoarm star polymer of  $63\,000\text{ g}\cdot\text{mol}^{-1}$ .

Complete conjugation was observed at reaction times as short as 20 min, showing no further increase in molecular weight with longer reaction times.

The conjugation of Cp-functional star precursor **13a** provided  $(\text{NBR})_2(\text{SAN})_2$  miktoarm star copolymers of  $20\,000\text{ g}\cdot\text{mol}^{-1}$  and a dispersity of 1.2 (Table 4.5, entry 1). Summation of molar masses of the building blocks leads to a theoretically expected molar mass of  $24\,000\text{ g}\cdot\text{mol}^{-1}$ . Several factors might explain the lowered molecular weights obtained from SEC. Molar masses of SAN polymers were calculated under consideration of its MHKS parameters.<sup>24</sup> In contrast, molar masses of NBRs and  $(\text{NBR})_2(\text{SAN})_2$  are relative values versus PS standards, as no MHKS parameters of these polymers were accessible. Considering the alteration of the hydrodynamic volume relative to the molecular weight when attaching the arms other than in a linear fashion, and the employment of different polymer types a simple summation of molar mass cannot be expected to yield accurate values.

Nevertheless, a slight shoulder toward lower molecular weight is observed in SEC analysis (Figure 4.17A). This shoulder is assigned to polymers that do not undergo conjugation to form 4-miktoarm star copolymers for reasons that are discussed in detail in the following paragraphs. In analogy, (NBR)<sub>2</sub>(SAN)<sub>2</sub> miktoarm star polymers are obtained with the higher molecular weight star precursor **13b** and dienophile SAN **7b**. SEC traces of the precursors and the conjugation product are illustrated in Figure 4.17B. The peak maximum of **(13b)(7b)<sub>2</sub>** (solid line) shifts toward lower retention time when compared to those of the SAN precursor **7b** (dashed line) or Cp-difunctional NBR **13b** (dotted line). Here, summation of molar masses of NBR **13b** and the two SAN building blocks **7b** calculates to 92 000 g·mol<sup>-1</sup>, whereas 63 000 g·mol<sup>-1</sup> is obtained experimentally (see Table 4.5, entry 2). The structures presented in the current chapter are the first reports of star shaped AN-BD copolymer architectures to date.

#### 4.3.5 Theoretical Aspects and Simulations

The herein presented data demonstrates the RAFT-HDA approach to be a powerful tool for the conjugation of NBR building blocks to access unique NBR block and miktoarm star copolymer architectures. However, molar masses of the obtained structures determined via SEC deviate from the molar masses theoretically expected from summation of those of the respective building blocks. Several reasons might be responsible for the observed discrepancy of theoretical and experimental molar mass data. As mentioned above, the conjugation of different polymer types and the lack of proper MHKS parameters for neither the NBR precursors nor the NBR conjugates are potential sources of systematic errors in molecular weight determination. Another factor is related to the preparation of the polymer building blocks via radical polymerization. Formation of nonfunctional chains – unable to undergo successive conjugation reactions due to the loss of chain-end functionality – is expected and was observed in small quantity when analyzing low molecular weight NBR using ESI-MS. Although formation of these species can be widely suppressed by choosing appropriate reaction conditions (that is, a low overall radical concentration), their contribution to incomplete polymer-polymer conjugation cannot be neglected. ESI mass spectrometry does

not allow a simple quantitative evaluation of the fraction of nonfunctional polymer and can only be applied for low molecular weight polymers. To assess the efficiency of the conjugation process, a plausibility study was performed evaluating the contribution of functional chains to the weight fraction of chains not partaking the block copolymer formation. The plausibility check was achieved by comparison of data obtained from SEC deconvolutions with data from PREDICI® simulations.\*\* From the PREDICI® simulations, the amount of nonfunctional precursor blocks is computed allowing for estimation of the maximum (weight fraction) attainable block copolymer. Based on the experimental data, PREDICI® models for the copolymerization of AN/BD employing bromide-functional controlling agent **1** and for the synthesis of SAN copolymers employing dithioester **3** were developed. A complete overview over the model is provided in chapter 4.2.10. Conversions and molar mass data of SAN and NBR polymerizations calculated from simulations show good agreement with experimental results. However, experimental  $M_n$  and conversion data of NBR with molar masses below  $10\,000\text{ g}\cdot\text{mol}^{-1}$  deviate from those obtained with the PREDICI® model. This observation may be associated with a more complex behavior of the system in the first hours of polymerization. Such a behavior is also indicated experimentally by a strong deviation of the evolution of molar mass with conversion from the linear character at the early polymerization stages. This process most probably has a higher impact on the overall polymerization when targeting short reaction times (and thus low molecular weight NBRs). Since the work aims at a semiquantitative discussion and good agreement with all other samples was obtained, the model was not further optimized. Nevertheless, values received in the simulations rather have a semiquantitative character and are used for a plausibility check.

To simulate weight fractions of nonfunctional polymer chains formed during polymerization, the obtained species were divided into chains possessing the chain-end functionality necessary for HDA conjugation and those not having these functionalities. Note that functionalization of the two individual building blocks was achieved with two approaches. Diene moieties are found at the NBR  $\alpha$ -chain-

---

\*\* SEC deconvolution and PREDICI simulations were performed by Dr. Lebohang Hlalele, Karlsruhe Institute of Technology, Institut für Technische Chemie und Polymerchemie.

end, which is the RAFT R-group, while the dienophile thiocarbonyl moiety is located at the  $\omega$ -chain-end (RAFT Z-group) of the SAN macromolecules. One of the main differences of the two approaches is the processes leading to the generation of nonfunctional polymer chains. While in the R-group approach all NBR chains except those derived from initiator radicals possess the diene functionality, SAN polymer chains lose their dienophile properties when chain termination events such as disproportionation or recombination occur. Simulations exhibited weight fractions of 4.9 to 5.5% of SAN polymers losing Z-group functionality during polymerization. For polymerization conditions see Table 4.3 (page 103), entries 11, 12 and 13, respectively. The increase is a result of chain termination events occurring throughout the polymerization, causing an accumulation of dead polymeric chains. In the AN/BD copolymerization simulations, a considerably higher weight fraction of nonfunctional NBR chains is observed. Here, percentages range from 6.2% (**6a**) to 7.2% (**6b**). In general, the R-group approach is expected to provide a higher degree of chain-end functionality in RAFT polymers than a Z-group approach. In light of the investigated systems, the inverse trend is obtained in the computational studies and is in line with experimental observations. AN/S copolymerizations provide narrow molecular weight distributions with  $D \leq 1.2$  for molar masses up to 80 000 g·mol<sup>-1</sup>, indicating excellent control. In contrast, molecular weight distributions obtained in AN/BD copolymerizations are slightly broadened even at low molecular weights, pointing to the formation of significant amounts of chains without the expected RAFT end-group functionality. The weight fraction of nonfunctionalized polymer chains obtained in simulations of <sup>t</sup>Br-functional NBRs **6** is equivalent to the weight fraction of nonfunctionalized chains in the Cp-capped NBRs **8**, when neglecting the weight difference of the chain-ends and assuming full conversion during the reaction with NiCp<sub>2</sub>. With a decreasing efficiency of the chain-end transformation into the Cp-capped polymer, a lower weight fraction of polymer chains able to undergo HDA conjugation *than* determined in the simulations is expected. Since no purification step after chain-end transformation is performed, weight fractions of nonfunctionalized chains in polymer **8** cannot be lower than those obtained from simulations for polymerizations of **6**.

To gain information on the coupling efficiency of the experimentally obtained block copolymer samples **8-b-7**, deconvolution of SEC traces was performed.<sup>23</sup> Deconvolution of the block copolymer SEC traces was carried out under consideration of the position of the peaks of the two precursor building blocks **8** and **7**. SEC traces of block copolymer **8b-b-7c** (black), **8b** (red), **7c** (blue) and the corresponding deconvoluted signals of the actual block copolymer (dashed line) and the residual polymers (dotted lines) are provided in Figure 4.18. A good peak fitting is obtained with an  $r^2$  value of 0.993. Integration allows for the determination of the weight fractions of block copolymer to 88.3% and the residual polymer to 10.7% (NBR) and 1.0% (SAN), respectively (Table 4.6, entry 3). It is noted that the deconvolution is leading to an underestimation of the actual fraction of block copolymer **8b-b-7c** by a few percent, since high molecular weight polymer is obtained but located beyond the area included in the Gaussian type deconvoluted block copolymer trace (dashed line). These higher molecular weight species might be a result of a chain length dependence of the rate coefficients of

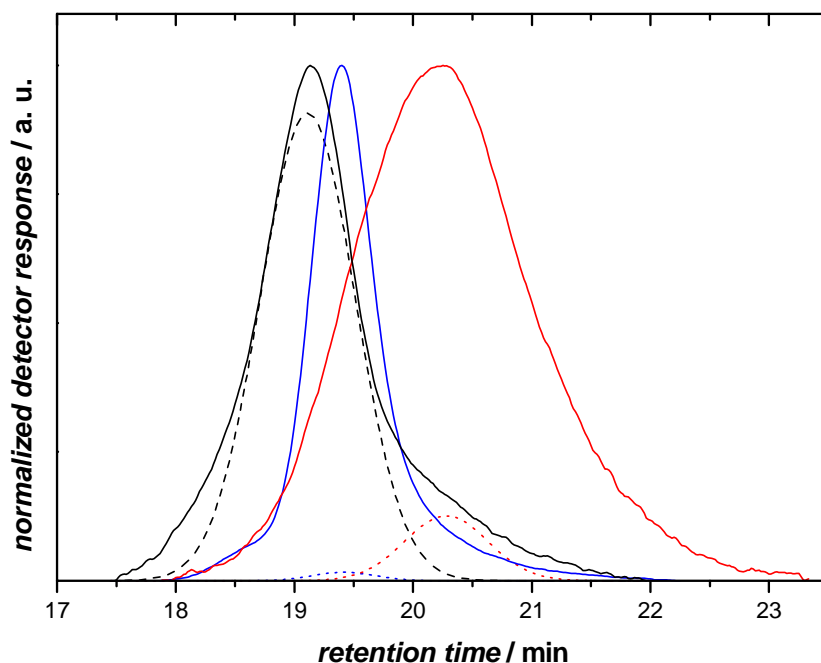


**Figure 4.18.** SEC traces of block copolymer **8b-b-7c** (black solid line), Cp-functional NBR **8b** (red solid line), dienophile SAN **7c** (blue solid line) and deconvolution data obtained via the PeakFit program. The dashed line represents the deconvoluted peak of the actual NBR-*b*-SAN block copolymer, the dotted lines indicate the deconvoluted side products, *i.e.* residual SAN (blue) or NBR (red line).

**Table 4.6.** Weight fraction of block/star copolymer as determined by SEC deconvolution and PREDICI® simulations.

entry	sample	weight fraction (%)					$r^2$
		block/star <sup>a</sup>	residual polymer <sup>a</sup>			block/star calculated <sup>b</sup>	
			NBR	SAN	3-arm star		
1	<b>8a-b-7a</b>	87.4	10.3	2.3	-	94.9	0.988
2	<b>8b-b-7b</b>	90.1	9.9	0	-	93.6	0.999
3	<b>8b-b-7c</b>	88.3	10.7	1.0	-	93.9	0.993
4	<b>(13b)(7b)<sub>2</sub></b>	80.7	19.3 <sup>c</sup>			n.d.	0.996

Conditions: <sup>a</sup> Determined from deconvolution of SEC traces of the block copolymer samples under consideration of peak maxima of the individual polymer building blocks. <sup>b</sup> Calculated from PREDICI® simulations employing Equation 4.1 (see the *Appendix*). <sup>c</sup> An overall value is provided, since a mixture of NBR, SAN, 4-miktoarm star and 3-miktoarm star polymers without knowledge of the actual position of the latter is obtained.

the conjugation process, evoking deviation from the Gaussian shaped signals.<sup>51</sup> In analogy, SEC traces of **8a-b-7a** is deconvoluted, revealing the sample to consist of 87.4% of the actual block copolymer, 10.3% of the NBR and 2.3% of SAN. The respective traces are provided in Figure 4.19; data are summarized in Table 4.6, entry 1.

The weight fractions of nonfunctionalized polymer chains obtained in PREDICI® simulations and the weight fractions of residual polymer building blocks determined via deconvolution cannot be compared directly, since the percentages correspond to different mass references. In the simulations, weight fractions are given as the ratio of the nonfunctional polymer material and the sum of functional and nonfunctional polymers *of similar type*, either NBR or SAN. In contrast, values obtained from deconvolution refer to the total mass of NBR-*b*-SAN sample including the respective unreacted NBR *and* SAN macromolecules. Thus, comparison of the weight fractions of residual chains obtained from SEC deconvolution and those determined from PREDICI® simulations requires transformation of the predicted relative weight fractions  $w_{\text{pred}}(\mathbf{8})$  and  $w_{\text{pred}}(\mathbf{7})$  of diene or dienophile functionalized polymer into a value characterizing the fraction of actual block copolymer **8-b-7** after conjugation has been performed. Calculations were performed according to Equation 4.1, explained in more detail in

the *Appendix*. The predicted relative weight fractions  $w_{\text{pred}}(\mathbf{8})$  and  $w_{\text{pred}}(\mathbf{7})$  are the ratios of functional polymer and the total weight of the individual NBR or SAN polymer sample, as obtained from PREDICI® simulations. The calculated fraction of actual block copolymer  $w_{\text{pred}}(\mathbf{8-b-7})$  is the ratio of the weight of polymer chains effectively possessing the desired NBR-*b*-SAN block structure and the total weight of the apparent block copolymer sample. The therein obtained values can be considered as an upper limit of the weight fraction of the actual block copolymer in the conjugated polymer sample that can be obtained under an ideal conjugation, since chain-end functionality is the limiting factor in the ligation process. Employing the values of simulated chain-end functionality for conjugation of Cp-functional NBR **8b** ( $w_{\text{pred}} = 92.8\%$ ) with dienophile SAN **7c** ( $w_{\text{pred}} = 94.5\%$ ) an upper limit of polymers possessing the actual block copolymer structure of 93.9% is obtained. This is in agreement with the value determined by deconvoluting the experimentally obtained SEC traces, giving 88.3% of actual **8b-b-7c** block copolymer (Table 4.6, entry 3). Consistent values are also obtained when

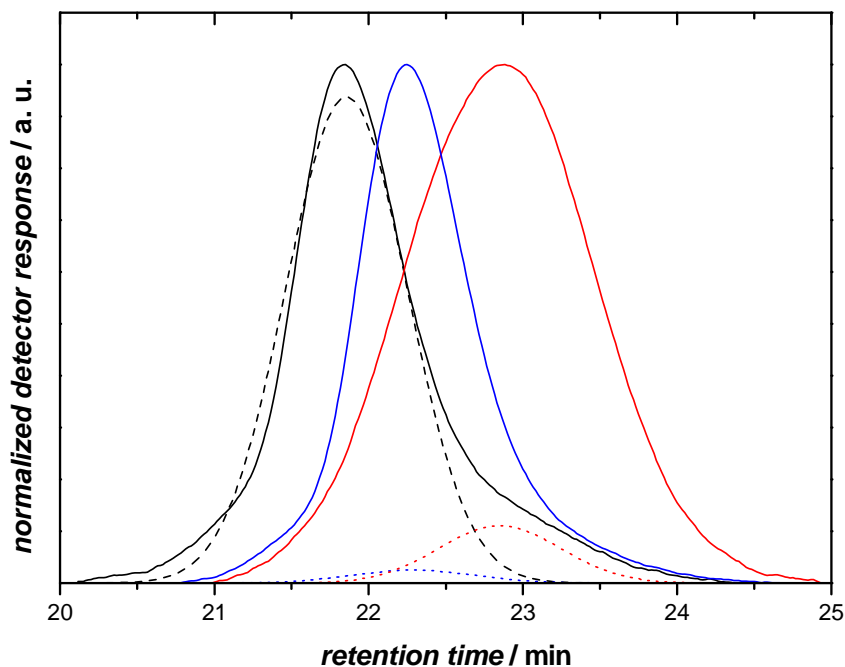


**Figure 4.19.** SEC traces of block copolymer **8a-b-7a** (black solid line), Cp-functional NBR **8a** (red solid line), dienophile SAN **7a** (blue solid line) and deconvolution data obtained via the PeakFit program. The dashed line represents the deconvoluted peak of the actual NBR-*b*-SAN block copolymer, the dotted lines indicate the deconvoluted side products, *i.e.* residual SAN (blue) or NBR (red line).

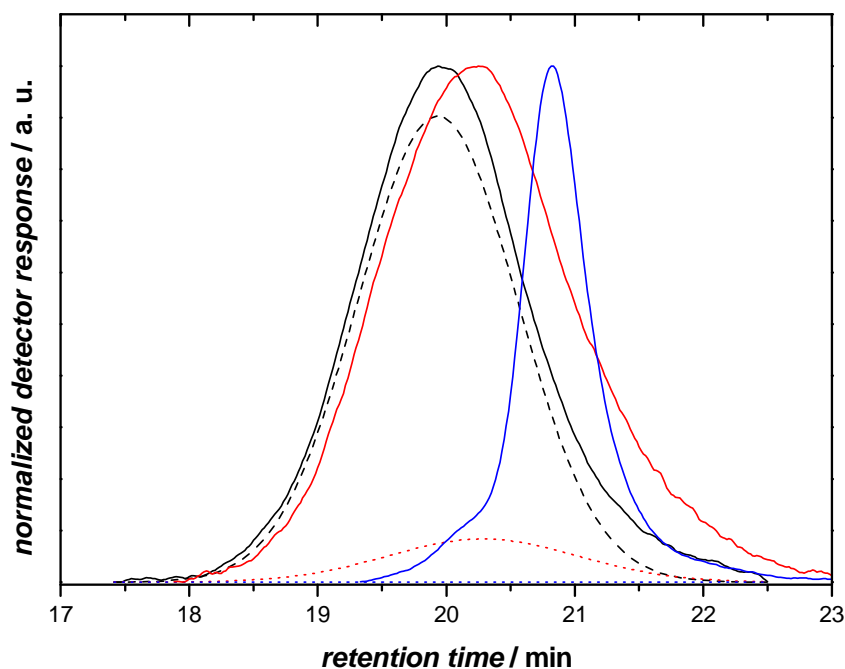


**Figure 4.20.** SEC traces of block copolymer **8b-b-7b** (black solid line), Cp-functional NBR **8b** (red solid line), dienophile SAN **7b** (blue solid line) and deconvolution data obtained via the PeakFit program. The dashed line represents the deconvoluted peak of the actual NBR-*b*-SAN block copolymer, the dotted lines indicate the deconvoluted side products, *i.e.* residual SAN (blue) or NBR (red line).

comparing simulated (94.9%) and SEC deconvolution (87.4%) values of actual NBR-*b*-SAN in block copolymer formation of **8a** ( $w_{\text{pred}} = 93.8\%$ ) and **7a** ( $w_{\text{pred}} = 95.8\%$ ), as shown in Table 4.6, entry 1. Taking into account the underestimation of the actual block copolymers in the deconvolutions of **8b-b-7c** and **8a-b-7a** due to the formation of high molecular weight **8-b-7** located outside the deconvoluted Gaussian curves (*vide supra*), the effective weight content of the actual block copolymer is higher than estimated from deconvolution. In the case where no high molecular weight tailing is observed (**8b-b-7b**, deconvolution provided in Figure 4.20), an excellent fit is obtained ( $r^2 = 0.999$ ) and a much improved correlation between block copolymer content derived from SEC deconvolution and PREDICI<sup>®</sup> is obtained. As summarized in Table 4.6, entry 2, deconvolution reveals 90.1% of actual block copolymer in excellent consistency with the upper limit weight fraction of actual block copolymer  $w_{\text{pred}}(\mathbf{8b-b-7b})$  calculated to 93.6% from simulated residual polymer values of **8b** ( $w_{\text{pred}} = 92.8\%$ ) and **7b** ( $w_{\text{pred}} = 94.8\%$ ). One has to keep in mind that PREDICI<sup>®</sup> simulations of NBR

and SAN polymerizations were performed assuming an ideal RAFT mechanism. Several processes not considered in the PREDICI® model – as indicated by the observed broad distributions of NBR in SEC measurements – might contribute to a decrease in chain-end fidelity further converging simulation and deconvolution values of the actual weight fractions of **8-b-7**.

Weight fractions of residual polymer of either nonfunctional SAN or NBR building blocks after conjugation obtained from SEC trace deconvolution do not agree with values calculated via PREDICI® simulations. Weight fractions of residual NBR as obtained from deconvolution are explicitly higher than an approximate equal distribution of residual SAN and NBR as expected from simulation data. This underestimation of residual SAN is attributed to the narrow SEC traces of SAN overlapping with the broad traces of NBR. The underestimation is most articulate for block copolymer **8b-b-7b**, where the narrow SAN trace is embedded entirely into the broad NBR trace. Nevertheless, the sum of residual NBR and SAN is a reliable value irrespective of its origin from the individual building blocks.

The herein presented data allow the conclusion that the observed incompleteness of the NBR-SAN HDA conjugation process is foremost a result of the presence of nonfunctional polymer chains formed during RAFT polymerization. From the deconvolution of SEC data, contributions of functional chains to the residual polymer not involved in the conjugation cannot be excluded. It is, however, expected that such contributions should be minimal, with a larger fraction being from nonfunctional SAN and NBR.

In case of the miktoarm stars, evaluation of the coupling efficiency is more complicated than for linear block copolymers. In addition to the targeted 4-miktoarm star copolymers and the unreacted NBR and SAN chains, formation of 3-miktoarm star polymers is expected. It was demonstrated earlier that formation of 4-arm star polystyrenes via the “arm-first” approach does not proceed to complete conversion and a considerable amount of 3-arm star polymer is obtained.<sup>8,52</sup> However, in the study presented in the current chapter the exact position of the SEC trace of the 3-miktoarm star polymer formed by reaction of one SAN block with the (bifunctional) NBR star precursor **13** cannot be determined.

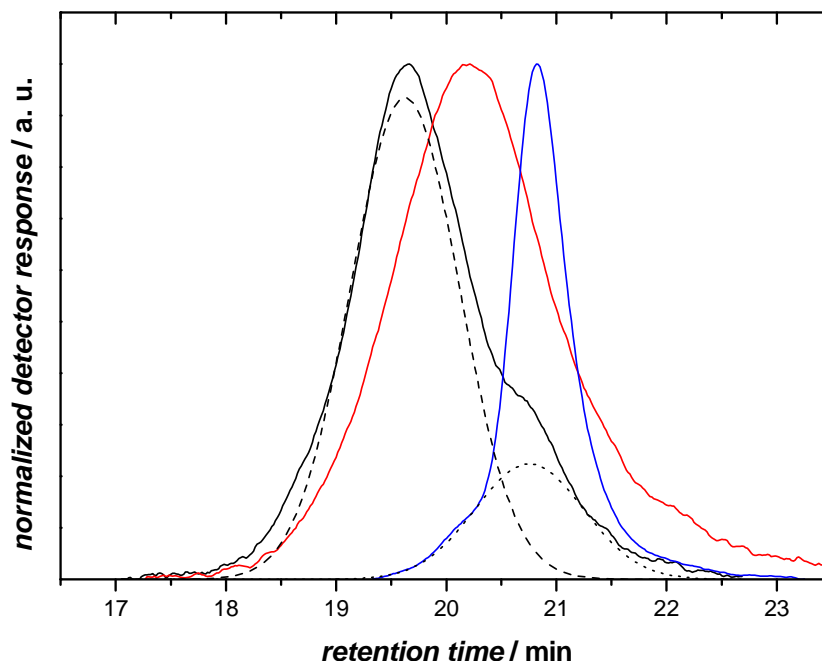


**Figure 4.21.** SEC traces of miktoarm star copolymer **(13b)(7b)<sub>2</sub>** (black solid line), Cp-functional star precursor **13b** (red solid line), dienophile SAN **7b** (blue solid line) and deconvolution data obtained via the Peak Fit program. The dashed line represents the deconvoluted peak of the 4-miktoarm star copolymer, the dotted line indicates the deconvoluted overall side products, *i.e.* residual SAN, NBR and 3-miktoarm star copolymer.

For that very reason, deconvolution of the miktoarm star copolymer is performed exemplarily for **(13b)(7b)<sub>2</sub>** by fitting to the 4-miktoarm star and one overall peak collectively containing the side products (Figure 4.21). The 4-miktoarm star copolymer accounts for 80.7% by weight with the remaining 19.3% being a result from the contribution of unreacted precursor blocks and possible 3-miktoarm star copolymer (Table 4.6, entry 4). Evaluation based on PREDICI® simulations is not performed, since no precise information on the content of 3-miktoarm star can be provided.

The increased quantity of residual polymer in case of the stars than for the block copolymers might be explained by steric constraints arising from the geometry of the conjugation. The Cp moieties are located in the center of the NBR star precursor; HDA cyclization requires unfolding of the macromolecule to allow access to the reactive moiety shielded by two linear chains. Steric hindrance increases further after a first SAN arm is attached, decelerating addition of a second SAN block to the 3-miktoarm star. With the insights obtained from the

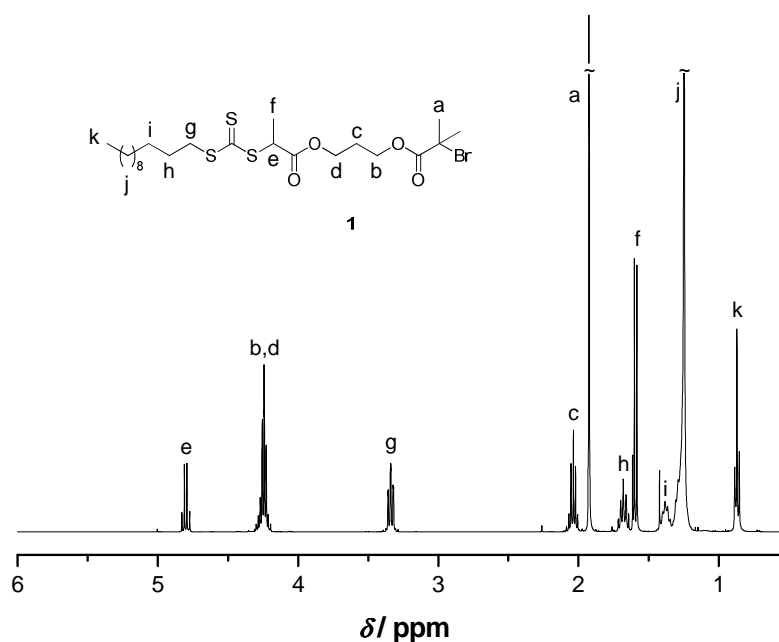
NBR-*b*-SAN block copolymer formation, the impact of the steric hindrance on incomplete star formation is estimated to account for around 10% of residual polymer.

#### 4.4 Conclusions

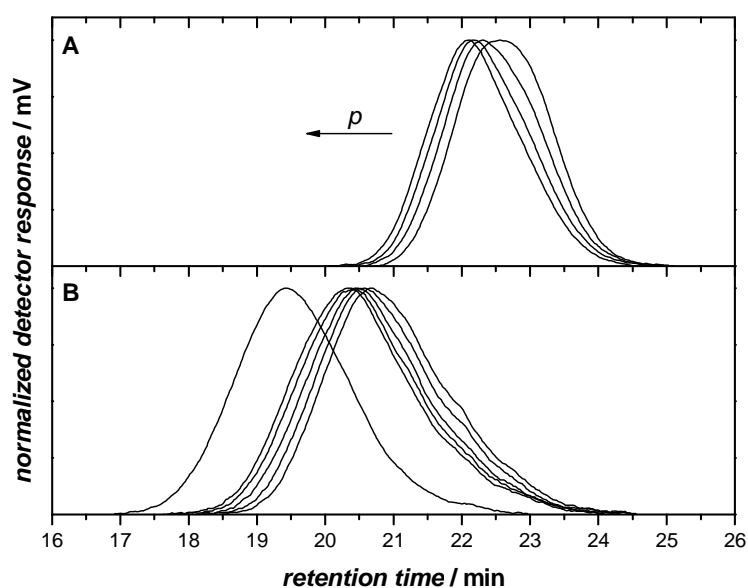
Ambient temperature RAFT-HDA ligation chemistry was successfully employed for the construction of block copolymers of NBR and SAN. The technique was shown to be a rapid and convenient method, allowing for the synthesis of NBR-*b*-SAN block copolymers over a broad range of molecular weights at nondemanding reaction conditions. NBR building blocks were obtained in RAFT copolymerizations employing a novel bromide-capped trithiocarbonate and a subsequent transformation of the bromide chain-end into a cyclopentadiene using nickelocene. Dienophile SAN polymers were accessible without any postpolymerization transformation. NBR-*b*-SAN block copolymers with molar masses of up to 110 000 g·mol<sup>-1</sup> were obtained and the protocol was further extended toward the synthesis of 4-miktoarm star copolymers.

The efficiency of the conjugation reactions was studied in detail in a semiquantitative manner by implementing a plausibility evaluation via kinetic simulations. Weight fractions of residual polymer – not participating in the modular conjugation – in block and miktoarm star copolymer samples were determined to range from 12 to 20% via deconvolution techniques. The values were compared to the calculated content of nonfunctionalized polymer chains arising from side reactions during the RAFT process as obtained in kinetic simulations. The study revealed the RAFT process to be responsible for the observed residual polymer not undergoing conjugation and further corroborates the efficiency of the HDA approach for the construction of complex macromolecular architectures. Nevertheless, the present study also demonstrates the limitations of reversible-deactivation radical polymerization protocols in the construction of macromolecular architectures.

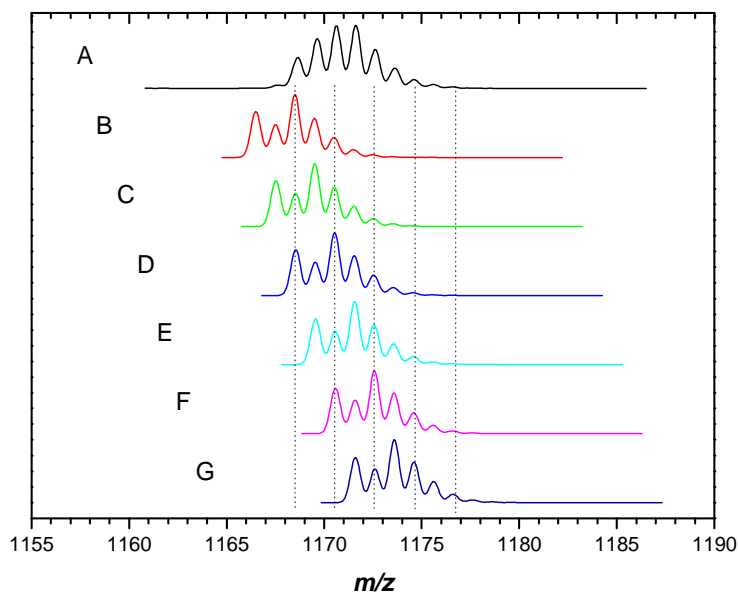
## 4.5 Appendix



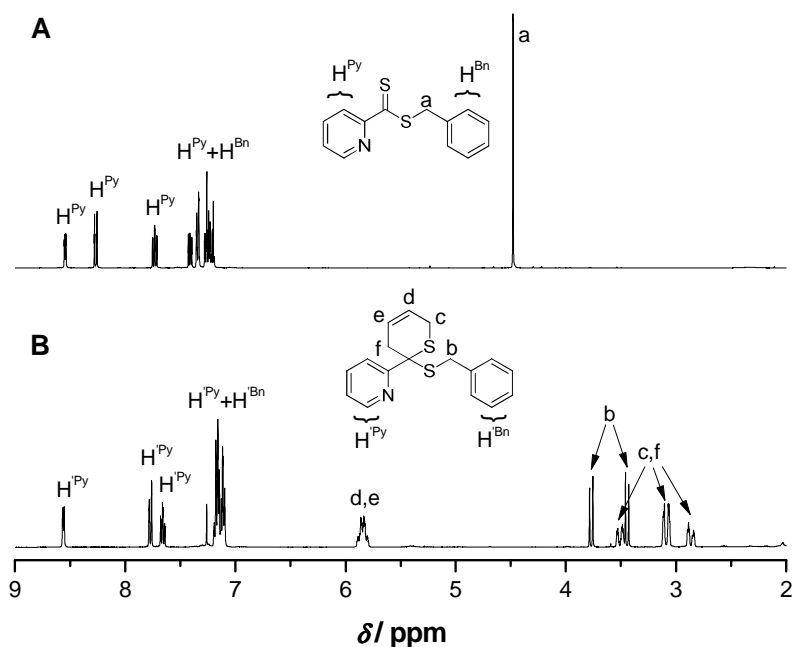
**Figure 4.22.**  $^1\text{H}$  NMR of  $t\text{Br}$ -functional RAFT agent **1** recorded in  $\text{CDCl}_3$ .



**Figure 4.23.** SEC traces of selected RAFT mediated polymerizations employing controlling agent **1**. Peak maxima shift toward lower retention times with increasing conversion under preservation of a monomodal molecular weight distribution. Conditions: A)  $[\text{RAFT}]_0 = 14.0 \text{ mmol}\cdot\text{l}^{-1}$ ,  $[\text{Ini}]_0 = 1.7 \text{ mmol}\cdot\text{l}^{-1}$ , samples taken after 4, 5, 6 and 7 h (Table 4.3, entry 4); B)  $[\text{RAFT}]_0 = 0.9 \text{ mmol}\cdot\text{l}^{-1}$ ,  $[\text{Ini}]_0 = 0.2 \text{ mmol}\cdot\text{l}^{-1}$ , samples taken after 2, 3, 4, 5, 6 and 22 h (Table 4.3, entry 6).



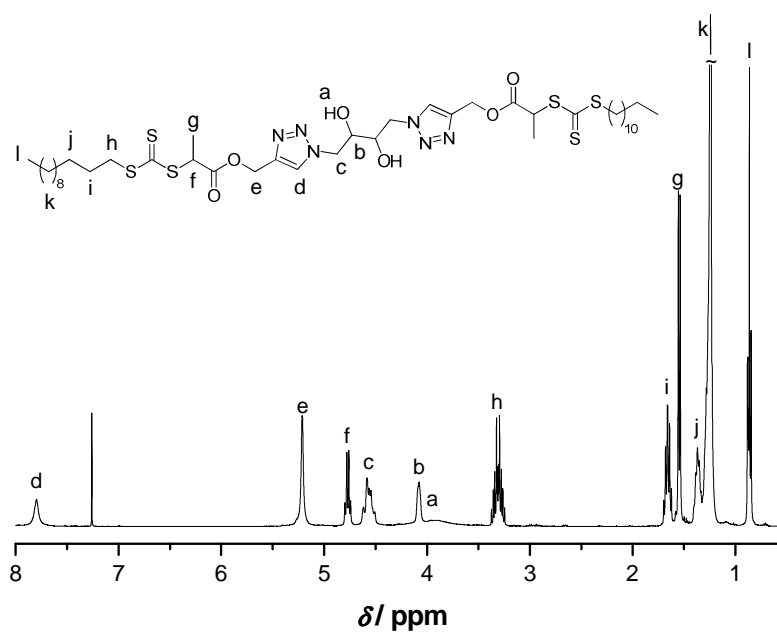
**Figure 4.24.** Comparative study of experimentally determined and theoretically calculated mass-to-charge ratios for the sodium adducts of a polymer **6** with  $m+n=11$  incorporated monomer units  $[\mathbf{6}_{11}+Na]^+$ . A) Magnified view into the region of 1155 to 1190 Da of an ESI-MS measurement of bromide-capped NBR **6c**. B-G) Simulated isotope patterns of bromide-capped NBR **6** with  $m+n=11$  repeat units and various  $m/n$  ratios, with  $m$  = number of incorporated AN, and  $n$  = number of incorporated BD monomer units. B)  $m/n = 7/4$ , C)  $6/5$ , D)  $5/6$ , E)  $4/7$ , F)  $3/8$  and G)  $2/9$ .



**Figure 4.25.**  $^1\text{H}$  NMR spectra ( $\text{CDCl}_3$ ) of A) controlling agent **3** and B) controlling agent **3** recorded after reaction with BD at  $100^\circ\text{C}$  and a successive purification via column chromatography (**3+BD**).

**Table 4.7.** Experimental details of Br-Cp transformation reactions.

entry		$m(\mathbf{6})/g$ or $m(\mathbf{12})/g$	$n(\text{NiCp}_2)$ (mmol)	$n(\text{PPh}_3)$ (mmol)	$n(\text{NaI})$ (mmol)	$V(\text{THF})$ (mL)
1	<b>6a</b> ⇒ <b>8a</b>	0.585	0.176	0.089	0.263	10
2	<b>6b</b> ⇒ <b>8b</b>	1.054	0.263	0.131	0.396	15
3	<b>6c</b> ⇒ <b>8c</b>	0.101	0.444	0.222	0.667	1.5
4	<b>6d</b> ⇒ <b>8d</b>	0.435	0.513	0.258	0.770	4
5	<b>12a</b> ⇒ <b>13a</b>	0.818	1.963	0.988	2.938	10
6	<b>12b</b> ⇒ <b>13b</b>	0.586	0.176	0.089	0.264	10

**Figure 4.26.**  $^1\text{H}$  NMR spectrum and signal assignments of hydroxyl-functional symmetrical controlling agent **10** recorded in  $\text{CDCl}_3$ .

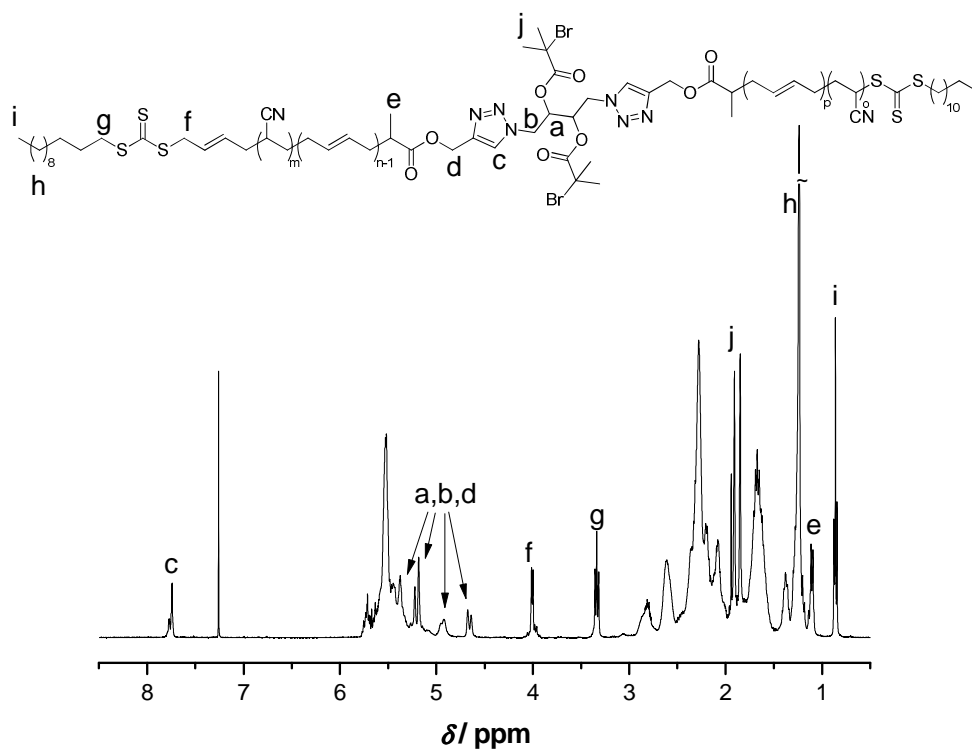


**Figure 4.27.**  $^1\text{H}$  NMR of midchain  $^4\text{Br}$ -functional NBR copolymer **12a** recorded in  $\text{CDCl}_3$ .

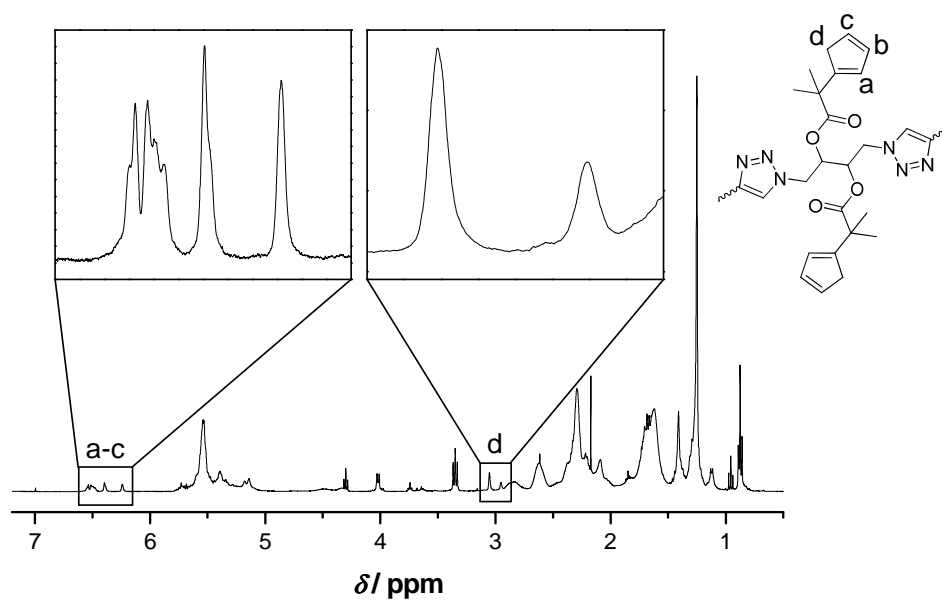


**Figure 4.28.**  $^1\text{H}$  NMR spectrum of the midchain Cp-functional star precursor **13a** recorded in  $\text{CDCl}_3$ .

**Table 4.8.** Comparison of conversion and  $M_n$  data for AN/BD copolymerizations.

experiment number	conversion (%)		$M_n$ (g·mol <sup>-1</sup> )	
	experimental	PREDICI®	Experimental	PREDICI®
<b>6e</b>	11.6	16.6	15 600	15 000
<b>6b</b>	12.3	15.3	39 000	36 000
<b>6f</b>	10.3	13.0	68 000	68 000
<b>6a</b>	29.1	11.0	5900	2900

**Table 4.9.** Comparison of conversion and  $M_n$  data for AN/S copolymerizations.

experiment number	conversion (%)		$M_n$ (g·mol <sup>-1</sup> )	
	experimental	PREDICI®	experimental	PREDICI®
<b>7a</b>	9.8	10.0	7900	7600
<b>7c</b>	11.2	5.0	76 000	56 000
<b>7b</b>	22.9	9.7	28 000	14 000

**Equation 4.1.** Calculation of the predicted weight fraction  $w_{pred}(\mathbf{8-b-7})$  of the actual block copolymer **8-b-7** of the total sample mass of the apparent block copolymer sample under consideration of the fraction of nonfunctional polymer chains present in the starting materials (*i.e.* building blocks **8** and **7**). Calculation was performed comprising the weight fractions of actual diene- and dienophile-functional polymers  $w_{pred}(\mathbf{8})$  and  $w_{pred}(\mathbf{7})$  within the starting materials, assuming full conversion of the HDA cyclization and an equimolar ratio of the actual diene- and dienophile-functionalized polymers **8** and **7** (excluding NBR and SAN polymer not possessing the diene oder dienophile functionality). Weight fractions of diene and dienophile polymers  $w_{pred}(\mathbf{8})$  and  $w_{pred}(\mathbf{7})$ , respectively, were obtained via PREDICI® simulations.  $M_n(\mathbf{8})$  and  $M_n(\mathbf{7})$  are the PS relative molar masses of the polymer building blocks as determined from SEC.

$$w_{pred}(\mathbf{8-b-7}) = \frac{M_n(\mathbf{8}) + M_n(\mathbf{7})}{M_n(\mathbf{8})/w_{pred}(\mathbf{8}) + M_n(\mathbf{7})/w_{pred}(\mathbf{7})}$$

## 4.6 References

1. Kaiser, A.; Brandau, S.; Klimpel, M.; Barner-Kowollik, C. *Macromol. Rapid Commun.* **2010**, *31*, 1616-1621.
2. Golas, P. L.; Tsarevsky, N. V.; Matyjaszewski, K. *Macromol. Rapid Commun.* **2008**, *29*, 1167-1171.
3. Agard, N. J.; Prescher, J. A.; Bertozzi, C. R. *J. Am. Chem. Soc.* **2004**, *126*, 15046-15047.
4. Codelli, J. A.; Baskin, J. M.; Agard, N. J.; Bertozzi, C. R. *J. Am. Chem. Soc.* **2008**, *130*, 11486-11493.
5. Tasdelen, M. A. *Polym. Chem.* **2011**, *2*, 2133-2145.
6. Sinnwell, S.; Synatschke, C. V.; Junkers, T.; Stenzel, M. H.; Barner-Kowollik, C. *Macromolecules* **2008**, *41*, 7904-7912.
7. Sinnwell, S.; Inglis, A. J.; Davis, T. P.; Stenzel, M. H.; Barner-Kowollik, C. *Chem. Commun.* **2008**, 2052-2054.
8. Inglis, A. J.; Sinnwell, S.; Davis, T. P.; Barner-Kowollik, C.; Stenzel, M. H. *Macromolecules* **2008**, *41*, 4120-4126.
9. Bousquet, A.; Barner-Kowollik, C.; Stenzel, M. H. *J. Polym. Sci. Part A: Polym. Chem.* **2010**, *48*, 1773-1781.
10. Nebhani, L.; Sinnwell, S.; Inglis, A. J.; Stenzel, M. H.; Barner-Kowollik, C.; Barner, L. *Macromol. Rapid Commun.* **2008**, *29*, 1431-1437.
11. Blinco, J. P.; Trouillet, V.; Bruns, M.; Gerstel, P.; Gliemann, H.; Barner-Kowollik, C. *Adv. Mater.* **2011**, *23*, 4435-4439.
12. Goldmann, A. S.; Tischer, T.; Barner, L.; Bruns, M.; Barner-Kowollik, C. *Biomacromolecules* **2011**, *12*, 1137-1145.
13. Urbani, C. N.; Bell, C. A.; Whittaker, M. R.; Monteiro, M. J. *Macromolecules* **2008**, *41*, 1057-1060.
14. Zhang, S.; Zhao, Y. *J. Am. Chem. Soc.* **2010**, *132*, 10642-10644.
15. Alberti, A.; Benaglia, M.; Guerra, M.; Gulea, M.; Hapiot, P.; Laus, M.; Macciantelli, D.; Masson, S.; Postma, A.; Sparnacci, K. *Macromolecules* **2005**, *38*, 7610-7618.

16. Dürr, C. J.; Emmerling, S. G. J.; Kaiser, A.; Brandau, S.; Habicht, A. K. T.; Klimpel, M.; Barner-Kowollik, C. *J. Polym. Sci. Part A: Polym. Chem.* **2012**, *50*, 174-180.
17. Barner-Kowollik, C.; Quinn, J. F.; Morsley, D. R.; Davis, T. P. *J. Polym. Sci. Part A: Polym. Chem.* **2001**, *39*, 1353-1365.
18. Vana, P.; Davis, T. P.; Barner-Kowollik, C. *Macromol. Theory Simul.* **2002**, *11*, 823-835.
19. Junkers, T.; Koo, S. P. S.; Barner-Kowollik, C. *Polym. Chem.* **2010**, *1*, 438-441.
20. Cherubin, T. *Über die Bestimmung von Copolymerisationsparametern in der radikalischen Copolymerisation von Acrylnitril mit Butadien*. Ph.D. Thesis, University of Essen, 1999.
21. Beuermann, S.; Buback, M. *Prog. Polym. Sci.* **2002**, *27*, 191-254.
22. Elizarrarás, D.; Morales, G.; de León, R. D.; Luciani, C.; Estenoz, D. *Macromol. Theory Simul.* **2008**, *17*, 180-197.
23. Inglis, A. J.; Barner-Kowollik, C. *Polym. Chem.* **2011**, *2*, 126-136.
24. Kim, W. N.; Burns, C. M. *Polym. Eng. Sci.* **1988**, *28*, 1115-1125.
25. Dietrich, M.; Glassner, M.; Gruending, T.; Schmid, C.; Falkenhagen, J.; Barner-Kowollik, C. *Polym. Chem.* **2010**, *1*, 634-644.
26. George, S.; Joseph, R.; Thomas, S.; Varughese, K. T. *Polymer* **1995**, *36*, 4405-4416.
27. Laus, M.; Papa, R.; Sparnacci, K.; Alberti, A.; Benaglia, M.; Macciantelli, D. *Macromolecules* **2001**, *34*, 7269-7275.
28. Inglis, A. J.; Sinnwell, S.; Stenzel, M. H.; Barner-Kowollik, C. *Angew. Chem. Int. Ed.* **2009**, *48*, 2411-2414.
29. Barner-Kowollik, C.; Du Prez, F. E.; Espeel, P.; Hawker, C. J.; Junkers, T.; Schlaad, H.; Van Camp, W. *Angew. Chem. Int. Ed.* **2011**, *50*, 60-62.
30. Wang, J.-S.; Matyjaszewski, K. *J. Am. Chem. Soc.* **1995**, *117*, 5614-5615.
31. Solomon, D. H.; Rizzardo, E.; Cacioli, P. *Polymerization Process and Polymers Produced Thereby*. US. Pat., 4 581 429, 1986.
32. Junkers, T.; Lovestead, T. M.; Barner-Kowollik, C., The RAFT Process as a Kinetic Tool: Accessing Fundamental Parameters of Free Radical

- Polymerization. In *Handbook of RAFT Polymerization*. 1<sup>st</sup> ed.; Barner-Kowollik, C., Ed.; Wiley-VCH: Weinheim, 2008; p 105 ff.
33. Li, Y.; Padias, A. B.; Hall, H. K. *J. Org. Chem.* **1993**, *58*, 7049-7058.
  34. Fossey, J. S.; Richards, C. J. *Organometallics* **2004**, *23*, 367-373.
  35. am Ende, D. J.; Whritenour, D. C.; Coe, J. W. *Org. Process Res. Dev.* **2007**, *11*, 1141-1146.
  36. Inglis, A. J.; Paulöhrl, T.; Barner-Kowollik, C. *Macromolecules* **2010**, *43*, 33-36.
  37. Barner-Kowollik, C.; Quinn, J. F.; Nguyen, T. L. U.; Heuts, J. P. A.; Davis, T. P. *Macromolecules* **2001**, *34*, 7849-7857.
  38. Bastin, R.; Albadri, H.; Gaumont, A.-C.; Gulea, M. *Org. Lett.* **2006**, *8*, 1033-1036.
  39. Chiefari, J.; Chong, Y. K.; Ercole, F.; Krstina, J.; Jeffery, J.; Le, T. P. T.; Mayadunne, R. T. A.; Meijs, G. F.; Moad, C. L.; Moad, G.; Rizzardo, E.; Thang, S. H. *Macromolecules* **1998**, *31*, 5559-5562.
  40. Barner-Kowollik, C. *Macromol. Rapid Commun.* **2009**, *30*, 1625-1631.
  41. Binder, W. H.; Sachsenhofer, R. *Macromol. Rapid Commun.* **2007**, *28*, 15-54.
  42. Binder, W. H.; Sachsenhofer, R. *Macromol. Rapid Commun.* **2008**, *29*, 952-981.
  43. Altintas, O.; Vogt, A. P.; Barner-Kowollik, C.; Tunca, U. *Polym. Chem.* **2012**, *3*, 34-45.
  44. Hadjichristidis, N.; Pitsikalis, M.; Pispas, S.; Iatrou, H. *Chem. Rev.* **2001**, *101*, 3747-3792.
  45. Cameron, D. J. A.; Shaver, M. P. *Chem. Soc. Rev.* **2011**, *40*, 1761-1776.
  46. Khanna, K.; Varshney, S.; Kakkar, A. *Polym. Chem.* **2010**, *1*.
  47. Moughton, A. O.; Hillmyer, M. A.; Lodge, T. P. *Macromolecules* **2011**, *45*, 2-19.
  48. Frieberg, B.; Glynos, E.; Sakellariou, G.; Green, P. F. *ACS Macro Lett.* **2012**, *1*, 636-640.
  49. Mansfeld, U.; Pietsch, C.; Hoogenboom, R.; Becer, C. R.; Schubert, U. S. *Polym. Chem.* **2010**, *1*, 1560-1598.
  50. Moad, G.; Rizzardo, E.; Thang, S. H. *Aust. J. Chem.* **2005**, *58*, 379-410.

- 
51. Preuss, C. M.; Barner-Kowollik, C. *Macromol. Theory Simul.* **2011**, *20*, 700-708.
  52. Gao, H.; Matyjaszewski, K. *Macromolecules* **2006**, *39*, 4960-4965.



# 5 ■ Photo-Induced Ligation of Acrylonitrile-Butadiene Rubber: Selective Tetrazole-Ene Coupling of Chain-End Functionalized Copolymers of 1,3-Butadiene<sup>††</sup>

## 5.1 Introduction

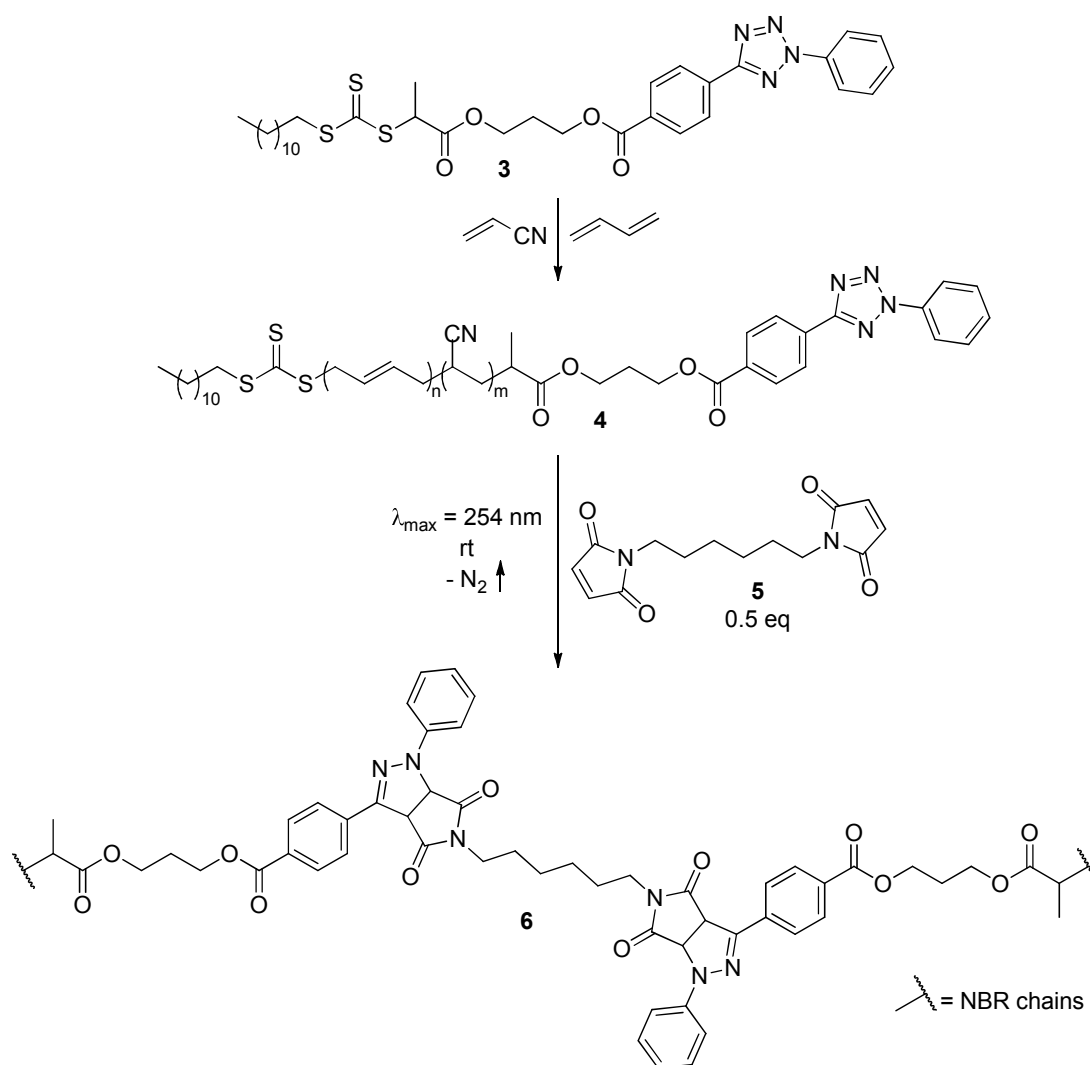
Within the last decade, orthogonal ligation techniques have found substantial interest in the field of polymer chemistry.<sup>1-4</sup> The most prominent ligation technique, the copper mediated azide-alkyne cycloaddition (CuAAC), was reinvented by Kolb, Finn and Sharpless<sup>5</sup> with the introduction of the “click” concept in 2001 and since then continuously refined. In recent years, strategies to improve catalysts in efficiency<sup>6</sup> and nature<sup>7</sup> were developed and catalyst-free strategies employing ring-strained cycloalkynes<sup>8</sup> were proposed. In addition, several other thermally,<sup>9-10</sup> chemically<sup>11-14</sup> or photochemically<sup>15-19</sup> triggered ligation protocols have been developed. An outstanding example of an orthogonal ligation chemistry is the UV-light triggered nitrile imine mediated tetrazole-ene coupling (NITEC).<sup>20-23</sup> First described in 1967 by Huisgen and coworkers,<sup>24</sup> the method is mainly applied in the field of biochemistry<sup>25-27</sup> and was used for bio-orthogonal conjugation of proteins *in vitro*<sup>28</sup> and *in vivo*.<sup>29-30</sup> Recently, polymer scientists have found interest in this technique free of catalysts and additives for the modification of polymersomes<sup>31</sup> or the spatially controlled immobilization of polymers on silicon or cellulose.<sup>32</sup> Mechanistically, the irreversible light triggered release of molecular nitrogen from a 2,5-tetrazole provides a nitrile imine dipole

---

<sup>††</sup> Adapted with permission from Dürr, C. J.; Lederhose, P.; Hlalele, L.; Abt, D.; Kaiser, A.; Brandau, S.; Barner-Kowollik, C. *Macromolecules* **2013**, *46*, 5915-5923. DOI: 10.1021/ma401154k. Copyright 2013 American Chemical Society.

that reacts *in situ* with olefins – either activated or unactivated – via formation of a pyrazoline structure (see chapter 2.3.6).

In the thesis at hand, the access of chain-end functionalized nitrile-butadiene rubber (NBR) via the recently developed RAFT mediated acrylonitrile (AN)/1,3-butadiene (BD) copolymerization protocol<sup>33-34</sup> is exploited for the synthesis of advanced macromolecular architectures of NBR via successive modular ligation strategies. Herein, block- and miktoarm star copolymers have been synthesized via hetero-Diels–Alder cyclization (chapter 4) and – by employing a CuAAC reaction pathway (chapter 3) – NBRs of molar masses above those that can be obtained in sequential RAFT polymerizations have been accessed.<sup>33</sup>



**Scheme 5.1** Overall strategy of the UV-induced modular coupling of NBR building blocks to obtain high molecular weight nitrile rubber.

In the present chapter, a photoinduced approach for the synthesis of linear high molecular weight NBR via the NITEC approach is described. Such an approach is highly desirable, since linear high molecular weight polymer of the technically important synthetic rubber cannot be obtained in a sequential RAFT process. With respect to an industrial application, the NITEC technique overcomes the limitations of other ligation techniques that derived from the need of metal catalysts, often exhibiting negative effects on NBR ageing properties.<sup>35</sup> The presented photochemical tetrazole-ene coupling technique reveals a high selectivity and solely proceeds with the specific linker molecule. A coupling of the tetrazole chain-ends with the ‘enes’ present in high concentrations within the NBR backbone is not observed.

The overall strategy of NBR coupling is depicted in Scheme 5.1. A novel tetrazole-functional controlling agent (**3**) – representing, to the best of our knowledge, the first ever reported photoreactive RAFT agent – was synthesized from 4-(2-phenyl-2H-tetrazol-5-yl)benzoic acid (**2**) in two consecutive esterification steps and employed in RAFT mediated radical copolymerization of AN and BD. In the presence of a small molecule linker, bis(maleimido)hexane (**5**), the RAFT based photoreactive polymers (**4**) were irradiated with UV-light ( $\lambda_{\text{max}} = 254 \text{ nm}$ ) to form the diaryl nitrile imine enophile *in situ*. The nitrile imine and the dipolarophile maleimide subsequently react to give the coupled NBR (**6**).

## 5.2 Experimental Section

### 5.2.1 Materials

Acrylonitrile (AN, > 99%, Acros), 1,3-butadiene (BD, > 99.5%, Air Liquide), *N,N'*-dicyclohexylcarbodiimide (DCC, 99%, Acros), 4-(dimethylamino)pyridine (DMAP, 99%, Aldrich), propane-1,3-diol (98%, Aldrich), benzenesulfonyl hydrazide (98%, ABCR), 4-formylbenzoic acid (97%, Aldrich), acetonitrile (Rotisol, HPLC grade), pyridine, (99%, ABCR), aniline (>99.5%, Aldrich), sodium nitrite (97+%, Acros), hydrochloric acid (37%, Roth), 1,1'-azobis(cyclohexane-1-carbonitrile) (98%, Aldrich), 1-ethylpiperidine hypophosphite (95%, Aldrich), 1-octene (98%, Aldrich), *trans*-3-octene (97%, ABCR) and chlorobenzene (99+%,

Acros) were used without further purification. 1,6-bis(maleimido)hexane (**5**) was obtained from BASF SE, Germany. Other solvents (synthesis grade) were obtained from VWR and used as received. 2-((dodecylsulfanyl)carbonothioyl)sulfanyl propanoic acid (DoPAT) was obtained from Lanxess Deutschland GmbH. 4-(2-phenyl-2H-tetrazol-5-yl)benzoic acid (**2**) was synthesized according to the literature.<sup>20</sup>

### 5.2.2 Synthesis of Tetrazole-Functional RAFT Agent **3**

DoPAT (2.000 g, 5.7 mmol), DMAP (0.014 g, 0.1 mmol) and 1,3-propanediol (1.299 g, 17.1 mmol) were dissolved in tetrahydrofuran (THF, 10 mL). The solution was cooled to 0 °C and DCC (1.290 g, 6.3 mmol) was added. The cooling bath was removed and the reaction mixture was stirred at ambient temperature for 16 h. THF was removed under reduced pressure. The obtained solid was dissolved in Et<sub>2</sub>O, extracted with 1 M aqueous hydrochloric acid (4 × 100 mL) and washed with saturated NaHCO<sub>3</sub> solution (100 mL). The organic layer was dried over MgSO<sub>4</sub> and Et<sub>2</sub>O was removed under reduced pressure. The crude product was purified via column chromatography on silica gel using hexane/ethyl acetate (3:1, v/v, *R<sub>f</sub>* 0.36) as the eluent. After drying under high vacuum compound **1** was obtained as a yellow oil (1.591 g, 68%).

<sup>1</sup>H NMR (400 MHz, CDCl<sub>3</sub>) δ 4.83 (q, *J* = 7.4 Hz, 1H, CH(CH<sub>3</sub>)), 4.31 – 4.28 (m, 2H, C(O)O-CH<sub>2</sub>), 3.69 (t, *J* = 7.4 Hz, 2H, CH<sub>2</sub>-OH), 3.34 (t, *J* = 7.4 Hz, 2H, S-CH<sub>2</sub>), 1.90 – 1.86 (m, 2H, O-CH<sub>2</sub>-CH<sub>2</sub>-CH<sub>2</sub>-OH), 1.70 – 1.66 (m, 2H, S-CH<sub>2</sub>-CH<sub>2</sub>), 1.59 (d, *J* = 7.4 Hz, 3H, CH(CH<sub>3</sub>)), 1.42 – 1.38 (m, 2H, S-CH<sub>2</sub>-CH<sub>2</sub>-CH<sub>2</sub>), 1.26 – 1.21 (m, 16H, CH<sub>3</sub>-(CH<sub>2</sub>)<sub>8</sub>), 0.86 (t, *J* = 7.4 Hz, 3H, CH<sub>2</sub>-CH<sub>3</sub>).

<sup>13</sup>C NMR (101 MHz, CDCl<sub>3</sub>) δ 222.27 (C(S)-S), 171.28 (C(O)-O), 62.00, 48.16, 37.37, 32.05, 29.76, 29.75, 29.68, 29.56, 29.47, 29.22, 29.03, 28.02, 22.82, 17.09, 14.25, 14.22 (CH<sub>2</sub>-CH<sub>3</sub>).

The hydroxyl-functional RAFT agent **1** (3.800 g, 9.3 mmol), DMAP (0.026 g, 0.02 mmol) and diaryl tetrazole **2** (2.890 g, 10.9 mmol) were dissolved in THF (20 mL). The solution was cooled to 0 °C and DCC (2.450 g, 11.9 mmol) was added. After stirring the reaction mixture for 16 h at ambient temperature THF was removed under reduced pressure. The obtained solid was dissolved in Et<sub>2</sub>O,

extracted with 1 M aqueous hydrochloric acid ( $4 \times 200$  mL) and washed with saturated  $\text{NaHCO}_3$  solution (200 mL). The organic layer was dried over  $\text{MgSO}_4$  and  $\text{Et}_2\text{O}$  was removed under reduced pressure. The crude product was purified via column chromatography on silica gel using hexane/ethyl acetate (3:1, v/v  $R_f$  0.47) as the eluent. After drying under high vacuum the title compound **3** was obtained as a yellow oil (2.760 g, 45%).

$^1\text{H}$  NMR (400 MHz,  $\text{CDCl}_3$ )  $\delta$  8.28 (d,  $J = 7.6$  Hz, 2H,  $\text{CH-C-C(O)O}$ ), 8.17 – 8.10 (m, 4H,  $\text{CH-CH-C-C(O)O}$ ,  $\text{C}_6\text{H}_5$ -*ortho*-H), 7.53 (t,  $J = 7.3$  Hz, 2H,  $\text{C}_6\text{H}_5$ -*meta*-H), 7.46 (t,  $J = 7.4$  Hz, 1H,  $\text{C}_6\text{H}_5$ -*para*-H), 4.81 (q,  $J = 7.1$  Hz, 1H,  $\text{CH}(\text{CH}_3)$ ), 4.45 (t,  $J = 7.9$  Hz, 2H, aryl- $\text{C(O)O-CH}_2$ ), 4.33 (t,  $J = 6.8$  Hz, 2H,  $\text{CH}(\text{CH}_3)\text{-C(O)O-CH}_2$ ), 3.32 (t,  $J = 7.2$  Hz, 2H, S- $\text{CH}_2$ ), 2.19 – 2.16 (m, 2H, O- $\text{CH}_2\text{-CH}_2\text{-CH}_2\text{-O}$ ), 1.66 – 1.60 (m,  $J = 7.1$  Hz, 2H, S- $\text{CH}_2\text{-CH}_2$ ), 1.59 (d,  $J = 7.2$  Hz, 3H,  $\text{CH}(\text{CH}_3)$ ), 1.38 – 1.34 (m, 2H, S- $\text{CH}_2\text{-CH}_2\text{-CH}_2$ ), 1.38 – 1.33 (m, 16H,  $\text{CH}_3\text{-(CH}_2)_8$ ), 0.86 (t,  $J = 7.2$  Hz, 3H,  $\text{CH}_2\text{-CH}_3$ ).

$^{13}\text{C}$  NMR (101 MHz,  $\text{CDCl}_3$ )  $\delta$  222.19 (C(S)-S), 171.33 ( $\text{CH}(\text{CH}_3)\text{-C(O)-O}$ ), 165.97 (aryl- $\text{C(O)-O}$ ), 164.46 (C(N-R)-N), 136.92, 131.88, 131.47, 130.38, 130.03, 129.88, 127.14, 120.06, 62.55, 61.83, 47.96, 37.44, 32.04, 29.76, 29.74, 29.68, 29.57, 29.47, 29.22, 29.05, 28.12, 27.99, 22.82, 16.87, 14.25 ( $\text{CH}_2\text{-CH}_3$ ).

### 5.2.3 Synthesis of Ethyl-Functionalized RAFT Agent **8**

DoPAT (2.000 g, 5.7 mmol), DMAP (0.014 g, 0.1 mmol) and ethanol (0.616 g, 13.4 mmol) were dissolved in THF (10 mL). After the solution was cooled to  $0^\circ\text{C}$ , DCC (1.290 g, 6.3 mmol) was added. The reaction mixture was stirred at ambient temperature for 16 h. THF was removed in vacuum. The obtained solid was dissolved in  $\text{Et}_2\text{O}$ , extracted with 1 M aqueous hydrochloric acid ( $4 \times 100$  mL) and washed with saturated  $\text{NaHCO}_3$  solution (100 mL). The organic layer was dried over  $\text{MgSO}_4$  and  $\text{Et}_2\text{O}$  was removed under reduced pressure. The crude product was purified via column chromatography on silica gel using hexane/ethyl acetate (3:1, v/v,  $R_f$  0.61) as the eluent. After drying under high vacuum compound **10** was obtained as yellow oil (1.430 g, 66%).

$^1\text{H}$  NMR (400 MHz,  $\text{CDCl}_3$ )  $\delta$  4.80 (q,  $J = 7.4$  Hz, 1H,  $\text{CH}(\text{CH}_3)$ ), 4.25 – 4.14 (m, 2H,  $\text{C(O)O-CH}_2$ ), 3.35 (t,  $J = 7.5$  Hz, 2H, S- $\text{CH}_2$ ), 1.74 – 1.63 (m, 2H, S- $\text{CH}_2\text{-CH}_2$ ), 1.59 (d,

$J = 7.5$  Hz, 3H, CH(CH<sub>3</sub>)), 1.46 – 1.34 (m, 2H, S-CH<sub>2</sub>-CH<sub>2</sub>-CH<sub>2</sub>), 1.34 – 1.18 (m, 19H, CH<sub>3</sub>-(CH<sub>2</sub>)<sub>8</sub>, O-CH<sub>2</sub>-CH<sub>3</sub>), 0.87 (t,  $J = 6.9$  Hz, 3H, CH<sub>2</sub>-CH<sub>2</sub>-CH<sub>3</sub>)

<sup>13</sup>C NMR (101 MHz, CDCl<sub>3</sub>)  $\delta$  222.27 (C(S)-S), 171.28 (C(O)-O), 62.00, 48.16, 37.37, 32.05, 29.76, 29.75, 29.68, 29.56, 29.47, 29.22, 29.03, 28.02, 22.82, 17.09, 14.25, 14.22.

#### 5.2.4 Coupling of Tetrazole-Functionalized NBR via NITEC

In a round bottom quartz glass flask, tetrazole-functionalized NBR was dissolved in acetonitrile. 0.5 eq of bismaleimide linker were added from a stock solution in acetonitrile (for details see Table 5.4, page 172). The solution was irradiated with UV-light of 254 nm (Lamag TLC lamp, 8 W) for 3 h. The solvent was removed under reduced pressure and polymers were analyzed without further purification.

#### 5.2.5 Polymerizations

RAFT mediated copolymerizations of AN and BD were performed in a pressure stable glass reactor in a setup described earlier.<sup>33</sup> Samples were taken after pre-set time intervals and precipitated in cold ethanol. Experimental details are provided in Table 5.2 (see page 158).

#### 5.2.6 DFT Calculations<sup>##</sup>

The HOMO and LUMO energies were calculated using the B3LYP/6-31G//B3LYP/6-31G model chemistry with GAMESS.

#### 5.2.7 Instrumentation

<sup>1</sup>H NMR and <sup>13</sup>C NMR spectra were recorded at ambient temperature on a Bruker Advance 400 NMR spectrometer or a Bruker AM 250 NMR spectrometer and referenced to the residual solvent signal.

Molecular weight determination was performed on a SEC system (PL-GPC 50 Plus, Polymer Laboratories) consisting of an auto injector, a guard column (PLgel Mixed C, 50 × 7.5 mm), three linear columns (PLgel Mixed C, 300 × 7.5 mm, 5  $\mu$ m bead-size) and a differential refractive index detector using THF as the eluent at 35

---

<sup>##</sup> DFT calculations were performed by Dr. Lebohang Hlalele, Karlsruhe Institute of Technology, Institut für Technische Chemie und Polymerchemie.

°C and a flow rate of 1 mL·min<sup>-1</sup>. The system was calibrated using narrow polystyrene (PS) standards (Polymer Standards Service) ranging from 160 to 6 × 10<sup>6</sup> g·mol<sup>-1</sup>. Samples were injected from solutions in THF (2 mg·mL<sup>-1</sup>) and molecular weight was evaluated with the Mark–Houwink–Kuhn–Sakurada (MHKS) parameters of NBR (the determination of the MHKS parameters of NBR is reported in Chapter 6).

ESI mass spectra were recorded on a LXQ mass spectrometer (ThermoFisher Scientific, San Jose, CA, USA) equipped with an atmospheric pressure ionization source operating in the nebulizer assisted electrospray mode. The system was calibrated with a standard containing caffeine, Met-Arg-Phe-Ala acetate and a mixture of fluorinated phosphazenes (Ultramark 1621), purchased from Aldrich. A spray voltage of 4.5 kV, a dimensionless sweep gas flow rate of 2 and a dimensionless sheath gas flow-rate of 12 were applied. The capillary voltage, the tube lens offset voltage and the capillary temperature were set to 60 V, 110 V and 275 °C, respectively. For SEC-ESI-MS measurements the mass spectrometer was coupled to a Series 1200 HPLC-system (Agilent, Santa Clara, CA, USA) with THF as the eluent in accordance to a setup described earlier.<sup>36</sup> Polymer samples were dissolved in THF at 2 mg·mL<sup>-1</sup> and injected onto the HPLC-system.

Fluorescence emission spectra were recorded in quartz cuvettes loaded with a sample volume of 230 µL on a Varian Cary Eclipse Fluorescence Spectrometer. UV absorption spectra were recorded on a Varian Cary 300 UV-vis spectrometer.

### 5.3 Results and Discussion

Cyclization of various diaryl nitrile imines with nonactivated olefins was reported to proceed within seconds.<sup>29</sup> In NBR polymerizations, incorporation of BD into the growing polymer chain predominantly occurs in a 1,4-mode resulting in the formation of internal double bonds distributed along the polymer backbone. These double bonds are potential “dipolarophiles” able to react with the nitrile imine dipole. Close to 10% of the BD incorporation occurs in a 1,2-mode giving pendant double bonds,<sup>37</sup> less sterically hindered and more readily available for cyclization than the internal ones. In 1972, Stille *et al.* investigated cyclizations of nitrile-

imines and residual double bonds of styrene-butadiene type or natural rubber type elastomers for their thermally induced crosslinking.<sup>38</sup> In their work, tetrazole-functionalized styrene monomers were synthesized and copolymerized into the elastomers as pendant nitrile imine dipole precursors. At elevated temperatures, crosslinked rubbers were obtained and characterized by solubility studies. Nitrogen release was observed at temperatures above 150 °C with tetrazole half lives in the range of several minutes. Since the reaction kinetics and cyclization affinities of diaryl nitrile imines toward olefins strongly depend on the substitution patterns of the aromates, a careful choice of substituents on the aromatic rings of the diary tetrazole is crucial to prevent crosslinking of the tetrazole-

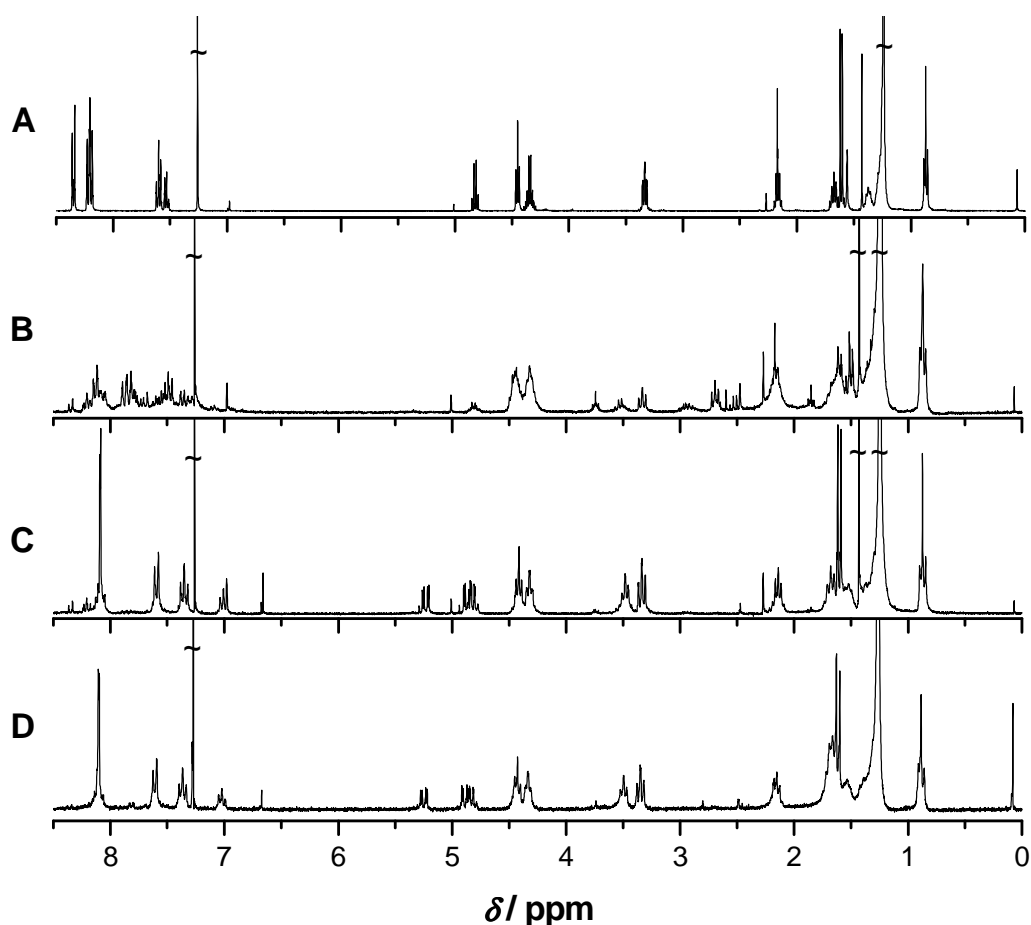


**Figure 5.1.** <sup>1</sup>H NMR spectra (CDCl<sub>3</sub>) of A) the diaryl tetrazole-functional RAFT agent **3** and B-D) the reaction mixtures obtained after irradiation with UV light of 254 nm at ambient temperature in acetonitrile in the presence of olefins: B) reactants: **3**, *trans*-3-octene (ratio 1:1), 3 h; C) reactants: **3**, *trans*-3-octene, linker **5** (1:1:0.5), 3 h; D) reactants: **3**, linker **5**, (ratio 1:1) 15 min. Acetonitrile was removed under reduced pressure prior to analysis.

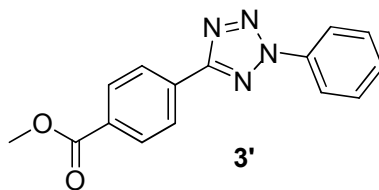


**Figure 5.2.** Chemical structure of the diaryl tetrazole precursor **3'** of the nitrile imine intermediate employed in the DFT calculation of the HOMO energy level of the 1,3-dipole for the discussion of the selectivity of the cycloadditions toward various olefins.

functionalized NBRs and to allow a selective coupling of the tetrazole-functionalized NBRs with the small molecular linker **5**. In the present study, thus a tetrazole was chosen exhibiting a cyclization reactivity sufficiently low to not proceed with the double bonds of the NBR backbone, yet sufficiently high to proceed to high conversion within a reasonable timeframe when adding maleimide linker **5**.

Orthogonality of the nitrile imine to the double bonds of the polymer backbone was proven experimentally in a  $^1\text{H}$  NMR model investigation depicted in Figure 5.1. Solutions of tetrazole **3** in acetonitrile were irradiated with UV light at  $\lambda_{\text{max}} = 254$  nm in the presence of 1-octene or *trans*-3-octene, chosen as model compounds mimicking the pendant and internal double bonds of the polymer backbone, respectively. While after irradiation in the presence of either *trans*-3-octene (Figure 5.1B) or 1-octene (not shown) the absence of aromatic resonances of the diaryl tetrazole protons at 8.4 ppm indicates a quantitative release of nitrogen, formation of the respective pyrazoline compounds is not observed and deactivation of the nitrile imine occurs via alternative pathways. In contrast, irradiation of **3** in the presence of maleimide quantitatively gives the pyrazoline adduct, as characterized by multiplets at 5.2 and 4.9 ppm (Figure 5.1D). When irradiating **3** in the presence of both, *trans*-3-octene and maleimide, sole formation of the maleimide cycloadduct was observed (Figure 5.1C). In 1,3-dipolar cycladdition reactions of type I (according to Sustmann's classification<sup>39</sup>) the reaction rate of the cycloaddition reaction increases with a decrease in the free-energy gap between the highest occupied molecular orbital (HOMO) of the enophile and the lowest unoccupied molecular orbital (LUMO) of the dipolarophile.<sup>40</sup> Lin and coworkers were able to exploit the interrelation of the

reaction rate and the free-energy gap by lifting the HOMO energy levels of the intermediate diaryl nitrile imines to reduce reaction times by tuning the aryl substitution pattern.<sup>29</sup> In analogy, the selectivity of the 1,3-dipolar cycloaddition toward maleimide observed in the present work can be explained by the molecular orbital (MO) energy levels of the reactants. The LUMO energy levels of 1-octene, *trans*-3-octene and maleimide were accessed by DFT calculations and are reported in Table 5.1, entry 2-4. When comparing the LUMO energy levels of the olefins with the HOMO energy level of the nitrile imine intermediate of diaryl tetrazole **3'** (Table 5.1, entry 1; for chemical structure see Figure 5.2), the free-energy gap between the MOs of the dipole and the dipolarophile increases in the order of maleimide < 1-octene < *trans*-3-octene, in line with the high reactivity observed for maleimide.<sup>§§</sup> To keep computational costs low, the HOMO energy level of the nitrile imine intermediate of tetrazole **3'** instead of **3** is used for discussion, since due to the distance of the trithiocarbonate and the ester moiety to the diaryl tetrazole moiety in compound **3** the dissimilar substitution pattern will not have a pronounced effect on the energy levels obtained. The difference of the HOMO energy level of the nitrile imine intermediate of tetrazole **3'** obtained in the current study and the energy level earlier reported by Wang *et al.*,<sup>29</sup> is a result of the

**Table 5.1.** Molecular orbital energies of the 1,3-dipole and the dipolarophile model compounds.<sup>a</sup>

entry	compound	$E_{\text{HOMO}}$ (eV)	$E_{\text{LUMO}}$ (eV)
1 <sup>b</sup>	<b>3'</b>	-5.249	-
2	maleimide	-	-2.996
3	1-octene	-	0.659
4	<i>trans</i> -3-octene	-	0.727
5	acetonitrile	-	0.947

<sup>a</sup> Energies of the molecular orbitals are obtained via DFT calculations (B3LYP/6-31G//B3LYP/6-31G) and are given as zero-point corrected values. <sup>b</sup> The HOMO energy level of the nitrile imine intermediate of tetrazole **3'** is reported. The chemical structure of **3'** is provided in Figure 5.2.

<sup>§§</sup> DFT calculations were performed by Dr. Lebohang Hlalele, Karlsruhe Institute of Technology, Institut für Technische Chemie und Polymerchemie.

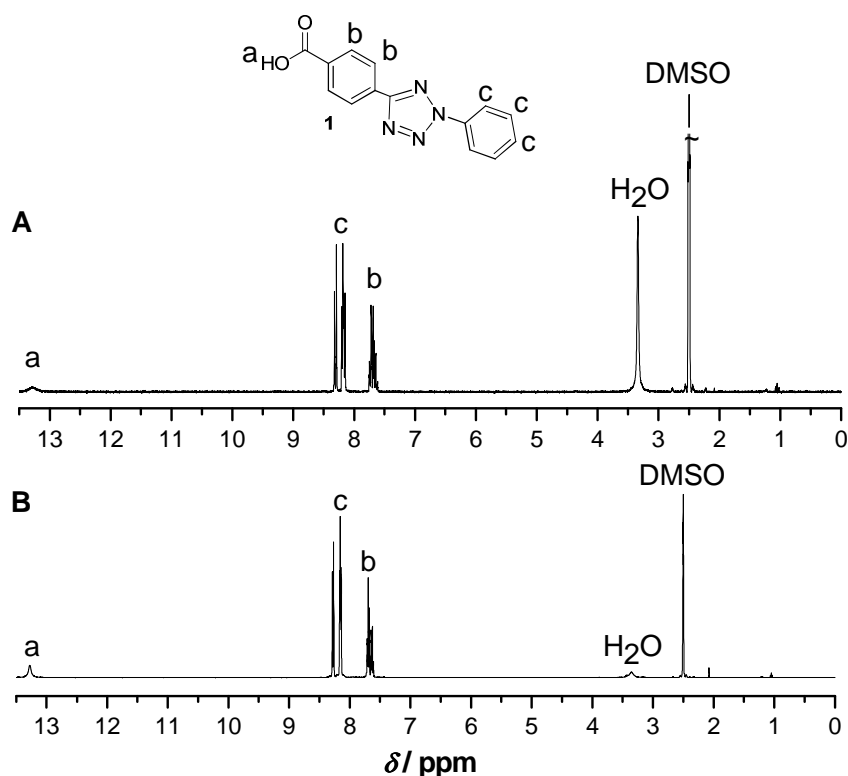


**Figure 5.3.** Investigation of the temperature stability of tetrazole **1**:  $^1\text{H}$  NMR spectra in  $\text{DMSO-d}_6$  A) before and B) after heating **1** to 100 °C for a period of 8 h.

difference in the model chemistries used (HF/3-21G//AM1 vs. B3LYP/6-31G//B3LYP/6-31G). The LUMO energy level of the nitrile moiety – a potential “ene” present in both the solvent and the NBR backbone – is positioned above the one of 1-octene. Nevertheless, light-induced coupling of tetrazole-functional polymers with acetonitrile was observed, when a plain solution of tetrazole-functional polymer was irradiated with UV (see Figure 5.15 and Figure 5.16 in the *Appendix* at the end of the present chapter) and can be explained with the high excess of solvent molecules relative to the polymer.

A high density of the chain-end functionality of polymers is a prerequisite for effective orthogonal ligation reactions on polymers. When orthogonal to the polymerization process, the utilization of functionalized controlling agents in RAFT polymerization allows for the synthesis of chain-end functionalized polymers with a high functional density without the need for postpolymerization modifications.<sup>41</sup> Due to a low propagation rate coefficient,<sup>42</sup> the solution-based reversible-deactivation radical copolymerization of AN and BD requires elevated

temperatures to obtain moderate conversions. The thermal stability of **3** in solution was proven by comparison of the  $^1\text{H}$  NMR spectra before and after heating the diaryl tetrazole at 100 °C for 8 h in DMSO- $d_6$  (Figure 5.3), allowing for the direct synthesis of tetrazole-functional polymers via the RAFT technique. The trithiocarbonate **3** was thus investigated toward its ability to control the free radical copolymerization of AN and BD. Polymerizations were performed at 100 °C in the absence of light. The obtained polymers **4a-f** range from oligomeric species to polymers with molar masses of up to 38 000  $\text{g}\cdot\text{mol}^{-1}$ , while dispersities below 1.5 were observed. A slightly higher dispersity of 1.6 is observed for NBR **4f** of much higher molecular weight. Experimental details for each individual polymerization are provided in Table 5.2. Molecular weights in the current study are reported as actual molar masses obtained from SEC via universal calibration employing the Mark-Houwink-Kuhn-Sakurada (MHKS) parameters of NBR, determined in context of the thesis at hand (see chapter 6). When comparing the molar masses obtained in the present chapter with those obtained under identical polymerization conditions reported in chapter 3 and 4 a decrease by a factor of

**Table 5.2.** Experimental details of RAFT mediated copolymerizations of AN/BD.<sup>a</sup>

entry	RAFT agent	[RAFT] <sub>0</sub> (mM)	[Ini] <sub>0</sub> (mM)	<i>t</i> (h)	<i>p</i> <sup>b</sup> (%)		<i>M</i> <sub>n</sub> ( $\text{g}\cdot\text{mol}^{-1}$ ) <sup>c</sup>	<i>D</i> <sup>c</sup>
1 <sup>d</sup>	<b>3</b>	91.1	5.5	3	37.2	<b>4a</b>	700 <sup>f</sup>	1.2
2 <sup>e</sup>	<b>3</b>	27.9	1.7	5.5	18.5	<b>4b</b>	1800	1.2
3	<b>3</b>	21.0	2.6	5	18.0	<b>4c</b>	3100	1.3
4	<b>3</b>	8.4	1.0	7	12.0	<b>4d</b>	4700	1.4
5	<b>3</b>	3.5	0.3	8	10.8	<b>4e</b>	9400	1.5
6	<b>3</b>	0.8	0.2	22	8.9	<b>4f</b>	38 000	1.6

<sup>a</sup> Conditions: NBR was synthesized with an overall monomer concentration of 9.5  $\text{mol}\cdot\text{L}^{-1}$  in chlorobenzene at 100 °C employing 1,1'-azobis(cyclohexane-1-carbonitrile) as a thermal initiator and polymers were recovered by precipitation in ethanol, except otherwise stated. <sup>b</sup> Conversion was determined gravimetrically. <sup>c</sup> Obtained from SEC via universal calibration employing the MHKS parameters of NBR. <sup>d</sup> Polymerization was performed in acetone; polymer was recovered by solvent evaporation. <sup>e</sup> Polymer was recovered by precipitation of polymer in cold hexane/Et<sub>2</sub>O. <sup>f</sup> As a result of the low molecular weight, a strong deviation of the molar mass obtained via universal calibration from the effective molar mass is observed. ESI-MS of polymer **4a** shows signals with the highest intensities at around 1100 Da.

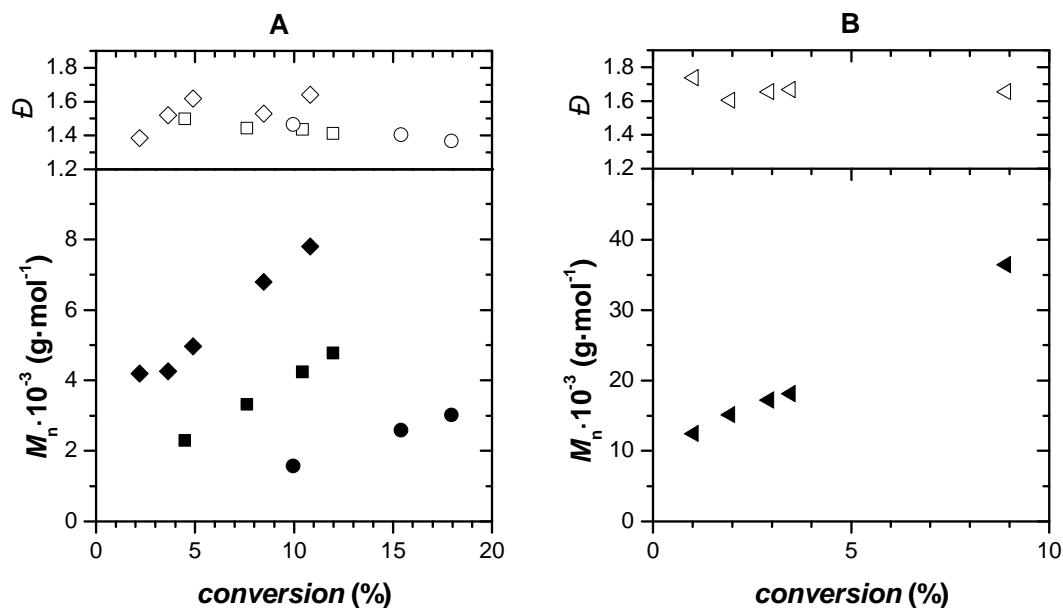


**Figure 5.4.** Evolution of molar mass and dispersity with conversion for a selection of RAFT mediated copolymerizations of AN and BD in their azeotropic ratio of 38/62 ( $[M]_0$  9.5 M). Polymerizations were performed in chlorobenzene at 100 °C, employing the tetrazole-functional controlling agent **3** and 1,1'-azobis(cyclohexane-1-carbonitrile) as the initiator. Conditions: A) rhombs:  $[3]_0$  3.5 mM,  $[Ini]_0$  0.3 mM (Table 5.2, entry 5); boxes:  $[3]_0$  8.4 mM,  $[Ini]_0$  1.0 mM (Table 5.2, entry 4); circles:  $[3]_0$  21.0 mM,  $[Ini]_0$  2.6 mM (Table 5.2, entry 3); B) triangles:  $[3]_0$  0.8 mM,  $[Ini]_0$  0.2 mM (Table 5.2, entry 6).

two in the values is observed. The decrease is a result of the higher  $K$  value of NBR relative to PS ( $49.5 \times 10^{-5} \text{ dL}\cdot\text{g}^{-1}$  vs  $14.1 \times 10^{-5} \text{ dL}\cdot\text{g}^{-1}$ ), since the  $\alpha$  values are almost identical for NBR and PS (0.689 vs. 0.70).<sup>43</sup>

In the copolymerizations employing the photoreactive trithiocarbonate **3**, a linear relation of molar mass with conversion is observed as depicted in Figure 5.4, indicating living characteristics. The deviation from the linear behavior at the early polymerization stages is due to a hybrid effect as previously described.<sup>44</sup> The high end-group functionality of the obtained polymers **4** was proven by SEC-ESI mass spectrometry analysis. A magnified view into the region of 700 to 1400 Da of the low molecular weight NBR **4a** is provided in Figure 5.5. The main signals are assigned to the sodium adducts  $[4_{m+n}Na]^+$  of the tetrazole-functional RAFT polymer, indicating formation of tetrazole-functionalized chains. Nevertheless, a small fraction of NBR **7** free of tetrazole functionality and unable to undergo further ligation is observed. These species are formed by the recombination of two propagating copolymer chains that were both initiated by the azo initiator

fragment and are an inevitable side product of the RAFT process.<sup>45</sup> The observed signal pattern (see inset, Figure 5.5) is a result of the masses of the BD and AN repeat units differing in 1 Da only. Each individual signal can be assigned to the superposition of the isotope pattern of polymer chains with a similar degree of polymerization,  $DP = m+n$ , yet different ratios of the AN to BD contents,  $m/n$ . <sup>1</sup>H NMR analysis of the tetrazole-functionalized NBR **4b** is provided in Figure 5.6A and further confirms the formation of functionalized chains. The multiplet resonances between 8.4 and 7.4 ppm are assigned to the aromatic diaryl tetrazole chain-end protons a-e of the polymer. Moreover, the signals of the methylene protons in  $\alpha$ -position to the ester moieties of the propyl linkage, f-g, are located at 4.4 and 4.2 ppm, respectively. Resonances at 0.9, 1.2 and 3.3 ppm indicate the presence of the Z-group dodecyl mercaptane chain-end as described in more detail for tetrazole-functional NBR **4a** in Figure 5.17 in the *Appendix*. Identical chain-end resonances are observed when analyzing polymers of higher molecular weight.

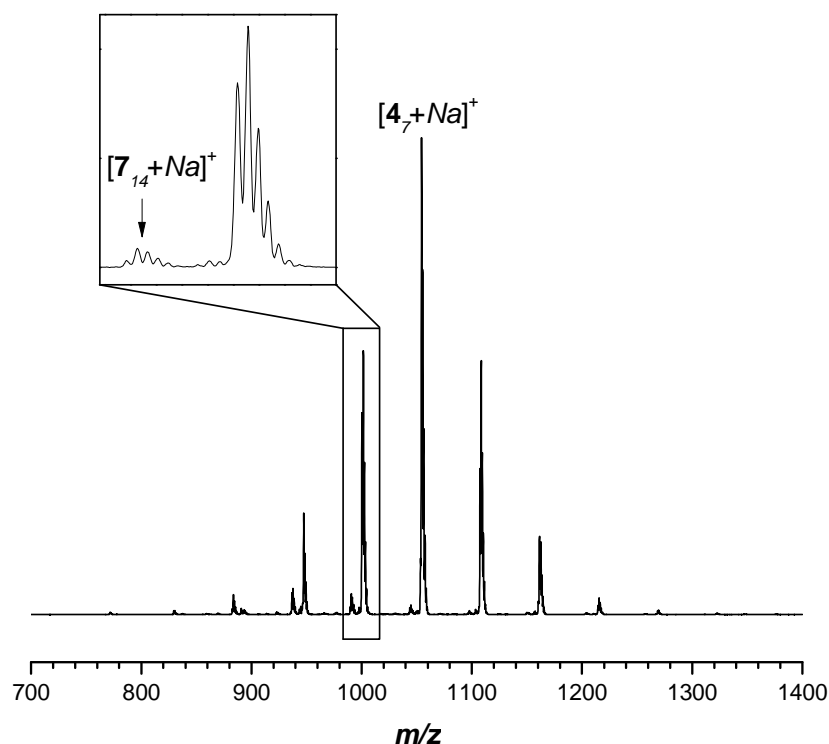


**Figure 5.5.** Magnified view into the region of 700 to 1400 Da of a SEC-ESI mass spectrum of the tetrazole-functionalized NBR **4a**. Polymer **7** is formed by recombination of two growing copolymer chains that were both initiated by the azo initiator fragment and is an inevitable side product of the RAFT process.

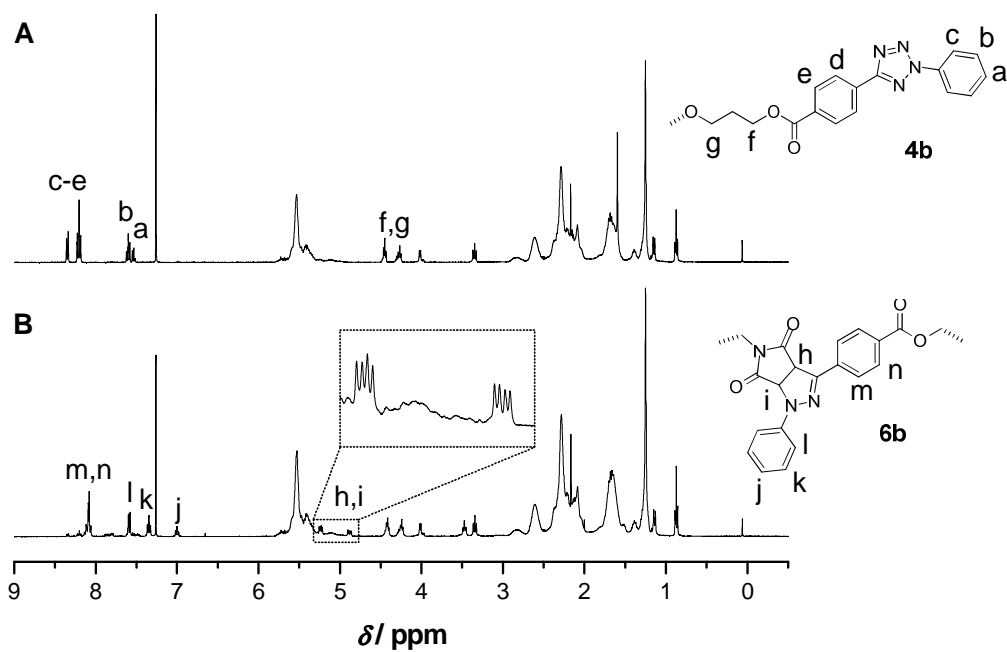


**Figure 5.6.**  $^1\text{H}$  NMR characterization of A) tetrazole-functionalized NBR **4b** of  $1800\text{ g}\cdot\text{mol}^{-1}$  and B) coupled NBR **6b** of  $3200\text{ g}\cdot\text{mol}^{-1}$ , both measured in  $\text{CDCl}_3$ .

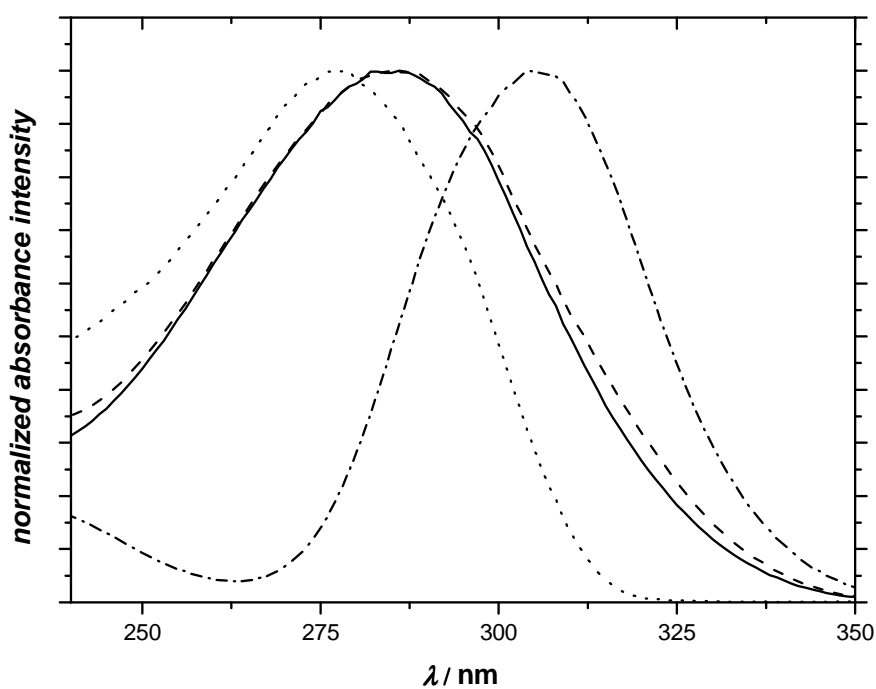


**Figure 5.7.** UV absorption spectra of tetrazole-functional controlling agent **3** (solid line), tetrazole-functional RAFT NBR **4a** (dashed line), trithiocarbonate **8** (dash-dotted line) and tetrazole **9** (dotted line).

In previous studies on photo-induced tetrazole-ene coupling, irradiation of tetrazoles to induce nitrogen release was performed at wavelengths ranging from 254 to 365 nm.<sup>20-23,25-32</sup> To choose an appropriate irradiation wavelength for the experiments, a UV absorption spectrum of the tetrazole-functional controlling agent **3** was recorded. As depicted in Figure 5.7, the UV absorption spectrum of RAFT agent **3** (solid line) features a broad absorption band exhibiting its maximum absorption at 286 nm and is similar to the UV absorption spectrum of tetrazole-functional NBR, exemplarily provided for NBR **4a** (dashed line). Nevertheless, the absorption of **3** (and **4**) is the result of the superposition of the absorption profiles of both, the tetrazole-functional R-group and the trithiocarbonate chain-end. Contributions of the two individual components were investigated with model compounds possessing either the trithiocarbonate or the diaryl tetrazole feature. The latter is represented by 3-hydroxypropyl 4-(2-phenyl-2H-tetrazol-5-yl)benzoate (**9**, see Figure 5.8), obtained from tetrazole **2** by esterification with an excess of 1,3-propanediol, and exhibits an absorption maximum of 275 nm (dotted line). The esterified compound was used instead of **2** to preclude a batho- or hypsochrome influence of the carboxylate on the light absorption properties of the chromophore. Absorption of the trithiocarbonate is represented by ethyl 2-(((dodecylthio)carbonothioyl)thio)propanoate (**8**, see Figure 5.8). The compound possesses a propanoate ester moiety and a dodecyl chain in vicinity to the trithiocarbonate – identical to the direct environment of the trithiocarbonate of controlling agent **3** – and shows its maximum absorption at 305 nm assigned to the  $\pi$ - $\pi^*$  transition of the trithiocarbonate (dash-dotted line). The polymerization via

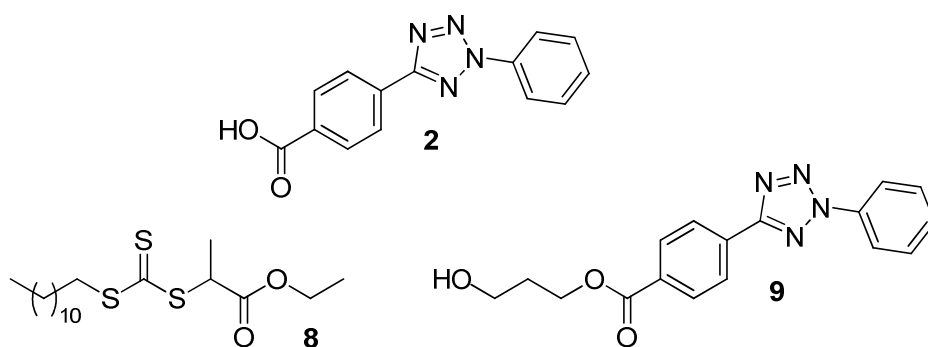


**Figure 5.8.** Model compounds employed in the determination of the UV absorption properties of the tetrazole-functionalized controlling agent **3**.

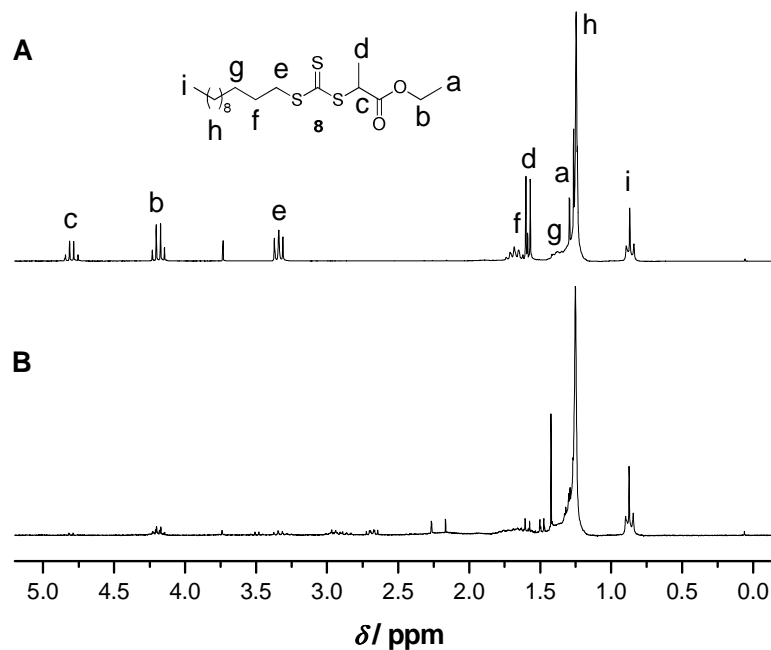


**Figure 5.9.**  $^1\text{H}$  NMR spectra ( $\text{CDCl}_3$ ) of alkyl-functional RAFT agent **8** A) before and B) after irradiation with UV light of 254 nm for 3 h, evidencing the decomposition of the trithiocarbonate under UV irradiation.

the RAFT process leads to an alteration of the direct environment of the trithiocarbonate, since the incorporation of monomers occurs in between the sulfur and the tertiary propanoate carbon after homolytic dissociation of the C-S single bond. Skrabania *et al.* reported a strong influence of the substitution patterns on the  $\pi$ - $\pi^*$  and  $n$ - $\pi^*$  transition of trithiocarbonates.<sup>46-47</sup> Nevertheless, since **3** and **4a** do not show a significant disparity in their absorption, insights obtained from the trithiocarbonate **8** can be used to describe the absorption of the tetrazole-functionalized polymers **4a-f**. Supported by these results, in the work described in the present chapter nitrogen release from the tetrazoles to allow for the ligation of the nitrile rubbers is triggered by irradiation with a UV source of  $\lambda_{\text{max}} = 254$  nm to facilitate the absorption of the tetrazole while minimizing the interference with the trithiocarbonate.

The behavior of trithiocarbonate RAFT agents under UV irradiation has been subject to intensive investigations. Driven by the search for UV initiated controlled polymerization strategies the radical decomposition pathways of trithiocarbonates have been elucidated.<sup>48-50</sup> In line with these experiments, the irradiation of trithiocarbonate **8** with UV light of 254 nm leads to a complete decomposition

within 3 h. As depicted in Figure 5.9, the decomposition is evidenced in  $^1\text{H}$  NMR spectroscopy by the loss of the propanoate methin and methyl proton resonances c and d at 4.8 and 1.6 ppm, respectively. Nevertheless, the UV induced coupling of the pure controlling agent **3** upon addition of 0.5 eq. of **5** quantitatively gave the respective pyrazoline **10** within 15 min without observing any decomposition of the trithiocarbonate. Formation of **10** is evidenced via  $^1\text{H}$  NMR spectroscopy provided in Figure 5.10 by the formation of multiplets of the methin protons d and e in  $\alpha$ -position to the imide carbonyls, resonating at 5.2 and 4.9 ppm. The conjugation further induces a shifting of the aromatic resonances a-c and f in comparison to those of tetrazole **3**. Moreover, resonances of the propanoate protons k and j in vicinity to the trithiocarbonate indicate that coupling is complete before decomposition of the trithiocarbonate occurs. However, prolonged irradiation is resulting in photobleaching of **10**. A magnified view into the  $^1\text{H}$  NMR spectra after irradiation of **3** in the presence of linker **5** for 15, 60 and 180 min is provided in Figure 5.11. While pure **10** is obtained after 15 and 60 min of irradiation, several aromatic signals are observed after 180 min of irradiation and indicate a decomposition of the pyrazoline coupling moiety.

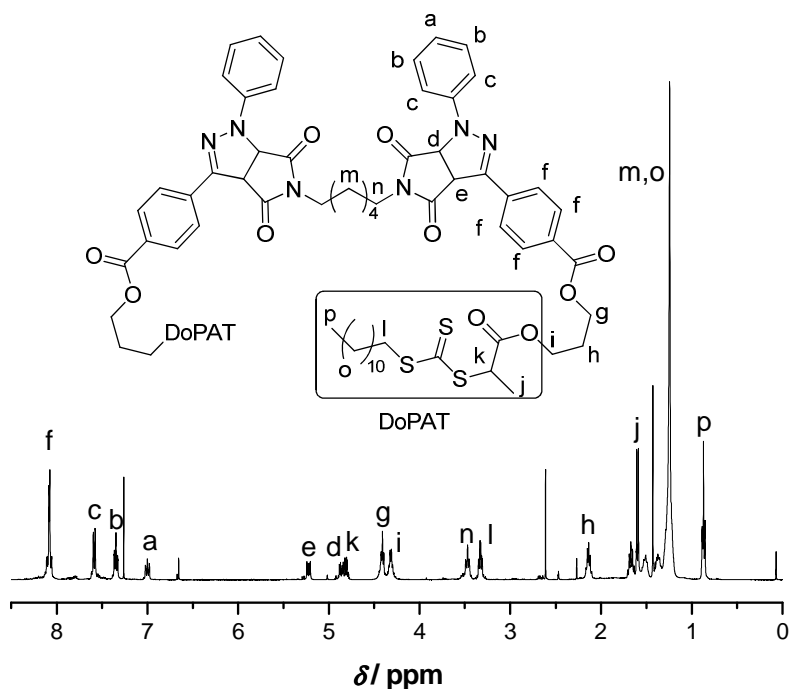


**Figure 5.10.**  $^1\text{H}$  NMR characterization ( $\text{CDCl}_3$ ) of compound **10** obtained in the NITEC reaction of tetrazole-functional controlling agent **3** with 0.5 equivalents of bis(maleimido)hexane (**5**) upon irradiation with UV light of 254 nm for 15 min.

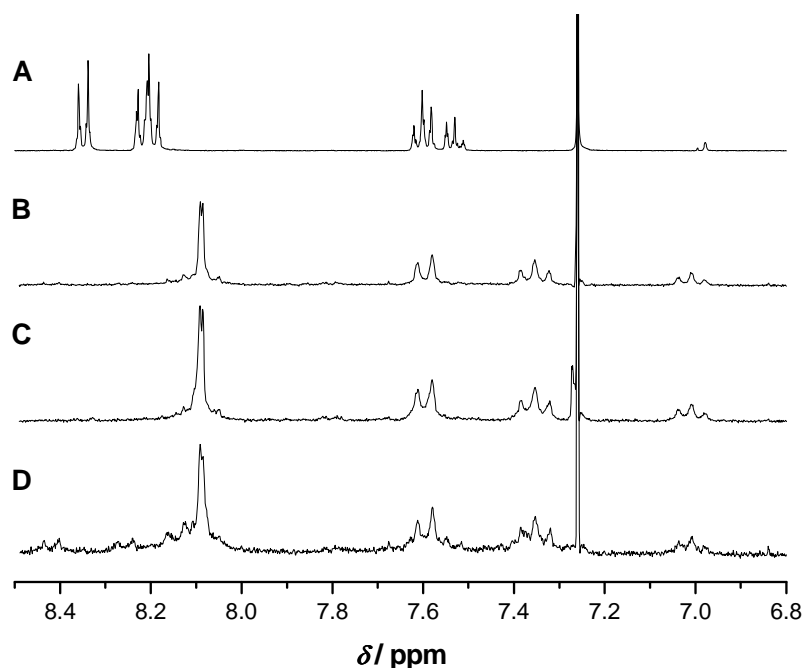


**Figure 5.11.** Magnified view into the region of 8.5-6.8 ppm of the  $^1\text{H}$  NMR spectra ( $\text{CDCl}_3$ ) following the NITEC reaction of tetrazole-functional RAFT agent **3** with 0.5 equivalents of linker **5**: A) before and B) after 15 min, C) after 60 min and D) after 180 min of irradiation with UV light of 254 nm.

In analogy to the UV induced coupling of tetrazole-functional controlling agent **3** giving the model compound **10**, NBRs **4** were subjected to UV irradiation in the presence of 0.5 equivalents of linker **5**. In contrast to the small molecule couplings described above, a prolonged irradiation time of 180 min was necessary to obtain the coupled polymers. The necessity of prolonged reaction time is hypothesized to be caused by a deceleration of the cyclization step of the *in situ* formed nitrile imine and the maleimide. Cyclization of the polymeric nitrile imine with the maleimide is diffusion controlled and determines reaction rates, since polymer unfolding and the convergence of the nitrile imine and the maleimide functionality is a prerequisite for the cyclization. In contrast, the UV-induced nitrogen release does not require the vicinity of the reactants and therefore may not exhibit a dependency on the dimension of the reactants.

The SEC traces of the tetrazole-functionalized NBR precursors before and after the UV induced ligation are depicted in Figure 5.12. Traces of the coupled NBRs **6** (solid lines) exhibit a distinct shift to lower retention time and thus higher molecular weight when compared to those of the respective tetrazole-

functionalized NBRs **4** (dashed lines). The SEC traces of the coupling of NBR **4b** is provided in Figure 5.12A. The peak retention time shifts from 23.8 to 22.8 min and accounts for an increase of the molar mass from 1800 g·mol<sup>-1</sup> to 3200 g·mol<sup>-1</sup> (for details see Table 5.3, entry 1). The discrepancy of the theoretically expected molar mass  $M_{n,exp}(\mathbf{6b})$  of 3900 g·mol<sup>-1</sup> (calculated from the sum of  $2 \times M_n(\mathbf{4b}) + M(\mathbf{5})$ ) and the experimentally observed molar mass can in part be explained with the commonly observed inaccuracy of molar masses in the low molecular weight region when calculated via universal calibration.<sup>51</sup> Nevertheless, the monomodal distribution of **6b** exhibits a slight tailing on the low molecular weight side. The tailing is a result of the presence of the nonfunctionalized polymer chains **7** unable to undergo conjugation.

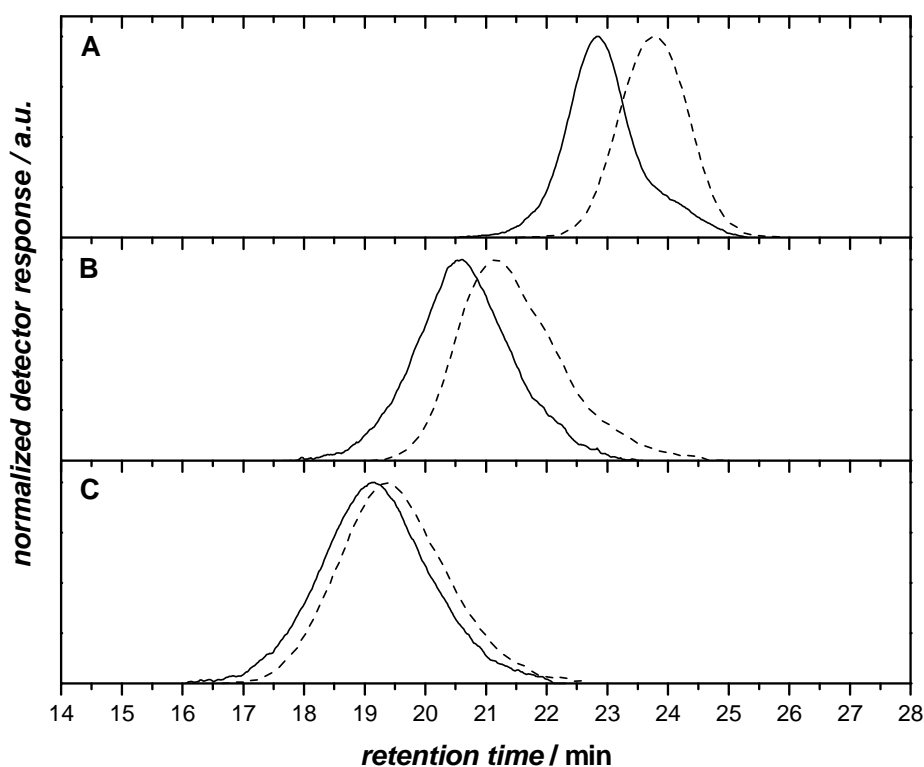


**Figure 5.12.** SEC traces of NBR coupling via the NITEC approach. SEC traces of coupled NBRs **6** are represented by solid lines, traces of tetrazole-functional polymers **4** are depicted as dashed lines. A) Coupling of NBR **4b** of 1800 g·mol<sup>-1</sup> giving NBR **6b** of 3200 g·mol<sup>-1</sup>, B) coupling of NBR **4e** of 9400 g·mol<sup>-1</sup> giving NBR **6e** of 17 000 g·mol<sup>-1</sup> and C) coupling of NBR **4f** of 38 000 g·mol<sup>-1</sup> giving NBR **6f** of 48 000 g·mol<sup>-1</sup>. SEC data was evaluated employing the MHKS parameters of NBR.

**Table 5.3.** SEC data of the light-induced coupling of NBR building blocks **4** in the presence of 0.5 equivalents of **5**.<sup>a</sup>

entry	tetrazole-functional NBR <b>4</b>			coupling product <b>6</b>		
		$M_n$ (g·mol <sup>-1</sup> ) <sup>b</sup>	$\mathcal{D}^b$		$M_n$ (g·mol <sup>-1</sup> ) <sup>b</sup>	$\mathcal{D}^b$
1	<b>4b</b>	1800	1.2	<b>6b</b>	3200	1.3
2	<b>4e</b>	9400	1.5	<b>6e</b>	17 000	1.5
3	<b>4f</b>	38 000	1.6	<b>6f</b>	48 000	1.7

<sup>a</sup> Conditions: Irradiation with UV-light of 254 nm for 3 h in acetonitrile. <sup>b</sup> Obtained from SEC via universal calibration employing the MHKS parameters of NBR.

Coupling of NBR **4e** of 9400 g·mol<sup>-1</sup>, depicted in Figure 5.12B provides NBR **6e** of 17 000 g·mol<sup>-1</sup> (Table 5.3, entry 2). Irradiation of NBR **4f** in the presence of **5** yields coupled NBR **6f** of 48 000 g·mol<sup>-1</sup> (Figure 5.12C), exhibiting a dispersity of 1.6 (Table 5.3, entry 3). In analogy to the coupling of **4b** and **4e**, here a decrease in dispersity is not observed during conjugation. Since polymer coupling is a convolution procedure, in an ideal ligation reaction a doubling of molar mass along with a decrease in dispersity is expected.<sup>52</sup> However, simulations of RAFT mediated copolymerizations of AN and BD theoretically confirmed the formation of up to 7 weight-% of nonfunctionalized polymers during polymerization, as it was shown in chapter 4. These polymer species do not possess the targeted RAFT R-group functionality and lead to molar masses of the coupled polymers below the theoretically expected values, even in cases where a full conversion of the functional chain-ends occurs. As a consequence, a broadening of the molecular weight distributions is observed when nonfunctionalized polymer species are present in polymer-polymer coupling reactions.

Since the NITEC is a pro-fluorescent reaction, fluorescence spectroscopy allows the investigation of the polymer coupling reactions. A UV-vis absorption spectrum of the fluorescent model compound **10** is provided in Figure 5.13 as a dashed-dotted line and reveals the presence of three local absorption maxima around 250 nm (I), 300 nm (II) and 380 nm (III). The fluorescence emission spectra of **10** exhibit increasing relative fluorescence intensities (FI) at excitation wavelengths  $\lambda_{\text{exc}}$  of 250 nm (dotted line), 300 nm (dashed line) and 384 nm (solid line) in the order of II < I < III and allow the assignment of the absorption maxima I and III to

the fluorescent chromophore. Absorption at 300 nm is caused by the trithiocarbonate moiety yet the occurrence of fluorescence most probably arises from the spectral overlap with absorption bands I and III. The feature at 500 nm observed in the emission spectrum at a  $\lambda_{\text{exc}}$  of 250 nm is a result of higher order transmissions.<sup>53</sup> Fluorescence emission spectra of the coupled NBRs **6** (not shown) exhibit features identical to **10**, proving the diaryl pyrazolines to be the moiety responsible for polymer-polymer coupling. The coincidence of the absorption wavelength of the fluorescent chromophore moiety with the wavelength employed for inducing the tetrazole-ene coupling of NBR building blocks, allows an *in situ* tracking of the cyclization progress with common fluorescence spectrometer equipment. Figure 5.14A shows the evolution of fluorescence emission of a 28  $\mu\text{M}$  solution of polymer **4d** in acetonitrile in the presence of 0.5 eq of the maleimide linker **5** over the first 70 min of the reaction, excited with a  $\lambda_{\text{exc}}$  of 254 nm. A steady increase of the FI is observed, yet the increase slows down with the progress of the reaction. A plot of the FI of the emission spectra at an emission wavelength  $\lambda_{\text{em}}$  of

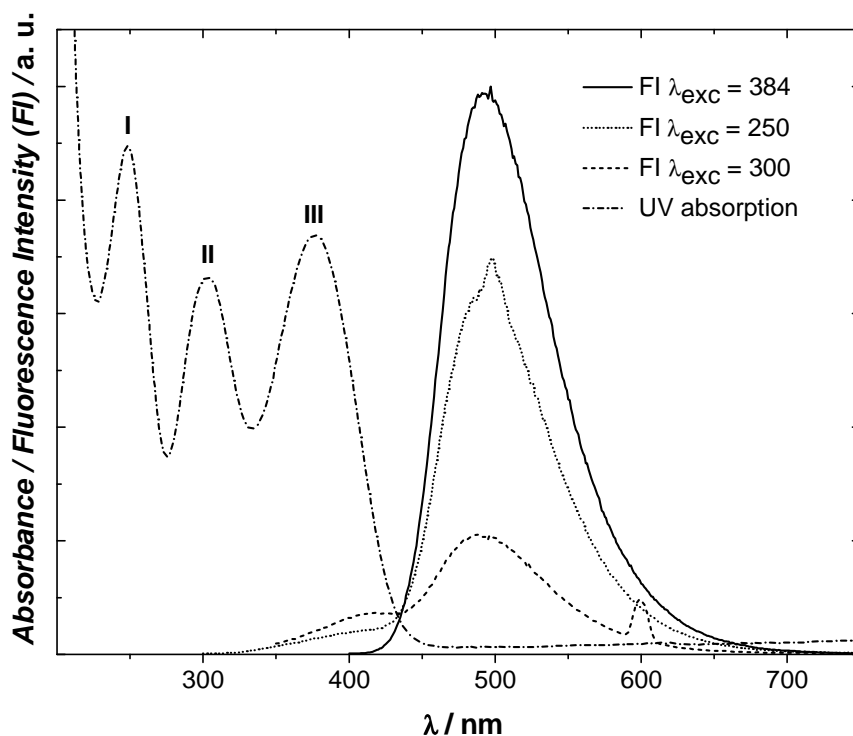


**Figure 5.13.** Illustration of the UV absorption spectrum (dash-dotted line) and the fluorescence emission spectra at  $\lambda_{\text{exc}}$  of 254 nm (dotted line), 300 nm (dashed line) and 384 nm (solid line) of the model compound **10** coupled via NITEC.

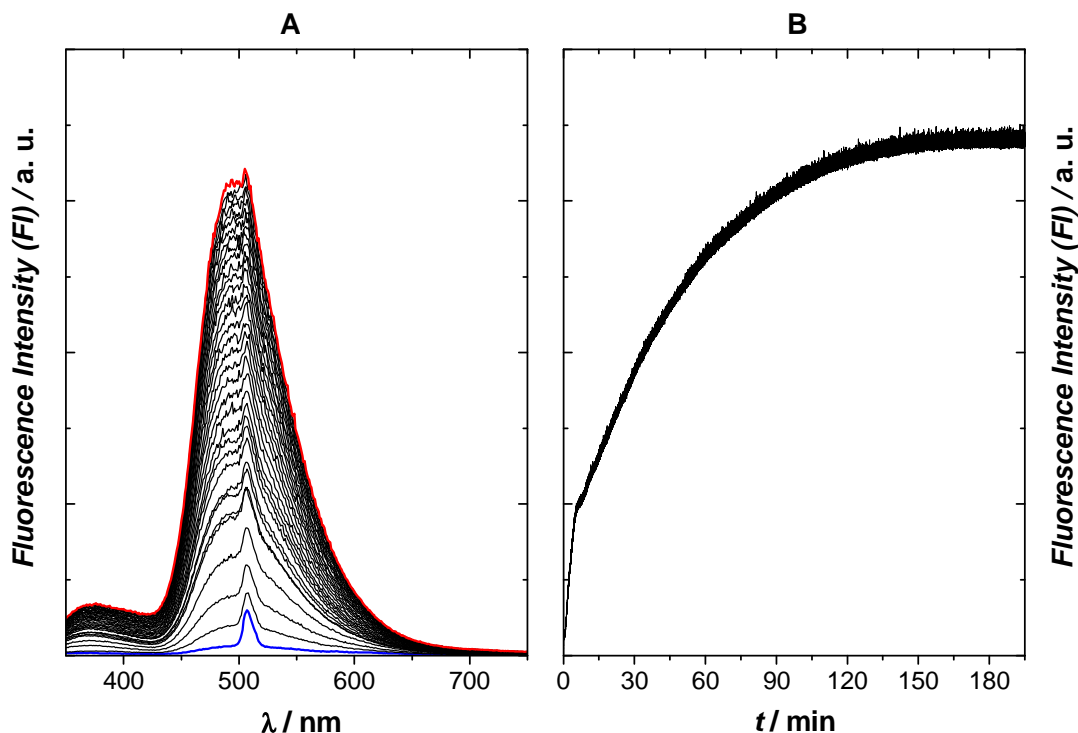


**Figure 5.14.** A) Fluorescence emission spectra at  $\lambda_{\text{exc}}$  of 254 nm of tetrazole-functional polymer **4d** in the presence of 0.5 eq of linker **5** measured at various irradiation times between the mixing of the starting materials (blue line) and 70 min of irradiation (red line). B) Evolution of the FI with irradiation time at an emission wavelength  $\lambda_{\text{em}}$  of 497 nm and an excitation wavelength  $\lambda_{\text{exc}}$  of 254 nm.

497 nm versus time, provided in Figure 5.14B, illustrates the plateauing of the FI at approximately 150 min of irradiation. The time dependent tracking of the reaction progress clearly evidences the necessity to perform the irradiation of polymeric tetrazoles on a longer timescale than required for small molecular analogs.

$^1\text{H}$  NMR spectroscopy of coupled polymer **6b** is provided exemplarily in Figure 5.6B (see page 161) and exhibits resonances of the pyrazoline methin protons h and i in  $\alpha$ -position to the carbonyls of the imide, resonating at 5.2 and 4.9 ppm and in part overlapping with resonances of the NBR backbone olefins (see inset). In analogy to the small molecule studies, transformation of the diaryl tetrazole **4b** into the pyrazoline structure of **6b** induces a shift of the protons of the aryl substituents from 8.3, 8.2, 7.6 and 7.5 ppm (observed in the spectrum of the tetrazole-functional polymer **4b**, Figure 5.6, page 161, signals a-e) to 8.1, 7.6, 7.3 and 7.0 ppm (Fig. 1B, signals j-n). Full conversion of the tetrazole-functional chain-ends is evidenced by the absence of the resonances a-e in the spectrum of the

coupled NBR **6b**. The small resonances in the aromatic region are traced back to bleaching effects as described for the conjugation model reaction of tetrazole-functional controlling agent **3** (*vide supra*). The measurements confirm that the ligation of the tetrazole-functional NBRs exclusively occurs with the reactive maleimide linker, without attacking olefins of the polymer backbone.

## 5.4 Conclusion

In conclusion, the nitrile imine mediated tetrazole-ene coupling was demonstrated to be a fast and efficient method for the coupling of industrially relevant NBR building blocks to obtain nitrile rubber of high molecular weight. The method provided is an extraordinarily pure example of NBR conjugation since it is free of catalysts, additives or chemical stimuli and purification or a postpolymerization transformation of the preformed polymer building blocks is not required prior to ligation. An appropriate choice of the dipolarophile linker and the nitrile imine precursor allowed the NITEC reaction to selectively proceed with the olefin linker. A reaction of the *in situ* formed enophile with the double bonds or the nitrile moieties of the incorporated monomer units within the polymer backbone – present in high excess relative to the dipolarophile linker molecule – was not observed. Underpinned by DFT calculations, the selectivity was explained by the reduced LUMO energy level of the maleimide linker compared to the nonactivated backbone olefins when employing a nitrile imine of moderate reactivity. An in-depth analysis of the coupled polymers revealed the maleimide derived fluorescent pyrazoline to be the element responsible for polymer-polymer coupling. The presented method is not limited to the coupling of linear NBR chains. By alteration of the architecture of the maleimide, block and star polymers and polymer brushes can be accessed. Moreover, the modification of surfaces with maleimide might allow the immobilization of NBR on solid substrates opening up a wide field of technical applications.

## 5.5 Appendix

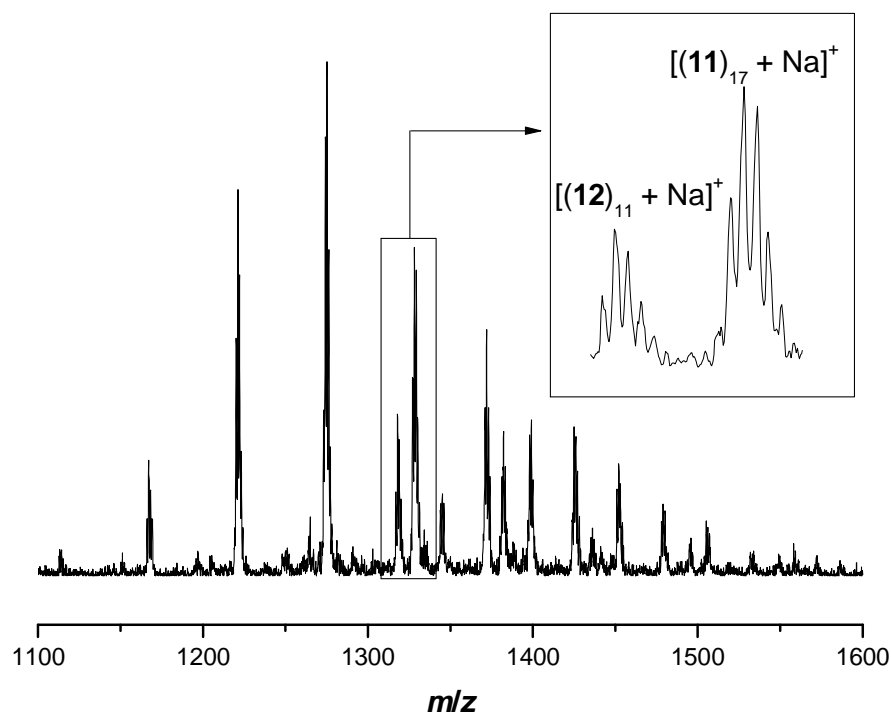


**Figure 5.15.** Magnified view into the region of 1100-1600 Da of the SEC-ESI mass spectrum of a polymer sample obtained after irradiation of a plain solution of tetrazole-functional NBR **4a** in acetonitrile with UV light of 254 nm for 3 h. For simplification of SEC-ESI-MS analysis, the UV labile trithiocarbonate chain-end was removed with 1,1'-azobis-(cyclohexane-1-carbonitrile) (0.34 mmol per gram of **4a**) in the presence of 1-ethylpiperidine hypophosphite (7.2 mmol per gram of **4a**) in toluene (35 mL per gram of **4a**) at 100 °C for 8 h prior to the irradiation, in analogy to a procedure described previously.<sup>54</sup> For signal assignments of structures **11** and **12** refer to Figure 5.16.

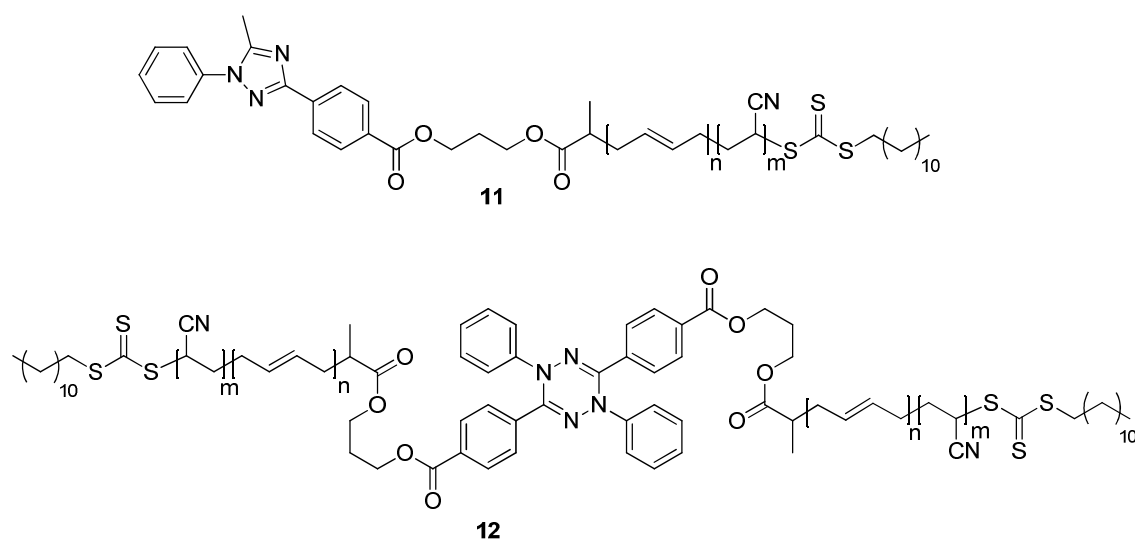


**Figure 5.16.** Structures of the side products formed during the irradiation of a plain solution of tetrazole-functional NBR **4a** with UV light of 254 nm for 3 h in acetonitrile. The side products were observed in ESI-MS when the UV labile trithiocarbonate was removed prior to irradiation. For simplification, the side products are depicted with the trithiocarbonate chain-end structures. The cycloadduct **11** is formed via the reaction of the nitrile moiety of acetonitrile with the nitrile imine of the NBR formed *in situ* from the tetrazole-functional NBRs via UV irradiation. The cycloadduct **12** is formed via the reaction of the nitrile imine moieties of two polymer chains.

**Table 5.4.** Experimental details for the light-induced coupling of NBR building blocks **4** in the presence of 0.5 equivalents of **5**.<sup>a</sup>

entry	coupling of	$m(\mathbf{4})$ (mg)	$V_{\text{total}}$ (ml) <sup>b</sup>
1	<b>4b</b>	40	6
2	<b>4e</b>	40	6
3	<b>4f</b>	120	6

<sup>a</sup> Conditions: Irradiation with UV-light of 254 nm for 3 h in acetonitrile. <sup>b</sup>  $V_{\text{total}}$  is the total reaction volume of the coupling experiments.

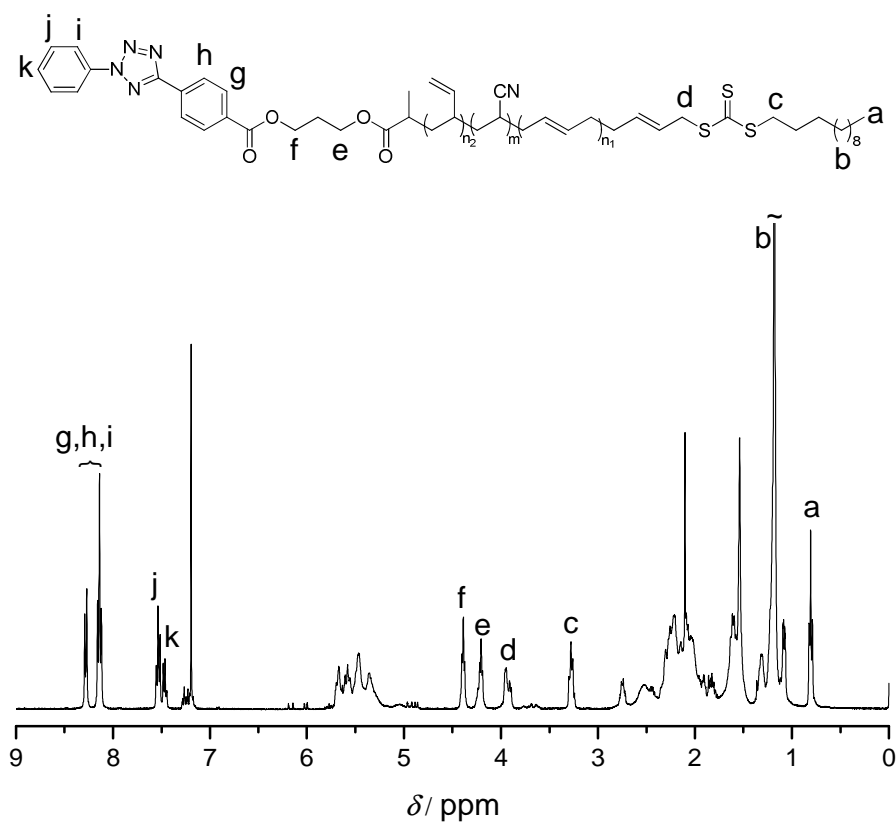


**Figure 5.17.** <sup>1</sup>H NMR characterization of the chain-end proton resonances of the tetrazole-functionalized NBR **4a**.

## 5.6 References

1. Becer, C. R.; Hoogenboom, R.; Schubert, U. S. *Angew. Chem. Int. Ed.* **2009**, *48*, 4900-4908.
2. Iha, R. K.; Wooley, K. L.; Nyström, A. M.; Burke, D. J.; Kade, M. J.; Hawker, C. *J. Chem. Rev.* **2009**, *109*, 5620-5686.
3. Barner-Kowollik, C.; Du Prez, F. E.; Espeel, P.; Hawker, C. J.; Junkers, T.; Schlaad, H.; Van Camp, W. *Angew. Chem. Int. Ed.* **2011**, *50*, 60-62.
4. Hawker, C. J.; Wooley, K. L. *Science* **2005**, *309*, 1200-1205.
5. Kolb, H. C.; Finn, M. G.; Sharpless, K. B. *Angew. Chem. Int. Ed.* **2001**, *40*, 2004-2021.
6. Yamada, Y. M. A.; Sarkar, S. M.; Uozumi, Y. *J. Am. Chem. Soc.* **2012**, *134*, 9285-9290.
7. Boren, B. C.; Narayan, S.; Rasmussen, L. K.; Zhang, L.; Zhao, H.; Lin, Z.; Jia, G.; Fokin, V. V. *J. Am. Chem. Soc.* **2008**, *130*, 8923-8930.
8. Agard, N. J.; Prescher, J. A.; Bertozzi, C. R. *J. Am. Chem. Soc.* **2004**, *126*, 15046-15047.
9. Tasdelen, M. A. *Polym. Chem.* **2011**, *2*, 2133-2145.
10. Gody, G.; Rossner, C.; Moraes, J.; Vana, P.; Maschmeyer, T.; Perrier, S. *J. Am. Chem. Soc.* **2012**, *134*, 12596-12603.
11. He, Y.; He, W.; Liu, D.; Gu, T.; Wei, R.; Wang, X. *Polym. Chem.* **2013**, *4*, 402-406.
12. Heredia, K. L.; Tolstyka, Z. P.; Maynard, H. D. *Macromolecules* **2007**, *40*, 4772-4779.
13. Blackman, M. L.; Royzen, M.; Fox, J. M. *J. Am. Chem. Soc.* **2008**, *130*, 13518-13519.
14. Singh, I.; Zarafshani, Z.; Lutz, J.-F. o.; Heaney, F. *Macromolecules* **2009**, *42*, 5411-5413.
15. Pauloehrl, T.; Delaittre, G.; Bruns, M.; Meißler, M.; Börner, H. G.; Bastmeyer, M.; Barner-Kowollik, C. *Angew. Chem. Int. Ed.* **2012**, *51*, 9181-9184.
16. Delaittre, G.; Pauloehrl, T.; Bastmeyer, M.; Barner-Kowollik, C. *Macromolecules* **2012**, *45*, 1792-1802.

17. Pauloehrl, T.; Delaittre, G.; Winkler, V.; Welle, A.; Bruns, M.; Börner, H. G.; Greiner, A. M.; Bastmeyer, M.; Barner-Kowollik, C. *Angew. Chem. Int. Ed.* **2012**, *51*, 1071-1074.
18. Pauloehrl, T.; Delaittre, G.; Bastmeyer, M.; Barner-Kowollik, C. *Polym. Chem.* **2012**, *3*, 1740-1749.
19. Poloukhtine, A. A.; Mbua, N. E.; Wolfert, M. A.; Boons, G.-J.; Popik, V. V. *J. Am. Chem. Soc.* **2009**, *131*, 15769-15776.
20. Song, W.; Wang, Y.; Qu, J.; Madden, M. M.; Lin, Q. *Angew. Chem. Int. Ed.* **2008**, *47*, 2832-2835.
21. Wang, Y.; Rivera Vera, C. I.; Lin, Q. *Org. Lett.* **2007**, *9*, 4155-4158.
22. Wang, Y.; Hu, W. J.; Song, W.; Lim, R. K. V.; Lin, Q. *Org. Lett.* **2008**, *10*, 3725-3728.
23. Yu, Z.; Ho, L. Y.; Wang, Z.; Lin, Q. *Bioorg. Med. Chem. Lett.* **2011**, *21*, 5033-5036.
24. Clovis, J. S.; Eckell, A.; Huisgen, R.; Sustmann, R. *Chem. Ber.* **1967**, *100*, 60-70.
25. Madden, M. M.; Rivera Vera, C. I.; Song, W.; Lin, Q. *Chem. Commun.* **2009**, 5588-5590.
26. Song, W.; Wang, Y.; Yu, Z.; Rivera Vera, C. I.; Qu, J.; Lin, Q. *ACS Chem. Biol.* **2010**, *5*, 875-885.
27. Yu, Z.; Lim, R. K. V.; Lin, Q. *Chem. Eur. J.* **2010**, *16*, 13325-13329.
28. Wang, J.; Zhang, W.; Song, W.; Wang, Y.; Yu, Z.; Li, J.; Wu, M.; Wang, L.; Zang, J.; Lin, Q. *J. Am. Chem. Soc.* **2010**, *132*, 14812-14818.
29. Wang, Y.; Song, W.; Hu, W. J.; Lin, Q. *Angew. Chem. Int. Ed.* **2009**, *48*, 5330-5333.
30. Song, W.; Wang, Y.; Qu, J.; Lin, Q. *J. Am. Chem. Soc.* **2008**, *130*, 9654-9655.
31. de Hoog, H.-P. M.; Nallani, M.; Liedberg, B. *Polym. Chem.* **2012**, *3*, 302-306.
32. Dietrich, M.; Delaittre, G.; Blinco, J. P.; Inglis, A. J.; Bruns, M.; Barner-Kowollik, C. *Adv. Funct. Mater.* **2012**, *22*, 304-312.
33. Kaiser, A.; Brandau, S.; Klimpel, M.; Barner-Kowollik, C. *Macromol. Rapid Commun.* **2010**, *31*, 1616-1621.

34. Dürr, C. J.; Emmerling, S. G. J.; Kaiser, A.; Brandau, S.; Habicht, A. K. T.; Klimpel, M.; Barner-Kowollik, C. *J. Polym. Sci. Part A: Polym. Chem.* **2012**, *50*, 174-180.
35. Nagdi, K. *Gummi-Werkstoffe: ein Ratgeber für Anwender ; Arten - Zusammensetzung - Verarbeitung - Eigenschaften - Beständigkeiten - Anwendungen - Prüfungen - Qualitätskontrolle - Klassifizierung - Chemie.* 3rd ed.; Gupta: Ratingen, 2004; p 431.
36. Dietrich, M.; Glassner, M.; Gruending, T.; Schmid, C.; Falkenhagen, J.; Barner-Kowollik, C. *Polym. Chem.* **2010**, *1*, 634-644.
37. Hertz, D. L.; Bussem, H.; Ray, T. W. *Rubber Chem. Technol.* **1995**, *68*, 540-546.
38. Stille, J. K.; Chen, A. T. *Macromolecules* **1972**, *5*, 377-384.
39. Sustmann, R. *Tetrahedron Lett.* **1971**, *12*, 2717-2720.
40. Houk, K. N.; Sims, J.; Watts, C. R.; Luskus, L. J. *J. Am. Chem. Soc.* **1973**, *95*, 7301-7315.
41. *Handbook of RAFT Polymerization.* Barner-Kowollik, C., Ed.; Wiley-VCH: Weinheim, 2009.
42. Hlalele, L.; Dürr, C. J.; Lederhose, P.; Kaiser, A.; Hüsgen, S.; Brandau, S.; Barner-Kowollik, C. *Macromolecules* **2013**, *46*, 2109-2117.
43. Strazielle, C.; Benoit, H.; Vogl, O. *Eur. Polym. J.* **1978**, *14*, 331-334.
44. Barner-Kowollik, C.; Quinn, J. F.; Nguyen, T. L. U.; Heuts, J. P. A.; Davis, T. P. *Macromolecules* **2001**, *34*, 7849-7857.
45. Moad, G.; Rizzardo, E.; Thang, S. H. *Aust. J. Chem.* **2005**, *58*, 379-410.
46. Skrabania, K. *The multifarious self-assembly of triblock copolymers : from multi-responsive polymers and multi-compartment micelles.* Ph.D. Thesis, University of Podsdam, 2008.
47. Skrabania, K.; Miasnikova, A.; Bivigou-Koumba, A. M.; Zehm, D.; Laschewsky, A. *Polym. Chem.* **2011**, *2*, 2074-2083.
48. Quinn, J. F.; Barner, L.; Barner-Kowollik, C.; Rizzardo, E.; Davis, T. P. *Macromolecules* **2002**, *35*, 7620-7627.
49. Lu, L.; Zhang, H.; Yang, N.; Cai, Y. *Macromolecules* **2006**, *39*, 3770-3776.

50. You, Y.-Z.; Hong, C.-Y.; Bai, R.-K.; Pan, C.-Y.; Wang, J. *Macromol. Chem. Phys.* **2002**, *203*, 477-483.
51. Chance, R. R.; Baniukiewicz, S. P.; Mintz, D.; Strate, G. V.; Hadjichristidis, N. *Int. J. Polym. Anal. Charact.* **1995**, *1*, 3-34.
52. Barner-Kowollik, C. *Macromol. Rapid Commun.* **2009**, *30*, 1625-1631.
53. Lakowicz, J. R. *Principles of fluorescence spectroscopy*. Springer: New York, 2009.
54. Vogt, A. P.; Sumerlin, B. S. *Macromolecules* **2008**, *41*, 7368-7373.



# 6 ■ Determining the Mark–Houwink Parameters of Nitrile Rubber: A Chromatographic Investigation of the NBR Microstructure<sup>\*\*\*</sup>

## 6.1 Introduction

In modern polymer chemistry, size exclusion chromatography (SEC) is the most prominent technique employed to determine the (average) molar mass and dispersity of synthetic polymers and biopolymers. Its widespread application results from it being a simple, rapid and versatile automated method not requiring complex sample preparation. With the appropriate choice of solvent, stationary phase and temperature, virtually all kind of soluble polymers can be separated according to their hydrodynamic volume  $V_h$ .  $V_h$  is defined as the volume of a hypothetical hard sphere exhibiting the same diffusion properties as the polymer coil in solution and is further described via the Stokes-Einstein relation. By calibrating a system with narrowly dispersed standards of known molecular weight, SEC allows accurate molecular weight determination.<sup>1</sup> However, standards and the samples of unknown molar mass need to be the same type of polymer, since separation of the macromolecules occurs based on the hydrodynamic volume and not by molecular weight. With knowledge of the Mark–Houwink–Kuhn–Sakurada (MHKS) parameters,  $K$  and  $\alpha$ , of the standards and the samples under investigation, reliable molecular weights can also be obtained when different types of polymer for calibration and samples are employed. The molecular weights of the

---

<sup>\*\*\*</sup> Dürr, C. J.; Hlalele, L.; Schneider-Baumann, M.; Kaiser, A.; Brandau, S.; Barner-Kowollik, C. *Polym. Chem.* **2013**, *4*, 4755-4767. DOI: 10.1039/C3PY00580A - Reproduced and adapted by permission of the Royal Society of Chemistry.

two polymer types are associated via the universal calibration principle stating that the product of intrinsic viscosity  $[\eta]$  and molecular weight  $M$  is proportional to the hydrodynamic volume.<sup>2-7</sup> In turn, intrinsic viscosity correlates with molecular weight  $M$  via the coefficients  $K$  and  $\alpha$  according to the Mark–Houwink relation,  $[\eta] = K \cdot M^\alpha$ . When SEC is coupled on-line to a viscometer, the MHKS parameters are not required for molecular weight determination via universal calibration.<sup>8-9</sup> Molecular weight determination via on-line viscometry is advantageous since MHKS parameters are solvent and temperature dependent. MHKS parameters are available for a wide variety of synthetic polymers. Nevertheless, several important polymers lack indexing of their MHKS parameters in physicochemical catalogs.

While produced in a volume of several hundred kilotons per year, nitrile-butadiene rubber (nitrile rubber, NBR) molecular weights in industry and academia are determined as polystyrene equivalent values,<sup>10</sup> since no MHKS parameters are reported to date. As highlighted by Guillaneuf *et al.*, knowledge of the actual molecular weight becomes particularly important when the efficiency of control is assessed in controlled polymerization,<sup>11</sup> a process recently introduced for the synthesis of NBR.<sup>12-14</sup>

Determination of true molecular weight and molecular weight distributions by SEC becomes complicated in case when polymers exhibit an inhomogeneous structural distribution. At any given retention time,  $t_{el}$ , SEC fractions of complex branched polymers are polydisperse in molecular weight albeit monodisperse in  $V_h$  – even in the absence of interactions between eluent and stationary phase other than size exclusion effects.<sup>1,15</sup> Molecular weight determination is complicated especially in the case of complex branched polymers, even though the structural homogeneity of SEC fractions has been proven for specific examples of hyperbranched polymers.<sup>16-17</sup> Multiple detection SEC allows an in-depth study of the mechanism of separation of complex polymers with a method first introduced by Gaborieau *et al.*<sup>18</sup> The method relates molecular weights determined by on-line light scattering and on-line viscometry with each other by calculating the local dispersity index as a function of  $t_{el}$  and was applied to the SEC separation of various polymers.<sup>19-22</sup> Nevertheless, for complex branched polymers, true molecular weight distributions remain challenging to obtain.<sup>23</sup>

NBR is a polymer with a high density of functional moieties vulnerable to reactive chemical environments.<sup>24</sup> Particularly the presence of the residual double bonds of the BD monomer in a radical environment provides a platform for a range of side reactions. BD, mainly incorporated in a 1,4-fashion, can be attacked by growing chains or initiator radicals, leading to the formation of branched polymers and – for very high radical concentrations – crosslinked polymer networks. This reactivity toward radical addition is even higher for vinyl double bonds, formed by 1,2-incorporation of BD, which is observed for close to 10% of the monomers.

The work presented in the current chapter aimed at the determination of MHKS parameters of nitrile rubber (prepared at azeotropic conditions). However, the high tendency of these polymers to form branched structures requires particular precautions since MHKS parameters may be valid for polymers of a unique microstructure only.<sup>25</sup> For this reason, an intensive study of the NBR microstructure by chromatographic means is provided. Due to the complexity of the polymers under investigation, topologies are discussed on a semi-quantitative basis. The experiments focus on establishing if the synthesized polymers are uniform in their microstructure. Insights into the polymer microstructure were obtained using triple detection SEC, revealing the presence of reaction condition dependent topologies. However, differences in the microstructure seem to be sufficiently subtle to allow for the determination of a single set of MHKS parameters. To the best of our knowledge, the provided study is the first report of MHKS parameters of NBR.

## 6.2 Experimental Section

### 6.2.1 Materials

Acrylonitrile (AN, > 99%, Acros), 1,3-butadiene (BD, > 99.5%, Air Liquide), 2,2'-azobis(*N*-butyl-2-methylpropionamide) (Wako Ltd.), chlorobenzene (Acros, 99+%) and ethanol (synthesis grade, VWR) were used as received. 2-((dodecylsulfanyl)carbonothioyl)sulfanyl propanoic acid (DoPAT) was obtained from Orica Pty Ltd., Melbourne, Australia. Tertiary dodecyl mercaptanes (TDM) were obtained from Lanxess and used without further purification.

### 6.2.2 Polymerizations

Copolymerizations of AN and BD were performed in chlorobenzene at 100 °C using a pressure stable glass reactor setup described earlier.<sup>12</sup> 2,2'-azobis(*N*-butyl-2-methylpropionamide) with a 10 h half-life decomposition temperature of 110 °C was employed as a thermal initiator. Control over the polymerization was achieved by either using TDM or DoPAT as chain transfer agents. Experimental conditions of the polymerizations performed in the current study are summarized in Table 6.1 (see page 184). Prior to SEC analysis, the polymer samples were purified by repeated precipitation in cold ethanol. Monomer-to-polymer conversion was determined gravimetrically.

### 6.2.3 NMR Measurements

<sup>1</sup>H NMR and <sup>13</sup>C NMR spectra were recorded at room temperature on a Bruker Advance 400 NMR spectrometer and referenced to the remaining solvent signal.<sup>26</sup>

### 6.2.4 Size Exclusion Chromatography and Data Evaluation

Triple-detection size exclusion chromatography to obtain local dispersities and MHKS parameters was performed on a modular system (Polymer Standards Service (PSS)/Agilent 1200 series) comprising a refractive index (RI) detector (PSS/Agilent 1200 series), a light-scattering unit (PSS SLD7000/BI-*M<sub>w</sub>A*, Brookhaven Instruments) and an ETA2010 viscometer (WGE Dr. Bures). Tetrahydrofuran (THF, HPLC grade) was used as the eluent and separation was performed on two linear columns (SDV-Lux-1000 Å and 10<sup>5</sup> Å, 5 μm, both obtained from PSS) at 25 °C with a flow rate of 1 mL·min<sup>-1</sup>. A calibration was established using narrow polystyrene (PS) standards (obtained from PSS) ranging from 160 to 6 × 10<sup>6</sup> g·mol<sup>-1</sup>, light scattering setup was performed with a highly disperse polystyrene sample of 1.25 × 10<sup>6</sup> g·mol<sup>-1</sup> (*M<sub>m</sub>*). The WinGPC software (PSS) was used for recording and evaluating light scattering and viscosity profiles (*i.e.* [η] or *M<sub>LS</sub>* as a function of retention time *t<sub>el</sub>*). Moreover, the WinGPC software was used to account for inter detector delay,<sup>27-29</sup> for the calculation of the overall intrinsic viscosity [η] (determined via on-line viscometry) and to calculate absolute molecular weights *M<sub>LS</sub>* (determined by on-line light scattering). [η], *M<sub>LS</sub>* and SEC

data as polystyrene equivalent values for all samples discussed in the current chapter are provided in Table 6.4 in the *Appendix* at the end of the current chapter. All further data processing was performed using the OriginPro 8.5G software package. To clarify the origin of molecular weights provided in the current chapter, absolute molecular weights obtained via light scattering are termed  $M_{LS}$  although equivalent to weight average molecular weights termed  $M_w$ .<sup>30</sup> Molecular weights obtained from viscometry are termed  $M_v$ . The terms  $M_n$  and  $M_m$  will be solely used for molecular weights obtained from conventional SEC.

On each measuring day the quality of the light scattering setup was tested by injecting a highly disperse polystyrene standard of known molecular weight (PSS). To account for errors resulting from sample injection, elution profiles of each single measurement were referenced to the solvent system peak occurring at 27.21 mL. A reduction of the signal-to-noise ratio in light scattering and viscosity profiles (that is  $M_{LS}$  or  $[\eta]$  vs.  $t_{el}$ ) data was achieved by linearly averaging the raw data – either  $\log([\eta] \cdot \text{g} \cdot \text{mL}^{-1})$  or  $\log(M_{LS} \cdot \text{mol} \cdot \text{g}^{-1})$  – over three consecutive sample injections. Over a broad range of retention time, sufficiently smooth curves for light scattering and intrinsic viscosity profiles versus  $t_{el}$  were obtained. As a consequence of the low sample concentrations in regions of very high molar masses, unreliable data is obtained at low  $t_{el}$  in on-line light scattering and viscometry. In the range of low molar masses (*i.e.* high  $t_{el}$ ) a strong variation of on-line light scattering is observed and is mainly a result of the low scattering intensity of low molecular weight material.

The refractive index increment  $dn/dc$  of NBR with azeotropic monomer incorporation was determined to be  $(126.8 \pm 1.8) \times 10^{-3} \text{ mL} \cdot \text{g}^{-1}$ . A universal calibration curve was established by fitting the logarithmic product of intrinsic viscosity (determined on-line) and the number average molecular weight (as provided by the supplier) of polystyrene standards using a third order polynomial function providing an excellent fit ( $r^2 = 0.999$ ).

Conventional molecular weight determination was performed on a SEC system (PL-GPC 50 Plus, Polymer Laboratories) consisting of an auto injector, a guard column (PLgel Mixed C,  $50 \times 7.5 \text{ mm}$ ), three linear columns (PLgel Mixed C,  $300 \times 7.5 \text{ mm}$ ,  $5 \mu\text{m}$  bead-size) and a differential RI detector using THF as the

eluent at 35 °C and a flow rate of 1 mL·min<sup>-1</sup>. The system was calibrated using a series of polystyrene standards ranging from 160 to 6 × 10<sup>6</sup> g·mol<sup>-1</sup>. Evaluation of data obtained in conventional SEC was performed using the Cirrus Software version 3.2.

### 6.3 Results and Discussion

Multi-angle laser light scattering (MALLS) and viscometry are state-of-the-art methods for the investigation of the molecular dimensions of polymers. While intrinsic viscosity is a direct measure of the volume fraction of the polymer in (dilute) solution, static light scattering provides information on the weight average molecular weight  $M_{LS}$  and the radius of gyration. For polymers, the latter is defined as the root mean square distance of the chain segments from its centre of gravity. Both methods provide valuable information on the polymer microstructure such as branching, as polymer microstructure influences the molecular dimensions by variation of the density of polymers in solution. In principle, branched structures exhibit lower radii of gyration than linear

**Table 6.1.** Experimental conditions of copolymerizations of AN and BD.<sup>a</sup>

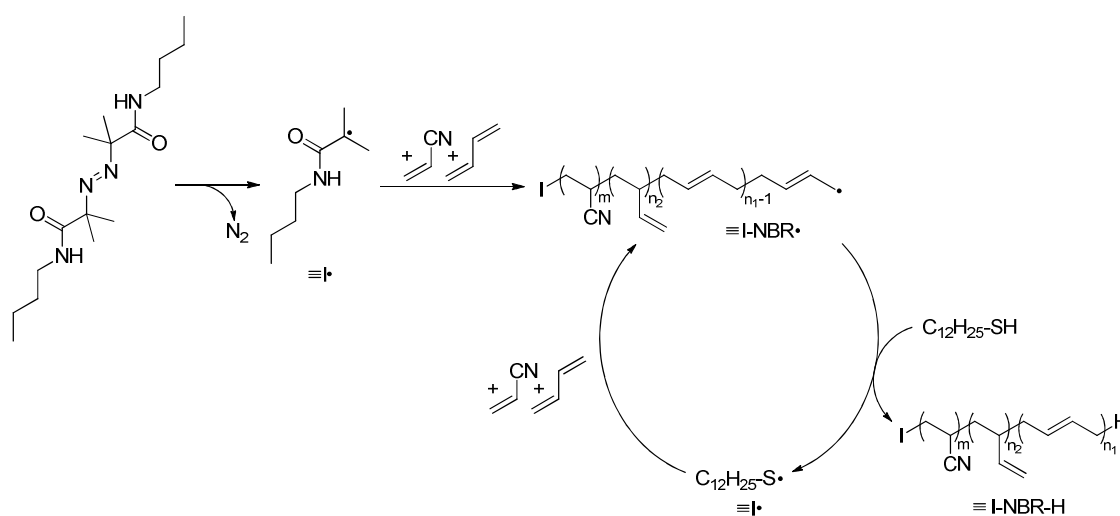
run	type of transfer agent	[T] <sub>0</sub> (mM)	[Ini] <sub>0</sub> (mM)	<i>t</i> (h)
A	conv. <sup>b</sup>	4.1	1.0	22
B	conv. <sup>b</sup>	4.1	2.5	22
C	conv. <sup>b</sup>	4.1	4.5	24
D	conv. <sup>b</sup>	4.1	8.5	24
E	conv. <sup>b</sup>	4.1	17.1	3.33
F	conv. <sup>b</sup>	4.1	34.1	3.66
G	RAFT <sup>c</sup>	0.3	1.0	22
H	RAFT <sup>c</sup>	1.3	8.5	24

<sup>a</sup> All polymerizations were performed in chlorobenzene at 100 °C. AN and BD were employed in the azeotropic ratio (38/62) with an initial overall monomer concentration [M]<sub>0</sub> of 6.75 mol·l<sup>-1</sup>. <sup>b</sup> Tertiary dodecyl mercaptanes were used in the conventional-type polymerizations. <sup>c</sup> RAFT mediated copolymerizations were performed using DoPAT as chain transfer agent.

analogs of similar molecular weight.<sup>31</sup> As it was shown for low-density polyethylene, branched polymers thus exhibit higher molecular weight than linear polymers of similar hydrodynamic volume.<sup>32</sup> In analogy, intrinsic viscosities of branched polymers are lower than those of linear polymers of the same molecular weight.<sup>25</sup>

A setup commonly used for the detailed investigation of molecular dimensions of polymers is triple detection SEC, a setup comprising a viscosity detector, a light scattering unit and a differential refractive index (RI) detector. The latter is required to obtain information on the concentration to allow for the determination of the distributions of data accessed from viscometry and light scattering detectors.<sup>33</sup> The hyphenation of these detectors with separation according to size exclusion mechanisms provides additional information on the relation of intrinsic viscosity and weight average molecular weights with hydrodynamic volume. In an ideal SEC mechanism – that is in absence of band broadening – fractions eluting from the column are monodisperse in hydrodynamic volume.

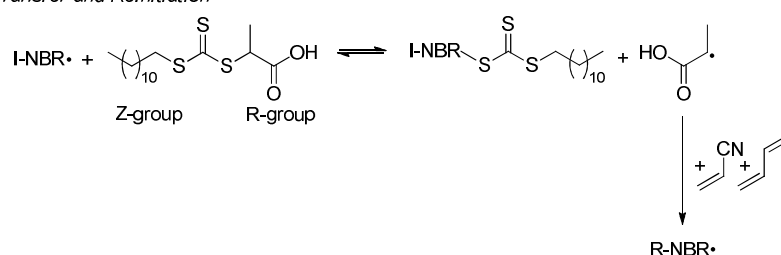
In the herein presented study triple detection SEC was employed to investigate the impact of reaction conditions during polymerization on the NBR microstructure. Since uniformity of polymer microstructure is a prerequisite for the determination of exclusive MHKS parameters, such insights are valuable information regarding the applicability of universal calibration using SEC



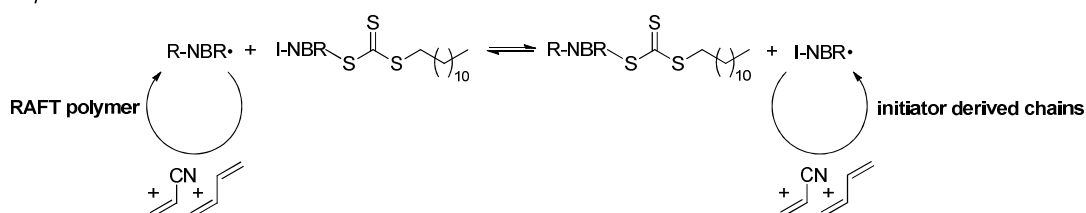
**Scheme 6.1.** Conventionally controlled free radical copolymerization of AN and BD.

instruments without on-line viscometry measurements. NBRs used in the present study were synthesized by radical copolymerization of AN and BD in organic solution. To control the molar masses of the synthetic rubbers, either tertiary dodecyl mercaptanes (TDM, polymerizations A-F, Table 6.1) or a trithiocarbonate (DoPAT, polymerizations G-H, Table 6.1) were used as a chain transfer agent. The mechanisms of the conventionally controlled polymerizations employing TDM and the RAFT mediated copolymerizations employing DoPAT are depicted in Scheme 6.1 and Scheme 6.2, respectively, and have been described elsewhere in more detail.<sup>12,34-37</sup> An azeotropic feed composition of 38 (AN) to 62 (BD) was employed to avoid compositional drifts during the copolymerizations. Such drifts would evoke a chemical-composition distribution complicating SEC evaluations.<sup>38</sup> As the NBR microstructure is most probably influenced by the radical environment, polymerizations with initial concentrations of the azo initiator 2,2'-azobis(*N*-butyl-2-methylpropionamide) in the range of 1.0 to 34.1 mmol·l<sup>-1</sup> were performed. Initial initiator concentrations increase in the order of polymerization runs A<B<C<D<E<F. In all these conventional chain transfer polymerizations using TDM, other reaction conditions such as temperature, monomer and transfer agent concentrations were identical to allow for a comparison of the obtained polymers. Weight average molecular weights  $M_{L,S}$  were in the range of 50 kg·mol<sup>-1</sup> to

*Reversible Chain Transfer and Reinitiation*



*Chain Equilibration*



**Scheme 6.2.** Reversible-deactivation radical copolymerization of AN and BD via the RAFT technique.

100 kg·mol<sup>-1</sup>, as determined by MALLS. During each polymerization run, a series of samples was taken at certain intervals and purified by repeated precipitation in cold ethanol. Evolution of conversion with polymerization time is depicted in Figure 6.1, exhibiting an increase in the slope with increasing initiator concentration. Reversible addition–fragmentation chain transfer (RAFT) mediated polymerizations G and H gave polymer samples with weight average molecular weights in the range of 15 kg·mol<sup>-1</sup> to 70 kg·mol<sup>-1</sup> by an appropriate choice of concentrations of initiator and transfer agent with all other reaction conditions identical to those in conventionally controlled free radical polymerizations A-F (for experimental details see Table 6.1). It is pointed out that – in contrast to the conditions applied in conventional RAFT polymerizations – a high initiator concentration relative to chain transfer agent is employed in reversible-deactivation<sup>39</sup> polymerizations G-H. These conditions will lead to an elevated generation of polymer chains with initiator fragments at either one or both ends of the polymer chain.<sup>40</sup> However, in the current study the key purpose for performing

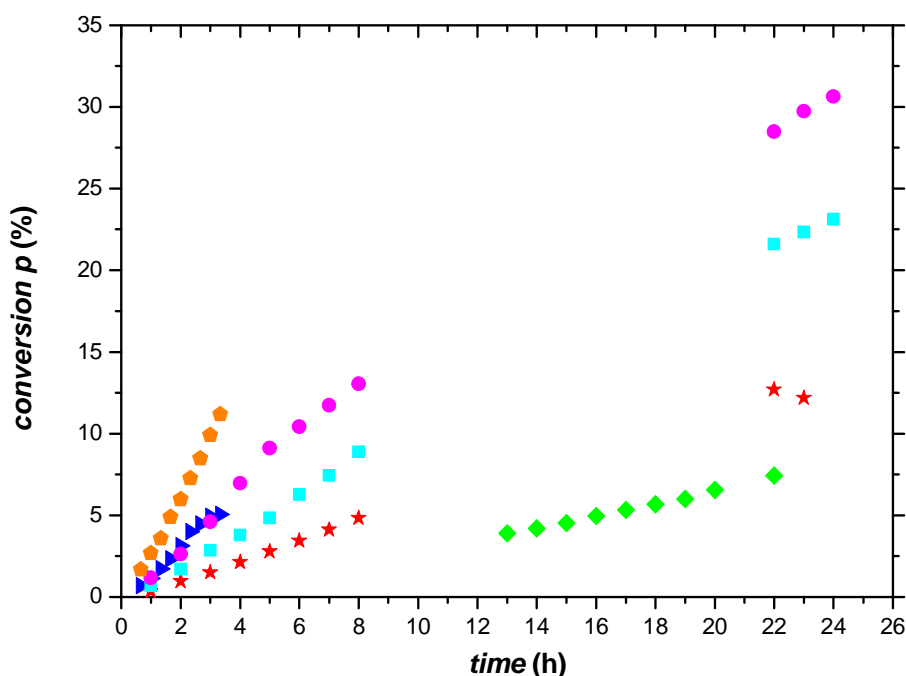


**Figure 6.1.** Evolution of conversion with reaction time for conventionally controlled free radical polymerizations with different initial initiator concentrations  $[Ini]_0$ : 1.0 mM (green, polymerization run A), 2.5 mM (red, run B), 4.5 mM (cyan, run C), 8.5 mM (magenta, run D), 17.1 mM (blue run E), 34.1 (orange, run F). All other reaction conditions are provided in Table 6.1.

RAFT polymerization was to adjust molecular weights of the NBR samples over a broad range. Since for modern SEC column packing materials analyte-stationary phase interaction attributed to effects other than size exclusion can be neglected, the diversity in the chemical nature of the chain-ends will not have an effect on the separation mechanism. Nevertheless, high initiator concentration and low concentration of controlling agent were a prerequisite to obtain conversion and molar masses required to meet the demands of detector sensitivity and sample preparation. Earlier studies evidenced that copolymerizations of AN and BD with initiator-to-RAFT agent ratios above unity can be performed without having a substantial negative effect on the controlled character of the polymerizations.<sup>12-13</sup>

A detailed overview over all samples investigated in the current study is provided in Table 6.4 in the *Appendix* at the end of the current chapter. Each sample was separated three times on the triple SEC instrument to allow for data averaging and to identify outliers arising from instrument related deviations. In the current study, samples will be termed by the polymerization run with subscripts giving the polymerization time (h), *e.g.* A<sub>15</sub> for a sample taken during polymerization run A after 15 h of polymerization.

### 6.3.1 Experimental Determination of the NBR Microstructure

Branching is experienced frequently in free radical polymerization and can occur by radical transfer reactions such as transfer to polymer or backbiting. For polyacrylates, these transfer reactions have been subject of intensive research and the underpinning mechanisms are elucidated to a very significant extent.<sup>41-42</sup> Other approaches to intentionally obtain branched polymers are the addition of bi- or multifunctional monomers or postpolymerization grafting reactions. In analogy to self condensing vinyl polymerization,<sup>43</sup> Vogt *et al.* used acrylate-capped trithiocarbonates to obtain statistically branched poly(*N*-isopropylacrylamide) and were able to vary the degree of branching from 0.045 to 0.16 by adjusting concentrations of trithiocarbonate and monomer.<sup>44</sup> In their study, an increase in the degree of branching was evidenced by a decrease of the slope  $\alpha$  when plotting intrinsic viscosity versus molecular weight as obtained by on-line SEC viscometry in a double logarithmic fashion (*i.e.* the Mark–Houwink plot).

In a similar approach, the individual NBR samples of the current study were investigated with regard to differences in the slope of their Mark–Houwink plots. In Figure 6.2, the double logarithmic plot of the intrinsic viscosity versus the weight average molecular weight  $M_{LS}$  of polymer samples from polymerization runs A-F is provided. For a better legibility, a single sample of each run is provided only. A specific trend in slope or position of the curves cannot be discerned. Nevertheless, the curves exhibit minor variations that might in part arise from differences in topology. Since variations are in the range of the signal-to-noise ratio of the measurements, this data cannot be used to evaluate branching in a qualitative or quantitative way. Note that three consecutive injections of each sample did provide identical Mark–Houwink plots, evidencing the reproducibility of the performed measurements.

Differences in the polymer microstructure referring to the radical concentration are revealed when studying the evolution of  $[\eta]$  and  $M_{LS}$  as a function of  $t_{el}$ . In Figure 6.3 and Figure 6.4, comparative plots of  $[\eta]$  and  $M_{LS}$  with  $t_{el}$  are provided

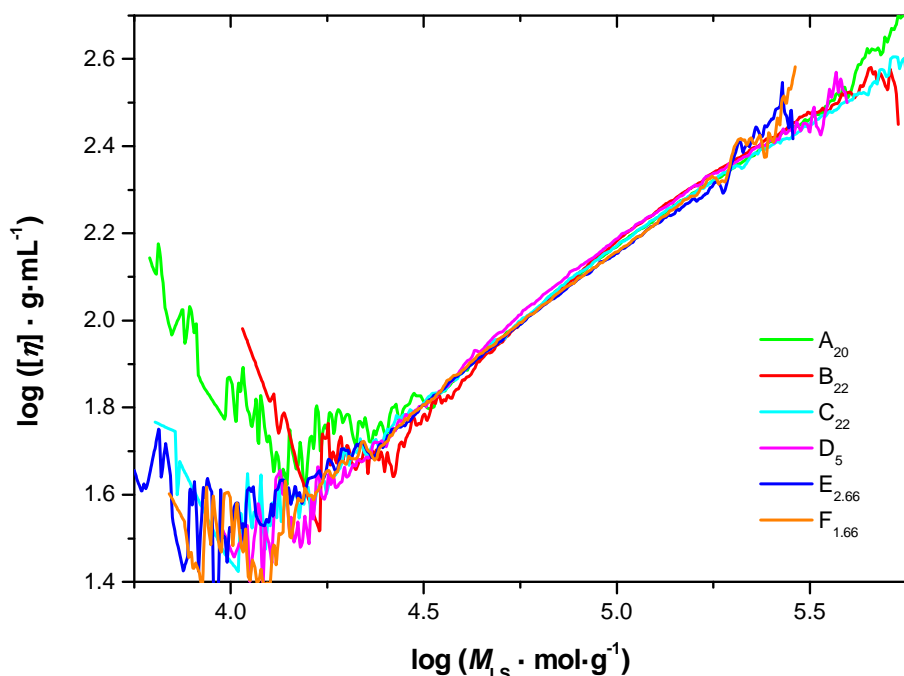


**Figure 6.2.** Double logarithmic plot of the intrinsic viscosity versus molecular weight as obtained by on-line viscometry and on-line light scattering for NBR samples taken from polymerizations A-F. Each line represents a single polymer sample: A<sub>20</sub> (green), B<sub>22</sub> (red), C<sub>22</sub> (cyan), D<sub>5</sub> (magenta), E<sub>2.66</sub> (blue), F<sub>1.66</sub> (orange). Note that curves are independent of the averaged (overall) molecular weight of the polymer sample.

exemplarily for all samples taken during polymerization runs A, performed with a low initial initiator concentration of 1 mM (blue lines), and run E, performed with a high initial initiator concentration of 17.1 mM (red lines). The individual lines represent  $[\eta]$  and  $M_{LS}$  profiles averaged over three consecutive injections of the same sample solution. Samples taken at polymerization times between 15 and 22 h (run A) and 1.33 to 3 h (run E) are plotted in the order of increasing conversion as illustrated by a deepening in color. Samples of these two polymerizations were chosen for discussion, since the strong difference in initiator concentration leads to a pronounced differentiation of the plots. When plotting  $[\eta]$  and  $M_{LS}$  for polymerization runs B-D, the curves are located in between those of polymerization runs A and E.  $[\eta]$  and  $M_{LS}$  data as a function of  $t_{el}$  of polymerization F with the highest initiator concentration of 34.1 mM do not show a pronounced deviation from polymerization run E, however. As in SEC separation occurs

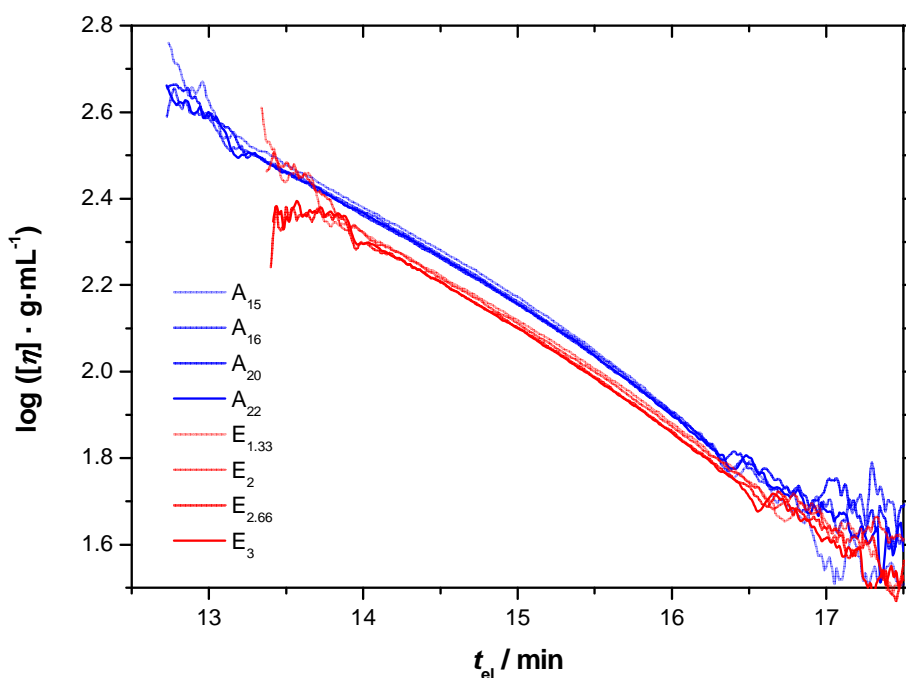


**Figure 6.3.** Logarithmic plot of the intrinsic viscosity as a function of retention time for polymerizations with two different initial initiator concentrations as obtained from on-line viscometry: Run A with a concentration of 1.0 mM (blue lines) and run E with a concentration of 17.1 mM (red lines). Each line represents the evolution of intrinsic viscosity for samples taken at a different polymerization time. Curves are given in the order of increasing conversion as visualized by a deepening in color. Each datapoint provided is an average value over three consecutive injections of the same sample solution.

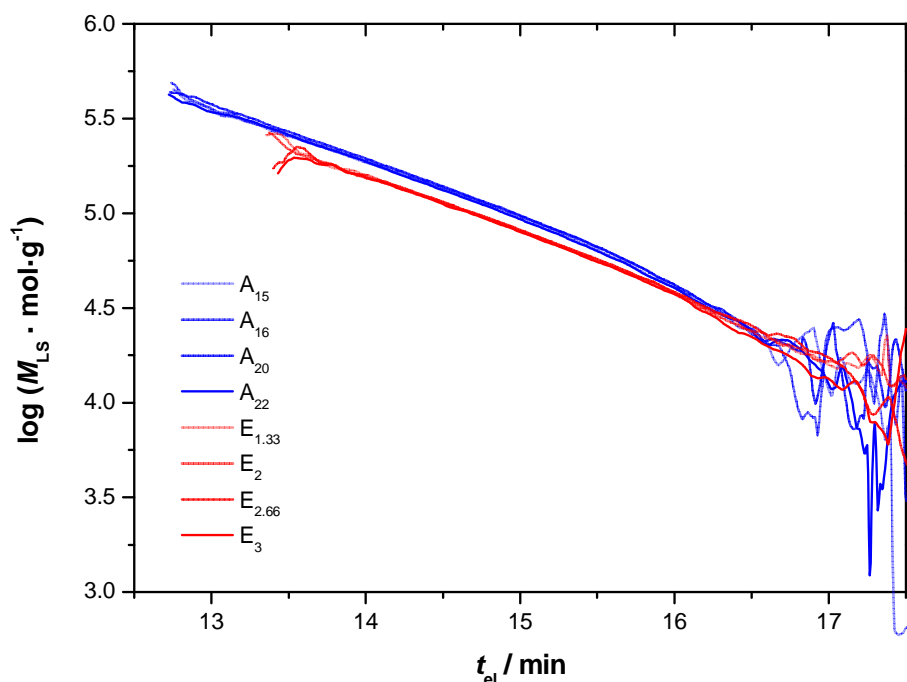


**Figure 6.4.** Logarithmic plot of the weight average molecular weight as a function of retention time for polymerizations with two different initial initiator concentrations as obtained from on-line MALLS: Run A with a concentration of 1.0 mM (blue lines) and run E with a concentration of 17.1 mM (red lines). Each line represents the evolution of intrinsic viscosity for a sample taken at a different polymerization time. Curves are given in the order of increasing conversion as visualized by a deepening in color. The data provided are an average over three consecutive sample injections.

according to size, an increase in retention time is equivalent to a decrease in hydrodynamic volume. The plots therefore provide insights into the interrelation of molecular dimension with weight averaged molecular weight and intrinsic viscosity, respectively. Figure 6.4 explicitly demonstrates that at an identical hydrodynamic volume polymers synthesized at high initial initiator concentrations exhibit a lower  $M_{LS}$  than polymers obtained in polymerizations with low initial initiator concentration. A similar trend is observed when comparing the intrinsic viscosity from both polymerization runs as provided in Figure 6.3. At similar  $t_{el}$ , a high initial concentration of initiator results in a lower intrinsic viscosity of polymer samples than of those polymerized with low  $[Ini]_0$ . In analogy, a lower intrinsic viscosity at similar  $t_{el}$  was observed for polymers obtained after a prolonged polymerization period within each individual polymerization run. Intrinsic viscosity at a particular  $t_{el}$  decreases in the order of  $A_{15} > A_{16} > A_{20} > A_{22}$  and  $E_{1.33} > E_2 > E_{2.66} > E_3$ , respectively. In turn, conversion increases with increasing

polymerization time. When comparing polymer coils of similar hydrodynamic volume,  $[\eta]$  is indirectly proportional to the density of the polymer chains in dilute solution. Keeping this in mind, such a behavior is expected, as earlier studies on poly(vinyl acetate) revealed an increase in the weight average molecular weight with conversion when comparing polymers of similar hydrodynamic volume.<sup>15</sup> Note that the variations in  $[\eta]$  and  $M_{LS}$  between polymerizations A and E cannot originate from the differences in conversion since despite initial initiator concentrations differ by a factor of 17, reaction times were adjusted to achieve similar overall conversion. Nevertheless, the variations in the hydrodynamic volume dependent intrinsic viscosity and molecular weight data evidence that differences in the microstructure of the polymers exist. The differences, however, do not translate into the Mark–Houwink plot (Figure 6.2) since changes in  $[\eta]$  and  $M_{LS}$  compensate each other.

Comparison of the microstructures of polymers obtained under different reaction conditions thus requires the simultaneous evaluation of data obtained from MALLS, viscometry and the information on hydrodynamic volume as given by the elution time. A method combining these three variables to describe structural inhomogeneity is the concept of local dispersity.<sup>45-47</sup> Local dispersity – first described with off-line methods<sup>15</sup> in the 1970s – can be derived from multi-detection SEC as shown by Gaborieau *et al.* for the evaluation of branching degrees of polyacrylates.<sup>18</sup> Local dispersity indices  $\mathcal{D}(t_{el})$  are determined as a function of retention time by the comparison of molecular weights as obtained by on-line viscometry ( $M_v$ ) and light scattering ( $M_{LS}$ ). In the case of complex branched polymers, a mixture of polymer species with a distribution of molecular weights elute at each retention time. The molecular weight from the on-line MALLS detector is obtained as a weight averaged value over all species present in the SEC fraction. Molecular weight  $M_v$ , as obtained via universal calibration from on-line viscometry data is providing number averaged masses at each fraction, as described theoretically by Hamielec and coworkers.<sup>48</sup> In analogy to the macroscopic dispersity, the local dispersity index is calculated by the ratio of weight average and number average molecular weight as a function of retention volume,  $\mathcal{D}(t_{el}) = M_{LS}(t_{el})/M_v(t_{el})$ .

Evaluation of triple SEC data was performed as described in the following. On-line viscometry and MALLS data were averaged over three consecutive injections prior to further processing. In contrast to several other studies of local dispersity indices, no raw data fitting was performed to avoid the interpretation of smooth but inaccurate data. While  $M_{LS}(t_{el})$  was directly obtained from on-line light scattering, transformation of  $[\eta]$  into  $M_v(t_{el})$  via the universal calibration principle was required. Therefore, a universal calibration curve was established with narrowly dispersed polystyrene samples and  $\log(M_v(t_{el}))$  of NBR was obtained by subtraction of  $\log[\eta]$  from the  $\log([\eta]_{PS} \cdot M_{PS})$  at each individual elution time, with  $[\eta]_{PS}$  and  $M_{PS}$  being intrinsic viscosity and weight average molecular weight of the polystyrene samples, respectively. Each of the described steps of data processing is documented for sample B<sub>22</sub> in Figure 6.12 to Figure 6.15 in the *Appendix*.

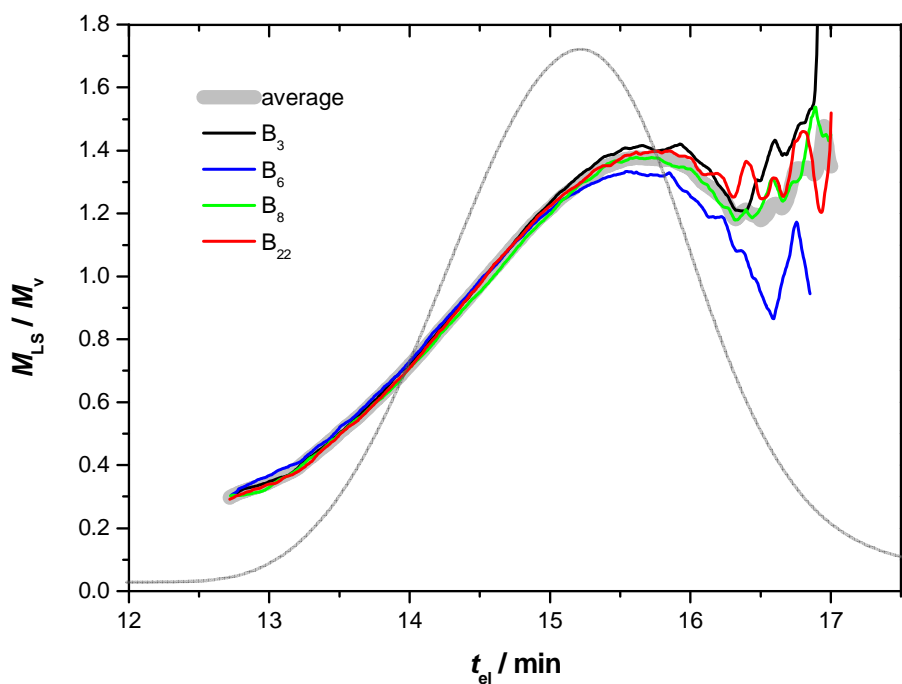


**Figure 6.5.** Plot of the local dispersity  $D(t_{el})$  calculated from on-line MALLS and on-line viscometry SEC. Each line represents the data obtained for a sample taken at different polymerization times during polymerization run B ( $[Ini]_0 = 2.5$  mM): B<sub>3</sub> (black line), B<sub>6</sub> (blue line), B<sub>8</sub> (green line) and B<sub>22</sub> (red line). A curve obtained from averaging over the samples is represented as a grey bold line. The signal of the refractive index detector of sample B<sub>8</sub> is provided exemplarily. Elugrams of samples B<sub>3</sub>, B<sub>6</sub> and B<sub>22</sub> do not show a pronounced difference in shape or position.

A plot of the local dispersity  $\mathcal{D}(t_{el})$  for samples taken during polymerization run B is provided in Figure 6.5.  $\mathcal{D}(t_{el})$  is depicted for samples taken after 3, 6, 8 and 22 h. The individual  $\mathcal{D}(t_{el})$  curves do not show a pronounced variation from the data averaged over local dispersities of the four different samples, represented by a bold gray line. Where present, variations in  $\mathcal{D}(t_{el})$  from the averaged plot are merely observed at high retention times and can be explained by the low sensitivity of the MALLS detector for low molecular weight material. Scattering of the data points is further enhanced by the low concentration of macromolecules in the region of high retention time (RI trace provided exemplarily for sample B<sub>8</sub> in Figure 6.5). The data provides evidence that under the applied polymerization conditions the microstructure of the NBRs does not change during the course of the polymerization B for polymerization times of up to 22 h.

The shape of the  $\mathcal{D}(t_{el})$  curves observed requires some additional explanation. Graphs of all samples exhibit an increase in  $\mathcal{D}(t_{el})$  with increasing  $t_{el}$ . Structural inhomogeneity is evoked by the presence of polymeric species of different molecular weights exhibiting similar hydrodynamic volumes, thus eluting in one

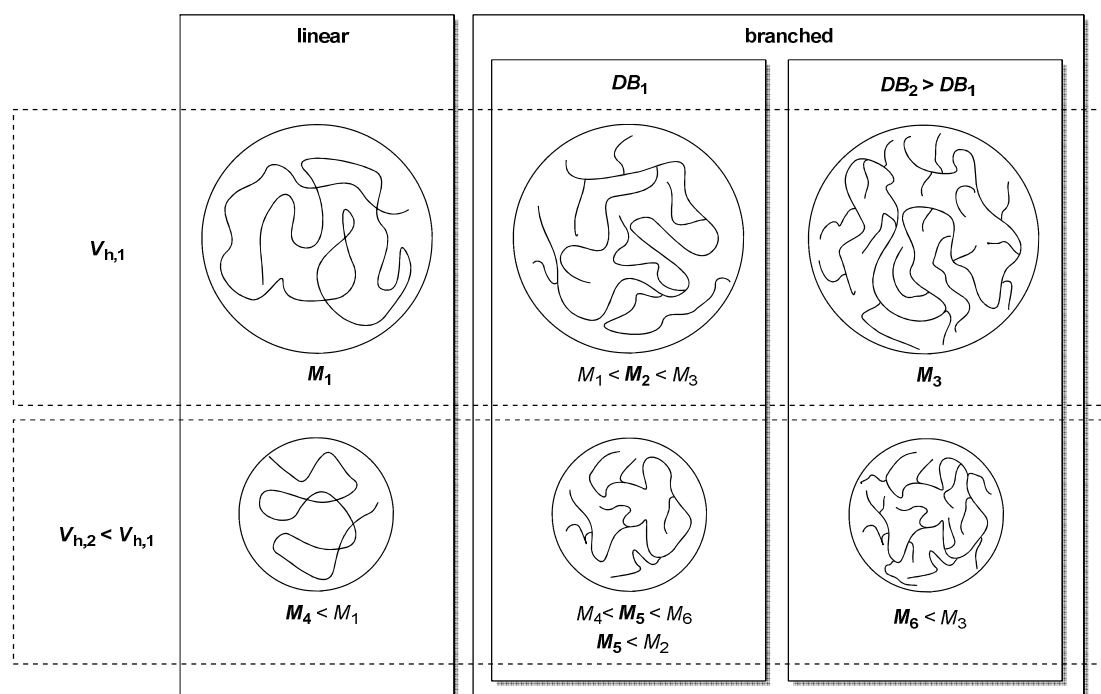


**Figure 6.6.** Illustration of the influence of molecular weight,  $M$ , and the degree of branching,  $DB$ , on the hydrodynamic volume,  $V_h$ .

fraction from the column. The different elution behavior of polymer chains of similar molar mass is a result of the different topologies arising from a variation in the degree of branching, as depicted in Figure 6.6. Molecular weight increases with the degree of branching for polymer coils showing the same hydrodynamic volume. While the hydrodynamic volume decreases with molecular weight for polymer chains of similar topology, polymer chains with a hydrodynamic volume  $V_{h,2}$  can exhibit higher molecular weights than polymers with a hydrodynamic volume  $V_{h,1} > V_{h,2}$ , when polymers of different degrees of branching are compared. For low molecular weight species (eluting at high  $t_{el}$ ) the impact of an increase in the number of branching points per incorporated monomer unit on the hydrodynamic volume is much more pronounced than for high molecular weight species (eluting at low  $t_{el}$ ). For polymer chains of low molecular weight – and thus a low absolute number of branching points per chain – an increase in the number of branching points will result in a marked decrease of hydrodynamic volume of the polymer coil in solution. The decrease in hydrodynamic volume is leading to an enhanced retention of the polymer on the size exclusion column. The polymer coil will then elute with other polymeric species, possessing a lower molecular weight, a lower degree of branching but identical hydrodynamic volume, inducing a high local dispersity at the given  $t_{el}$ . If we consider a similar case for polymer chains of high molecular weight, an increase in the degree of branching will result in an elution behavior of polymer coils shifted toward higher retention times, too. However, polymer chains of high molecular weight will exhibit a high absolute number of branching points per chain, leading to compact coils with elevated molecular densities in solution. For these species, an additional branching point will not induce a pronounced decrease in hydrodynamic volume, as the structures are already quite compact. Here, the rather insignificant impact of an additional branching point on hydrodynamic volume makes fractions to appear more uniform than in case of low molecular weight polymer chains, even at similar branching frequencies, resulting in  $\mathcal{D}(t_{el})$  close to unity. Nevertheless, at low retention times,  $\mathcal{D}(t_{el}) < 1$  is observed. Obviously, local dispersities should not be interpreted in full analogy to macroscopic dispersities. From a macroscopic point of view, dispersities below unity cannot be observed, since weight averaged molecular

weights solely lie above number averaged values. The method rather needs to be understood as a method relating two independent methods of molecular weight determination with each other. Uniform (linear) polyacrylates were shown to give  $\mathcal{D}(t_{el})$  around unity over the full range of  $t_{el}$ .<sup>18</sup> A deviation of the local dispersity from unity thus is interpreted as a variation in topology toward a nonuniform microstructure. As observed in earlier studies, local dispersities considerably lower than unity are mainly obtained in regions of low sample concentration and were explained by the inaccuracy of molecular weight determination resulting from low detector responses at low sample concentrations.<sup>21,49</sup>  $\mathcal{D}(t_{el})$  values below unity are observed for all NBR samples in regions of low sample concentration. However, the low concentration cannot be the only reason, since  $\mathcal{D}(t_{el}) < 1$  is also observed in regions of concentrations sufficiently high for accurate MALLS measurements. Moreover, smooth and reproducible data are obtained in all measurements. Low sample concentration would merely result in a pronounced scattering of datapoints, not observed in regions of  $t_{el}$  discussed in the current chapter. Another potential source of inaccuracy in molecular weight determination is related to column efficiency. If band broadening occurs, fractions eluting from the column are polydisperse in hydrodynamic volume. However, monodisperse hydrodynamic volume is a prerequisite for calculating number averaged molecular weights  $M_v$  as a function of  $t_{el}$  via the universal calibration principle derived by Hamielec and Ouano.<sup>48</sup> Failure of this premise results in inaccurate values of  $M_v$ ,<sup>50</sup> and thus  $\mathcal{D}(t_{el})$ , without effecting  $[\eta]$  and  $M_{LS}$  of the overall samples. Nevertheless, since measurements and data processing for all samples were identical, relative values can be interpreted qualitatively, irrespective absolute values of  $\mathcal{D}(t_{el})$ . This is no drawback for the current study, since in any case local dispersity on principle cannot be employed for a quantitative determination of the degree of branching.

Local dispersities  $\mathcal{D}(t_{el})$  as a function of elution time for samples taken from polymerizations A-F were obtained in analogy to the processing described exemplarily for polymerization B. Plots of  $\mathcal{D}(t_{el})$  of samples taken during all polymerization runs exhibit a shape similar to the plot described in detail for polymerization run B. Data are provided for each run in separate graphs (Figure 6.16 to Figure 6.20 in the *Appendix*). For each polymerization experiment, local

dispersity data of individual samples are provided together with a plot obtained from averaging local dispersity over all taken samples (bold grey line). In polymerizations C-F,  $\mathcal{D}(t_{el})$  of the individual samples shows an increased scattering of data points from the averaged curve when compared to the plots of  $\mathcal{D}(t_{el})$  of polymerizations A and B. This variation can be traced back to an alteration of the microstructures during the course of the polymerizations, not pronounced at low radical concentrations. Moreover, a trend of a decreasing slope of the  $\mathcal{D}(t_{el})$  can be discerned with increasing reaction time within each polymerization run. This decrease can be interpreted as an increased uniformity of the polymer chains obtained at higher conversion than those obtained at the early polymerization stages. While short- and long-chain branching in free radical polymerizations mainly occurs via radical transfer reactions such as back-biting, transfer to polymer or  $\beta$ -scission, copolymerization with BD offers additional channels of (long-chain) branching. Since BD is a bifunctional monomer, branching of nitrile rubber can also occur by incorporation of either the internal or vinylic double bonds of incorporated BD within the polymer backbone. In conventional free radical copolymerization, radical life times are short; around 1 s lies in between initiation and termination of a single polymer chain.<sup>51</sup> The probability of terminated polymer chains to be attacked by a growing radical chain (either radical transfer or incorporation of residual double bonds) increases with increasing resting time in the radical environments. Since at the beginning of polymerizations concentration of unreacted monomer is high compared to those of incorporated monomer units, only a fraction of polymer chains might have been attacked by growing radical chains. With increasing reaction time and a decreasing excess of unreacted monomers, the increasing probability of being attacked by radicals results in branched topologies of all chains present, expressed in an increased uniformity of the polymer. Compositional drifts as a cause for the apparent change of polymer microstructure can be ruled out, since this would be accompanied by a clear trend of increasing or decreasing refractive index increment with reaction time, not observed in any of the polymerizations.<sup>52</sup>

To compare the influence of radical concentration on NBR topologies,  $\mathcal{D}(t_{el})$  of polymerization runs A-F is plotted in Figure 6.7. The provided curves are data

obtained from averaging local dispersity over all samples taken from each individual polymerization run, *i.e.* data provided as bold grey lines in Figure 6.5 and Figure 6.16 to Figure 6.20. Local dispersities of samples obtained under different reaction conditions show a clear variation in the position of  $\mathcal{D}$  as a function of  $t_{el}$ . With increasing radical concentration in the polymerizations, a negative shift of the curves on the  $\mathcal{D}$ -axis is observed. Local dispersities of polymerizations A-C with low concentrations, represented by the green, red and cyan line, respectively, are almost similar in shape and position. Nevertheless, at a given  $t_{el}$ , the obtained curves from polymerizations performed with higher radical concentrations show a distinct shift toward lower  $\mathcal{D}(t_{el})$  and arrange in the order of C>D>E>F. The plot obtained for polymerization run F, however, in comparison to polymerization run E, does not exhibit a decrease in  $\mathcal{D}(t_{el})$  as substantial as observed for the pairs C-D and D-E. Due to the common inaccuracy of chromatographic separation of around 10%, not too much attention is given to the

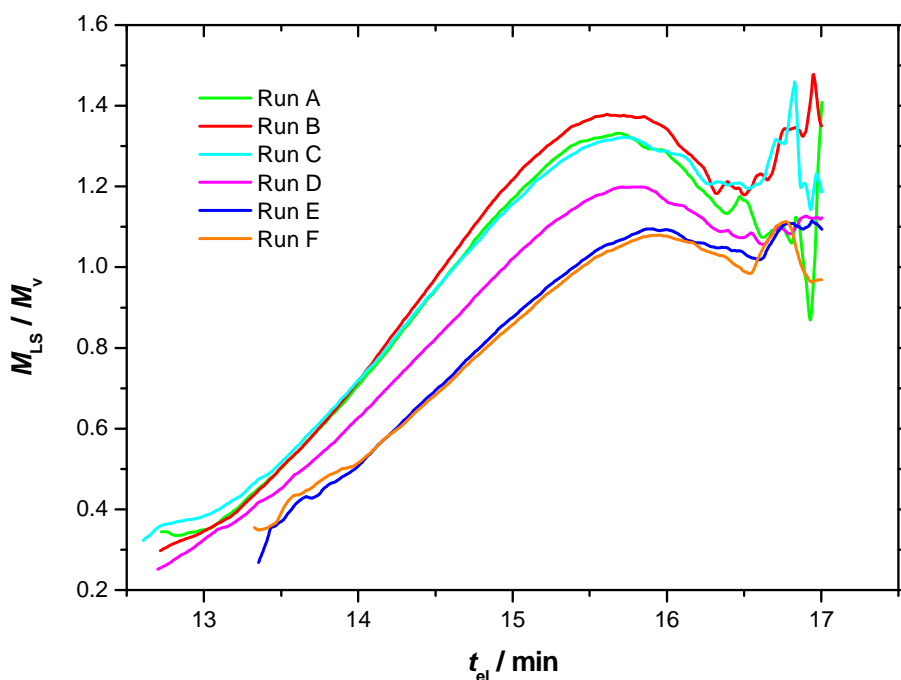


**Figure 6.7.** Comparative plot of local dispersities  $\mathcal{D}(t_{el})$  of nitrile rubber obtained in polymerizations experiencing different radical environments. Individual curves provided are obtained from averaging  $\mathcal{D}(t_{el})$  over all samples taken during polymerization run A (green curve,  $[\text{Ini}]_0 = 1.0 \text{ mM}$ ), run B (red curve,  $[\text{Ini}]_0 = 2.5 \text{ mM}$ ), run C (cyan curve,  $[\text{Ini}]_0 = 4.5 \text{ mM}$ ), run D (magenta curve,  $[\text{Ini}]_0 = 8.5 \text{ mM}$ ), run E (blue curve,  $[\text{Ini}]_0 = 17.1 \text{ mM}$ ) and run F (orange curve,  $34.1 \text{ mM}$ ).

absolute positions of the local dispersity plots. Nevertheless, the qualitative increase of negative shift of  $\mathcal{D}(t_{el})$  with increasing radical concentration is proof for the changes in NBR microstructure. Pronounced differences in the quantitative  $^{13}\text{C}$  NMR spectra of nitrile rubber obtained under the different polymerization conditions were not observed (see Figure 6.21 in the *Appendix*). The variation in the microstructure might thus be too subtle to be observed in NMR measurements. Nevertheless, the NMR experiments may also indicate differences in the nature of the branching topology while the polymers exhibit a similar branching density. In analogy, Cotts *et al.* observed changes in the branching topology of polyethylenes varying from linear chains to arborescent globular structures when studying polymers synthesized under different ethylene pressures.<sup>53</sup> In their study, light scattering evidenced differences in the polymer microstructure while the total branching as observed in  $^{13}\text{C}$  NMR measurements remained unchanged.

The concept of local dispersity can also be applied for the visualization of the change in microstructure during the course of reversible-deactivation radical copolymerization of AN and BD. In Figure 6.8, local dispersities as a function of  $t_{el}$  are depicted as solid lines for samples taken after 4, 6, 7, 8, 22 and 24 h of RAFT mediated copolymerization H. The polymerization was performed with an initial initiator concentration of 8.5 mM and with reaction conditions identical to those applied in conventional free radical copolymerization D. A gradual positive shift of the  $\mathcal{D}(t_{el})$  at a given  $t_{el}$  is observed with increasing conversion. While local dispersity plots of samples taken between 4 and 8 h of polymerization (black, magenta, cyan and blue curves) exhibit low slopes, curves obtained at 22 and 24 h of polymerization (green and red) are much steeper. Moreover, the shape of local dispersity plots obtained after long reaction times approaches the shape of local dispersity of polymers obtained from conventionally controlled free radical copolymerizations, exemplarily depicted for sample D<sub>8</sub> (blue dotted line). The latter sample is obtained under conditions equivalent to the preparation of sample H<sub>8</sub>, except conventional chain transfer was applied. The reason for the plots of H<sub>4</sub>, H<sub>6</sub>, H<sub>7</sub> and H<sub>8</sub> expanding over a smaller range of retention time than those of H<sub>22</sub> and H<sub>24</sub> is the lower overall molecular weight of those samples, as in RAFT polymerization molecular weight increases with conversion. RI traces of H<sub>6</sub> and

$H_{24}$  are provided exemplarily as dashed lines. Note the minor scattering of  $\mathcal{D}(t_{el})$  data of  $H_4$ ,  $H_6$ ,  $H_7$  and  $H_8$  in the region of 16.5 to 17.5 min resulting from an improved signal-to-noise ratio due to the high sample concentration in the region of low hydrodynamic volume.

The small slope of  $\mathcal{D}(t_{el})$  observed for samples taken during the first hours of the RAFT mediated copolymerization H might be interpreted as a proof for the high uniformity of the polymers obtained. Controlled radical polymerization was shown to give rise to a lower degree of branching, when polymerization of *n*-butyl acrylate was performed under otherwise similar conditions to conventional free radical polymerization.<sup>54</sup> The authors suggested a validity of the findings for polymerizations of other monomers that undergo chain transfer to monomer and computational studies could prove the lower degree of branching in ATRP of acrylates when compared to free radical copolymerization.<sup>55</sup> The herein presented

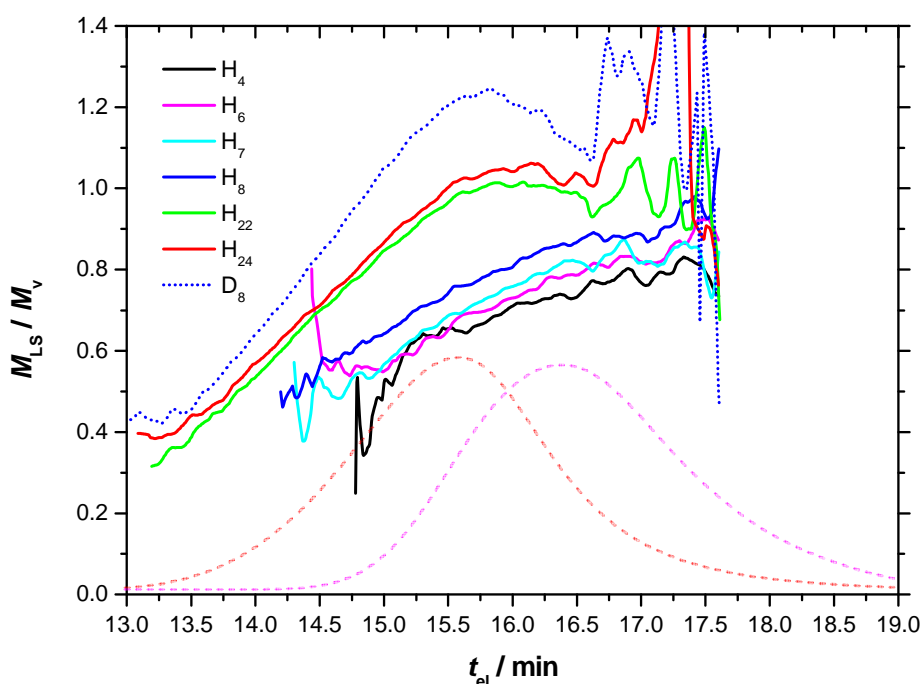


**Figure 6.8.** Graphical illustration of the change in polymer microstructure during the RAFT mediated copolymerization of AN and BD with an initial initiator concentration of 8.5 mM (polymerization run H).  $\mathcal{D}(t_{el})$  is depicted for samples  $H_4$  (black),  $H_6$  (magenta),  $H_7$  (cyan),  $H_8$  (blue),  $H_{22}$  (green),  $H_{24}$  (red) and  $D_8$  (blue dotted line). The latter was obtained from free radical copolymerization in the presence of dodecyl mercaptanes as the conventional chain transfer agents under conditions identical to those applied in RAFT mediated copolymerization H. The signal of the refractive index detector (a.u.) is given exemplarily for  $H_6$  (magenta dashed line) and  $H_{24}$  (red dashed line).

data show that with increasing polymerization times, the uniformity the polymers exhibit within the first hours of RAFT mediated polymerizations is reduced and structures approach those typically obtained in conventional free radical copolymerizations. Local dispersity of nitrile rubber obtained in polymerization G with an initial initiator concentration of 1.0 mM is provided in Figure 6.22 in the *Appendix*, showing a similar change in topology over the course of the polymerization. At a given  $t_{el}$ , samples obtained at higher polymerization times exhibit higher values for  $\mathcal{D}(t_{el})$ . Nevertheless, at polymerization times of up to 22 h, nitrile rubber of rather uniform microstructure is obtained. This behavior can be attributed to both a lower overall radical concentration and a higher concentration of transfer agent relative to radical concentration.  $\mathcal{D}(t_{el})$  span over a shorter range than in the case of conventional free radical copolymerization under equivalent conditions, with  $\mathcal{D}(t_{el})$  provided exemplarily for sample A<sub>22</sub> (red dotted line).

### 6.3.2 Can a Unique Set of MHKS Parameters be Obtained for NBR?

Molecular weight determination is among the most important polymer characterization techniques and detailed molecular weight information is crucial for many applications. Properties of materials strongly depend on the chain lengths of the polymers employed in the production thereof. Especially in applications where precise concentration knowledge is required, *i.e.* in modular polymer-polymer ligation reactions, exact number molecular weight averages need to be known. A method for the synthesis of high molecular weight NBR via the copper mediated azide-alkyne cycloaddition of chain-end functionalized NBRs was introduced in chapter 3. Moreover, in chapter 4 hetero-Diels–Alder reactions were shown to be a powerful tool for the construction of block and miktoarm star copolymer architectures of nitrile rubber. Since MHKS parameters for NBR have not been accessible, in these studies the determination of the exact reactant concentrations has been performed with methods alternative to SEC, such as stoichiometry variation or NMR studies. Nevertheless, with SEC being a convenient method for molecular weight determination, knowledge of MHKS parameters of NBR is highly desirable. However, a uniform microstructure is an important prerequisite for molecular weight determination via universal calibration using

MHKS parameters. Polymers of different topology will require the determination of topology-dependent MHKS parameters.

The above presented results unambiguously evidence that nitrile rubber obtained under different reaction conditions exhibits dissimilar microstructures, most probably caused by the radical environment during the polymerizations. In addition, polymer microstructure can be considered invariant over the course of the polymerization in particular cases only. However, changes seem to be subtle, as  $^{13}\text{C}$  NMR did not reveal pronounced structural differences. It is therefore mandatory to establish, if despite these structural differences, a universal set of MHKS parameters can be determined for NBR.

In general, MHKS parameters of polymers are obtained by linear regression of the double logarithmic plot of  $[\eta]$  as a function of weight average molecular weight for a series of polymer samples. Ideally, molecular weights of the polymer samples vary over a broad range. At molar masses below  $10\,000\text{ g}\cdot\text{mol}^{-1}$  MHKS parameters were shown by several studies to give inaccurate data.<sup>56</sup> A more accurate molecular weight determination for samples of low molar mass is obtained when using methods introduced by Stockmayer and Fixman<sup>57</sup> or Sadron and Rempp.<sup>58</sup> A logarithmic plot of the intrinsic viscosity versus molecular weight for all samples discussed in the current study is provided in Figure 6.9. The plotted values,  $[\eta]$  and  $M_{\text{LS}}$ , are obtained as weight averaged values by triple detection SEC,<sup>59</sup> averaged over the entire distribution of the polymer samples. Data for three consecutive injections of each sample is provided giving consistent values within an error adequate for the techniques applied ( $<5\%$  in  $M_{\text{LS}}$ ,  $<3\%$  in  $[\eta]$ ). While  $M_{\text{LS}}$  and  $[\eta]$  of samples taken during RAFT mediated copolymerizations G-H span over a broad range, NBRs obtained in each polymerization A-F employing conventional chain transfer agents only exhibit a minor variation in  $M_{\text{LS}}$  and  $[\eta]$  over polymerization times up to 24 h and mainly locate at the high molecular weight end of Figure 6.9.

Linear regression of the  $\log [\eta]$  versus  $\log M_{\text{LS}}$  data gave a slope of  $0.689 \pm 0.010$  with an intercept of  $(-1.306 \pm 0.048) \cdot \log (\text{mL}\cdot\text{g}^{-1})$ , shown as a solid line in Figure 6.9. An adequate regression ( $r^2 = 0.979$ ) was obtained and regular residues scatter evenly around the best fit.  $K$  and  $\alpha$  can be directly extracted from the regression since intrinsic viscosity and molecular weight are related with one another by the

Mark–Houwink equation, given in its logarithmic form as  $\log [\eta] = \log K + \alpha \cdot \log M_{LS}$ . Consequently, MHKS parameters of NBR samples (25 °C, THF) can be deduced as  $K = (49.5 \pm 5.5) \times 10^{-5} \text{ dL} \cdot \text{g}^{-1}$  and  $\alpha = 0.689 \pm 0.010$ . Given the fact that the samples do not show a unique microstructure, the error margin obtained for the MHKS parameters is reasonably low. A potential source of inaccuracy of the obtained MHKS parameters is – since a copolymer is investigated – a drift in monomer composition. However, compositional drifts can be ruled out as this would be manifested by a gradual change in the refractive index increments,  $dn/dc$ , with conversion, which was not observed in the polymerizations A-H. To the best of our knowledge, this is the first time MHKS parameters are reported for nitrile rubber. It should be noted that MHKS parameters for NBR with monomer composition other than the azeotrope composition (38/62) need to be determined in separate experiments and are not considered in the present study. Nevertheless, nitrile

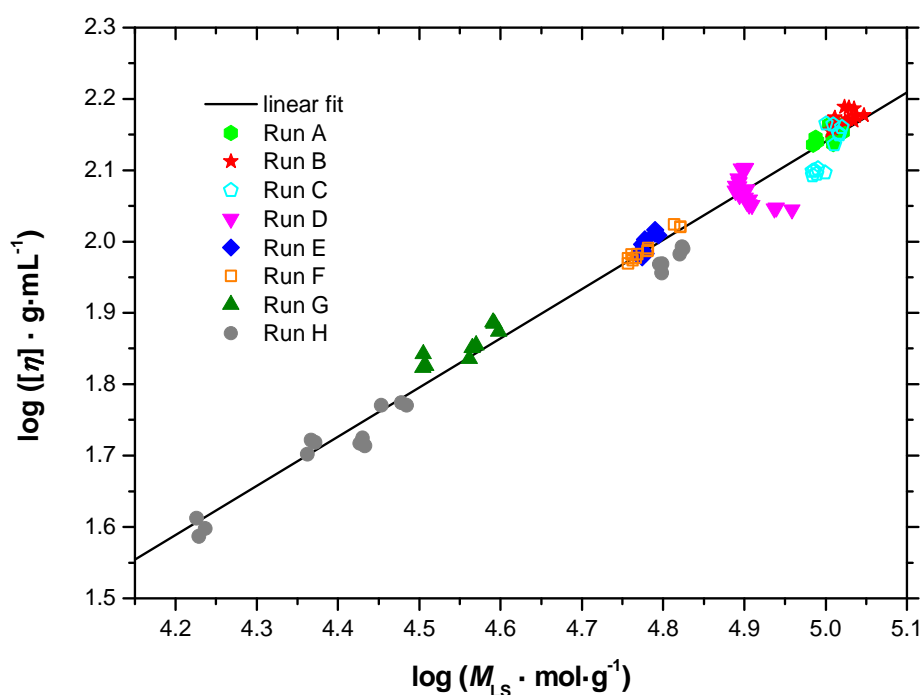


**Figure 6.9.** Double logarithmic plot of the weight average intrinsic viscosity  $[\eta]$  measured via on-line viscometry as a function of the weight average molecular weight  $M_{LS}$  as obtained from on-line MALLS for a series of NBR samples. For each sample,  $[\eta]$  and  $M_{LS}$  of three individual injections is provided: Polymerization run A (green), run B (red), run C (cyan), run D (magenta), run E (blue), run F (orange), run G (dark green) and run H (grey). Linear regression of  $\log [\eta]$  used to determine the MHKS parameters is depicted as a black solid line, yielding a slope of 0.689 and an intercept of -1.306.

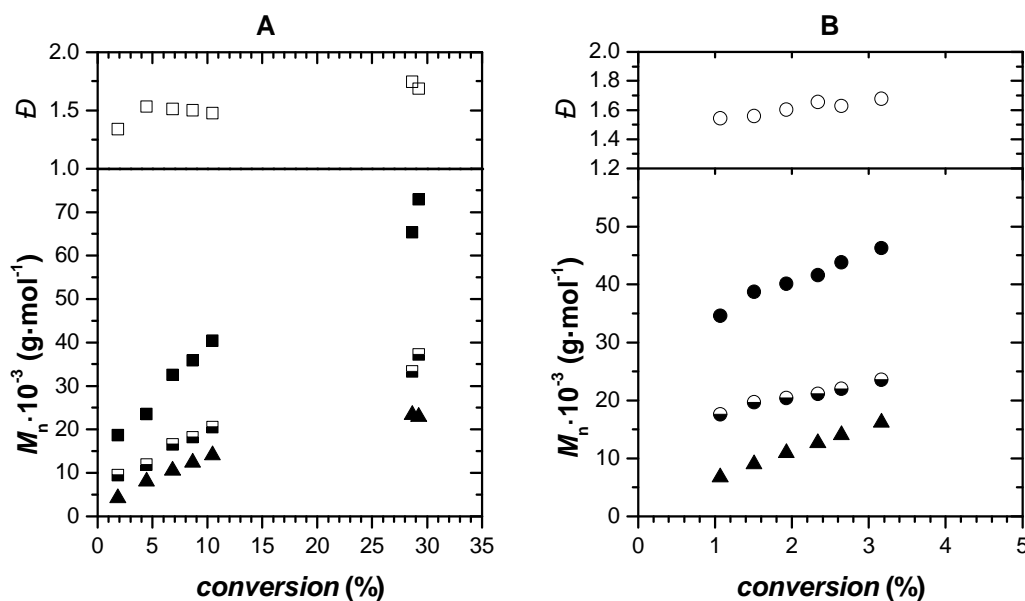


**Figure 6.10.** Evolution of molar mass with conversion for RAFT mediated polymerizations H (Figure 6.10A) and G (Figure 6.10B) with molar masses accessed via different methods. Polystyrene equivalent molar masses obtained from conventional SEC are represented by filled symbols, molar masses obtained from universal calibration using MHKS-parameters determined herein ( $K = 49.5 \times 10^{-5} \text{ dL} \cdot \text{g}^{-1}$ ,  $\alpha = 0.689$ ) are provided as half filled symbols.  $M_n$  theoretically expected from RAFT polymerization under consideration of initiator derived chains is calculated according to Equation 6.1 and Table 6.5 (provided in the *Appendix*) and is depicted by triangles. Dispersity  $\mathcal{D}$  is provided as obtained with conventional SEC as polystyrene equivalent values (empty symbols) only. Note the different scales of diagram A and B in  $M_n$  and conversion.

rubber with azeotrope composition has the highest market volume, thus the experiments focus on the azeotrope.

The herein obtained MHKS parameters were employed to determine molar masses of NBR samples taken during polymerizations G and H via universal calibration and the masses were compared to those obtained as polystyrene equivalent values. SEC was performed on a conventional system with differential refractive index detector only. In Figure 6.10, molar masses determined with the MHKS parameters for NBR are depicted for RAFT mediated polymerizations H (Figure 6.10A) and G (Figure 6.10B) as a function of conversion and are represented by half filled symbols. Molar masses as determined relative to polystyrene are depicted as filled symbols with the respective dispersity given as empty symbols. Dispersities of NBR samples as obtained by universal calibration do not show a strong variation to those obtained as polystyrene equivalent values (empty symbols) and thus are not provided in Figure 6.10. Such a behavior is

expected, since the relation of  $M_n$  and  $M_m$  is influenced by the slope of the Mark-Houwink plot, which is similar for NBR and polystyrene (0.689 vs. 0.70) thus giving similar dispersities.<sup>60</sup> In all examples, samples obtained from conventional calibration exhibit molar masses of about twice the value obtained via universal calibration. Since polymerizations G and H are RAFT polymerizations, the theoretically expected molar masses can be calculated based on conversion and reaction time. Calculations were performed according to Equation 6.1 under consideration of initiator derived chains<sup>35</sup> and are represented as triangles in Figure 6.10. Consideration of such chains is necessary since a high initiator concentration relative to controlling agent is employed (for mechanism of formation see Scheme 6.2, page 186). As depicted in Figure 6.11, the presence of initiator derived chains is evidenced by <sup>1</sup>H NMR spectroscopy, showing resonances of both the RAFT Z-group and the initiator fragment. Moreover, calculations were made assuming an initiator efficiency  $f$  of 0.7 and recombination as the predominant mechanism of chain termination (*i.e.*  $d = 1$ ). The latter assumption is justified by the reactivity ratios of AN and BD, leading to the almost exclusive presence of polymer chains with BD terminal units at any time during polymerization. Initiator efficiencies of azo initiators commonly range between 0.5 and 0.7. The higher limit was chosen for the calculations, allowing the obtained theoretical values to be discussed as lower limits of the expected molar masses. The molar masses obtained via universal calibration exhibit some positive deviation from the theoretical values. Nevertheless, the correlation is much improved compared to the polystyrene equivalent molar masses obtained from polystyrene based calibration SEC. Since the RAFT process is complex and cannot

**Equation 6.1.** Theoretically expected number average molar masses of nitrile rubber (azeotropic conditions) obtained in RAFT mediated copolymerizations G and H. The equation input values of conversion  $p$ , reaction time  $t$ , the initial concentration of RAFT agent  $[RAFT]_0$  and the initial initiator concentration  $[Ini]_0$  are provided in Table 6.5 in the Appendix.

$$\bar{M}_n(\text{calc.}) = \frac{[M]_0 \cdot p}{[RAFT]_0 + df[Ini]_0 \left(1 - \exp\left(-\frac{\ln 2}{\tau_{1/2}} \cdot t\right)\right)} m_M + m_{RAFT}$$

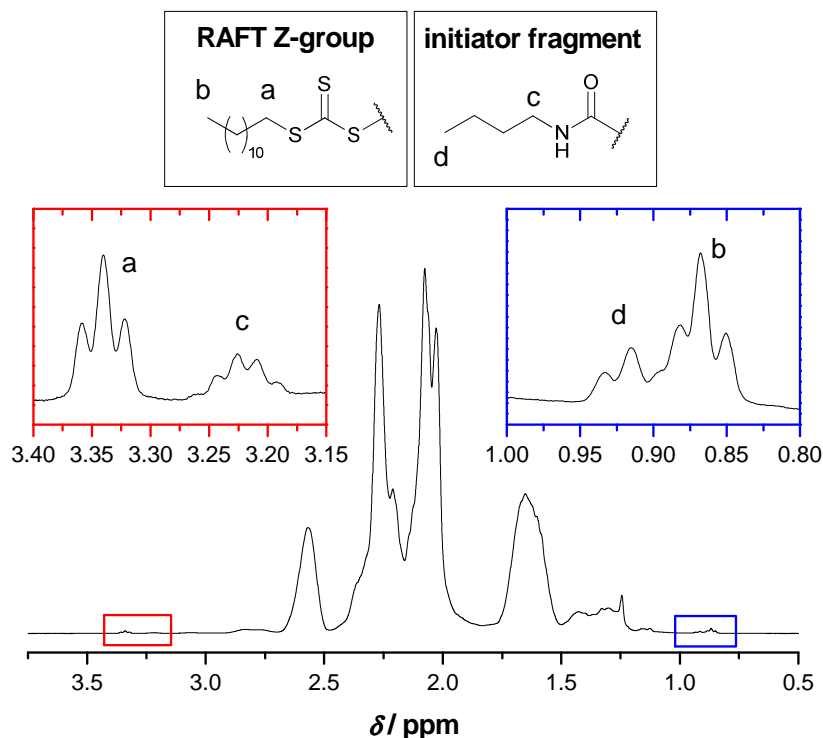


**Figure 6.11.** Aliphatic region of the  $^1\text{H}$  NMR spectrum ( $\text{CDCl}_3$ ) of sample  $G_{22}$  obtained in the RAFT mediated copolymerization of AN and BD, evidencing the presence of RAFT polymers and initiator derived chains.

sufficiently be described with Equation 6.1, theoretical calculations are an approximation further complicated by the presence of a hybrid behavior, commonly observed in RAFT mediated AN/BD copolymerizations.<sup>61</sup> Nevertheless, the good agreement of theoretical and experimental data is certainly a hint that the provided MHKS parameters lead to a better molar mass estimation than a calibration based on polystyrene equivalents.

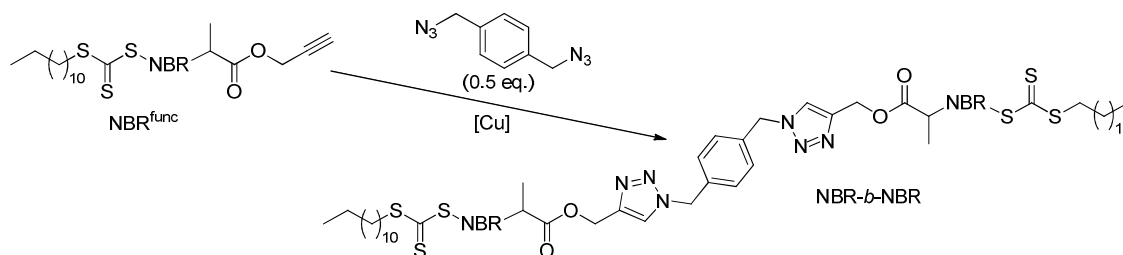
A firm proof for the applicability of the derived MHKS parameters determined in the current study is evident when comparing weight average molecular weight data  $M_w$  obtained from light scattering and universal calibration.  $M_w$  and  $M_{LS}$  data of nitrile rubber samples synthesized in polymerization runs G and H are given in Table 6.2. Universal calibration was performed using conventional SEC equipment and the MHKS parameters obtained herein. Polystyrene equivalent weight average molecular weights are given for completeness and show values of approximately twice  $M_{LS}$ . In contrast, molecular weights obtained from universal calibration and

**Table 6.2.** Weight average molecular weight  $M_m$  of NBR samples of polymerizations G and H obtained from conventional calibration, universal calibration using MHKS parameters determined herein and on-line MALLS.

sample	conv. calibration <sup>a</sup>	univ. calibration <sup>b</sup>	light scattering <sup>c</sup>
	$M_m$ (kg·mol <sup>-1</sup> )	$M_m$ (kg·mol <sup>-1</sup> )	$M_{LS}$ (kg·mol <sup>-1</sup> )
G <sub>17</sub>	64	33	32
G <sub>20</sub>	71	37	37
G <sub>22</sub>	78	40	39
H <sub>4</sub>	36	18	17
H <sub>6</sub>	49	25	23
H <sub>7</sub>	54	27	27
H <sub>8</sub>	60	30	30
H <sub>22</sub>	114	59	63
H <sub>24</sub>	123	63	67

<sup>a</sup> Polystyrene equivalent values. <sup>b</sup> obtained on conventional SEC equipment using MHKS parameters determined in the current study. <sup>c</sup> Absolute molecular weights obtained in on-line MALLS.

light scattering show good agreement over a broad molecular weight range and consistency is observed for samples taken in both RAFT mediated polymerization runs G and H. The data confirm that the MHKS parameters of nitrile rubber determined in the current study give accurate values independent of molecular weight and polymerization conditions. This is an important observation, since triple detection SEC analyses provided evidence of microstructure variances with the progress of polymerization and the variation of reaction conditions.



**Scheme 6.3.** Concept of orthogonal conjugation of alkyne-functionalized nitrile rubber to obtain high molecular weight NBR via the copper mediated azide-alkyne cycloaddition.

In chapter 3, alkyne-functionalized nitrile rubber (NBR<sup>func</sup>) has been the subject of orthogonal conjugation upon addition of small molecule diazide linkers to obtain high molecular weight NBR-*b*-NBR by a concept depicted in Scheme 6.3. Quantitative conversion of chain-end functionality has been confirmed via NMR and mass spectrometry measurements. Since no MHKS parameters of NBR were accessible at the time the experiments were performed, merely qualitative information evidencing the conjugation were obtained from SEC showing shifts of the peak retention times. The SEC data was thus re-evaluated with the MHKS parameters obtained in the current study. Molar masses  $M_{n,univ}$  of NBR<sup>func</sup> obtained from universal calibration with the MHKS parameters are provided in Table 6.3, giving values between 0.5 and 35 kg·mol<sup>-1</sup>. As coupling of polymers showing molecular weight distributions is a convolution process and molar mass is considered as a quantitative measure in modular conjugations,<sup>62-63</sup> a doubling of

**Table 6.3.** Comparison of conventional versus universal calibration molecular weight data of NBR-NBR conjugation experiments.<sup>a</sup>

NBR <sup>func</sup>		NBR- <i>b</i> -NBR			
universal calibration <sup>b</sup> $M_{n,univ}$ (g·mol <sup>-1</sup> )	conventional calibration <sup>c</sup> $M_{n,conv}$ (g·mol <sup>-1</sup> )	$\delta_{conv}$ <sup>d</sup> (%)	$M_{n,exp}$ <sup>e</sup> expected (g·mol <sup>-1</sup> )	universal calibration <sup>b</sup> $M_{n,univ}$ (g·mol <sup>-1</sup> )	$\delta_{univ}$ <sup>f</sup> (%)
0.5	2.5	150	1.0	1.2	20
3.0	10.6	77	6.0	5.2	13
5.2	17.4	67	10.4	8.6	17
19.9	72	80	40	37	8
35	97	39	70	50	29

<sup>a</sup> Experimental data is taken from Table 3.2, chapter 3. <sup>b</sup> Evaluation of SEC data was performed with MHKS parameters obtained in the current study. <sup>c</sup> Reported as polystyrene relative values obtained from conventional SEC. A calibration curve was established with narrowly dispersed polystyrene standards. <sup>d</sup> Deviation of the conventional calibration molar mass  $M_{n,conv}$  from the expected molar mass  $M_{n,exp}$ , calculated via  $\delta_{conv} = |M_{n,conv} - M_{n,exp}| / M_{n,exp}$ . <sup>e</sup> Molar mass expected from the conjugation being a convolution process:  $M_{n,exp}(\text{NBR-}b\text{-NBR}) = 2 \times M_{n,univ}(\text{NBR}^{func})$ . <sup>f</sup> Deviation of the universal calibration molar mass  $M_{n,univ}$  from the expected molar mass  $M_{n,exp}$ , calculated via  $\delta_{univ} = |M_{n,univ} - M_{n,exp}| / M_{n,exp}$ .

$M_n$  is expected during polymer-polymer conjugation. In Table 6.3, the molar masses  $M_{n,conv}$  and  $M_{n,univ}$  of the coupled polymers NBR-*b*-NBR determined via conventional (*i.e.* relative to polystyrene) and universal calibration, respectively, are compared to the theoretically expected values  $M_{n,exp}$ . The theoretically expected molar masses are calculated by doubling the molar masses  $M_{n,univ}$  of the chain-end functional precursors NBR<sup>func</sup> under the assumption of a full preservation of the chain-end functionality during the polymerization and a full conversion during the coupling process. The molar masses  $M_{n,conv}$  obtained in conventional calibration give molar masses of the coupled polymers ranging from 2.5 to 97 kg·mol<sup>-1</sup>, thus a deviation ( $\delta_{conv}$ ) of 39 to 150% from the expected molar masses is observed. In contrast, the molar masses  $M_{n,univ}$  of NBR-*b*-NBR obtained in universal calibration range from 1.2 to 50 kg·mol<sup>-1</sup> and show a much improved agreement with the theory; deviations ( $\delta_{univ}$ ) lie between 8 and 29%. Nevertheless, molar masses of NBR-*b*-NBR arrange below the theoretically expected values. Since in the previous study the completeness of orthogonal conjugation reactions was confirmed with independent methods, the improved consistency of molar mass data obtained in universal calibration is a further indication for the quality of the MHKS parameters of nitrile rubber obtained herein.

## 6.4 Conclusions

In the present chapter, NBR microstructure was shown to be dependent on the radical polymerization conditions. Variation of the polymer microstructure was evidenced by triple SEC measurements, making use of the simultaneous determination of molecular weights with two independent methods, namely on-line viscometry and on-line light scattering. The variation in the polymer microstructure of nitrile rubber obtained by the conventionally controlled free radical polymerizations was shown to originate from different radical environments during the polymerization process, depending on the reaction conditions. Experimental data are provided showing differences in microstructure not only when comparing nitrile rubber obtained under different polymerization conditions, yet the microstructure also shows a gradual variation during the

course of the polymerization. Such behavior is more pronounced when polymerizations are performed in the presence of high initial initiator concentrations. Moreover, triple SEC measurements give insight into the variation of NBR microstructure when the polymerizations are performed under reversible-deactivation conditions (RAFT). At low conversion, rather uniform polymer is obtained. With increasing conversion, a loss of the controlled character is evidenced, and microstructures approach those of nitrile rubber obtained in conventional free radical copolymerizations. The aim of the SEC based investigation was a semi-quantitative elucidation whether uniform structures are obtained in radical copolymerizations of AN and BD. Such a uniform structural composition is a prerequisite for the applicability of a unique set of MHKS parameters in universal calibration. Despite the fact that differences in polymer microstructure are observed, a single set of MHKS parameters is applicable. Linear regression of the Mark–Houwink plots of samples polymerized under different conditions gives values of  $K = (49.5 \pm 5.5) \times 10^{-5} \text{ dL}\cdot\text{g}^{-1}$  and  $\alpha = 0.689 \pm 0.010$  (25 °C, THF) with low error margin. The weight average molecular weights of nitrile rubber determined via universal calibration with the MHKS parameters show a good correlation with the absolute molecular weights determined via light scattering, underpinning the veracity of the obtained parameters.

## 6.5 Appendix

**Table 6.4.** Experimental details and analytical data of NBR samples investigated in the study. In the current chapter the samples are termed by quoting the polymerization run and the time samples were taken during polymerization, *e.g.* A<sub>15</sub> for the first entry.<sup>a</sup>

run	<i>t</i> (h)	<i>p</i> <sup>b</sup> (%)	<i>M</i> <sub>n</sub> <sup>c</sup> (kg·mol <sup>-1</sup> )	<i>M</i> <sub>m</sub> <sup>c</sup> (kg·mol <sup>-1</sup> )	<i>D</i> <sup>c</sup>		[ <i>η</i> ] <sup>d</sup> (ml·g <sup>-1</sup> )	<i>M</i> <sub>LS</sub> <sup>e</sup> (kg·mol <sup>-1</sup> )
A	15	4.5	122	197	1.6	a	146.1	103.5
						b	154.8	103.0
						c	146.0	101.0
A	16	4.9	120	189	1.7	a	145.1	104.8
						b	142.5	104.9
						c	144.2	103.3
A	20	6.6	111	187	1.7	a	139.6	101.9
						b	138.7	102.1
						c	137.1	102.2
A	22	7.4	110	184	1.7	a	138.2	97.7
						b	139.8	97.2
						c	136.7	96.5
B	3	1.5	120	204	1.7	a	149.1	102.6
						b	150.3	111.4
						c	149.8	108.9
B	6	3.4	118	203	1.7	a	154.4	105.5
						b	154.0	106.8
						c	153.5	108.4
B	8	4.8	122	199	1.6	a	143.9	102.2
						b	142.9	101.4
						c	144.8	102.5
B	22	12.7	94	176	1.9	a	147.7	108.2
						b	147.3	105.6
						c	148.3	106.6
C	5	4.8	116	198	1.7	a	146.4	100.1
						b	144.7	104.7
						c	145.9	102.1

C	8	8.9	113	188	1.7	a	142.0	103.7
						b	141.2	104.0
						c	136.8	136.8
C	22	21.6	90	173	1.9	a	126.5	97.8
						b	123.8	96.4
						c	124.4	97.5
C	24	23.1	84	170	2.0	a	125.0	99.9
						b	125.6	96.3
						c	125.8	96.8
D	3	4.6	93	156	1.7	a	126.6	78.7
						b	126.7	79.7
						c	126.8	79.6
D	5	9.1	86	145	1.7	a	119.8	77.5
						b	122.5	78.1
						c	121.0	78.3
D	7	11.7	91	150	1.7	a	117.8	77.3
						b	116.2	78.4
						c	118.3	80.0
D	8	13.0	85	148	1.7	a	113.7	80.0
						b	119.4	78.2
						c	115.1	79.6
D	22	28.5	85	156	1.8	a	112.6	81.2
						b	112.6	80.5
						c	114.6	80.5
D	24	30	85	157	1.8	a	111.6	86.9
						b	111.2	86.5
						c	110.8	90.9
E	1.33	1.7	73	120	1.6	a	102.0	62.2
						b	102.6	61.7
						c	103.8	61.7
E	2	3.1	73	116	1.6	a	100.7	59.9
						b	99.1	59.4
						c	99.86	59.9

E	2.66	4.5	68	112	1.6	a	96.2	60.1
						b	95.0	59.5
						c	96.5	59.0
E	3	4.9	70	113	1.6	a	95.8	59.2
						b	95.9	58.7
						c	95.7	59.7
F	1	2.7	81	126	1.6	a	105.7	65.1
						b	104.8	66.3
						c	105.0	66.3
F	1.66	4.9	74	116	1.6	a	98.0	60.4
						b	97.0	60.3
						c	97.2	60.4
F	2.66	8.5	71	113	1.6	a	93.1	57.1
						b	94.8	57.1
						c	95.9	57.7
F	3.33	11.2	74	112	1.5	a	94.2	57.9
						b	96.0	58.7
						c	94.9	58.4
G	17	1.9	40	64	1.6	a	69.6	32.0
						b	67.0	32.2
						c	66.6	32.0
G	20	2.6	44	71	1.6	a	68.6	36.5
						b	71.0	36.7
						c	71.6	37.2
G	22	3.2	46	78	1.7	a	74.9	39.6
						b	77.2	39.0
						c	76.8	39.1
H	4	4.5	24	36	1.5	a	41.0	16.8
						b	38.6	16.9
						c	39.6	17.2
H	6	6.8	33	49	1.5	a	52.3	23.6
						b	52.7	23.3
						c	50.4	23.0

H	7	8.7	36	54	1.5	a	52.1	26.7
						b	53.0	26.9
						c	51.8	27.1
H	8	10.5	40	60	1.5	a	58.9	28.4
						b	58.9	30.5
						c	59.5	30.1
H	22	28.7	65	114	1.7	a	92.9	62.4
						b	90.3	62.8
						c	93.1	63.0
H	24	29.3	73	123	1.7	a	97.7	66.8
						b	96.0	66.1
						c	98.3	66.6

<sup>a</sup> Experimental details of the polymerizations are provided in Table 6.1 in chapter 6, page 184. <sup>b</sup> Conversion was determined gravimetrically. <sup>c</sup> Determined by conventional SEC as polystyrene relative values. <sup>d</sup> Overall intrinsic viscosity determined by on-line viscometry. <sup>e</sup> Absolute molecular weight determined by on-line MALLS. <sup>f</sup> Sample not used in averaging of light scattering and viscometry profiles ( $M_{LS}$  vs.  $t_{el}$ ,  $[\eta]$  vs.  $t_{el}$ ). Here, irreproducible data was obtained, most probably due to technical issues.

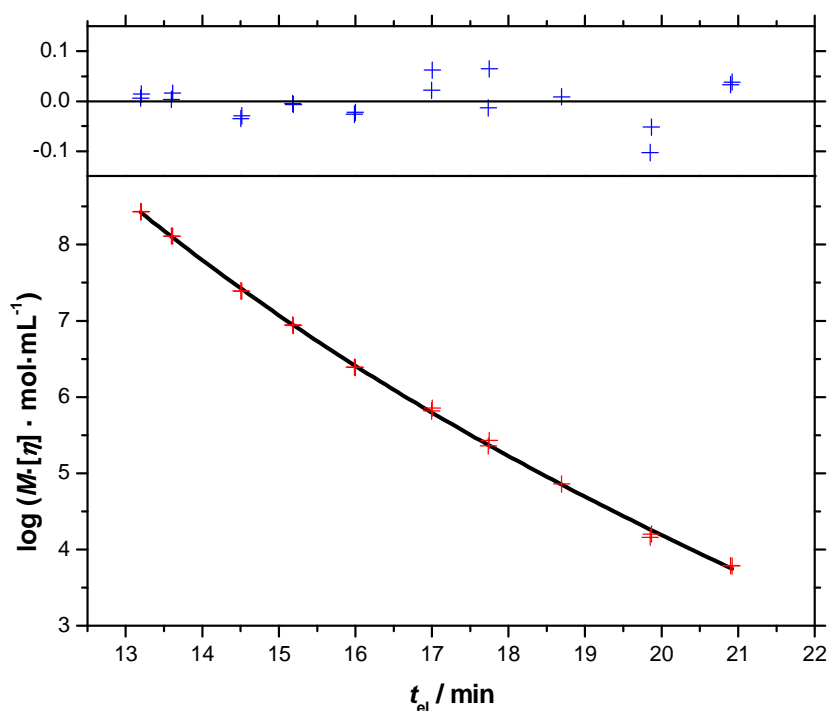


**Figure 6.12.** 3<sup>rd</sup> order polynomial fit (black solid line) of the universal calibration data (red) as a function of retention time. Intrinsic viscosity was determined by on-line viscometry; molar masses were used as provided by the supplier. A regular residual analysis is depicted in the upper panel (blue data points). An excellent fit with an  $r^2$  value of 0.999 is obtained.

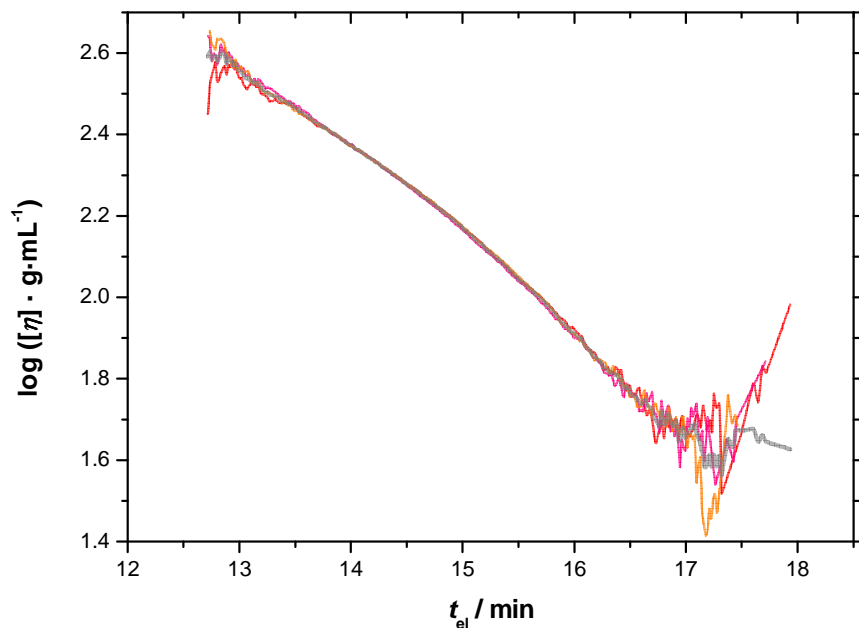


**Figure 6.13.** Evolution of intrinsic viscosity,  $\log([\eta] \cdot \text{g} \cdot \text{mL}^{-1})$ , with elution time  $t_{\text{el}}$  measured on-line exemplarily depicted for sample B<sub>22</sub>. The curves of three consecutive injections (red, orange and pink lines) are averaged (grey line) using the Origin Software to obtain an improved signal-to-noise ratio.

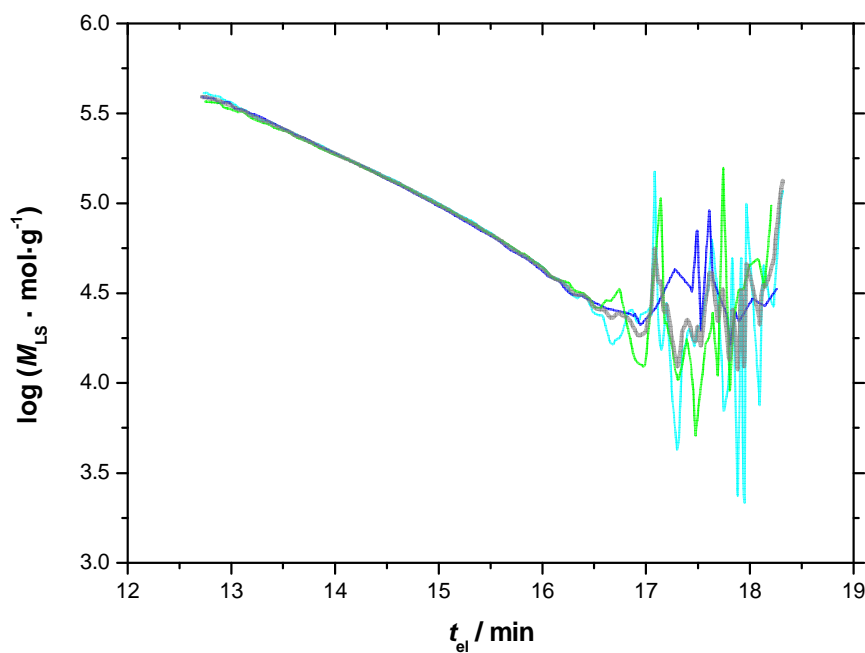


**Figure 6.14.** Evolution of molecular weight,  $\log(M_{\text{LS}} \cdot \text{mol} \cdot \text{g}^{-1})$ , versus elution time  $t_{\text{el}}$  of sample B<sub>22</sub> measured via on-line light scattering. The curves of three consecutive injections (blue, green and cyan lines) are averaged (grey line) using the Origin Software to obtain an improved signal-to-noise ratio.

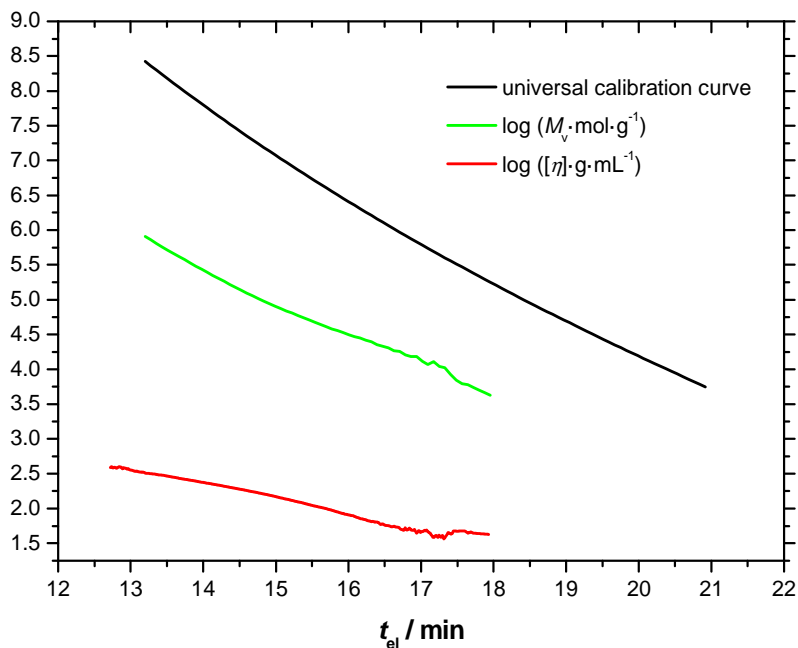


**Figure 6.15.** Determination of  $\log(M_v \cdot \text{mol} \cdot \text{g}^{-1})$  of sample B<sub>22</sub> (green line) as a function of  $t_{el}$  from its viscosity profile (red line),  $\log([\eta] \cdot \text{g} \cdot \text{mL}^{-1})$ , by universal calibration.  $\log(M_v \cdot \text{mol} \cdot \text{g}^{-1})$  is obtained by subtracting  $\log([\eta] \cdot \text{g} \cdot \text{mL}^{-1})$  from the universal calibration curve established for narrowly dispersed polystyrene samples (black line).

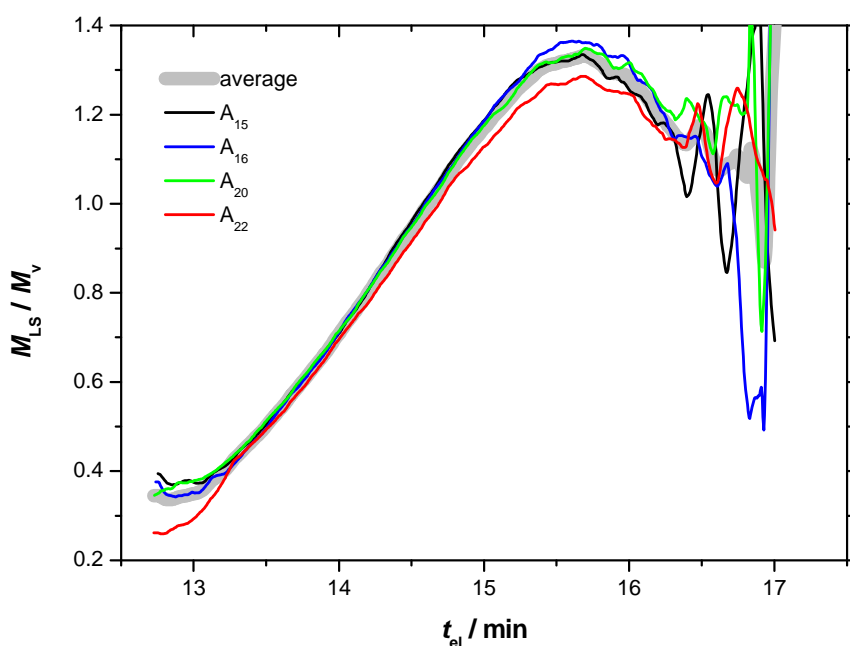


**Figure 6.16.** Plot of the local dispersity  $\mathcal{D}(t_{el})$  calculated from on-line MALLS and on-line viscometry SEC. The lines represent the data obtained for samples taken at different polymerization times during polymerization run A ( $[\text{Ini}]_0 = 1 \text{ mM}$ ): A<sub>15</sub> (black line), A<sub>16</sub> (blue line), A<sub>20</sub> (green line) and A<sub>22</sub> (red line). The curve obtained from averaging over all samples is represented as a grey bold line.

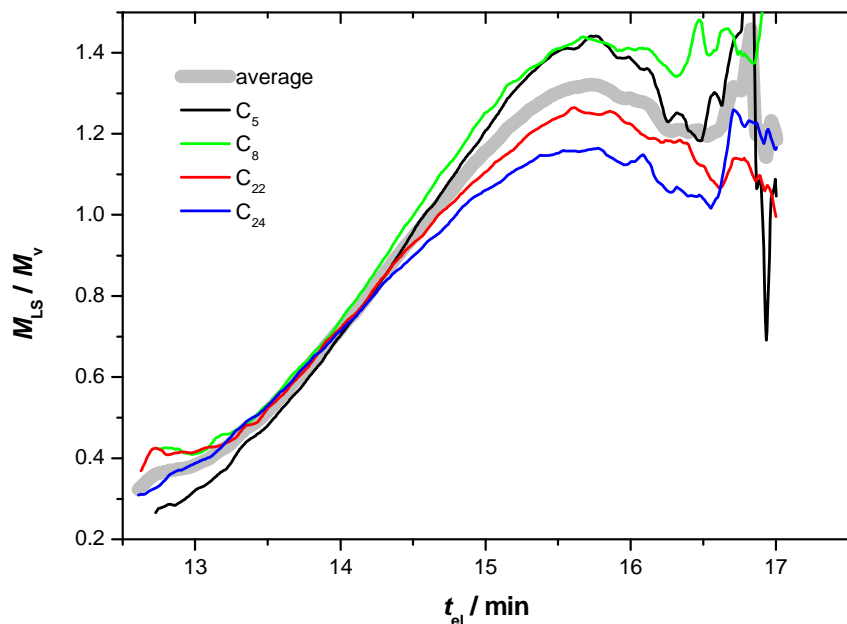


**Figure 6.17.** Plot of the local dispersity  $D(t_{el})$  calculated from on-line MALLS and on-line viscometry SEC. The lines represent the data obtained for samples taken at different polymerization times during polymerization run C ( $[Ini]_0 = 4.5$  mM):  $C_5$  (black line),  $C_8$  (green line),  $C_{22}$  (red line) and  $C_{24}$  (blue line). The curve obtained from averaging over all samples is represented as a grey bold line.

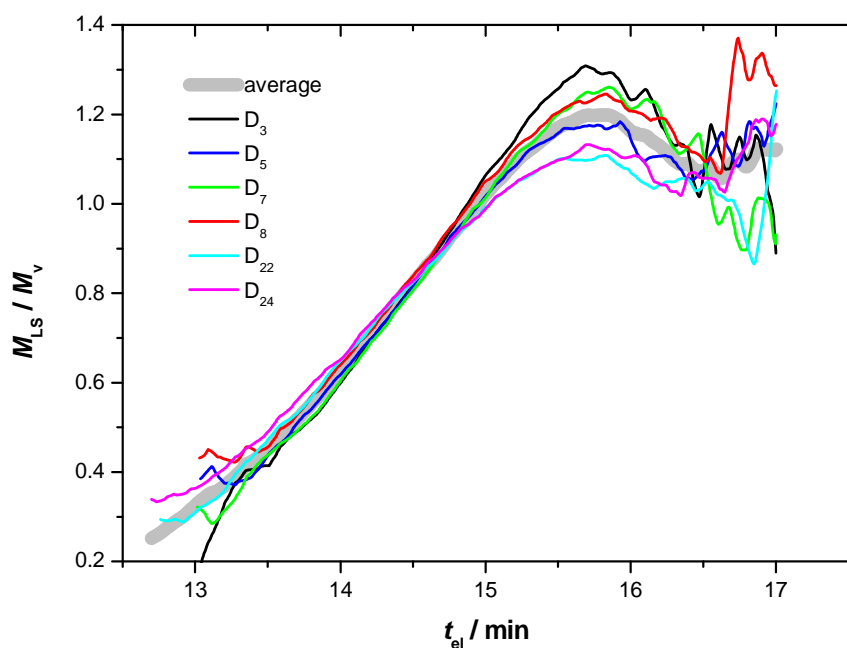


**Figure 6.18.** Plot of the local dispersity  $D(t_{el})$  calculated from on-line MALLS and on-line viscometry SEC. The lines represent the data obtained for samples taken at different polymerization times during polymerization run D ( $[Ini]_0 = 8.5$  mM):  $D_3$  (black line),  $D_5$  (blue line),  $D_7$  (green line),  $D_8$  (red line),  $D_{22}$  (cyan line) and  $D_{24}$  (magenta line). The curve obtained from averaging over all samples is represented as a grey bold line.

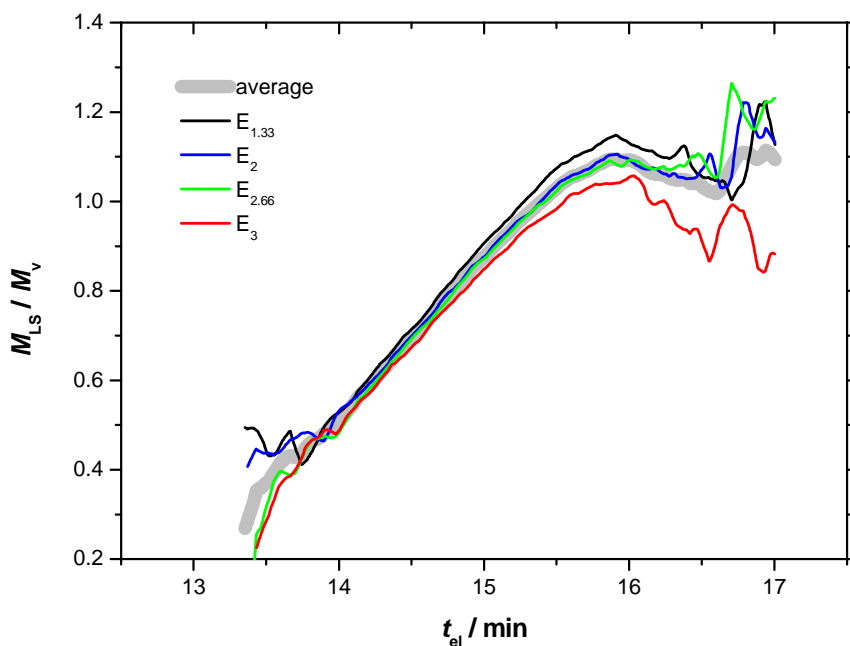


**Figure 6.19.** Plot of the local dispersity  $\mathcal{D}(t_{el})$  calculated from on-line MALLS and on-line viscometry SEC. The lines represent the data obtained for samples taken at different polymerization times during polymerization run E ( $[Ini]_0 = 17.1$  mM):  $E_{1.33}$  (black line),  $E_2$  (blue line),  $E_{2.66}$  (green line) and  $E_3$  (red line). The curve obtained from averaging over all samples is represented as a grey bold line.

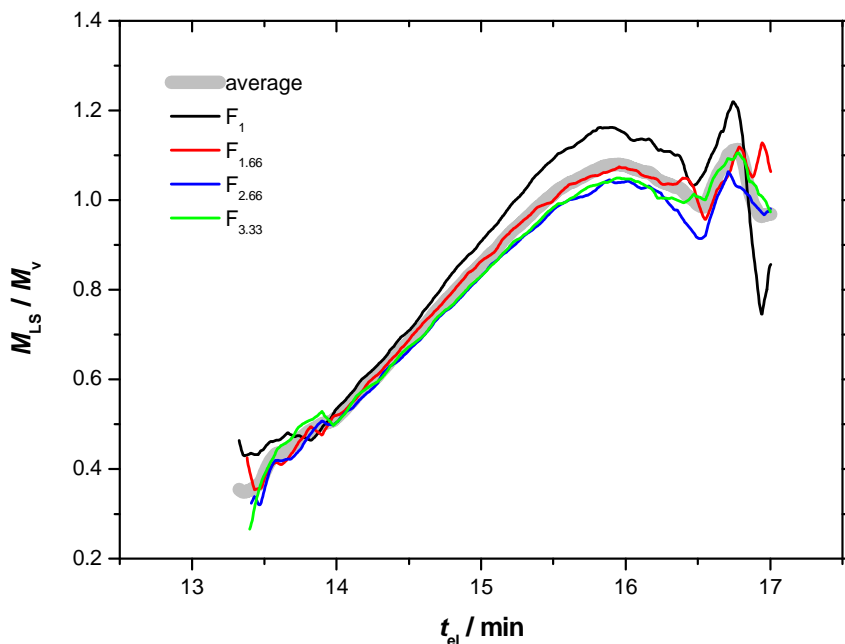


**Figure 6.20.** Plot of the local dispersity  $\mathcal{D}(t_{el})$  calculated from on-line MALLS and on-line viscometry SEC. The lines represent the data obtained for samples taken at different polymerization times during polymerization run F ( $[Ini]_0 = 34.1$  mM):  $F_1$  (black line),  $F_{1.66}$  (red line),  $F_{2.66}$  (blue line) and  $F_{3.33}$  (green line). The curve obtained from averaging over all samples is represented as a grey bold line.

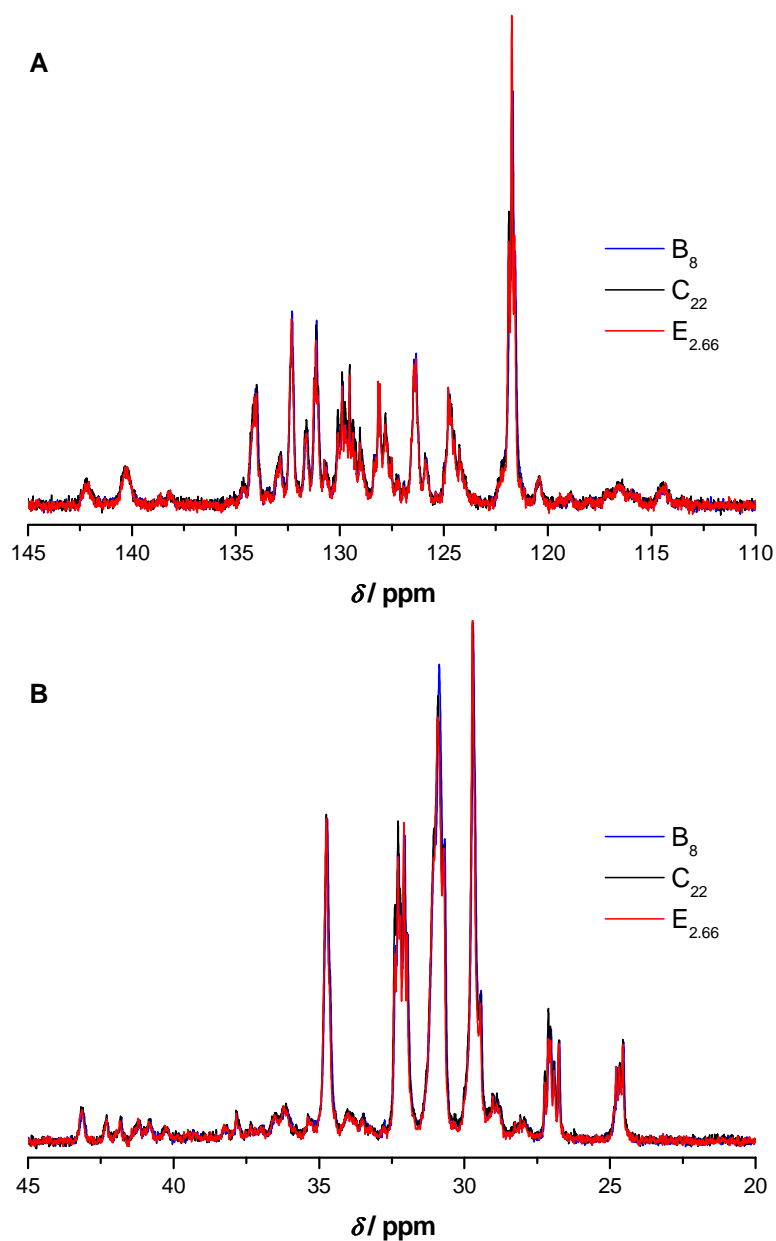


**Figure 6.21.** Magnified view into the region of A) 145 to 110 ppm and B) 45 to 20 ppm of the superimposed  $^{13}\text{C}$  NMR spectra (ambient temperature,  $\text{C}_2\text{D}_2\text{Cl}_4$ ) of nitrile rubbers  $\text{B}_8$ ,  $\text{C}_{22}$  and  $\text{E}_{2.66}$  obtained in conventionally controlled free radical copolymerization of AN and BD.  $^{13}\text{C}$  NMR signal assignments of NBR are described in detail elsewhere.<sup>64-65</sup>

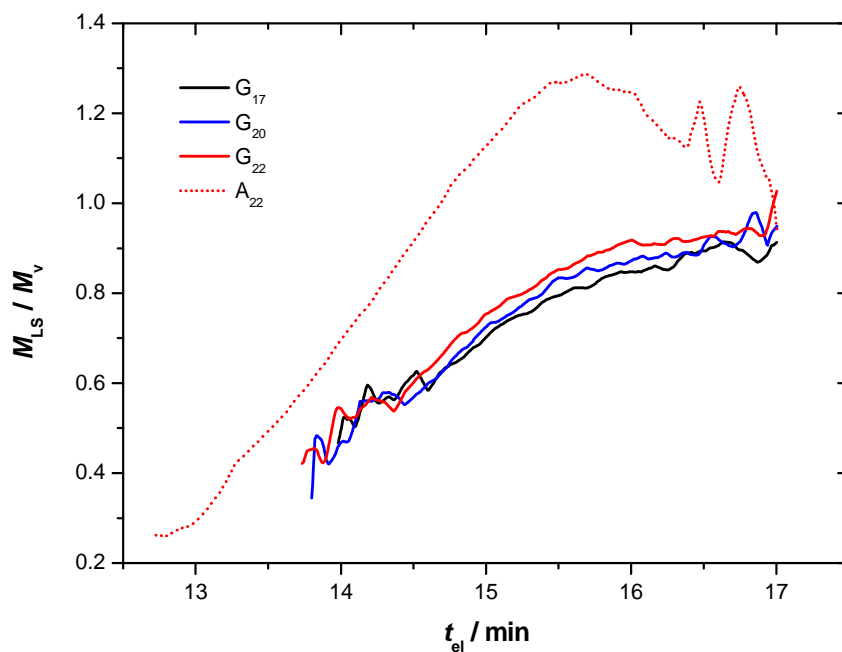


**Figure 6.22.** Graphical illustration of the change in polymer microstructure during the RAFT mediated copolymerization of AN and BD with an initial initiator concentration of 1.0 mM (polymerization run G).  $\mathcal{D}(t_{el})$  is depicted for samples  $G_{17}$  (black solid line),  $G_{20}$  (blue solid line),  $G_{22}$  (red solid line) and  $A_{22}$  (red dotted line). The latter was obtained from conventionally controlled free radical copolymerization under conditions identical to those applied in RAFT mediated copolymerization G.

**Table 6.5.** Experimental data and reaction conditions employed in the calculation of the theoretical molar masses of the RAFT mediated copolymerizations G and H via Equation 6.1 (see page 205).

polymerization run	$t$ (h)	$p^a$ (%)	$[\text{Ini}]_0$ (mM)	$[\text{RAFT}]_0$ (mM)
G	13	1.1	1.0	0.3
G	15	1.5	1.0	0.3
G	17	1.9	1.0	0.3
G	19	2.3	1.0	0.3
G	20	2.6	1.0	0.3
G	22	3.2	1.0	0.3
H	2	1.9	8.5	1.3
H	4	4.5	8.5	1.3
H	6	6.8	8.5	1.3
H	7	8.7	8.5	1.3
H	8	10.5	8.5	1.3
H	22	28.7	8.5	1.3
H	24	29.3	8.5	1.3

<sup>a</sup> Conversion was determined gravimetrically.

## 6.6 References

1. Kostanski, L. K.; Keller, D. M.; Hamielec, A. E. *J. Biochem. Bioph. Methods* **2004**, *58*, 159-186.
2. Grubisic, Z.; Rempp, P.; Benoit, H. *J. Polym. Sci. Part B: Polym. Lett.* **1967**, *5*, 753-759.
3. Jackson, C.; Chen, Y.-J.; Mays, J. W. *J. Appl. Polym. Sci.* **1996**, *61*, 865-874.
4. Coll, H. *Sep. Sci.* **1970**, *5*, 273-282.
5. Wild, L.; Guliana, R. *Journal of Polymer Science Part A-2: Polymer Physics* **1967**, *5*, 1087-1101.
6. Temyanko, E.; Russo, P. S.; Ricks, H. *Macromolecules* **2000**, *34*, 582-586.
7. Dubin, P. L.; Principi, J. M. *Macromolecules* **1989**, *22*, 1891-1896.
8. Coote, M. L.; Davis, T. P. *J. Polym. Sci. Part B: Polym. Phys.* **1999**, *37*, 2557-2570.
9. Striegel, A. M. *Anal. Chem.* **2005**, *77*, 104 A-113 A.
10. OECD. *Test No. 118: Determination of the Number-Average Molecular Weight and the Molecular Weight Distribution of Polymers using Gel Permeation Chromatography*. OECD Publishing.
11. Guillaneuf, Y.; Castignolles, P. *J. Polym. Sci. Part A: Polym. Chem.* **2008**, *46*, 897-911.
12. Kaiser, A.; Brandau, S.; Klimpel, M.; Barner-Kowollik, C. *Macromol. Rapid Commun.* **2010**, *31*, 1616-1621.
13. Dürr, C. J.; Emmerling, S. G. J.; Kaiser, A.; Brandau, S.; Habicht, A. K. T.; Klimpel, M.; Barner-Kowollik, C. *J. Polym. Sci. Part A: Polym. Chem.* **2012**, *50*, 174-180.
14. Klimpel, M.; Brandau, S.; Westeppe, U.; Barner-Kowollik, C.; Kaiser, A. *Nitrilkautschuke und deren Herstellung in organischen Lösungsmitteln*. WO Pat., 2011/032832 A1, 2011.
15. Hamielec, A. E.; Ouano, A. C.; Nebenzahl, L. L. *J. Liq. Chromatogr.* **1978**, *1*, 527-554.
16. Simon, P. F. W.; Müller, A. H. E.; Pakula, T. *Macromolecules* **2001**, *34*, 1677-1684.

17. Konkolewicz, D.; Gray-Weale, A. A.; Gilbert, R. G. *J. Polym. Sci. Part A: Polym. Chem.* **2007**, *45*, 3112-3115.
18. Gaborieau, M.; Nicolas, J.; Save, M.; Charleux, B.; Vairon, J.-P.; Gilbert, R. G.; Castignolles, P. *J. Chromatogr. A* **2008**, *1190*, 215-223.
19. Castignolles, P. *Macromol. Rapid Commun.* **2009**, *30*, 1995-2001.
20. Castignolles, P.; Graf, R.; Parkinson, M.; Wilhelm, M.; Gaborieau, M. *Polymer* **2009**, *50*, 2373-2383.
21. Junkers, T.; Schneider-Baumann, M.; Koo, S. S. P.; Castignolles, P.; Barner-Kowollik, C. *Macromolecules* **2010**, *43*, 10427-10434.
22. Gaborieau, M.; Castignolles, P. *Anal. Bioanal. Chem.* **2011**, *399*, 1413-1423.
23. Gaborieau, M.; Gilbert, R. G.; Gray-Weale, A.; Hernandez, J. M.; Castignolles, P. *Macromol. Theory Simul.* **2007**, *16*, 13-28.
24. Hertz, D. L.; Bussem, H.; Ray, T. W. *Rubber Chem. Technol.* **1995**, *68*, 540-546.
25. Scholte, T. G.; Meijerink, N. L. J. *Br. Polym. J.* **1977**, *9*, 133-139.
26. Gottlieb, H. E.; Kotlyar, V.; Nudelman, A. *J. Org. Chem.* **1997**, *62*, 7512-7515.
27. Zammit, M. D.; Davis, T. P. *Polymer* **1997**, *38*, 4455-4468.
28. Zammit, M. D.; Davis, T. P.; Suddaby, K. G. *Polymer* **1998**, *39*, 5789-5798.
29. Pigeon, M. G.; Rudin, A. *J. Appl. Polym. Sci.* **1995**, *57*, 287-301.
30. Hiorns, R. C.; Boucher, R. J.; Duhlev, R.; Hellwich, K. H.; Hodge, P.; Jenkins, A. D.; Jones, R. G.; Kahovec, J.; Moad, G.; Ober, C. K.; Smith, D. W.; Stepto, R. F. T.; Vairon, J. P.; Vohlidal, J. *Pure Appl. Chem.* **2012**, *84*, 2167-2169.
31. Terao, K.; Mays, J. W. *Eur. Polym. J.* **2004**, *40*, 1623-1627.
32. Mirabella, F. M.; Ford, E. A. *J. Polym. Sci. Part B: Polym. Phys.* **1987**, *25*, 777-790.
33. Held, D.; Kilz, P. *Macromol. Symp.* **2005**, *231*, 145-165.
34. Cherubin, T. *Über die Bestimmung von Copolymerisationsparametern in der radikalischen Copolymerisation von Acrylnitril mit Butadien*. Ph.D. Thesis, University of Essen, 1999.
35. Moad, G.; Rizzardo, E.; Thang, S. H. *Aust. J. Chem.* **2005**, *58*, 379-410.
36. Moad, G.; Rizzardo, E.; Thang, S. H. *Aust. J. Chem.* **2009**, *62*, 1402-1472.
37. Moad, G.; Rizzardo, E.; Thang, S. H. *Aust. J. Chem.* **2012**, *65*, 985-1076.

38. Uliyanchenko, E.; van der Wal, S.; Schoenmakers, P. J. *Polym. Chem.* **2012**, *3*, 2313-2335.
39. Jenkins, A. D.; Jones, R. G.; Moad, G. *Pure Appl. Chem.* **2010**, *82*, 483-491.
40. Lowe, A. B.; McCormick, C. L., RAFT Polymerization in Homogeneous Aqueous Media: Initiation Systems, RAFT Agent Stability, Monomers and Polymer Structures. In *Handbook of RAFT Polymerization*. 1<sup>st</sup> ed.; Barner-Kowollik, C., Ed.; Wiley-VCH: Weinheim, 2008; p 235 ff.
41. Ahmad, N. M.; Heatley, F.; Lovell, P. A. *Macromolecules* **1998**, *31*, 2822-2827.
42. Nikitin, A. N.; Hutchinson, R. A. *Macromolecules* **2005**, *38*, 1581-1590.
43. Fréchet, J. M. J.; Henmi, M.; Gitsov, I.; Aoshima, S.; Leduc, M. R.; Grubbs, R. B. *Science* **1995**, *269*, 1080-1083.
44. Vogt, A. P.; Sumerlin, B. S. *Macromolecules* **2008**, *41*, 7368-7373.
45. Hamielec, A. *Pure Appl. Chem.* **1982**, *54*, 293-307.
46. Degoulet, C.; Nicolai, T.; Durand, D.; Busnel, J. P. *Macromolecules* **1995**, *28*, 6819-6824.
47. Thitiratsakul, R.; Balke, S. T.; Mourey, T. H.; Schunk, T. C. *Int. J. Polym. Anal. Charact.* **1998**, *4*, 357-377.
48. Hamielec, A. E.; Ouano, A. C. *J. Liq. Chromatogr.* **1978**, *1*, 111-120.
49. Tackx, P.; Bosscher, F. *Anal. Commun.* **1997**, *34*, 295-297.
50. Gidley, M. J.; Hanashiro, I.; Hani, N. M.; Hill, S. E.; Huber, A.; Jane, J.-L.; Liu, Q.; Morris, G. A.; Rolland-Sabaté, A.; Striegel, A. M.; Gilbert, R. G. *Carbohydr. Polym.* **2010**, *79*, 255-261.
51. *Handbook of Radical Polymerization*. Matyjaszewski, K.; Davis, T. P., Eds.; Wiley-Interscience: Hoboken, 2002.
52. Radke, W.; Simon, P. F. W.; Müller, A. H. E. *Macromolecules* **1996**, *29*, 4926-4930.
53. Cotts, P. M.; Guan, Z.; McCord, E.; McLain, S. *Macromolecules* **2000**, *33*, 6945-6952.
54. Ahmad, N. M.; Charleux, B.; Farcet, C.; Ferguson, C. J.; Gaynor, S. G.; Hawket, B. S.; Heatley, F.; Klumperman, B.; Konkolewicz, D.; Lovell, P. A.;

- Matyjaszewski, K.; Venkatesh, R. *Macromol. Rapid Commun.* **2009**, *30*, 2002-2021.
55. Konkolewicz, D.; Sosnowski, S.; D'hooge, D. R.; Szymanski, R.; Reyniers, M.-F.; Marin, G. B.; Matyjaszewski, K. *Macromolecules* **2011**, *44*, 8361-8373.
56. Chance, R. R.; Baniukiewicz, S. P.; Mintz, D.; Strate, G. V.; Hadjichristidis, N. *Int. J. Polym. Anal. Charact.* **1995**, *1*, 3-34.
57. Stockmayer, W. H.; Fixman, M. *J. Polym. Sci. Part C: Polym. Symp.* **1963**, *1*, 137-141.
58. Sadron, C.; Rempp, P. *J. Polym. Sci.* **1958**, *29*, 127-140.
59. Radke, W.; Müller, A. H. E. *Macromolecules* **2005**, *38*, 3949-3960.
60. Strazielle, C.; Benoit, H.; Vogl, O. *Eur. Polym. J.* **1978**, *14*, 331-334.
61. Barner-Kowollik, C.; Quinn, J. F.; Nguyen, T. L. U.; Heuts, J. P. A.; Davis, T. P. *Macromolecules* **2001**, *34*, 7849-7857.
62. Barner-Kowollik, C. *Macromol. Rapid Commun.* **2009**, *30*, 1625-1631.
63. Preuss, C. M.; Barner-Kowollik, C. *Macromol. Theory Simul.* **2011**, *20*, 700-708.
64. Kondo, A.; Ohtani, H.; Kosugi, Y.; Tsuge, S.; Kubo, Y.; Asada, N.; Inaki, H.; Yoshioka, A. *Macromolecules* **1988**, *21*, 2918-2924.
65. Li, L.; Chan, C.-M.; Weng, L. T. *Macromolecules* **1997**, *30*, 3698-3700.



# 7 ■ Concluding Remarks and Outlook

Nitrile-butadiene rubber (NBR) is among the most important technical rubber products with broad applications in the automotive and aeronautical industry. With the increasing demand for mobility within the emerging economies, the need for NBR will certainly rise within the next decades. Moreover, the further development of sophisticated materials will require access to a broad range of specialty polymers and simple, yet efficient methods for their synthesis. In the thesis at hand, the lack of efficient strategies for the construction of advanced macromolecular architectures of NBR was addressed.

The copper mediated azide-alkyne cycloaddition (CuAAC) has been exploited for the synthesis of high molecular weight NBR architectures. Chain-end functionalized NBR building blocks were prepared by reversible addition-fragmentation chain transfer (RAFT) polymerization employing a novel alkyne-functionalized trithiocarbonate transfer agent. Modular ligation of the building blocks with a small molecular diazide allowed for the generation of linear NBR of up to  $100\,000\text{ g}\cdot\text{mol}^{-1}$  and dispersities below 1.6. As previous studies on the reversible-deactivation radical copolymerization of acrylonitrile (AN) and 1,3-butadiene (BD) have shown, NBR of such high molar mass displaying a narrow molecular weight distribution cannot be obtained in a sequential RAFT process. Moreover, a controlled crosslinking of NBR was achieved via the introduction of pendant alkyne-functionalities by terpolymerization of AN and BD with propargyl methacrylate and a subsequent cycloaddition reaction with a small molecular diazide.

Cyclopentadiene (Cp)-functionalized NBR proved to be an efficient polymer building block for the synthesis of NBR-*b*-poly(styrene-*co*-acrylonitrile) block

copolymers and 4-miktoarm star copolymers via the reversible addition-fragmentation chain transfer-hetero-Diels-Alder (RAFT-HDA) cyclization technique. The Cp-functionalized building blocks were obtained via a halide-Cp transformation of bromide-functionalized polymer precursors utilizing nickelocene. These precursors were accessed via RAFT mediated copolymerization of AN and BD employing two novel bromo-functionalized trithiocarbonate controlling agents. The dienophile poly(styrene-*co*-acrylonitrile) building blocks were obtained without any postpolymerization modification in RAFT mediated polymerization employing pyridinyl dithioester controlling agents. A semiquantitative evaluation of the coupling reactions via simulation and deconvolution techniques revealed the RAFT process to be responsible for up to 13% of nonfunctionalized polymeric material unable to undergo conjugation.

In an approach alternative to the CuAAC, tetrazole-functionalized NBR building blocks were employed to obtain linear NBR of high molecular weight. The coupling was performed upon irradiation with UV light in the presence of a small molecular bismaleimido linker via the nitrile imine mediated tetrazole-ene coupling (NITEC) technique. By an appropriate choice of the aryl substituents of the diaryl tetrazole chain termini, a selective coupling of the polymeric nitrile imine intermediate with the bifunctional linker was obtained. A reaction of the nitrile imine intermediate with the carbon-carbon double bonds or the nitrile moieties – both potential dipolarophiles and present in high concentrations within the polymer chain – was not observed. Underpinned by DFT calculations, the selectivity of the cyclization was identified to result from the low energy level of the lowest unoccupied molecular orbital (LUMO) of the olefinic dilinker.

The three presented coupling techniques, *i.e.* CuAAC, RAFT-HDA and the NITEC, were shown to be efficient strategies for the construction of advanced macromolecular architectures of NBR. However, the NITEC approach provides an important advantage over CuAAC and RAFT-HDA. The tetrazole-ene coupling of NBR building blocks is an extraordinarily pure example of modular conjugation. The tetrazole-functional polymer building blocks can be directly obtained in RAFT mediated polymerization without any postpolymerization modification. Moreover, the cyclization is triggered by irradiation with UV light in the absence of additives,

while molecular nitrogen is the only byproduct formed. The two alternative methods either require a postpolymerization modification – as in case of the RAFT-HDA approach – or proceed in the presence of catalytic species that, in case of the CuAAC technique, require an additional purification step after the coupling has been completed. Nevertheless, all three methods have proven to be fast, efficient and versatile and provide the first-ever reported set of modular ligation techniques for the construction of advanced macromolecular architectures of NBR. Due to the modular character of the approaches, the herein developed techniques may further serve as a basis for the synthesis of other sophisticated NBR structures. For example, the simple structural variation of the small molecular linker molecules will allow for the access of numerous novel materials with unprecedented property profiles. Moreover, in light of the high number of applications of NBR as sealings or dampers, especially the surface modification of solid substrates with NBR building blocks might open up a wide field for innovative products. In this context, the potential ability of the photo-induced NITEC technique for the spatially resolved modification of solid substrates is highlighted. The possibility to access veritable molar masses of NBR employing the herein determined Mark–Houwink–Kuhn–Sakurada parameters will fundamentally simplify future investigations in academia and industry where exact information on concentration and chain length is required.



## List of Abbreviations

$[\eta]$	intrinsic viscosity
$A$	pre-exponential factor
a. u.	arbitrary units
AGET	activators generated by electron transfer
Ala	alanine
AN	acrylonitrile
Arg	arginine
ARGET	activators regenerated by electron transfer
ATRP	atom transfer radical polymerization
BD	1,3-butadiene
BHT	butylated hydroxytoluene
br	broad (NMR)
BR	butadiene rubber
CC	column chromatography
COD	cyclooctadiene
Cp	cyclopentadiene
CR	chloroprene rubber
CSIRO	Commonwealth Scientific and Industrial Research Organization
CuAAC	copper mediated 1,3-dipolar azide-alkyne cycloaddition
d	dublet (NMR)
$\mathcal{D}$	dispersity index
$\mathcal{D}(t_{ei})$	local dispersity index
DA	Diels–Alder
$DB$	degree of branching
DCC	<i>N,N'</i> -dicyclohexylcarbodiimide
DFT	density functional theory
DMAP	4-(dimethylamino)pyridine

---

DMF	<i>N,N</i> -dimethylformamide
DMSO	dimethyl sulfoxide
$dn/dc$	refractive index increment
DoPAT	2-((dodecylsulfanyl)carbonothioyl)sulfanyl propanoic acid
DP <sub>n</sub>	degree of polymerization
$E_a$	activation energy
EPDM	ethylene propylene diene monomer
eq	equivalent
ESI	electrospray ionization
FI	fluorescence intensity
FT	Fourier transform
HDA	hetero-Diels–Alder
HNBR	hydrogenated nitrile-butadiene rubber
HOMO	highest unoccupied molecular orbital
HPLC	high performance liquid chromatography
I·	initiator fragment
Ini	radical initiator
ICAR	initiators for continuous activator regeneration
IIR	butyl rubber
IR	infrared
$J$	dipole-dipole coupling constant (NMR)
$K, \alpha$	Mark–Houwink–Kuhn–Sakurada parameters
L	ligand
LUMO	lowest unoccupied molecular orbital
$M$	molecular weight
M	monomer
m	multiplet (NMR)
$m/z$	mass-to-charge ratio
MADIX	macromolecular design by interchange of xanthates
MALLS	multi-angle laser light scattering
Met	methionine

---

MHKS	Mark–Houwink–Kuhn–Sakurada
$M_{LS}$	weight average molecular weight obtained in light scattering
$M_m$	weight average molecular weight
MMA	methyl methacrylate
$M_n$	number average molecular weight
$M_{n,conv}$	molar mass determined via conventional calibration
$M_{n,exp}$	expected molar mass
$M_{n,univ}$	molar mass determined via universal calibration
MO	molecular orbital
MS	mass spectrometry
$M_v$	molar mass determined via on-line viscometry
Na <sub>2</sub> EDTA	ethylenediaminetetraacetic acid disodium salt
NBR	nitrile-butadiene rubber
NiCp <sub>2</sub>	nickelocene
NITEC	nitrile imine mediated tetrazole-ene coupling
NMP	nitroxide mediated polymerization
NMR	nuclear magnetic resonance
<i>p</i>	conversion
Phe	phenylalanine
PMA	prop-2-ynyl methacrylate
PMDETA	<i>N,N,N',N'',N'''</i> -pentamethyldiethylenetriamine
PPh <sub>3</sub>	triphenylphosphine
ppm	parts per million
PS	polystyrene
q	quadruplet (NMR)
RAFT	reversible addition–fragmentation chain transfer
$R_f$	retardation factor
RI	refractive index
RuAAC	ruthenium mediated 1,3-dipolar azide-alkyne cycloaddition
s	singlet (NMR)
S	styrene

---

SAN	poly(styrene- <i>co</i> -acrylonitrile)
SBR	stryrene-butadiene rubber
SEC	size exclusion chromatography
$t$	time
t	triplet (NMR)
$^t\text{Br}$	tertiary bromoalkane
TDM	tertiary dodecyl mercaptanes
$t_{\text{el}}$	elution time, retention time
TEMPO	2,2,6,6-tetramethylpiperidine 1-oxyl
TFA	trifluoroacetic acid
THF	tetrahydrofuran
TLC	thinlayer chromatography
TMS	trimethylsilyl
UV	ultraviolet
UV-vis	ultraviolet-visible
$V$	volume
$V_{\text{h}}$	hydrodynamic volume
$V_{\text{total}}$	total volume
$w_{\text{pred}}$	predicted relative weight fraction
$\lambda_{\text{em}}$	emission wavelength
$\lambda_{\text{exc}}$	excitation wavelength

# Curriculum Vitae

Date of Birth                      February 6<sup>th</sup>, 1985  
Place of Birth                      Lüneburg, Germany  
Nationality                          German

## Education

05/2010 – Present                **Doctoral Studies in Chemistry**  
Under the supervision of Prof. Dr. Christopher Barner-  
Kowollik  
Karlsruhe Institute of Technology (KIT), Germany

03/2010                                **Diploma in Chemistry**  
Diploma thesis:  
Mechanistic Insights into Isomerizing Carbonylation  
of Methyl Oleate  
Under the supervision of Prof. Dr. Stefan Mecking  
University of Konstanz, Germany

10/2004 – 03/2010                **Studies in Chemistry**  
University of Konstanz, Germany

08/2008 – 01/2009                **Studies in Chemistry**  
Queen's University, Kingston, Ontario, Canada

09/1995 – 07/2004                **High School Certificate**  
Sonthofen, Germany

## Employment History

05/2010 - Present                Institut für Technische Chemie und Polymerchemie  
Karlsruhe Institute of Technology (KIT), Germany  
Scientific coworker



# List of Publications and Conference Contributions

## Refereed Journal Publications

- (11) *Photo-Induced Ligation of Acrylonitrile-Butadiene Rubber: Selective Tetrazole-Ene Coupling of Chain-End Functionalized Copolymers of 1,3-Butadiene*  
Dürr, C. J.; Lederhose, P.; Hlalele, L.; Abt, D.; Kaiser, A.; Brandau, S.; Barner-Kowollik, C. *Macromolecules* **2013**, *46*, 5915-5923.
- (10) *Determining the Mark-Houwink Parameters of Nitrile Rubber: A Chromatographic Investigation of the NBR Microstructure*  
Dürr, C. J.; Hlalele, L.; Schneider-Baumann, M.; Kaiser, A.; Brandau, S.; Barner-Kowollik, C. *Polym. Chem.* **2013**, *4*, 4755-4767.
- (9) *A One-Pot Route to Poly(carboxybetaine acrylamide) Functionalized SWCNTs and Further Modification with DNA*  
Yameen, B.; Rodriguez-Emmenegger, C.; Ahmed, I.; Preuss, C. M.; Dürr, C. J.; Zydziak, N.; Trouillet, V.; Fruk, L.; Barner-Kowollik, C. *Chem. Commun.* **2013**, *49*, 6734-6736.
- (8) *Mechanistic Insights into the UV-Induced Radical Copolymerization of 1,3-Butadiene with Acrylonitrile*  
Hlalele, L.; Dürr, C. J.; Lederhose, P.; Huesgen, S.; Kaiser, A.; Brandau, S.; Barner-Kowollik, C. *Macromolecules* **2013**, *46*, 2109-2117..
- (7) *Mild and Efficient Modular Synthesis of Poly(acrylonitrile-co-butadiene) Block and Miktoarm Star Copolymer Architectures*  
Dürr, C. J.; Hlalele, L.; Kaiser, A.; Brandau, S.; Barner-Kowollik, C. *Macromolecules* **2013**, *46*, 49-62.
- (6) *Mechanistic Features of Isomerizing Alkoxyacylation of Methyl Oleate*  
Roesle, P.; Dürr, C. J.; Möller, H. M.; Cavallo, L.; Caporaso, L.; Mecking, S. *J. Am. Chem. Soc.* **2012**, *134*, 17696-17703.

- (5) *High Molecular Weight Acrylonitrile-Butadiene Architectures via a Combination of RAFT Polymerization and Orthogonal Copper Mediated Azide-Alkyne Cycloaddition*  
Dürr, C. J.; Emmerling, S. G. J.; Lederhose, P.; Kaiser, A.; Brandau, S.; Klimpel, M.; Barner-Kowollik, C. *Polym. Chem.* **2012**, *3*, 1048–1060.
- (4) *A Detailed Investigation of the Experimental Conditions for the Reversible Addition Fragmentation Chain Transfer-Mediated Copolymerization of Acrylonitrile and Butadiene*  
Dürr, C. J.; Emmerling, S. G. J.; Kaiser, A.; Brandau, S.; Habicht, A. K. T.; Klimpel, M.; Barner-Kowollik, C. *J. Polym. Sci. – Polym. Chem.* **2012**, *50*, 174–180.
- (3) *Dimethyl Titanocene Y: A Valuable Precursor for Libraries of Cytotoxic Titanocene Derivatives*  
Immel, T. A.; Martin, J. T.; Dürr, C. J.; Groth, U.; Huhn, T. *J. Inorg. Biochem.* **2010**, *104*, 863–867.
- (2) *A Solvent Having Switchable Hydrophilicity*  
Jessop, P. G.; Phan, L.; Carrier, A.; Robinson, S.; Dürr, C. J.; Harjani, J. R. *Green Chem.* **2010**, *2*, 809–814.
- (1) *405 nm Absorption Detection in Nanoliter Volumes*  
Waechter, H.; Bescherer, K.; Dürr, C. J.; Oleschuk, R. D.; Loock, H.-P. *Anal. Chem.* **2009**, *81*, 9048–9054.

## Patents

- (1) *Verfahren zur Herstellung von Nitrilkautschuken in organischen Lösungsmitteln, Process for Producing Nitrile Rubbers in Organic Solvents*  
Brandau, S.; Kaiser, A.; Klimpel, M.; Barner-Kowollik, C.; Dürr, C. J.; Emmerling, S. G. J. EP 2 554 558, WO 2013/017610.

## Conference Contributions

- (2) *High Molecular Weight Acrylonitrile-Butadiene Architectures via a Combination of RAFT Polymerization and Orthogonal Copper Mediated Azide-Alkyne Cycloaddition*  
Dürr, C. J.; Emmerling, S. G. J.; Kaiser, A.; Brandau, S.; Barner-Kowollik, C. *Warwick Polymer Conference 2012*, Coventry, United Kingdom.
- (1) *Synthesis of Acrylonitrile-Butadiene Rubber (NBR) via RAFT Techniques*  
Kaiser, A.; Brandau S.; Dürr, C. J.; Emmerling, S. G. J.; Klimpel, M.; Barner-Kowollik, C. *Makromolekulares Kolloquium 2011*, Freiburg, Germany.



## Acknowledgement – Danksagung

First of all I would like to thank my thesis advisor Prof. Dr. Christopher Barner-Kowollik for giving me the opportunity to work on the exciting topic, for the restless support and dedication, the numerous fruitful discussions and for placing his trust in me.

Lanxess Deutschland GmbH is thanked for funding the project and the excellent collaboration. Very special thanks go to Dr. Sven Brandau, Dr. Andreas Kaiser, Stefan Hüsgen and Dr. Michael Klimpel for the fruitful discussions and the permanent support.

Dr. Andreas Kaiser, Dr. Sebastian Emmerling and Dr. Lebohang Hlalele are thanked for the great teamwork. Dr. Andreas Kaiser is thanked for introducing me to the beforehand unknown topic and for sharing precious technical experience.

I thank Paul Lederhose for his excellent contribution to the work on the photo-induced ligation of NBR building blocks (presented in chapter 5) in the context of his diploma thesis.

Axel Habicht, Paul Lederhose and Doris Abt are thanked for their support in various projects as “Hiwis” and “Vertiefer” students.

I thank Dr. Maria Schneider for her great devotion to the triple SEC measurements. Peter Gerstel, Dr. Anja Goldmann, Evelyn Stühling and Gabriele Herrmann are thanked for the organizational and administrative work.

Dr. Lebohang Hlalele is thanked for performing polymerization simulations, SEC deconvolution and DFT calculations.

I would like to acknowledge all those who performed measurements: Michael Kaupp, Kim Öhlenschläger and Astrid Hirschbiel for SEC-ESI-MS measurements and Dr. Leonie Barner for elemental analysis. Lukas Stolzer is thanked for his help with the fluorescence measurements.

I thank Christiane Lang, Dr. Lebohang Hlalele and my dad for proof reading.

I would like to thank the whole macroarc group for the warm atmosphere, the support and the great time we had together. Special thanks go to the “Westhochschule” team; thank you for the fruitful discussions, the helping hands

when they were needed and the encouraging words. My special thanks also go to the “OC” team for kindly integrating me into the macroarc group.

Finally, I would like to thank my family Claudi and Isabella. Thank you for your permanent support and the little smiles. Thank you for making every moment so special.